INTRINSICALLY PHOTOSENSITIVE RETINAL GANGLION CELLS: DIVERSITY OF FORM AND FUNCTION

A DISSERTATION
SUBMITTED TO THE FACULTY OF THE GRADUATE SCHOOL
OF THE UNIVERSITY OF MINNESOTA

Tiffany M. Schmidt

IN PARTIAL FULFILLMENT OF THE REQUIREMENTS
FOR THE DEGREE OF
DOCTOR OF PHILOSOPHY

Associate Professor Paulo Kofuji, Advisor

DECEMBER 2010

© TIFFANY M SCHMIDT 2010

Acknowledgements

-I would first and foremost like to thank my husband, Nate, for steadfast support of my chosen career path, for always providing a listening ear when needed, and for sticking with me on every step of this adventure.

-I thank my family, especially my mother, for being supportive of me, and always being proud of me.

-I would like to thank my fellow graduate students (especially Rachel Penrod and Stephanie Fretham) for providing an outlet for problem solving, troubleshooting, and escapism when necessary.

-I would lastly, but certainly not least, like to thank my advisor, Paulo, for hours of scientific discussion, for the unfailing support and encouragement in my career path, for teaching me to be a scientist, and for his friendship.

Abstract of Dissertation

A subpopulation of retinal ganglion cells (RGCs) express the photopigment melanopsin, rendering them intrinsically photosensitive (ipRGCs). These ganglion cell photoreceptors are critical for several non-image forming behaviors including circadian entrainment and the pupillary light reflex. Initially thought to be a uniform population, later studies demonstrated that there was at least some degree of morphological and physiological diversity in the ipRGC population. Technical limitations, however, had prevented the comprehensive study of ipRGCs at the single cell level. The purpose of this project was to utilize a mouse model in which ipRGCs are labeled *in vivo* with enhanced green fluorescent protein to identify and target single ipRGCs for morphological and physiological analyses. The central hypothesis of the research presented herein is that distinct morphological ipRGC subtypes have distinct physiological properties and synaptic inputs, resulting in unique light information sent to target nuclei in the brain by the various ipRGC subpopulations. This work has confirmed the existence and further analyzed the morphological and physiological properties of at least three ipRGC subtypes: M1 cells with dendrites stratifying in the OFF sublamina of the inner plexiform layer (IPL), M2 cells with dendrites stratifying in the ON sublamina of the IPL, and M3 cells with dendrites bistratifying in both the ON and OFF sublaminas of the IPL. We find that these cell types do indeed possess distinct intrinsic light responses and intrinsic membrane properties. Furthermore, we find that these subpopulations are differentially influenced by cone-mediated signals. Finally, we find that the cation channel involved in ipRGC signal transduction is not composed solely of the canonical transient receptor

potential channel (TRPC) subunit 3, 6, or 7. However, we do find that TRPC6 is involved in mediating the melanopsin-evoked light response in both M1 and M2 cells, with both subtypes showing a reduction in the magnitude of the intrinsic light response in *TRPC6*$^{-/-}$ animals. Collectively, the differential influence of intrinsic, melanopsin-mediated phototransduction and synaptically-evoked extrinsic inputs on the integrated light-evoked response of ipRGC subtypes indicates that these subtypes may serve as conduits for distinct light information sent to the brain. We discuss the implications of these findings and propose a model for the differential influence of distinct ipRGC subtypes on various non-image forming behaviors.

Table of Contents

List of Tables

List of Figures

Chapter 1

Chapter 2

Chapter 3

Chapter 4

List of Abbreviations

RGC	Retinal Ganglion Cell
ipRGC	Intrinsically Photosensitive Retinal Ganglion Cell
BC	Bipolar Cell
AC	Amacrine Cell
IPL	Inner Plexiform Layer
INL	Inner Nuclear Layer
GCL	Ganglion Cell Layer
RPE	Retinal Pigmented Epithelium
TRPC	Canonical Transient Receptor Potential Channel
Opn4	Melanopsin Gene
WT	Wild-Type
EGFP	Enhanced Green Fluorescent Protein
NIF	Non-Image Forming
SCN	Suprachiasmatic Nucleus
OPN	Olivary Pretectal Nucleus
PLR	Pupillary Light Reflex
(v or d)LGN	(Ventral or Dorsal) Lateral Geniculate Nucleus
SC	Superior Colliculus

Contributions

The following contributions were made by individuals other than Tiffany M. Schmidt and Paulo Kofuji:

Chapter 2: *Kenichiro Taniguchi* performed immunohistochemical and PCR procedures.

Chapter 6: *Claudio E. Perez-Leighton* performed immunohistochemical experiments, PCR experiments, and multi-electrode array recordings.

Joel Abromovitz and Lutz Birnbaumer generated and characterized TRPC7$^{-/-}$ mouse line.

CHAPTER 1

Introduction and Overview

Light is a profoundly important regulator of biology and behavior in living things. In mammals, in addition to its role in image-forming vision, light influences a variety of non-image forming (NIF) functions including pineal melatonin synthesis, daily activity rhythms, and sleep, all of which must be synchronized to the environmental light dark cycle (Herzog, 2007). Additionally, in humans, light exposure influences mood, arousal, concentration, and mental health (Hanifin and Brainard, 2007). In mammals including humans, the eyes are absolutely required for light information to influence these various NIF functions (Foster et al., 1991; Czeisler et al., 1995; Bellingham and Foster, 2002). Within the eye of mammals, there exists a specialized retinal ganglion cell (RGC) photoreceptor. Discovered only recently, these specialized RGCs have now been demonstrated to be highly influential in mediating, if not absolutely critical for, a variety of NIF functions. This makes investigation of RGC photoreceptors critical for a deeper understanding not only of NIF behaviors, but of diseases and disorders associated with behavioral dysfunction of the circadian timing system.

Retinal organization and image forming vision

The retina is the neural tissue responsible for signaling light information to target brain nuclei. It is a highly organized structure, consisting of six different types of neurons (Dowling and Werblin, 1969; Werblin and Dowling, 1969; Dowling, 1970). The outermost retina consists of the rod and cone photoreceptors which express opsin photopigments allowing them to respond directly to changes in light. The rods and cones then transduce and signal light information from the environment via synapses in the outer plexiform layer to the bipolar cells (BCs), the cell bodies of which lie in the

inner nuclear layer. This signal is then relayed to the retinal ganglion cells (RGCs), the cell bodies of which lie in the ganglion cell layer (GCL). Along the way the signal is modulated by the horizontal and amacrine cells, which act as inhibitory interneurons. The RGCs are the projection neurons of the retina, and project axons to various visual nuclei in the brain (Wassle, 2004).

Retinal signaling can be divided anatomically and physiologically into two streams, the ON and OFF pathways. In the dark, the photoreceptors are depolarized and constantly releasing glutamate. Upon an increase in environmental illumination, the rod and cone photoreceptors hyperpolarize and subsequently decrease glutamate release in a graded manner which causes a depolarization of ON BCs and consequent increase in glutamate release from ON BCs onto the ON RGCs, the dendrites of which are located in the inner half of the IPL in the ON sublamina. In parallel, the decrease in glutamate release from photoreceptors causes a hyperpolarization of OFF BCs and consequent decrease in glutamate release from OFF BCs onto OFF RGCs, the dendrites of which are located in the outer half of the IPL in the OFF sublamina (Dowling and Werblin, 1969; Werblin and Dowling, 1969; Famiglietti and Kolb, 1976; Wassle, 2004). These parallel pathways are illustrated for the cone system in Figure 1. These two streams of information are conveyed to the lateral geniculate nucleus of the thalamus and on to the primary visual cortex where they mediate image forming vision, or conscious visual perception of images.

The non-image forming visual system

Virtually all living organisms exhibit daily oscillations in physiology and/or behavior known as circadian rhythms. In mammals these oscillations include daily

changes in pineal melatonin synthesis, daily activity rhythms, and sleep (Herzog, 2007). It is critical that these rhythms be aligned with the solar day in order to correlate behavior and physiology with the environmental cycle of light and dark. To accomplish this feat, the circadian rhythm is entrained to the environmental light dark cycle via light information from the eyes through a process known as circadian photoentrainment.

In mammals, the master pacemaker in the brain is comprised of two small nuclei situated on either side of the third ventricle just above the optic nerve called the suprachiasmatic nuclei of the hypothalamus (SCN). The cells in the SCN form an oscillating network of cells that synchronize the endogenous clocks of a variety of other structures (Yoo et al., 2004). If the SCN is lesioned, the various body clocks will desynchronize and disrupt normal physiological function (Yoo et al., 2004). In the absence of light input, the SCN continues to synchronize body rhythms with an endogenous period slightly different (shorter in the case of the mouse) from that of the solar day. However, light information conveyed from the retina via the retinohypothalamic tract, entrains the circadian rhythm to the environmental cycle of light and dark and the 24 hour day (Moore and Lenn, 1972; Johnson et al., 1988; Rea, 1998). This entrainment can be altered or shifted, via presentation of a light pulse during the dark period, a process called phase-shifting. Depending on the circadian time at which the light stimulus is presented, this can cause an advance, or a delay in activity rhythms (Altimus et al., 2009).

Perhaps the other most commonly studied NIF function is the pupillary light reflex (PLR). Light input from the eye travels to the olivary pretectal nucleus (OPN), the nucleus involved in driving this behavior (Trejo and Cicerone, 1984; Clarke and

Ikeda, 1985). This information is then sent on to the Edinger Westphal nuclei and on to the ciliary ganglion to cause constriction or dilation of the pupil in response to changes in environmental illumination.

A novel inner retinal photoreceptor mediates non-image forming vision

The rods and cones were historically thought to be the only photosensitive cells in the retina. However, the presence of a third retinal photoreceptor began to be suspected as it became clear that some blind individuals with outer retinal degeneration still retained certain non-image forming (NIF) visual functions such as photoentrainment of the circadian rhythm and pineal melatonin synthesis to the daily cycle of light and dark, despite loss of all conscious visual perception (Czeisler et al., 1995; Lockley et al., 1997). In support of these observations, mice without functional rods or cones were found to be capable of circadian photoentrainment and had a functional PLR (Freedman et al., 1999; Lucas et al., 2001). Furthermore, these behaviors showed a unique spectral tuning with a λ_{max} ~ 480 nm, shifted toward the blue end of the spectrum from the λ_{max} of rods which is ~ 500 nm and M cones of ~ 511 nm (Jacobs et al., 1991; Yoshimura and Ebihara, 1996; Freedman et al., 1999; Lucas et al., 2001; Nikonov et al., 2006).

During this same period, the melanopsin gene was cloned from the dermal melanophores of *Xenopus laevis* (Provencio et al., 1998). Soon after that, researchers identified melanopsin-positive RGCs in the GCL of mouse and human retinas using *in situ* hybridization (Provencio et al., 2000). These findings were confirmed soon after with antibody staining in the mouse retina (Provencio et al., 2002). Together with behavioral and spectral data from mice with outer photoreceptor degeneration, these

findings suggested the existence of a third, novel class of photoreceptor in the mammalian retina (Provencio et al., 2000; Provencio et al., 2002).

The suprachiasmatic nucleus (SCN) of the hypothalamus is the central circadian pacemaker in mammals, and is responsible for synchronizing the endogenous clocks throughout the body to the master clock (Hastings et al., 2003; Hastings, 2004; Yoo et al., 2004). Light information from the retina entrains the master circadian clock to the environmental cycle of light and dark, a process required to keep physiological timing in line with the solar day (Foster et al., 1991). Light information reaches the SCN via a direct RGC projection called the retinohypothalamic tract (RHT)(Moore and Lenn, 1972; Pickard, 1980; Rea, 1998). The fact that the 1) SCN is the central circadian pacemaker in mammals, 2) that the SCN receives an RGC projection, 3) that individuals or mice without functional rod/cone photoreceptors but retaining RGCs still showed circadian entrainment, and 4) that RGCs in mammals had been shown to express the photopigment melanopsin led investigators to examine SCN-projecting RGCs as the possible elusive circadian photoreceptor.

By introducing a retrograde tracer into the SCN and then targeting fluorescently-labeled SCN-projecting RGCs in the retina of the rat, David Berson and colleagues demonstrated that the RGCs that project to the SCN are indeed intrinsically photosensitive (ip) (Berson et al., 2002). In other words, SCN-projecting RGCs, unlike other RGCs are able to respond directly to light, even when all rod/cone signaling in the retina are blocked. Moreover, ipRGCs respond to light with a λ_{max} ~480 nm, identical to that seen in circadian or PLR behaviors of functionally blind mice with outer photoreceptor degeneration (Yoshimura and Ebihara, 1996; Freedman et al., 1999;

Lucas et al., 2001; Berson et al., 2002). These cells have properties distinct from the rod/cone photoreceptors, including sluggish onset and offset kinetics, light-evoked depolarization as opposed to hyperpolarization, and a very sustained depolarization and calcium elevation during light stimulation (Berson et al., 2002; Sekaran et al., 2003; Tu et al., 2005; Wong et al., 2005; Hartwick et al., 2007). These cells serve as environmental irradiance detectors (Berson et al., 2002; Dacey et al., 2005) and were likely first discovered by Barlow and Levick, who termed a small proportion of cat retinal ganglion cells (<1%) "luminance units," which they hypothesized played a role in the PLR (Barlow and Levick, 1969).

A concurrent study to that of Berson et al. (2002) by Hattar et al. utilizing a melanopsin null mouse model where tau lacZ is knocked in to the melanopsin locus (*Opn4*$^{taulacZ/taulacZ}$ referred to subsequently as *Opn4*$^{-/-}$), demonstrated that these ipRGCs express the photopigment melanopsin, which is responsible for rendering them intrinsically photosensitive (Hattar et al., 2002). Later studies demonstrated the sufficiency of melanopsin to act as a photopigment capable of rendering other cell types photosensitive through the use of heterologous expression of melanopsin in human embryonic kidney cells, neurons, or oocytes (Melyan et al., 2005; Panda et al., 2005; Qiu et al., 2005). There are ~800 tau-lacZ positive cells in the retinas of *Opn4*$^{-/-}$ mice, meaning that these cells form 1-2% of the total rodent RGC population (Hattar et al., 2002).

When the central projections of ipRGCs were examined using tau-lacZ labeling in the brains of *Opn4*$^{+/-}$ or *Opn4*$^{-/-}$ mice, these cells were found to project to a variety of structures involved in NIF vision. ipRGCs were found to substantially innervate the

core of the SCN, consistent with a role for ipRGCs in circadian photoentrainment as well as the shell of the OPN, which is the nucleus responsible for driving the PLR (Hattar et al., 2002; Hattar et al., 2006)(Figure 2). Additionally, ipRGCs were found to innervate the intergeniculate leaflet (IGL) and the ventral lateral geniculate nucleus (vLGN), both structures thought to be involved in circadian behaviors (Hattar et al., 2002; Hattar et al., 2006). Other structures found to receive projections of ipRGCs included: the lateral habenula, the peri-supraoptic nucleus, the superior colliculus, and the subparaventricular zone (Hattar et al., 2006)(Figure 2).

ipRGC phototransduction

Phototransduction of ipRGCs differs substantially from that of rods and cones in many ways. Firstly, rod and cone photoreceptors hyperpolarize in response to light. When light is captured by rhodopsin or cone opsin in mammals, this activates the G-protein transducin, resulting in a decrease in cGMP and subsequent closure of a cyclic-nucleotide-gated (CNG) channel, hyperpolarization of the photoreceptor, and decrease in glutamate release. ipRGCs, however, depolarize in response to light stimulation of the melanopsin photopigment (Hankins et al., 2008). Melanopsin itself is evolutionarily more closely related to invertebrate rhodopsin than vertebrate rhodopsin (Nickle and Robinson, 2007) which, similar to ipRGCs, depolarize in response to light stimulation. Thus it is currently believed that the signal transduction cascade in ipRGCs is similar to that of invertebrate photoreceptors with melanopsin activation resulting in activation of Gq, PLC activation, and subsequent opening of a cation-permeable canonical transient receptor potential (TRPC) channel (Lamb et al., 2007; Nickle and Robinson, 2007; Hankins et al., 2008). Second, melanopsin, like invertebrate photoreceptors, is thought

to be bistable, meaning that intervening long-wavelength light exposure allows the chromophore to revert from all-*trans* to 11-*cis* retinal without relying on the retinoid cycle of either the retinal pigmented epithelium (RPE) or the Müller cells. Rods rely completely on the RPE retinoid cycle pathway for chromophore recycling while cones also make use of the endogenous retinoid capability of Müller cells (Wang et al., 2009; Wang and Kefalov, 2009). It is currently unknown whether ipRGCs are indeed bistable, utilize Müller cells for chromophore regeneration, or both. However, it has been demonstrated that the PLR of humans as well as the firing of SCN neurons can be potentiated by an intervening long wavelength light between stimulations at the preferred wavelength for melanopsin of 480 nm (Mure et al., 2007; Zhu et al., 2007; Mure et al., 2009; but see Mawad and Van Gelder, 2008). It has also been demonstrated in heterologous expression systems and using melanopsin from *Amphioxus* that melanopsin itself can act in a bistable manner (Melyan et al., 2005; Terakita et al., 2008). However, there is also evidence that ipRGCs interact closely with Müller cells (Viney et al., 2007), and thus ipRGCs could also make use of this pathway to regenerate chromophore. ipRGCs, though they show a reduced sensitivity in mice where the RPE is unable to regenerate chromophore due to lack of a key enzyme involved in the retinoid cycle, *rpe65*, melanopsin phototransduction remains intact (Doyle et al., 2006; Tu et al., 2006). The chromophore regeneration of melanopsin is currently an active area of research.

Both rods/cones and melanopsin mediate non-image forming behaviors

The finding that ipRGCs express the photopigment melanopsin raised the question, what role does the melanopsin photopigment vs. rod/cone signaling play in

NIF behaviors? Mice with nonfunctional/entirely lacking rods/cones or else lacking the photopigment melanopsin both retain functional circadian photoentrainment and PLR, but with slight detectable deficits. For example, mice lacking rod/cone function fully constrict their pupils in response to bright light stimulation, but have an increased threshold at which this behavior first occurs (Lucas et al., 2001; Semo et al., 2003; Barnard et al., 2004). Mice lacking melanopsin, in contrast, retain similar sensitivity of their PLR, but are only able to constrict their pupils to 80% of maximum and are unable to maintain constriction for long periods, highlighting a role for the melanopsin photopigment in driving the PLR at bright light intensities and over long durations (Lucas et al., 2003; Panda et al., 2003; Gamlin et al., 2007; Zhu et al., 2007).

Similar patterns to that of the PLR deficits are observed in circadian photoentrainment when mice lack either rod/cone function or melanopsin photopigment. Wild-type mice will generally show a phase-delay of increasing magnitude when successively brighter lights are presented early in the subjective night. In mice lacking rod/cone function, phase-shifting is observed (Takahashi et al., 1984; Freedman et al., 1999; Hattar et al., 2003; Barnard et al., 2004) but with an action spectrum matching that of the photopigment melanopsin (Yoshimura and Ebihara, 1996) . Furthermore, mice lacking the melanopsin photopigment show phase shifts in response to a light pulse, albeit of reduced magnitude even at the brightest light intensities (Panda et al., 2002; Ruby et al., 2002)

Collectively, these studies support the idea that rod/cone input as well as melanopsin signaling work in concert to mediate non-image forming vision. When known components of rod/cone phototransduction are disrupted in conjunction with the

knockout of the melanopsin protein, all major visual accessory functions in mice are lost (Hattar et al., 2003). Thus, it appears that with the discovery of ipRGCs, all of the major photoreceptive systems in the retina have been discovered.

ipRGCs in development

A unique feature of ipRGCs is their light sensitivity early in development. ipRGCs are present and expressing the photopigment melanopsin from birth in rat and mouse and are thus capable of responding to light from birth (Hannibal and Fahrenkrug, 2004a; Sekaran et al., 2005; Lupi et al., 2006) Furthermore, ipRGCs are forming functional connections with the SCN at that time as light can induce c-fos expression in the SCN of WT but not *Opn4*$^{-/-}$ mouse pups at postnatal day (P)0 (Weaver and Reppert, 1995; Hannibal and Fahrenkrug, 2004a; Lupi et al., 2006). Indeed, extracellular multielectrode array (MEA) recordings of retinas at P8 reveal robust light evoked RGC spiking that is absent in *Opn4*$^{-/-}$ mice (Tu et al., 2005). This is in contrast to other types of RGC, which do not begin to show light responses until around the time of eye opening when synaptic circuitry becomes functional (Sernagor, 2005). Thus, the NIF visual system could be receiving light-evoked signals at a much earlier time point than other RGC brain targets, leaving open the question of whether these cells play a role in patterning of brain projections, behavior, or retinal wiring early in development.

ipRGCs receive synaptic input

Not only are ipRGCs intrinsically photosensitive, but evidence also indicates that ipRGCs, like other types of RGCs, receive synaptic inputs from bipolar and amacrine cells relaying rod/cone signals. Electron microscopy studies have demonstrated ribbon synapses closely apposed to melanopsin immunoreactive dendrites

in the ON sublamina of the IPL. This same study also found inhibitory synapses to melanopsin dendrites in both ON and OFF stratifying melanopsin immunoreactive dendrites (Belenky et al., 2003). Corroborating these findings, a study using viral tracing techniques to label ipRGCs and their input neurons in the INL demonstrated the presence of ipRGCs having dendrites stratifying in the OFF (Type 1 or M1), ON (Type 2 or M2), or both the ON and OFF (Type 3 or M3) sublaminas of the IPL (Viney et al., 2007). All three types were found to receive synapses from ACs, with the Type 1 receiving inputs from the dopaminergic amacrine cells, corroborating findings that OFF-stratifying ipRGCs, which stratify in the outermost sublamina of the IPL, form a discrete plexus with the dopaminergic amacrine cells (Viney et al., 2007; Vugler et al., 2007). Type 2 cells were found to receive input from a different type of as-yet-unidentified AC (Viney et al., 2007). The BCs presynaptic to these subtypes were nearly impossible to determine as the pseudorabies virus used in that study did not cross the ribbon synapses with high efficiency. However, Viney et al. did propose input to Type 2 ipRGCs from Type 8 BCs (Viney et al., 2007) based on a few GFP-labeled BCs.

Physiological studies have also identified functional synaptic inputs to ipRGCs. In the primate, ipRGCs stratifying in either the ON or OFF sublaminas were found to have L/M-ON/S-OFF receptive field organization (Dacey et al., 2005). In the rat, MEA recordings demonstrated that likely all ipRGCs receive synaptic input (Wong et al., 2007). Thus, ipRGCs must integrate their intrinsic, melanopsin-mediated phototransduction with synaptic signals relayed from the rods/cones of the outer retina.

ipRGCs are the sole conduits for mediation of NIF behaviors

Previous research had suggested that perhaps RGCs other than ipRGCs also innervate NIF nuclei (Gooley et al., 2001; Gooley et al., 2003; Morin et al., 2003; Sollars et al., 2003). Thus, though it was clear that ipRGCs relay melanopsin-mediated signals to NIF nuclei and that ipRGCs receive synaptic signals from the rods/cones, it was unclear whether the outer retinal signaling of rods/cones was primarily being relayed to NIF nuclei via the ipRGCs themselves, via "regular" RGCs, or both. Several laboratories addressed this question simultaneously using various techniques to selectively ablate ipRGCs. When near complete ablation of the ipRGC population was achieved, severe impairment to abolishment of NIF behaviors such as the PLR, circadian entrainment, and sleep induction by light were observed (Altimus et al., 2008; Goz et al., 2008; Guler et al., 2008; Hatori et al., 2008b). Collectively these studies demonstrated that ipRGCs are the primary conduits for rod/cone and melanopsin-mediated light input to NIF nuclei to mediate NIF behaviors, highlighting the critical role of ipRGCs in a variety of light-influenced physiological functions.

The current project

Despite an understanding of the importance of ipRGCs in mediating NIF behaviors, an understanding of how ipRGCs signal light information to the brain was lacking. Until the present studies were performed, identification and single-cell analysis of ipRGCs necessitated retrograde labeling of ipRGCs from the SCN of primarily rats. This technique precludes the use of younger mice and also only allows sampling from the SCN-projecting ipRGCs. Additionally, early studies hinted that ipRGC population might be more morphologically and physiologically diverse than initially thought, indicating that further analysis of the properties of ipRGCs at the single-cell level was

necessary to understand how these RGC photoreceptors signal light information to the brain.

Knowing that ipRGCs are the conduits for both rod/cone and melanopsin-mediated influence on NIF behaviors, the overall goal of the studies presented herein is to understand how ipRGCs integrate intrinsic and synaptic signals to relay light information to the brain. The central hypothesis of this study is that distinct morphological subpopulations of ipRGC differentially relay light information to the brain and play distinct roles in influencing NIF behaviors. More specifically, the goals of this project are to understand: 1) the diversity that exists within the ipRGC population 2) the intrinsic properties of ipRGCs and 3) the synaptic influences on ipRGCs and how these signals are integrated with the intrinsic light response.

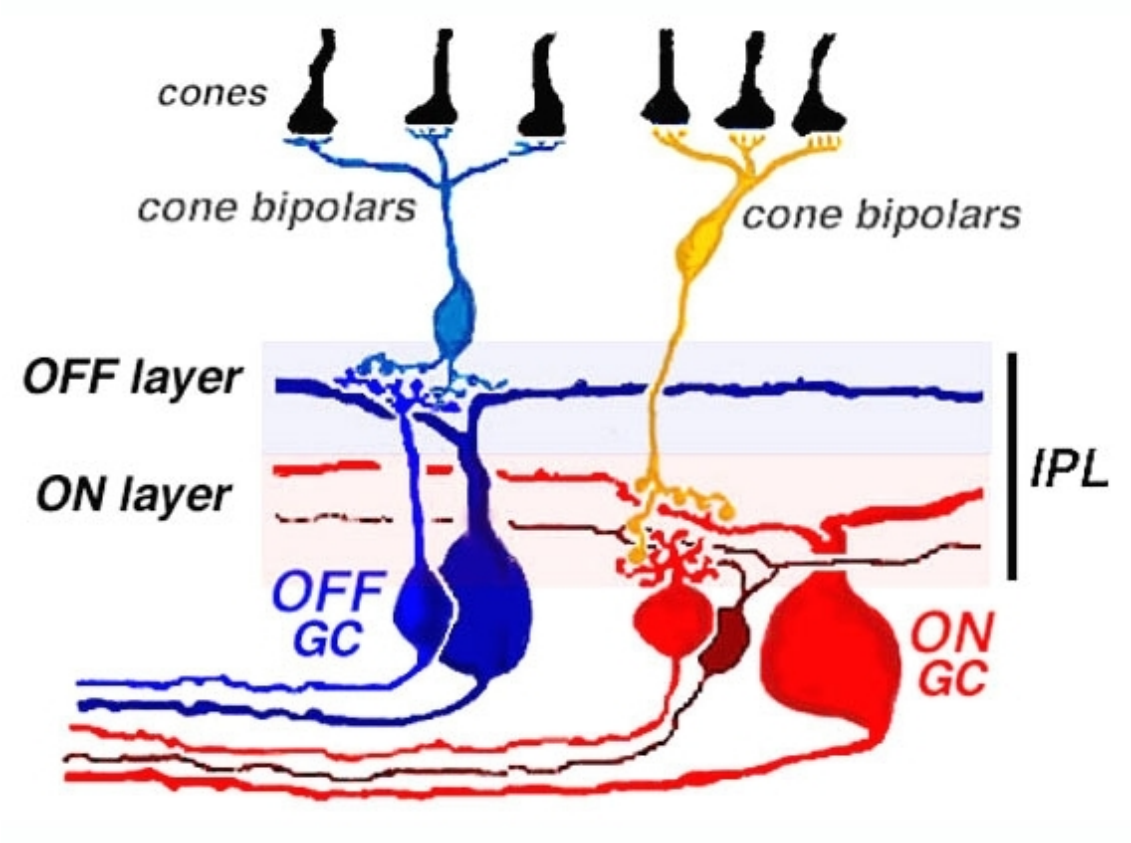

Figure 1. ON and OFF cone pathways in the mammalian retina (Nelson et al., 1978).
RGCs stratifying in the OFF sublamina (blue GCs) of the IPL receive excitatory inputs from OFF bipolar cells (blue cone bipolar cells in diagram) and signal light decrements. RGCs stratifying in the ON sublamina (red ganglion cells) of the IPL receive excitatory inputs from ON bipolar cells (yellow cone bipolar cells in diagram) and signal light increments.

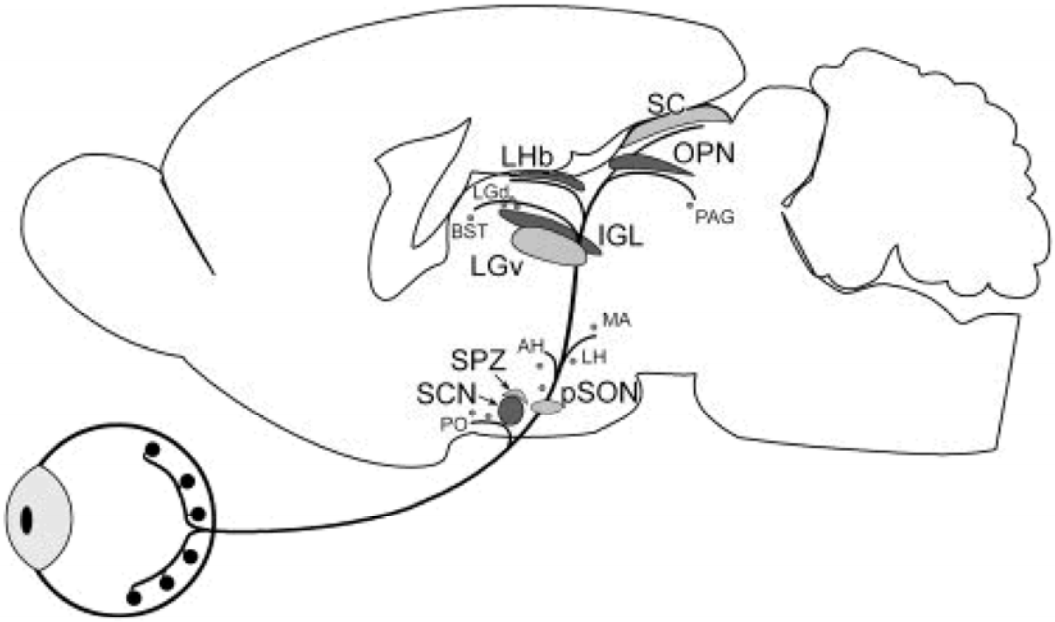

Figure 2. Brain targets of ipRGCs (Hattar et al., 2006).
Major targets of ipRGCs are shown in dark gray. Secondary targets are shown in light gray. Minor targets indicated by smaller lettering and dots.

CHAPTER 2

Intrinsic and extrinsic light responses in melanopsin-expressing ganglion cells during mouse development.

Schmidt TM, Taniguchi K, and Kofuji P (2008) *J Neurophysiol* 100:371-384

ABSTRACT

Melanopsin (Opn4) is a photopigment found in a subset of retinal ganglion cells that project to various brain areas. These neurons are "intrinsically" photosensitive (ipRGCs) and are implicated in non-image forming responses to environmental light such as the pupillary light reflex and circadian entrainment. Recent evidence indicates that ipRGCs respond to light at birth, but questions remain as to whether and when they undergo significant functional changes. We employed BAC transgenesis to engineer a mouse line in which Enhanced Green Fluorescent Protein (EGFP) is expressed under the control of the melanopsin promoter. Double immunolabeling for EGFP and melanopsin demonstrates their co-localization in ganglion cells of mutant mouse retinas. Electrophysiological recordings of ipRGCs in neonatal mice (postnatal days (P) 0-7) demonstrated that these cells responded to light with small and sluggish depolarization. However, starting at P11we observed ipRGCs that responded to light with a larger and faster onset (<1 s) and offset (<1 s) depolarization. These faster, larger depolarizations were observed in most ipRGCs by early adult ages. However, upon application of a cocktail of synaptic blockers, we found that all cells responded to light with slow onset (>2.5 s) and offset (>10 s) depolarization, revealing the "intrinsic", melanopsin-mediated light responses. The "extrinsic," cone/rod influence on ipRGCs correlates with their extensive dendritic stratification in the inner plexiform layer. Collectively, these results demonstrate that ipRGCs make use of melanopsin for phototransduction before eye opening and that these cells further integrate signals derived from the outer retina as the retina matures.

INTRODUCTION

Many aspects of behavior and physiology exhibit daily oscillations known as circadian rhythms (Hastings et al., 2003; Herzog, 2007). In mammals, circadian rhythms are driven by a biological clock found in the suprachiasmatic nuclei (SCN) (Hastings, 2004; Maywood et al., 2006). These intrinsic circadian rhythms are synchronized to the environmental cycle of day and night by the process of photoentrainment, which uses environmental light information to entrain the biological clock. In mammals, the signal for photoentrainment arises from a subset of retinal ganglion cells (RGCs) that send projections to the SCN. These ganglion cells that project to the SCN express melanopsin and are intrinsically photosensitive (ipRGCs) (Berson et al., 2002; Hattar et al., 2002). The sensitivity, spectral tuning, and slow kinetics of these ipRGCs closely match those of the photic entrainment mechanism, suggesting that these ganglion cells form the primary pathway for circadian entrainment (Fu et al., 2005a; Fu et al., 2005b; Kumbalasiri and Provencio, 2005; Peirson and Foster, 2006; Berson, 2007).

Furthermore, there is evidence that ipRGCs are capable of phototransduction in newborn mice when rods and cones are not yet formed (Hannibal and Fahrenkrug, 2004a; Sekaran et al., 2005). Calcium imaging and multi-electrode array recordings from wild type and melanopsin null mouse retinas suggest that ipRGCs are photosensitive at early postnatal stages (P0-5) (Sekaran et al., 2005; Tu et al., 2005). Light-evoked Fos induction in the SCN of mice can be detected as early as P0 (Hannibal and Fahrenkrug, 2004a; Lupi et al., 2006), indicating that ipRGCs are the first functional photosensitive cells in the retina.

While ipRGCs respond to light via melanopsin-mediated phototransduction, there are a number of reports that indicate that these cells also receive signals from cone/rod pathways (Belenky et al., 2003; Dacey et al., 2005; Perez-Leon et al., 2006; Wong et al., 2007). Perez-Leon et al. (2006), using retrograde labeling from the SCN of rats and whole-cell recordings, reported that ~5% of ipRGCs demonstrate light-evoked synaptic inputs, while (Wong et al., 2007) reported, using multi-electrode array recordings in rat retina, that all ipRGCs receive synaptic input from the outer retina. Furthermore, Lupi et al., 2006 demonstrated light-evoked c-Fos induction in the SCN of melanopsin knockout mice as early as P14, indicating rod/cone signaling to the SCN. However, it is unclear whether the rod/cone mediated signals reaching the SCN at P14 are a result of the formation synaptic inputs onto ipRGCs or the result of inputs from other types of ganglion cells to the SCN. Additionally, because previous assessments of early postnatal ipRGC light responses have been performed in the presence of synaptic blockers (Sekaran et al., 2005; Tu et al., 2005), it is still unclear at what point in development ipRGCs begin to show synaptically driven light responses and what the functional impact of those synaptic connections might be. Because of the differences between the image-forming and non-image forming streams in the visual system, it is possible that these two visual systems do not develop coincidentally (Sernagor, 2005).

The goal of this study was to record light responses of ipRGCs throughout development and to determine the timing and functional impact of the formation of extrinsic inputs onto these cells. We investigated the properties of developing ipRGCs during the first postnatal weeks using a novel transgenic mouse model in which ipRGCs are labeled *in vivo* with EGFP. We found that ipRGC light responses during this period

transition from being driven solely by “intrinsic” phototransduction, to being driven by both “intrinsic” and “extrinsic” phototransduction right around the time of eye opening. Emergence of cone/rod modulation of ipRGCs is coincident with the stratification of their dendrites in the inner plexiform layer (IPL), mainly in the ON sublamina. Overall, these results indicate that ipRGCs undergo major changes in their light sensitivity and synaptic connectivity during a crucial period in visual development.

MATERIALS AND METHODS

Generation of *Opn4-EGFP* Bacterial Artificial Chromosome (BAC) transgenic mouse line

BAC recombination was performed by using protocols and reagents from a BAC Modification Kit (Gene Bridges, Heidelberg, Germany) which relies on ET-recombination method (Muyrers et al., 1999). The BAC clone RP24-107C11, containing ~29 Kb and ~155 Kb of DNA flanking the 5' and 3' ends of the *Opn4* gene locus respectively, was obtained from the BAC resource at Children's Hospital Oakland Research Institute, and a cassette containing an EGFP-PolyA (Clontech, Mountain View, CA) and a Kanamycin/Neomycin resistance gene flanked by two FRT sites was inserted. Briefly, we used Polymerase Chain Reaction (PCR) to amplify the *Opn4* gene homology arms and the EGFP-FRT- Kanamycin/Neomycin -FRT cassette. *Opn4* arm 1 consisted of a 50-bp fragment upstream of the ATG in exon 1 (5'-GGACCGATCCCTGATCTTTCCATGGCCTTAGCTCCTCTGAGAGCCTGAGC-3'). *Opn4* gene arm 2 was a 50-bp product downstream of the stop codon of exon 9 (5'-CACAGTCACATGCAGATATTCCCCTAGATACAGATCATACTTAGACCCTG-3'). The EGFP-FRT- Kanamycin/Neomycin -FRT cassette was derived from the pIGCN21 plasmid (kindly provided by Neal Copeland and Nancy Jenkins, NCI) in which we replaced the EGFP-cre gene with EGFP-polyA. *E. coli* cells carrying RP24-107C11 BAC and the plasmid pRedET were electroporated with *Opn4* (arm 1)-EGFP-FRT-Neo/Kan-FRT-*Opn4* (arm 2) PCR product, and homologously recombined positive clones were selected with kanamycin and chloramphenicol. The Kanamycin/Neomycin cassette was then removed by electroporating the plasmid

containing flp recombinase (plasmid 706-FLP, GeneBridges, Heidelberg, Germany), resulting in an *Opn4-EGFP* BAC. Homologous recombination was confirmed by PCR and by sequencing the BAC using primers that flanked the upstream of *Opn4* arm1 to *EGFP* cassette and downstream of *Opn4* arm2 to *EGFP* cassette. The *Opn4-EGFP* BAC DNA was prepared using a modified alkaline lysis protocol (Nucleobond kit, Clontech, Mountain View, CA), and circular intact DNA was microinjected into fertilized embryos (FVB/NCR strain) by standard pronuclear injection techniques at the McLaughlin Research Institute (Great Falls, MT). Genomic DNA isolated from tissue was purified using Puragene kit (Gentra Systems, Minneapolis, MN), and founder mice carrying the BAC transgene were identified by PCR with primer sets 5'-GACATTAAGCAGTCAGCAGC -3' (in *Opn4* gene) and 5'-GTGGTGCAGATGAACTTCAG -3' (in EGFP), yielding a ~380-bp product. One founder line was produced that transmitted the transgene in a normal Mendelian inheritance pattern with all offspring appearing grossly normal. Animals were cared for in accordance with guidelines described in the Guide for the Care and Use of Laboratory Animals, using protocols approved by the University of Minnesota Institutional Animal Care and Use Committee.

RT-PCR Analyses

First strand cDNA was synthesized from total RNA templates using random primers and the superscript II reverse transcriptase (Invitrogen, Carlsbad, CA). One to two micrograms of total RNA was brought to 11 µl in diethyl pyrocarbonate (DEPC)-treated water and combined with 1 µl random hexamers (50 ng/µl). The mixture was heated at 65^{o}C for 5 min and then incubated on ice. The remaining components for

reverse transcription were then added and incubated for 10 min as follows: 4 µl of 5x synthesis buffer, 2 µl 0.1 M DTT, 1 µl 10 mM dNTP mix and 1 µl (200 units) superscript reverse transcriptase. The reaction mix was left at room temperature (RT) for 10 min, incubated at 42^{o}C for 50 min and the reaction terminated by incubating at 70^{o}C for 15 min. Oligonucleotides corresponding to EGFP sequences were: 1) sense 5'-CCGACCACATGAAGCAGCACGA -3'; 2) antisense 5'-CGTTCTTCTGCTTGTCGGCCATG-3'. Oligonucleotides corresponding to b-actin sequences were: 1)sense 5'-ATGGATGACGATATCGCTGCGC-3'; 2)antisense 5'-TTCACGGTTGGCCTTAGGGTTCAG-3'.

PCR reactions contained (in a final volume of 50 µl): 5 µl of RT reaction (0.5-1 µg of first strand cDNA), 1 µM of sense and antisense primers, 25 µl of 2x PCR buffer HotStar Taq(Qiagen, Valencia, CA). Thirty cycles were performed on the samples using a MJ Mini Thermocycler (Biorad, Hercules, CA) as follows: 1) denaturation at 94^{o}C for 30 s; 2) annealing at 57^{o}C for 30 s; 3) extension at 72^{o}C for 30 s. This was followed by a final extension cycle at 72^{o}C for 10 min and a soak cycle at 4^{o}C. Reaction products were analyzed by electrophoresis on 2% agarose gels. Amplicon sizes were determined in agarose DNA gels following electrophoresis with 1Kb DNA ladder markers (Invitrogen, Carlsbad, CA).

Antibodies

The following primary antibodies were used: rabbit anti-melanopsin (obtained from I. Provencio, UF006, University of Virginia), rabbit anti-EGFP (Invitrogen, Carlsbad, CA), mouse anti-EGFP (Invitrogen, Carlsbad, CA) goat anti-choline acetyl transferase (ChAT) (Millipore, Bedford, MA). For secondary antibodies, we used

AlexaFluor antibodies (Invitrogen, Carlsbad, CA) produced in goat or donkey, including anti-rabbit 488 and 594; anti-mouse 488 and 594; anti-goat 488 and 594.

Immunocytochemistry

Mice were sacrificed with CO_2 asphyxiation, and were intracardially perfused with 4 % paraformaldehyde-0.1 M phosphate buffer (PFA). Retinas were dissected in phosphate-buffered saline, pH 7.4 (PBS) and were fixed overnight in PFA at 4 °C. The next day, retinas were washed extensively in PBS, and then blocked overnight in PBS containing 10 % goat or donkey serum, and 0.5 % Triton X-100 at room temperature. Primary antibody incubation was carried out for three days at 4°C in PBS containing 1% goat or donkey serum, 0.5% Triton X-100. Samples were washed 3x15 min each in PBS, then were incubated in secondary antibodies for two days at 4 °C. Retinas were washed 3x15 min in PBS, then were mounted in Vectashield (Vector Laboratories, Burlingame, CA). When the experiment was carried out using a pipette solution containing 0.5% biocytin (Sigma, Saint Louis, MO) or neurobiotin (Vector Laboratories, Burlingame, CA), patch pipettes were carefully detached from the recorded cells, and the retinas were then fixed with PFA overnight at 4°C. Neurobiotin or biocytin was visualized with rhodamine−conjugated streptavidin (Jackson Immunoresearch Laboratories, West Grove, PA).

Image analysis

The fluorescent specimens were imaged with Olympus Fluoview 1000 confocal microscope, using a 40X or 60X oil immersion lens. Excitation at different wavelengths was performed sequentially to prevent bleed-through of images. Optical sections were collected at 0.2- 1.0 μm intervals, and reconstructions of several optical

images onto a single plane were performed using ImageJ software (http://rsb.info.nih.gov/ij/). The brightness and contrast of the images were adjusted using ImageJ software. For analysis of dendritic stratification in the IPL, we used ChAT immunostaining to reveal bands corresponding to the projections of cholinergic amacrine cells. These bands were used as reference landmarks for sublamina a (OFF sublamina) and b (ON sublamina) and were used to categorize ipRGC dendritic arborization. For dendritic analysis, three-dimensional reconstructions of the dendritic processes of each biocytin/neurobiotin-filled neuron were made from Z-series stacks of confocal images. The projection images were semi-automatically traced with NIH ImageJ using the NeuronJ plugin (http://www.imagescience.org/meijering/software/neuronj/). Total dendritic length and dendritic field size of each filled cell were analyzed. Dendritic field area was calculated by drawing a convex polygon linking the dendritic terminals. The dendritic field area was then calculated and the diameter expressed as that of a circle having an equal area.

Electrophysiology

Whole cell recordings were performed on acutely isolated whole-mount retinas of *Opn4-EGFP* mice. Animals were anesthetized with isoflurane and then euthanized by pneumothorax and the eyes were enucleated. Retinas were removed from eyecups and placed in Ames' solution containing 23 mM sodium bicarbonate bubbled in 95% oxygen/5% carbon dioxide at room temperature. Prior to recording, the vitreous was removed and retinas were treated with Ames' solution (Sigma, Saint Louis, MO) containing collagenase/hyaluronidase (240 U/ml and 1000 U/ml, respectively) at room temperature for 20 minutes. For animals younger than P11 the

collagenase/hylaluronidase treatment was shortened to 5 minutes. Retinas were then mounted with the vitreal surface up in a custom made chamber (Newman and Bartosch, 1999) and perfused with Ames' solution bubbled with 95% oxygen/5% carbon dioxide at room temperature. Euthanasia and dissections were performed in ambient room light. Dissections were performed under a standard dissection microscope which was also used to mount retinas in the recording chamber. At all other times following dissection, retinas were kept in a dark room with only minimal ambient light. The recording chamber was mounted on the stage of an upright microscope (E600 FN, Nikon, Tokyo, Japan) equipped with differential interference contrast optics and epifluorescence. Recordings were performed at room temperature (21-23 ^{o}C) using a Axopatch 200B amplifier (Axon Instruments, Molecular Devices, Sunnyvale, CA) with fire-polished borosilicate pipettes (3-7 mΩ) (Sutter Instruments, Novato, CA) filled with (in mM) 125 KGluconate, 2 $CaCl_2$, 2 $MgCl_2$, 10 EGTA, 10 HEPES, 0.5 NaGTP, and 2 Na_2ATP, pH with KOH (pH 7.2). All traces were sampled at 5-10 KHz and low-pass filtered at 2-5 KHz. Current and voltage acquisitions were performed with a Digidata 1320 D/A and A/D converter connected to PC computer running pCLAMP 10 software (Axon Instruments). Liquid junction potentials (6.1 mV) were corrected for all recordings. In full-field white light experiments, cells were given 3-5 minutes following visualization of GFP under fluorescence prior to stimulation with white light. In these experiments, each cell was stimulated only once after patching. In irradiance-response experiments, retinas were allowed to dark adapt for 5 minutes before first stimulus, and light stimuli following the first were spaced three minutes apart to allow the cell to return to baseline.

Whole-cell currents were analyzed off-line with Clampfit (Axon Instruments) and membrane potential values were averaged over 1 s sliding time windows with IgorPro 6.0 (Portland, OR). Baseline Vm was measured by taking the average membrane voltage over ten seconds of baseline prior to light stimulation. Measurements of cell capacitance and resistance were derived from those currents evoked by stepping the cell potential to a 10 mV hyperpolarized value for 20 ms from a holding potential of -60 mV. Only cells with an access resistance of less than 20 MΩ were used for these calculations. Charge Q was estimated by time integration of evoked current during the step voltage. Membrane resistance was estimated from the steady state evoked current during the step voltage. Light responses were defined as the maximum depolarization of the averaged trace during or following light stimulation within a 50s time window. On latency was defined as the time to reach 50% of the maximum response after light on (latency to half-maximum). Off latency was defined as the time of decay to 50% of the maximum light response at or following light off. Because of extensive averaging of traces prior to analysis, time of light on and off were defined based on the beginning of the on and off components of an averaged response from a reference trace and then extrapolated to other traces. Curve fits for normalized, averaged irradiance response data were determined by nonlinear regression using Origin 7.5 (MicroCal Inc., Northampton, MA) according to the logistic dose-response function $y = A_2 + [A_1 - A_2/(1 + (IR/IR_{50})^{nH})]$, where A_1 is the maximum response plateau, A_2 is the minimum response plateau, IR is irradiance, IR_{50} is the irradiance values that generate half-maximal response, and n_H is the Hill slope . Light stimuli for some experiments were full-field, broadband white light (7.6×10^{14} photons/cm^2.s at 480 nm) delivered

from below the retina using the microscope's 100 W halogen lamp and transillumination optics. An electromechanical shutter (Vincent Associates, Rochester, NY) was used to control the duration and timing of the light stimulus. In irradiance-response experiments, light stimulation was performed using a Xenon lamp feeding the camera port. A filter wheel fitted with various neutral density filters and narrow band pass filters (Chroma Technologies, Rockingham, VT) and shutter (Lambda-3, Sutter Instruments) was used to control the wavelength, intensity, and duration of light stimuli. Irradiance measurements were made with a calibrated radiometer model S370 (UDT instruments, San Diego, CA).

Pharmacology

To block transmission of signals from the outer retina to ipRGCs, we blocked bipolar cell light responses with a cocktail consisting of 250 μM DL-2-amino-4-phosphonobutyrate (DL-AP4, a group III metabotropic glutamate receptor agonist), 10 μM 6,7-dinitroquinoxaline-2,3-dione (DNQX) or 75 μM 6-cyano-7-nitroquinoxaline-2,3-dione (CNQX) (AMPA/kainate receptor antagonists). DL-AP4, CNQX, and DNQX were purchased from Tocris (Ellisville, MO, USA). To block gap junctions, we used the gap junction blocker meclofenamic acid (Sigma, St. Louis, MO) at a working concentration of 200 μM. The retinas were preincubated with meclofenamic acid for 20 minutes prior to recordings.

Statistics

Statistical analyses were performed using Origin 7.5 (MicroCal Inc., Northampton, MA). Statistical comparison of means was made using either a Student's *t*-test or one-way *Analysis of Variance* (*ANOVA*), and significance was concluded when

$P < 0.05$. Post-Hoc analyses were done using Tukey's Honestly Significant Difference. Data are presented as mean plus or minus standard error of the mean (SEM).

RESULTS

Generation and validation of *Opn4-EGFP* BAC transgenic mice

Visualization of ipRGCs in newborn and early postnatal mouse retinas is difficult given the need for injection of retrograde tracers into SCN or other brain areas innervated by these cells (for example Berson et al., 2002; Lucas et al., 2003; Dacey et al., 2005). Therefore, to study the functional and morphological properties of ipRGCs during early postnatal development, we have taken a BAC transgenic approach to allow for the *in vivo* labeling of ipRGCs in the mouse retina with EGFP. For generation of this transgenic mouse line, we used a BAC containing the *Opn4* gene and 29 Kb of the 5' and 155 Kb of the 3' sequences (Figure 1A). In this BAC, the coding sequence for *Opn4*, which is contained in multiple exons, was replaced with EGFP and polyadenylation sequences by *in vitro* recombination (Yang et al., 1997). From this recombinant BAC, a single founder mouse line was generated. Adult and young animals from the *Opn4-EGFP* line appeared behaviorally normal, with no gross abnormalities in motor activity. We detected intrinsic EGFP fluorescence only in the retina (Figure 1B), with no detectable fluorescence found in paraformaldehyde-fixed samples of brain tissue (data not shown). RT-PCR analysis of EGFP expression also confirmed the restricted expression of EGFP to the retina (Figure 2). EGFP fluorescence in the ganglion cell layer was easily visible through the microscope under epifluorescent illumination. Cells of varying intensity could be readily identified, with some cells showing a very strong EGFP signal and others, though still visible, showing weaker fluorescent labeling.

To validate this mouse line as a reporter of melanopsin expression, it was essential to demonstrate that there was a correlation of expression between the reporter gene EGFP and endogenous melanopsin in RGCs. By using anti-melanopsin and anti-EGFP antibodies in whole mount retinas from *Opn4-EGFP* mice, we were able to verify that EGFP expression colocalized with melanopsin expression in RGCs (Figure 1C). While EGFP expression was localized to the cytosol of the soma and dendrites, as would be expected for expression of cytoplasmic EGFP (Figure 1C, left panels), the expression of melanopsin was restricted to the plasma membrane of RGC somas and processes (Figure 1C, middle panels). Of cells that were EGFP positive, 95.6% (306/320 EGFP positive cells) in P17-24 retinas and 99.0% (417/421 EGFP positive cells) in P5-7 retinas also stained positive for melanopsin. Of cells that stained positive for melanopsin 97.8% (306/313 melanopsin positive cells) in P17-24 retinas and 99.8% (417/418 melanopsin positive cells) in P5-7 retinas also stained positive for EGFP (Figure 1C and data not shown). The strong coexpression of EGFP and melanopsin demonstrates that EGFP is indeed being expressed with high coincidence in RGCs that express melanopsin.

We next wanted to functionally validate that EGFP positive cells in this reporter mouse are intrinsically photosensitive as would be expected if EGFP is indeed being expressed in ipRGCs. To test this, we performed whole-cell recordings of light responses of EGFP positive cells at a variety of ages from early postnatal (P0-2 and P5-7) to early adult (P17-24). Intrinsic EGFP fluorescence in the retinas of these mice was detectable at P0. EGFP positive cells were also visible in the inner nuclear layer (INL) at P17-24, and EGFP expression in these cells colocalized with melanopsin expression

(data not shown). This is consistent with previous research showing that some melanopsin positive cell bodies are found in the INL (Berson et al., 2002; Hattar et al., 2002; Dacey et al., 2005). Recordings were performed in a whole mount retinal preparation that preserves light responsiveness of retinal cells (Metea and Newman, 2006), presumably due to remaining retinal pigmented epithelial cells in this preparation. To identify ganglion cells, retinas were visualized under infrared illumination and then EGFP positive cells in the ganglion cell layer (GCL) were localized by brief exposure to 480 nm illumination. To determine intrinsic photosensitivity of EGFP positive cells, we performed recordings in the presence of an AMPA/kainate (DNQX / CNQX) glutamate receptor antagonist and a metabotropic (DL-AP4) glutamate receptor agonist to block signaling to RGCs from the outer retina via the ON and OFF bipolar cell pathways. EGFP positive cells at every age tested showed an increase in firing rate following a 5 s full-field white light stimulus (Figure 3). Smoothing of voltage responses reveals the characteristic slow, tonic depolarization first reported by (Berson et al., 2002) (on latency: P0-2: 4.5 ± 0.8 s, n=14; P5-7: 2.0 ± 0.1 s, n=5; P17-24: 2.7 ± 0.7 s, n=10). The ipRGC response declined to baseline levels only after several seconds following termination of the light stimulus (off latency: P0-2: 22.8 ± 2.3 s, n=14; P5-7: 52.0 ± 11.4 s, n=5; P17-24: 16.3 ± 3.0 s, n=10). At P17-24, the average peak depolarization amounted to 6.8 ± 0.8 mV (n=10), which is similar to the average peak depolarizations of 5.9 ± 0.8 mV (n=14) and 7.2 ± 1.0 mV (n=5) at early postnatal stages (P0-2 and P5-7 respectively) ($P < 0.8$, one-way *ANOVA*). Overall, the kinetics of light responses obtained from EGFP positive cells in the presence of synaptic blockers are consistent with those reported for rat and mouse ipRGCs (Berson et al., 2002; Hattar et al., 2002;

Warren et al., 2006), and demonstrate that EGFP positive cells in this reporter mouse line are indeed intrinsically photosensitive.

Of note, in the presence of synaptic blockers it was common to see pre-stimulus spontaneous firing at P0-2, P5-7, and P17-24. In the absence of synaptic blockers, it was more common to see pre-stimulus spontaneous firing prior to light stimulation in cells at P17-24 compared to P0-14, which is likely indicative of the partially light adapted state of the retinas. However, there were also cells at every age (including P17-24) for which we observed no background firing, consistent with previous studies demonstrating very low levels of spontaneous activity for these cells in the absence of light stimulation (data not shown)(Berson et al., 2002; Warren et al., 2003).

ipRGCs change how they respond to light throughout development

Previously, calcium imaging and multielectrode array techniques were used to analyze the responsiveness of ipRGCs to light at early developmental stages (Sekaran et al., 2005; Tu et al., 2005). These reports made use of various synaptic blockers or knockout mice to isolate adult cells with intrinsic light sensitivity and compare them to early postnatal cells. With the genetic labeling of ipRGCs, it was our goal to compare the functional properties of ipRGCs during the first three postnatal weeks of development in the absence of synaptic blockers. We compared the light responses of ipRGCs to a 5 s full field white light stimulus at four different developmental periods during the first three postnatal weeks of development: just after birth (P0-2), before eye opening (P5-7), around the time of eye opening (P11-14), and early adulthood (P17-24) (Sernagor et al., 2001). The ability to perform whole-cell recordings of cells at these various ages allowed us to measure resting membrane potential (Vm), capacitance of

the membrane (Cm) and resistance of the membrane (Rm) of cells throughout development (Table 1). The higher capacitance of cells at P5-7 and P11-14 than of those at P0-2 or P17-24 would support the idea that ipRGCs are gap-junctionally coupled during these stages. As a preliminary test of this hypothesis, we measured the capacitance and resistance of cells at each of these four stages in the presence of 200 μM meclofenamic acid (MFA), a potent antagonist of several types of neuronal gap junctions in the retina (Pan et al., 2007) . We expected that if cells were coupled at these stages, the presence of MFA would decrease the average Cm. Indeed, we found that in the presence of MFA the Cm was significantly lower in cells at P5-7 ($P < 0.005$, Student's *t*-test) , P11-14 ($P < 0.0001$, Student's *t*-test), and interestingly, also at P17-24 ($P < 0.002$, Student's *t*-test), but not at P0-2 ($P > 0.6$, Student's *t*-test) (Table1). This is consistent with the idea that ipRGCs are gap-junctionally coupled as early as P5 in the developing mouse retina, and continue to be electrically coupled with other retinal cells into early adulthood (Sekaran et al., 2003; Sekaran et al., 2005; Tu et al., 2005). The results concerning Rm however, are less clear. If Rm at any of these stages is influenced by gap junctional coupling, we would expect the presence of MFA to increase Rm. At P17-24 cells in MFA did have a significantly higher Rm than cells in the control condition ($P< 0.009$, Student's *t*-test), but at P0-2 cells in MFA had a significantly lower Rm than cells in the control condition. There was no effect of MFA on the Rm of cells at P5-7 ($P > 0.07$, Student's *t*-test) or P11-14 ($P > 0.3$, Student's *t*-test). It is unclear why these differential effects of MFA on Rm occurred at different ages, but previous research has shown that MFA can affect other channel types

(especially potassium channels) within neurons in addition to gap junctions, which could affect the Rm of the cells (Lee and Wang, 1999; Peretz et al., 2005).

Examples of light responses seen during each period are shown in Figure 4A. At P0-2 and P5-7, all of the cells responded to light with the characteristic long latency and sustained depolarization characteristic of melanopsin-mediated responses. Additionally, at early stages (P0-7), periodic bursts of action potentials independent of light stimulation were observed in 79% of cells (62/78) in accordance with previous studies (Wong, 1999) (Figure 5). The average peak light-evoked depolarization increased during development with significantly larger responses at P17-24 (18.6 ± 1.2 mV, n=21) than at P0-2 (7.7 ± 1.9 mV, n = 8), P5-7 (9.7 ± 1.1 mV, n=25) or P11-14 (14.5 ± 0.8 mV, n = 39) (P <0.001, one-way *ANOVA*) (Figure 4B). Interestingly between P11 and P14, some of the cells (15/39) displayed a rapid onset response of short latency. This initial fast component was always excitatory, and cells remained depolarized for the duration of the light stimulus. Following light off, cells displayed a rapid repolarization of short latency. Spike frequency remained elevated even after the decay time criteria was met, consistent with a residual melanopsin-mediated response. These rapid onset and offset kinetics were observed in most (17/21 for full-field white light, and 22/26 for 610 nm or 480 nm light, total of 39/47) cells at P17-24. One-way *ANOVA*s revealed that the on and off latencies of cells at P17-24 were indeed significantly faster than cells at P0-2 and P5-7 (on latency: $P < 0.001$, one-way *ANOVA*; off latency: $P< 0.001$, one-way *ANOVA*)(Figure *4C-D*). Because traces were averaged over a 1s sliding time window prior to analysis of on and off latencies, it is likely that the kinetics of the light responses are somewhat distorted. On and off latencies for cells

receiving extrinsic inputs are much faster than those measured from averaged traces, with both being on the order of < 200 ms when measured from the raw traces (data not shown). However, without averaging, measurements of membrane voltages are difficult to perform objectively on spiking cells, especially in younger animals where the slower intrinsic response dominates. Therefore, to compare kinetics across ages, we chose to quantify and compare these values using smoothed traces.

The differential kinetics of light responses seen in early adult ipRGCs would be consistent with these cells receiving cone/rod-mediated signals from the outer retina, as was recently demonstrated by studies in primate and rat retina (Dacey et al., 2005; Wong et al., 2007). To test this, we recorded light responses of cells to full field white light stimuli at P17-24 before and after application of synaptic blockers (DL-AP4 and DNQX/CNQX) to block cone/rod mediated ON and OFF pathways (Figure 6A-C). Indeed, in the presence of a cocktail of synaptic blockers, the on and off latencies for light-evoked depolarizations were significantly increased compared to controls (on latency: 0.6 ± 0.02 s vs. 2.7 ± 0.7 s, n=10; $P < 0.01$, Student's t-test; off latency: 0.4 ± 0.1 s vs. 16.3 ± 3.0 s, n=10; $P<0.001$, Student's t-test) (Figure 6E-F). Additionally, maximum depolarization significantly decreased after synaptic blockade (17.7 ± 1.3 mV vs. 6.8 ± 0.8 mV, n=10; $P < 0.0001$, Student's t-test) (Figure 6D). From these observations it is reasonable to conclude that the two types of kinetics observed in ipRGC light responses are the result of two different systems: 1) the intrinsic response, mediated by melanopsin and insensitive to synaptic blockers, and 2) the extrinsic response, mediated by cone/rod driven pathways and sensitive to synaptic blockers.

Responses of ipRGCs to various levels of irradiance during development

We expected that the outer retinal signals from rods/cones present by P17-24 might serve to increase the sensitivity of adult cells to light in comparison to ipRGCs at P5-7 which rely solely on intrinsic signals for light responsiveness (Dacey et al., 2005; Wong et al., 2007). To test this**,** we compared the light responsiveness of ipRGCs at various developmental periods (P5-7 and P17-24) to increasing intensities of 5 s 480 nm or 610 nm light stimuli. As expected, ipRGCs responded to increasing irradiance with stronger depolarizations of shorter latency, eventually saturating. Examples of light responses for each age period to increasing intensities of 480 nm light stimuli are shown in Figure 7. When ipRGC responses to increasing irradiance levels were normalized and then averaged for groups P5-7 and P17-24 and plotted according to light intensity, there was an indication that adult cells are more sensitive to 480 nm than P5-7 cells by approximately one log unit of irradiance (Figure 8A), a trend that was also evident for 610 nm light stimulation (Figure 8B). The light responses at P5-7 lie in the photopic range (Dacey et al., 2005), consistent with previous results indicating low levels of light sensitivity for melanopsin (Sekaran et al., 2005; Tu et al., 2005).

If the higher sensitivity at P17-24 is generated by synaptic signals originating from the outer retina, then these differences should vanish in the presence of synaptic blockers. To test this, we performed additional irradiance-response experiments as described above, but in the presence of a synaptic blocker cocktail (DNQX and DL-AP4). Irradiance-response curves of cell responses in the presence of synaptic blockers for P5-7 and P17-24 are shown in Figure 8C-D. In the presence of synaptic blockers, the higher sensitivity of cells at P17-24 to both 480 nm and 610 nm light was diminished. This indicates that the increased sensitivity of P17-24 ipRGCs is due to the

presence of functional extrinsic inputs at this age and not to an enhancement of sensitivity in the intrinsic system between P5-7 and P17-24.

Because ipRGCs are receiving functional synaptic inputs at P17-24, but not at P5-7, it would be reasonable to expect that the spectral sensitivity of ipRGCs at P17-24 would be shifted toward a λ_{max} more consistent with mid-wavelength cone driven input, which has a λ_{max} of ~510nm. However, we would expect that ipRGCs at P5-7 would have a λ_{max} of ~480 nm (Berson et al., 2002; Dacey et al., 2005) because spectral sensitivity of these cells is presumably determined only by the intrinsic system. To test this hypothesis, average light responses to increasing intensities of 610 nm light at P17-24 and P5-7 in the absence of synaptic blockers were normalized to averaged 480 nm responses within the same age group. We then estimated the λ_{max} for each group based on the differences in sensitivity to these two wavelengths (Lamb, 1995). Indeed, we saw a shift in the λ_{max} from ~480 nm at P5-7 to ~490 nm at P17-24, demonstrating a shift in the spectral sensitivity of ipRGCs at adult stages to longer wavelengths, consistent with the idea that these cells are receiving mid-wavelength cone driven input, in addition to being influenced by the intrinsic system.

Dendritic stratification and arborization of ipRGCs during development

The strong modulation of ipRGCs at adult stages due to synaptic inputs implies that these cells receive afferent connections from bipolar or amacrine cells in the IPL. A well-known developmental event in retinal maturation is the progressive segregation of RGC dendrites into the a and b sublaminas of the IPL, which is a morphological rearrangement crucial for the emergence of the ON and OFF pathways (Sernagor et al., 2001). We investigated whether ipRGC dendritic arborization and stratification in the

IPL changes throughout the first postnatal weeks of development. To examine how the stratification of ipRGC dendrites progresses from P0-2 and P5-7 to adult morphology we filled individual ipRGCs at P0-2, P5-7, or P17-24 with either 0.5% biocytin or neurobiotin. We then utilized streptavidin conjugated with rhodamine to visualize the soma and dendritic processes of the biocytin/neurobiotin filled cells. Retinas were also stained for Choline Acetyl Transferase (ChAT), a marker of cholinergic amacrine cells in the GCL and in the INL. ChAT is expressed very early in retinal development (Stacy and Wong, 2003), and its staining allowed us to visually identify the relative locations of the ON and OFF sublaminas of the IPL. At P0-2 and P5-7 it was difficult to visualize the different sublaminas of the IPL using the ChAT antibody staining, though it did appear that ipRGCs were monostratified at these ages (Figure 9D and E). Two distinct levels of stratification of ipRGC dendrites were seen at P17-24, corresponding to stratification in the ON-(inner) and OFF- (outer) sublaminas. Examples of ipRGC stratification within the IPL, measured from 27 cells (P17-24) are shown in Figure 9A-C. For one group of cells the dendrites stratified at the inner (ON) sublamina of the IPL, near the GCL (14/27 cells) (Figure 9B). In a second group of cells the dendrites stratified at the outer borders of the IPL (OFF sublamina) near the INL (6/27 cells) (Figure 9A). We also observed a third group of cells that displayed distinct stratification in both the inner (ON) and outer (OFF) sublaminas of the IPL (7/27 cells) (Figure 9C). Three subtypes of ipRGCs were also described by (Viney et al., 2007) using transsynaptic viral tracing techniques in mice. Following their terminology, we found that in P17-24 mice, ~ 22% of cells were Type I with dendritic stratification restricted to the OFF sublamina in the IPL, ~52% of cells were Type II with dendritic

arborization restricted to the ON sublamina, and ~ 26% of cells were Type III with bistratified dendritic arbors in both the ON and OFF sublaminas. Quantification of dendritic field diameter and total dendritic length of the neurobiotin/biocytin filled cells shows that there is an increase in dendritic field diameter (Mean ± SEM in μm: P0-2=107 ± 8; P5-7=182 ± 53; P17-24=339 ± 18) and total dendritic length (Mean ± SEM in μm: P0-2=976 ± 53; P5-7=1688 ± 142; P17-24=3337 ± 359) with age (Figure 9F).

Inner and outer stratifying ipRGCs in primates have both been found to be intrinsically photosensitive (Dacey et al. 2005). Though intrinsic photosensitivity has been confirmed in rodent Type I (M1, outer-stratifying) ipRGCs (Berson et al. 2002), this has yet to be demonstrated directly in rodent Type II (M2, inner-stratifying) ipRGCs (Hattar et al. 2006; Baver et al. 2008). In order to directly demonstrate intrinsic photosensitivity of Type II ipRGCs in the mouse, we dye-filled EGFP positive cells from adult (P53-54) mice with neurobiotin and recorded light responses to a 30 s white light stimulus in the presence of a cocktail of synaptic blockers (10 μM DNQX and 250 μM DL-AP4) to block signaling from the outer retina. We then co-immunostained for ChAT and performed immunocytochemistry as described above to determine the stratification subtype of the filled cell. By filling only one cell per preparation, we were able to directly correlate the light response of a given cell to its dendritic stratification subtype. As expected, Type II cells responded to a 30 s white-light stimulus with a sluggish, sustained depolarization in the presence of synaptic blockers (*n*=5), confirming the intrinsic photosensitivity of inner-stratifying, Type II ipRGCs. Figure 9 (G-H) shows an example of the intrinsic light response and dendritic stratification of a single adult Type II ipRGC.

DISCUSSION

The results of our study indicate that melanopsin-expressing ganglion cells undergo major functional remodeling during early postnatal development in mice. Although calcium imaging and multi-electrode recordings of mouse retinas have indicated light responsiveness of ipRGCs during early neonatal stages, these studies have relied on various pharmacological blockers and knockout mice to isolate and compare their intrinsic light responses at early neonatal and adult stages (Sekaran et al., 2005); (Tu et al., 2005). We employed a novel transgenic mouse model to identify ipRGCs *in situ,* allowing for the electrophysiological recording of these cells in the absence of synaptic blockers. We followed the time course of development of synaptic connections onto these cells, and we compared the "intrinsically" and "extrinsically" mediated light responses of ipRGCs during the developmental periods before and after eye opening in the mouse.

It was important to first validate the BAC transgenic mouse model in which expression of EGFP is driven by the melanopsin promoter. The fidelity of this reporter mouse line for melanopsin expression was demonstrated by: 1) co-localization of EGFP and melanopsin expression in subpopulations of ganglion cells, 2) lack of expression of EGFP in other tissues and 3) functional demonstration of intrinsic light responses in EGFP-positive cells. Overall, the intrinsic light responses recorded from EGFP positive cells were similar to those previously described in rat and mouse ipRGCs identified using cell tracers or extracellular recordings (Berson et al., 2002; Hattar et al., 2002; Warren et al., 2006). In our experiments, under conditions in which synaptic influences from rods and cones were blocked pharmacologically, EGFP-

positive cells sampled during the first three postnatal weeks of development displayed a slow and sustained depolarization upon light stimulation, consistent with melanopsin phototransduction (Berson et al., 2002; Hattar et al., 2002; Warren et al., 2006).

With the ability to visually identify individual ipRGCs, we were able to record and fill these cells with the small-molecular-weight dye biocytin or neurobiotin. Morphological reconstructions of filled ipRGCs show that cells at P17-24 have extensive dendritic arborization in the IPL ON and OFF sublaminas. We recognized three types of ipRGCs, the most frequent of which showed dendritic stratification restricted to the ON sublamina, another in which the dendrites terminated in the OFF sublamina and another subpopulation in which the dendrites bistratified in both sublaminas. Likewise, there was a progressive increase in dendritic field size and complexity during the analyzed period. The synaptically driven depolarizing light responses at P17-24 are consistent with the larger subpopulation of ipRGCs observed with dendrites terminating only in the ON sublamina. This is in contrast to findings in rat ipRGCs, in which it was reported that ipRGC dendrites terminate mainly in the OFF sublamina (Berson et al., 2002; Hattar et al., 2002). However a recent study using transsynaptic viral tracing in mice also found three distinctly stratifying ipRGC populations. This study found that the ON and OFF stratifications were equally predominant, and that a smaller proportion of cells were ON/OFF stratified (Viney et al., 2007). Additionally, evidence from melanopsin knockout mice and from the use of antibody staining to the N and C termini of the melanopsin protein has identified at least two populations of distinctly stratifying ipRGCs within the retina termed M1 (which appear to stratify in the outer IPL, analogous to Type I) and M2 (which may stratify

only in the proximal IPL, analogous to Type II) (Hattar et al., 2006; Baver et al., 2008). Baver et al. (2008) saw ~56% of ipRGCs staining as M1 (OFF stratifying) and ~46% staining as M2 (ON stratifying) while Viney et al. (2007) saw ~39% Type I (OFF stratifying), ~41% Type II (ON stratifying), and ~20% Type II (ON/OFF bistratified). Our results are in support of three distinct types of dendritic stratification within the population of ipRGCs, similar to the findings of Viney et al. (2007), but we observed ~22% Type I, 52% Type II, and 26% Type III. At this time, it is not clear what the source of discrepancy between proportion of dendritic stratification types seen in this study versus those of Baver et al. (2008) or Viney et al. (2007) could be. It is possible that ON stratifying cells were somehow oversampled in our experimental system where EGFP positive cells were selected at random for dye filling, while in other systems a large proportion of ipRGCs were labeled in bulk using viral tracing or antibody staining. ON and OFF stratifying ipRGCs have also been identified in primate retina, with OFF stratifying cells being the predominant subtype (Dacey et al., 2005; Jusuf et al., 2007). Though two types of stratification have been identified in primate and demonstrated to be intrinsically photosensitive (Dacey et al. 2005), this study was the first to directly demonstrate intrinsic photosensitivity of Type II melanopsin RGCs in the rodent, confirming the intrinsic photosensitivity of another morphological subtype of melanopsin-expressing RGC. Perhaps the most intriguing aspect of these differences in stratification is the fact that while individual ipRGCs clearly demonstrate specific segregation within different sublaminas of the IPL, adult ipRGCs appear to receive synaptically driven depolarization only at light on. A careful analysis of the specific types of synaptic connections onto each of these ipRGC morphological subtypes, as

well as an analysis of any differences in their intrinsic responses, will be a necessary next step in characterizing the different morphological subtypes of ipRGCs.

This study was the first to follow the developmental time course of the emergence of functional signaling from the outer retina to ipRGCs. Perhaps the major finding in this study was that photoresponses of ipRGCs changed dramatically between the periods before and after eye opening. By the second postnatal week (P11-14), synaptically-driven light responses evoked by cone/rod pathways were already detected in ipRGCs using whole-cell current clamp recordings. This is consistent with research on development of the image-forming visual system, which has shown that functional synaptic connectivity between ganglion cells and the outer retina is first detectable around the time of eye-opening (Sernagor et al., 2001), demonstrating that in this case, the image and non-image forming visual pathways do develop with a similar time course. At least in our experiments, in which the retinas were partially light adapted (see methods), we noticed that at three postnatal weeks, almost all ipRGCs depolarized with a markedly accelerated onset and offset to light stimulus in contrast to the slower response kinetics observed in the first postnatal week of development. There was also a gain of sensitivity of about one log unit of irradiance for both 480 nm and 610 nm at later developmental stages (P17-24). The fact that almost all ipRGCs at P17-24 responded to light with cone/rod-mediated depolarization suggests that synaptically-driven influence is a general property of these cells. Perez-Leon et al., using whole-cell voltage clamp recordings observed only ~5 % of ipRGCs exhibiting synaptically-driven light responses (Perez-Leon et al., 2006). In contrast, Wong et al., using multi-electrode recording techniques, found that virtually every ipRGC exhibited a synaptically-

mediated light response (Wong et al., 2007). Our results indicate that at adult stages the ipRGCs are signaling to various brain areas via a summation of the "intrinsic" slow response and "extrinsic",” fast response originating from outer retinal pathways. It is important to note that our recordings were performed at room temperature, and this should be taken into account when comparing quantitative measurements of light responses in this study to those in studies in which recordings were done at more physiological temperatures.

In this mouse line, EGFP is presumably expressed in the entire population of ipRGCs that innervate various non-image forming central structures such as the SCN, pretectum and the intergeniculate leaflet (Hattar et al., 2006). This idea is supported by the strong colocalization of EGFP and melanopsin expression. The relatively homogenous and consistent synaptically mediated light responses in ipRGCs argues against the notion that these cells convey irradiance signals to the SCN with sluggish depolarization kinetics and with maximal spectral sensitivity centered at 480 nm (Berson, 2003). Instead, the properties of ipRGC responses observed in early adult animals (P17-24) are remarkably similar to those seen in the melanopsin-expressing cells of primates that project to the lateral geniculate nucleus and olivary pretectal nucleus (Dacey et al., 2005). Medium and long-wavelength cones provide strong excitatory inputs to these ipRGCs providing spectral sensitivity and kinetics to light responses distinct from those provided by the melanopsin system (Dacey et al., 2005).

Because we employed 480 nm light for EGFP detection, we performed electrophysiological recordings in retinas that were partially light adapted, thus reducing or even eliminating any contribution of the rods to the ipRGC extrinsic light

response. The dynamic range of the photoresponses in the absence of synaptic blockers with 610 nm is in the range of 10^{13} to 10^{16} photon/cm^2.s, consistent with synaptically-driven light responses mediated by cones, most likely of the medium wavelength subtype. A recent report using a mouse model of medium wavelength cone degeneration found that these photoreceptors have significant role in circadian entrainment (Dkhissi-Benyahya et al., 2007). Our findings that synaptic inputs are conferring upon ipRGCs an overall higher sensitivity to light, as well as shifting the λ_{max} of these cells from ~480 nm toward that of medium wavelength cones are in agreement with this idea. These results thus indicate an important role of medium wavelength cones in providing light responsiveness to ipRGCs, and the shift in λ_{max} for adult ipRGCs to ~490 nm more closely matches the λ_{max} of ~500 nm reported for phase-shifting in hamsters (Takahashi et al., 1984) and the λ_{max} of ~510 nm reported for SCN neurons in rat under photopic conditions (Aggelopoulos and Meissl, 2000).This reinforces the notion that cone photoreceptors have an important contribution to non-image forming light responses in mammalian organisms.

The exclusive reliance of ipRGCs upon melanopsin-mediated phototransduction at earlier stages (P0-11) seems to indicate a lesser need at this developmental period for the distinct spectral tuning and kinetics provided by the cone/rod pathways. The suggested role of the cone/rod pathways in providing better discrimination of spectral changes at dawn and dusk (Panda, 2007) and therefore stronger synchronization of the circadian clock may not be as relevant at mouse early newborn stages before eye opening, at a time when maternal care is provided on an almost full time basis. However, global detection of irradiance levels by the melanopsin system might still be

physiologically relevant even at early developmental stages to convey signals related to sleep-wake cycle and hormonal regulation. Indeed, it is possible to induce cFos expression in the SCN of neonatal mice *in vivo* by exposing rat and mouse pups to light, implying a potential role for photoentrainment of the circadian clock even at early ages (Hannibal and Fahrenkrug, 2004a; Lupi et al., 2006). Another possible role for irradiance detection by the melanopsin system at early developmental stages is that light responses of ipRGCs may subserve an important role in driving the overall network activity of the inner retina by consolidating the development of RGCs (Sernagor, 2005). Appropriate targeting of RGC axons during retinal development relies upon activity-dependent refinement and consolidation of connections (Wong, 1999). Several studies have indicated that RGC activity also plays a crucial role in the formation of visual cortex organization and in the stratification of RGC dendrites (Sernagor et al., 2001). To what extent ipRGCs contribute to the waves of depolarization before eye opening is presently unknown, but their ability to detect light at these early postnatal stages (albeit with low sensitivity, about 10^{12} to 10^{14} photon/cm^2.s for 480 nm at P0-7), leaves open the possibility that these cells are somehow involved in the specific targeting and dendritic arborization that are occurring during this time period.

The development of this EGFP reporter mouse has also allowed us to measure the intrinsic membrane properties of these cells at early ages, something that is not possible using the extracellular techniques that have been used previously. The findings that membrane capacitance is significantly decreased in the presence of the gap junctional blocker MFA at P5-7, P11-14, and P17-24 is consistent with the idea that ipRGCs are electrically coupled during these periods. Indeed, these results are in

agreement with previous reports, using calcium imaging or multielectrode array, of correlated firing between ipRGCs and other ganglion cells at P5-10 (Sekaran et al., 2005; Tu et al., 2005). Prior to this study, Sekaran et al.reported, using calcium imaging in *rd/rd cl* mice, that adult ipRGCs were coupled and that this coupling could be blocked using carbenoxelone (Sekaran et al., 2003). Our data in P17-24 mice in which the rods and cones are still intact provides additional evidence of coupling between adult ipRGCs. Interestingly, Tu et al. using multielectrode recordings in *rd/rd* mice, did not find any correlated firing in adult retinas (Tu et al., 2005). It remains to be determined to which types of cells ipRGCs are coupling and whether this coupling remains constant or changes during development.

Overall our findings reveal marked developmental changes of ipRGCs in the mouse retina during a period in which neuronal differentiation, synaptogenesis and cell death are all occurring with high frequency. Morphological expansion of ipRGC dendrites and their subsequent specific stratification in the inner plexiform layer is accompanied by the formation of functional connectivity with vertical pathways from the cone/rod systems. As development progresses, ipRGCs transition from being driven solely by intrinsic light responses to forming functional connections with vertical pathways from the cone/rod systems while still retaining their intrinsic photosensitivity. Such changes may reflect distinct roles for these cells at different time points throughout retinal development.

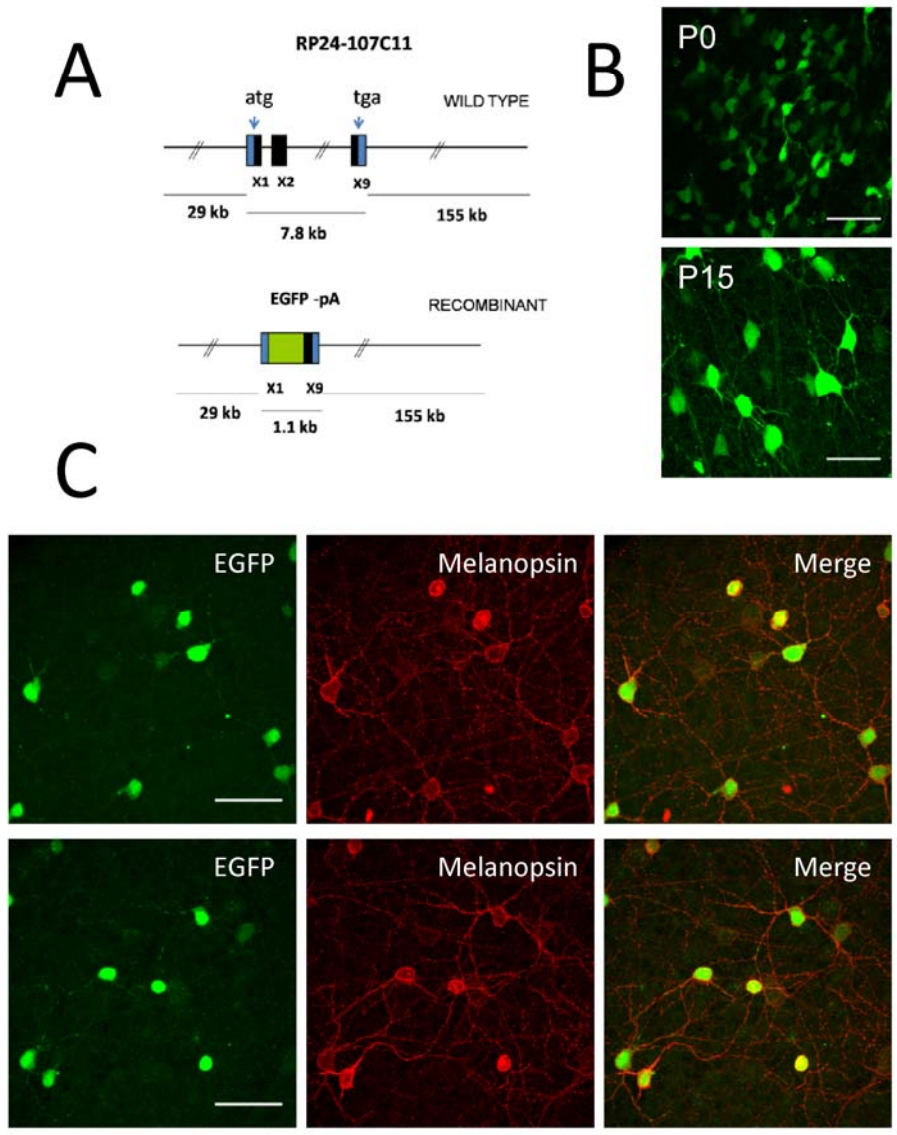

Figure 1: Generation and initial characterization of Opn4-EGFP mouse line.
(A) Schematic representation of the transgene *Opn4-EGFP*. The 192 Kb mouse genomic bacterial artificial chromosome (BAC) clone RP24-107C11 containing the entire transcriptional unit of *Opn4* together with 29 Kb of upstream and 155 Kb of downstream sequence was engineered to harbor *EGFP* coding sequences followed by a polyadenylation signal (pA) in the coding region of the *Opn4* gene by homologous recombination in *E. coli*. X1, X2 and X9 represent exon 1, exon 2 and exon 9 with the start codon in exon 1 (ATG) and stop codon (TGA) in exon 9. (B) Confocal images of intrinsic EGFP signals in whole mount retinas of *Opn4-EGFP* mouse at P0 (upper panel) and P15 (lower panel). (C) Immunostaining for EGFP (green) and melanopsin (red) of adult (P21) whole mount *EGFP-Opn4* retinas. Scale bar: 50 μm (B-C).

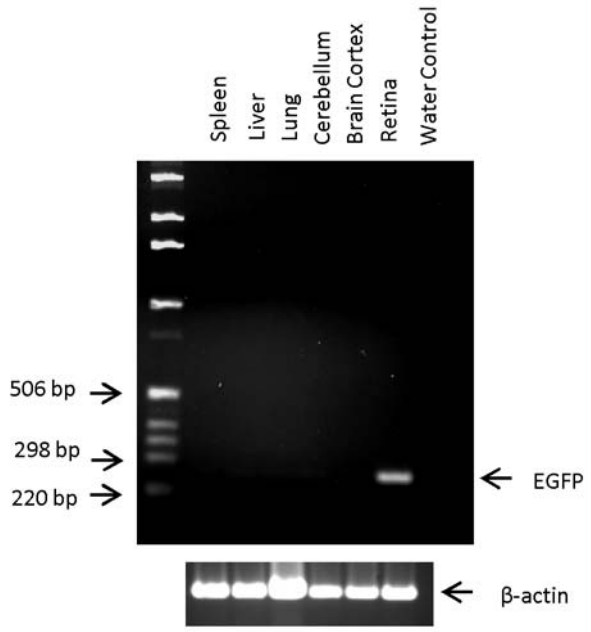

Figure 2: PCR analysis for expression of EGFP mRNA inOpn4-EGFP mouse spleen, liver, lung, cerebellum, brain cortex and retina.
Product of the expected size (255-bp) for EGFP was obtained only from retinal RNA. Beta-actin, in contrast, was detected in all tissues probed.

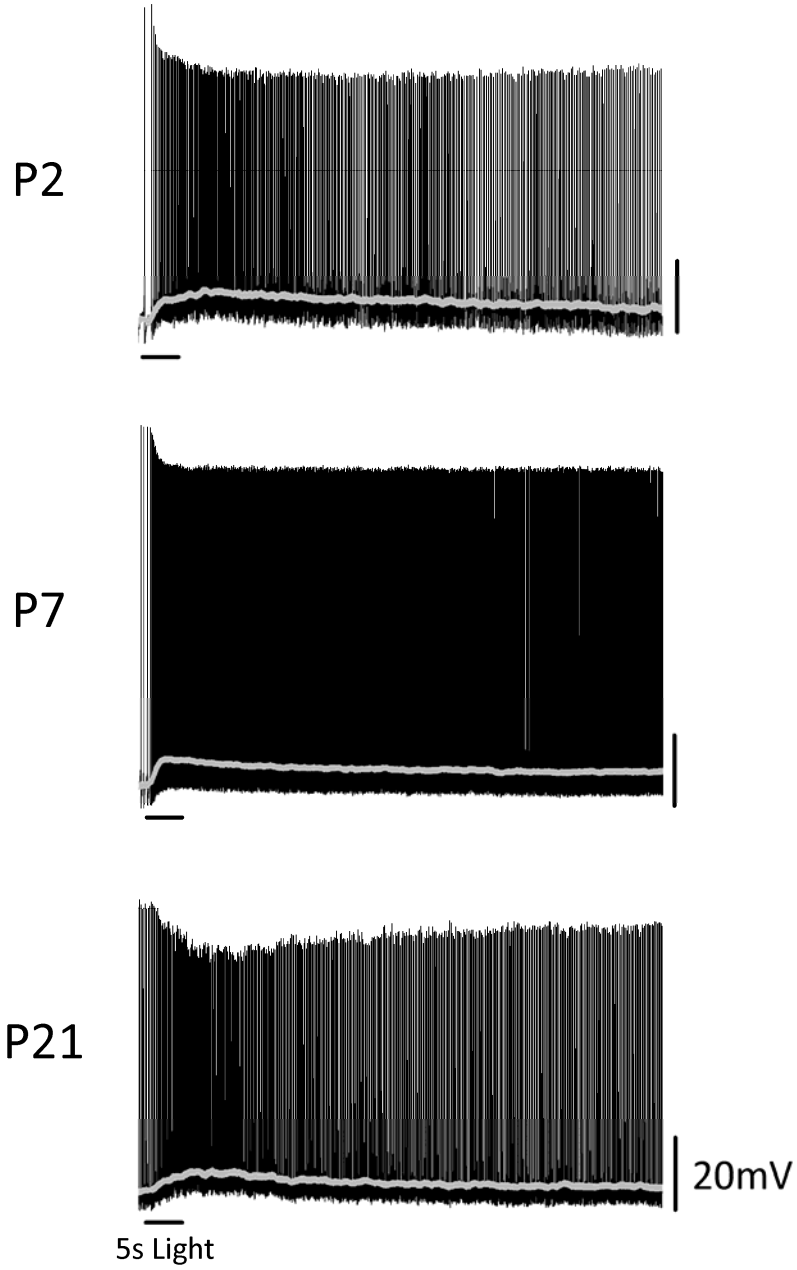

Figure 3: Intrinsic light responses of EGFP-positive ganglion cells in whole mount Opn4-EGFP retinas.
Membrane potential of EGFP positive ganglion cells was recorded in current clamp mode at ages P2, P7 and P21. A full-field white light stimulus of 5 s duration was applied to the retina. A cocktail of pharmacological blockers was also included to prevent any rod or cone-driven influences in the light responses. Gray line shows membrane potential values averaged over a 1 s sliding time window.

Table 1: Intrinsic electrical properties of ipRGCs recorded at various stages of postnatal development in the absence or presence of meclofenamic acid (MFA). Values reported as Mean ± SEM. Vm: Resting membrane potential; Cm: membrane capacitance; Rm: membrane resistance; MFA: meclofenamic acid. *indicates significant difference from control condition ($P < 0.05$). † 2 outliers (>2 standard deviations from the mean) were removed from the analysis.

Age Group	Vm (mV)	Cm (pF) Control	Cm (pF) MFA	Rm (MΩ) Control	Rm (MΩ) MFA
P0-2	-52.9 ± 1.9 (*n*=8)	32.8 ± 1.7 (*n*=13)	33.9 ± 2.0 (*n*=7)	868.7 ± 51.8 (*n*=13)	607.9 ± 103.5* (*n*=7)
P5-7	-57.0 ± 1.3 (*n*=25)	55.5 ± 1.6 (*n*=17)	48.7 ± 1.6* † (*n*=18)	403.9 ± 50.1 (*n*=17)	432.4± 55.3 (*n*=20)
P11-14	-55.0 ± 0.9 (*n*=39)	58.5 ± 1.7 (*n*=19)	38.8 ± 2.6* (*n*=21)	414.4 ± 46.5 (*n*=19)	369.9 ± 25.2 (*n*=21)
P17-24	-50.5 ± 1.0 (*n*=19)	41.6 ± 1.7 (*n*=20)	31.6 ± 2.3* (*n*=15)	370.2 ± 36.1 (*n*=20)	515.9 ± 36.5* (*n*=15)

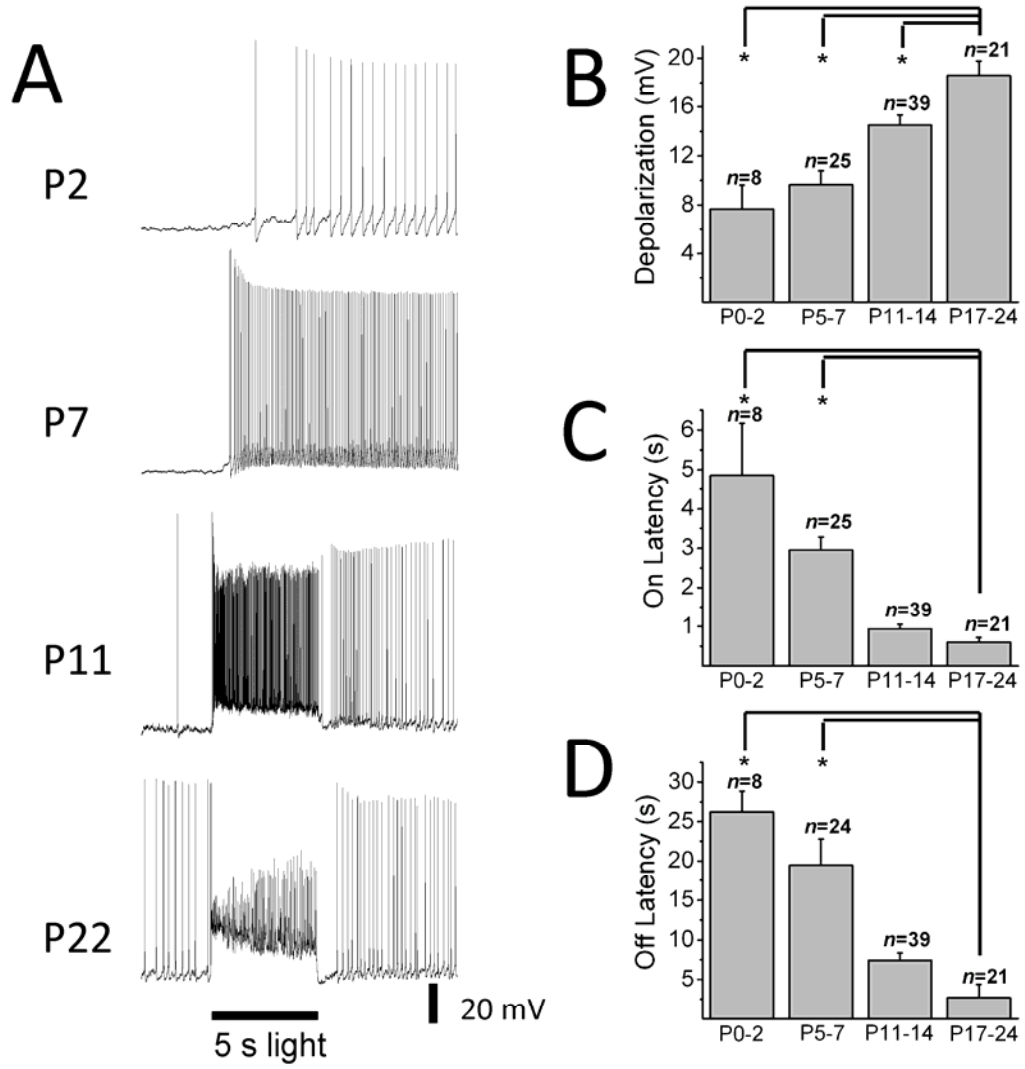

Figure 4: Light evoked responses of ipRGCs at various stages of mouse development.
(A) Recordings of representative light responses at P2, P7, P11 and P22 in response to a 5 s full field white light stimulus in the absence of synaptic blockers. Amplitude (Mean ± SEM) of average depolarization (B) on latency (C) and off latency (D) are shown for the various stages of mouse development. (on latency: P0-2=4.9 ± 1.3 s; P5-7=3.0 ± 0.3 s; P11-14=0.9 ± 0.1 s; P17-24=0.6 ± 0.1 s)(off latency: P0-2=26.2 ± 2.6 s; P5-7=19.5 ± 3.4 s; P11-14=7.4 ± 0.9 s; P17-24=2.7 ± 1.7 s) Error bars represent SEM. *$P < 0.001$.

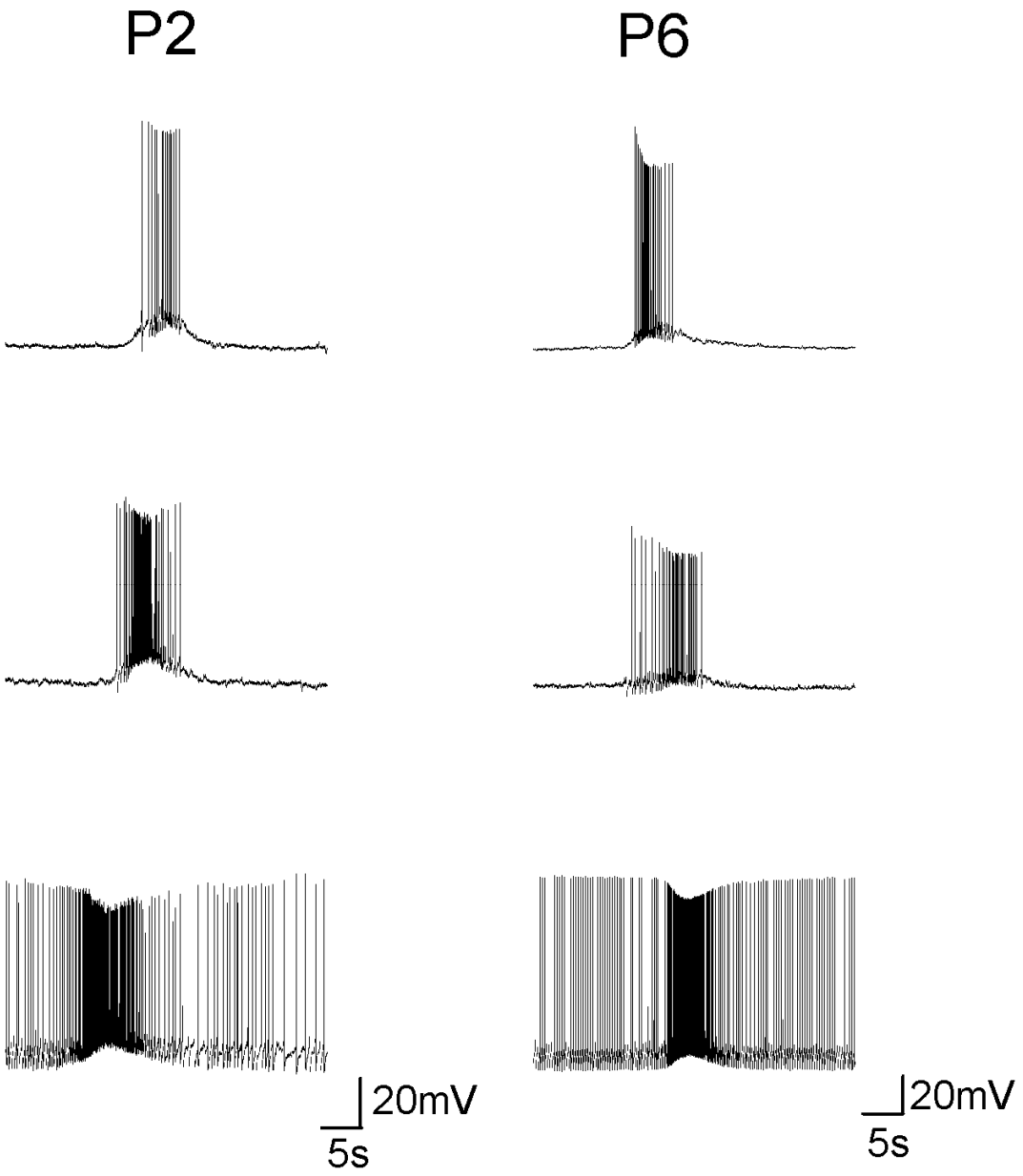

Figure 5: Bursts of depolarization during the first postnatal week in ipRGCs of Opn4-EGFP mice.
Spontaneous bursts of depolarization were detected in ipRGCs at early postnatal stages (P0-7) in the absence of light stimulation. Examples are shown at P2 (left column) and P6 (right column).

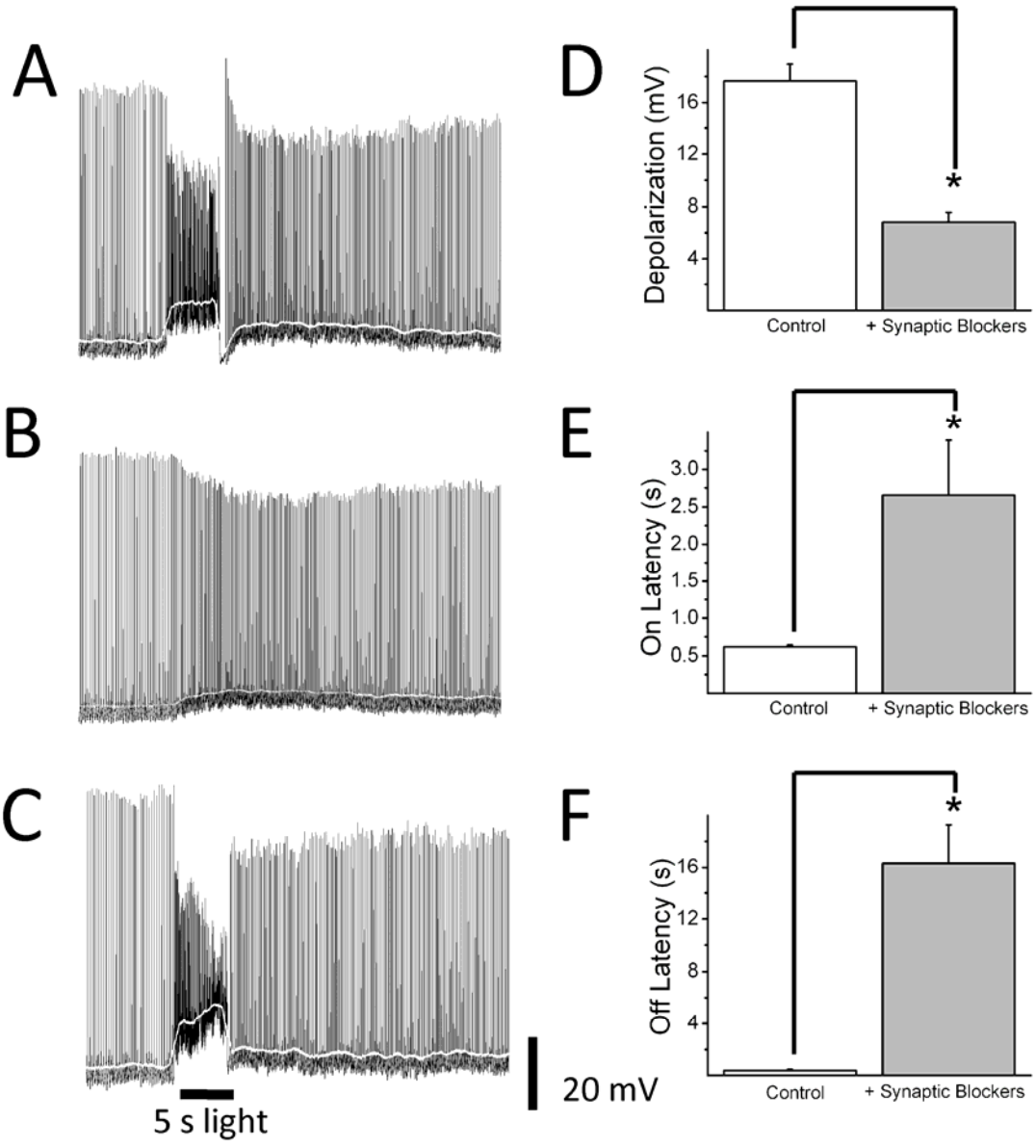

Figure 6: Influence of glutamatergic synaptic inputs on ipRGC light-evoked responses.
Representative traces of an ipRGC response to a 5 s full field white light stimulus from a P21 mouse recorded in the absence (A) or presence (B) of a cocktail of glutamatergic receptor blockers. Traces in (C) show the same cell upon washout of the synaptic blockers. Amplitude (Mean ± SEM, $n = 10$) of depolarization (D) on latency (E) and off latency (F) are shown in the absence and presence of synaptic blockers. White line shows membrane potential values averaged over a 1 s sliding time window. Error bars represent SEM. *$P < 0.01$.

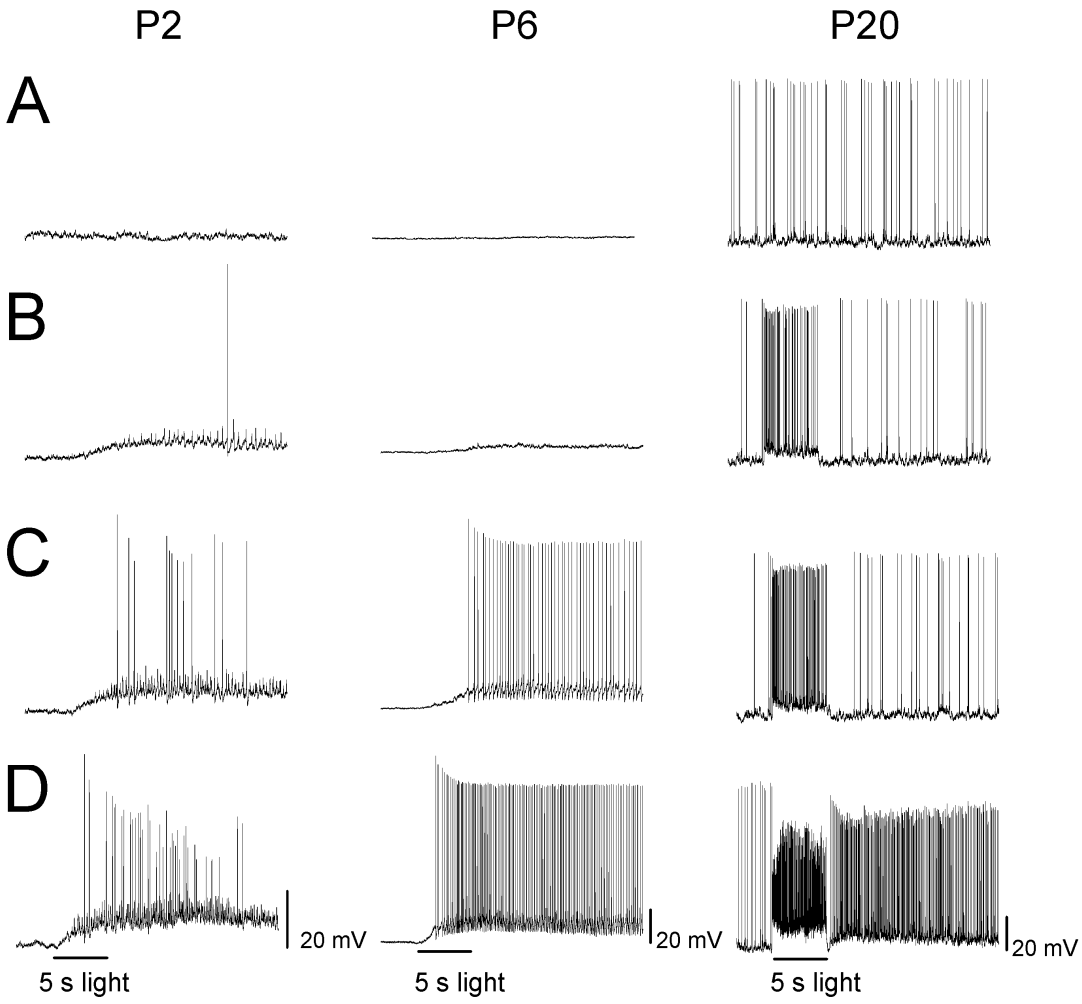

Figure 7: Light evoked responses of ipRGCs to increasing (top to bottom) intensities of 5 s full field 480 nm light stimulation.
Representative light responses at P2 (left column), P6 (middle column) and P20 (right column). Stimulus intensity (in photons/cm^2.s) for P2: 7.63 x 10^{11} (A), 7.63 x 10^{12} (B), 2.29 x 10^{13} (C), 7.63 x 10^{13} (D). Stimulus intensity (in photons/cm^2.s) for P6: 2.4 x 10^{11} (A), 2.28 x 10^{11} (B), 2.29 x 10^{14} (C), 7.63 x 10^{14} (D). Stimulus intensity (in photons/cm^2.s) for P20: 7.63 x 10^{10} (A), 7.63 x 10^{11} (B), 2.44 x 10^{12} (C), 6.10 x 10^{14} (D).

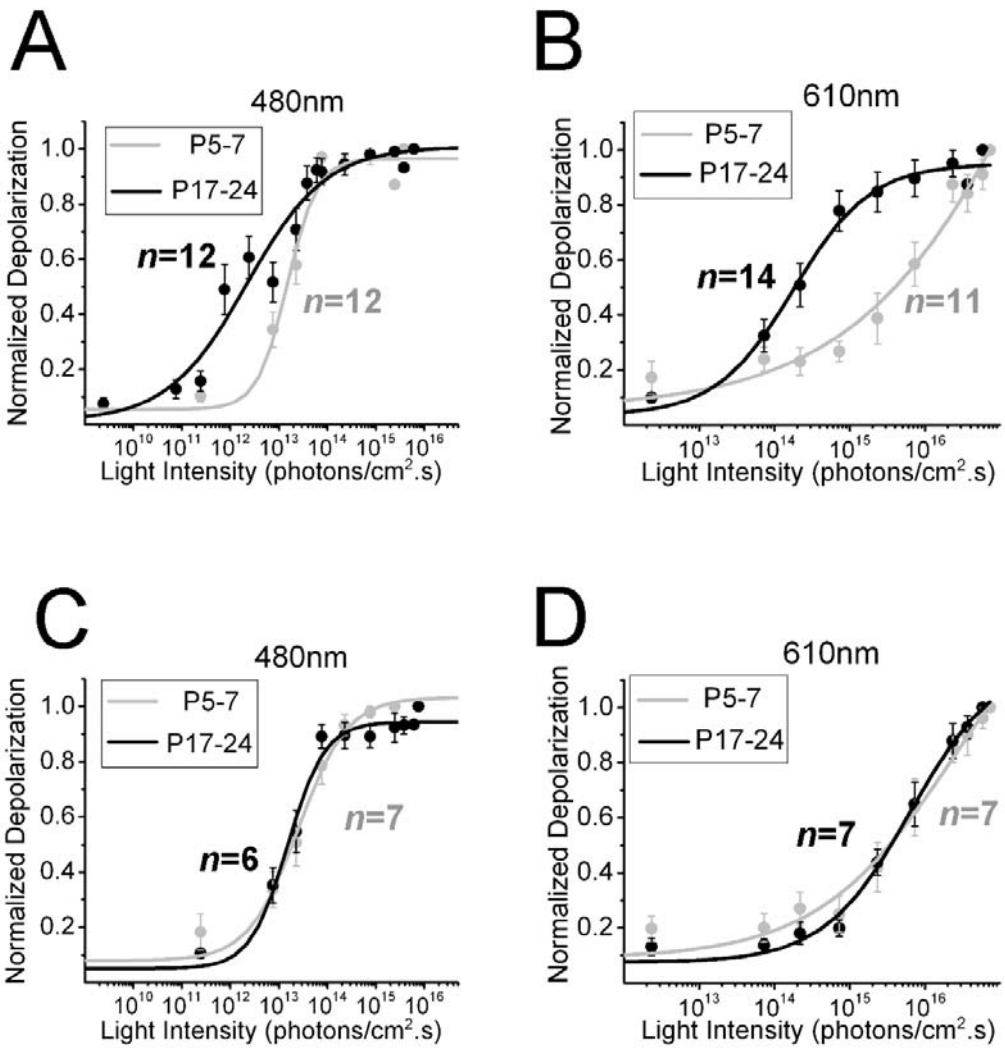

Figure 8: Differences in sensitivity of light-evoked responses in P17-24 and P5-7 retinas.

(A-D) Irradiance-response curves to 480 nm and 610 nm light in the absence (A-B) and presence (C-D) of glutamatergic synaptic blockers. Irradiance yielding half-maximal response (IR50) in photons/cm^2.s $IR50_{P17\text{-}24}$~2.09 x 10^{12}, $IR50_{P5\text{-}7}$~1.47 x 10^{13} (A) $IR50_{P17\text{-}24}$~1.83 x 10^{14}, $IR50_{P5\text{-}7}$~3.81 x 10^{15} (B) $IR50_{P17\text{-}24}$~1.54 x 10^{13}, $IR50_{P5\text{-}7}$~1.93 x 10^{13} (C) $IR50_{P17\text{-}24}$~3.51 x 10^{15}, $IR50_{P5\text{-}7}$~3.11 x 10^{15} (D).

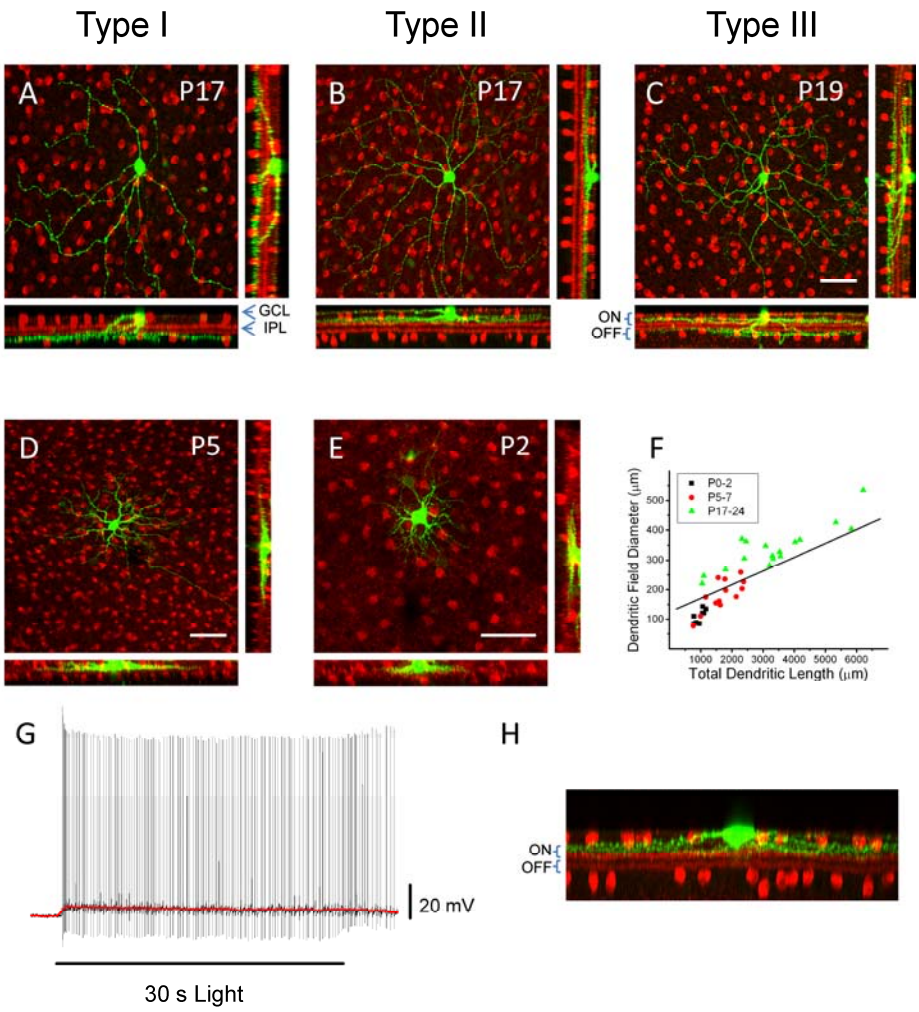

Figure 9: Morphological diversity of ipRGCs during mouse development.
Whole mount retinas of ipRGCs filled with biocytin/neurobiotin (in green) and immunostained ChAT (in red) to visualize cholinergic amacrine cells (A, B, C, D, E). Top row: examples of three types of ipRGCs in P17-24 mice. ChAT positive cell bodies are in the GCL and the INL, while their projections form two bands visible in the rotated images that run along the ON and OFF sublamina of the IPL (bottom and right panels of A-E). (A) monostratified ipRGC (P17) with dendritic arborization in the OFF sublamina of the IPL (Type I ipRGC), (B) monostratified ipRGC (P17) with dendritic arborization in the ON sublamina of the IPL (Type II ipRGC), (C) bistratified ipRGC (P19) with ON and OFF segregated arborization with respect to the two anti-ChAT labeled bands (Type III ipRGC). (D-E) Examples of ipRGC confocal images taken from P5 and P2 mice. (F) Dendritic length and dendritic field diameter of individual ipRGCs at P0-2, P5-7 and P17-24. (G) Example of intrinsic light response (p53) of Type II cell to a 30 s white light stimulus recorded in current clamp mode in the presence of synaptic blockers. Red line shows membrane potential values averaged over a 1 s sliding time window. (H) Dendritic stratification of cell from (G) in the ON sublamina of the IPL. ChAT: choline acetyl transferase; GCL: ganglion cell layer; IPL: inner plexiform layer. Scale bars: 50 μm for A-E.

CHAPTER 3

Functional and morphological differences among intrinsically photosensitive retinal ganglion cells

Schmidt TM and Kofuji P (2009) *J Neurosci* 29(2): 476-482

ABSTRACT

A subset of ganglion cells in the mammalian retina express the photopigment melanopsin and are intrinsically photosensitive (ipRGCs). These cells are implicated in non-image forming visual responses to environmental light such as the pupillary light reflex, seasonal adaptations in physiology, photic inhibition of nocturnal melatonin release, and modulation of sleep, alertness and activity. Morphological studies have confirmed the existence of at least three distinct subpopulations of ipRGCs, but studies of the physiology of ipRGCs at the single cell level have focused mainly upon M1 cells, the dendrites of which stratify solely in sublamina a (OFF sublamina) of the retinal inner plexiform layer (IPL). Little work has been done to compare the functional properties of M1 cells to those of M2 cells, the dendrites of which stratify solely in sublamina b (ON sublamina) of the IPL. The goal of the current study was to compare the morphology, intrinsic light response, and intrinsic membrane properties of M1 and M2 cells in the mouse retina. Here we demonstrate additional morphological differences between M1 and M2 cells as well as distinct physiological characteristics of both the intrinsic light responses and intrinsic membrane properties. M2 cells displayed a more complex dendritic arborization and higher input resistance, yet showed lower light sensitivity and lower maximal light responses than M1 cells. These data indicate morphological and functional heterogeneity among ipRGCs.

INTRODUCTION

Retinal ganglion cells (RGCs) in the mammalian retina expressing the photopigment melanopsin comprise a distinct subpopulation of RGCs and are intrinsically photosensitive (ipRGCs) (Berson et al., 2002); (Hattar et al., 2002). These ipRGCs project to several brain areas including the suprachiasmatic nuclei (SCN) of the hypothalamus which drive the mammalian circadian rhythm, and the olivary pretectal nuclei (OPN), which control the pupillary light reflex (PLR) (Hattar et al. 2006). These cells are now thought to be the sole pathway through which non-image forming visual responses are conveyed to both the SCN and OPN (Guler et al., 2008); (Hatori et al., 2008a). Previous work has identified at least three morphologically distinct subpopulations of ipRGCs: those that stratify solely in sublamina a (OFF sublamina) of the retinal inner plexiform layer (IPL), termed M1 (or Type I), those that stratify solely in sublamina b (ON sublamina) of the IPL, termed M2 (or Type II), and those that bistratify in both the a and b sublaminas of the IPL, termed Type III (Hattar et al., 2006; Viney et al., 2007; Baver et al., 2008; Schmidt et al., 2008). Furthermore, previous research has indicated that M1 cells form the primary projection to the SCN (80 % M1/20 % M2), while M1 and M2 cells project to the OPN in approximately equivalent proportions (45 % M1/55 % M2) (Baver et al., 2008).

Calcium imaging and multielectrode array (MEA) recordings from adult ipRGCs in the whole mount retina have demonstrated diversity in their intrinsic light responses (Sekaran et al., 2003; Tu et al., 2005). However, whole-cell recordings of intrinsic light responses from ipRGCs have either mainly been made from ipRGCs retrogradely labeled from the SCN, a population consisting mainly of M1 cells (Berson

et al., 2002; Baver et al., 2008; Badea et al., 2009) or have not been separately considered based on morphological subtype (Schmidt et al., 2008). Thus the physiological diversity in the intrinsic ipRGC light responses demonstrated using extracellular recording techniques remains untested at the single cell level. Because these cells are the sole pathway for non-image forming visual responses to the brain and because of the specificity of projections to different brain areas, a deeper understanding of the physiology of the different morphological subpopulations of ipRGCs is critical to understanding how these cells signal light information to the non-image forming centers of the brain (Guler et al., 2008; Hatori et al. 2008).

The goal of the current study was to use a transgenic mouse model in which ipRGCs are labeled *in vivo* with enhanced green fluorescent protein (EGFP) (Schmidt et al., 2008) to determine what, if any, physiological diversity in the intrinsic light response or intrinsic membrane properties may underlie the previously identified morphological diversity in the ipRGC population. In this paper, we identify stark differences in the dendritic arbor complexity, light response characteristics, light sensitivity, and intrinsic membrane properties of M1 and M2 cells, highlighting major physiological and additional morphological diversity within the ipRGC population.

MATERIALS AND METHODS

Animals

Recordings were performed on postnatal (P) 22-40 animals from the *Opn4-EGFP* mouse line described previously (Schmidt et al., 2008). Animals were cared for in accordance with guidelines described in *Guide for the Care and Use of Laboratory Animals*, using protocols approved by the University of Minnesota Institutional Care and Use Committee.

Electrophysiology

Dissections were performed as described previously (Schmidt et al., 2008). Briefly, retinas were removed from the eyecups and bubbled with 95% O2-5%CO2 bicarbonate buffered Ames' solution (Sigma, St. Louis, MO) at room temperature in a dark room with minimal ambient light. Prior to recording, retinas were treated with Ames' solution containing collagenase/hyaluronidase (240 and 1000 U/ml, respectively) at room temperature for 15 minutes to remove vitreous. No adverse effects of this treatment on retinal health were observed.

Recordings were performed using an Axon 700B Amplifier (Molecular Devices, Union City, CA) with extracellular solution containing 95% O_2-5%CO_2 bicarbonate buffered Ames' solution (Sigma, St. Louis, MO) at 32-34^{o}C. For current clamp recordings, pipettes were filled with (in mM): 125 K-gluconate, 2 $CaCl_2$, 2 $MgCl_2$, 10 EGTA, 10 HEPES, 0.5 NaGTP, and 2 Na_2ATP, pH to 7.2 with KOH. For voltage clamp recordings, pipettes were filled with (in mM): 125 CsMethanesulfonate, 10 $CsCl_2$, 5 EGTA, 1 $MgCl_2$, 2 Na_2ATP, 10 NaHepes, 10 Phosphocreatine, 2 QX314, 0.5 NaGTP, pH to 7.6 with KOH. Intracellular solutions also contained 10 μM Alexafluor-

594 hydrazide (AF-594)(Invitrogen, Carlsbad, CA) and dendritic stratification was classified by focusing in the proximal and distal layers of the IPL. To ensure that we were successfully able to identify stratification subtype using this technique, we filled single ipRGCs in three individual retinas with neurobiotin and AF-594 and classified their stratification using AF-594. Retinas were then processed for immunocytochemistry and coimmunostained for choline acetyl transferase (ChAT) as described previously (Schmidt et al. 2008). An independent observer then classified the stratification of these cells based on confocal images of the neurobiotin staining with streptavidin. Stratification was correctly identified using AF-594 in all three cases (data not shown), demonstrating the fidelity of this technique in identifying stratification directly following recordings from individual cells. If a cell was bistratified or if its stratification could not be identified, that cell was excluded from subsequent analyses. Liquid junction potentials (6.1 mV) were corrected for all recordings. In full-field white light experiments, cells were given 3-5 minutes following visualization of EGFP under epifluorescence prior to a single stimulation with light.

For nucleated patch experiments, tightly sealed whole cell recording was obtained prior to pulling out a nucleated patch. A nucleated patch was formed by slowly (1-2 min) pulling the patch pipette away from the whole cell while applying a gentle negative pressure (Sather et al., 1992). Effectiveness of formation of a nucleated patch was monitored by following the capacitive transients during the course of the experiment.

Whole cell currents, and current step data were analyzed off-line with Clampfit (Molecular Devices) and membrane potential values were measured from raw traces for

white-light experiments and over a 1 s sliding time window for irradiance-response and nucleated patch experiments to maximize the signal to noise ratio using Igor Pro. For spike analysis, threshold for spike detection was set at 0 mV for all traces. For hyperpolarizing current steps, membrane voltage was measured from the average value over the last 10 ms of the 1 s current pulse. Resting membrane potential (Vm) values were calculated by taking the average membrane voltage of the first 10 s of baseline prior to any light stimulation. For light response experiments, cells whose resting membrane potential (Vm) did not reach -40 mV were excluded from the analyses. Cell capacitance (Cm) and input resistance (R_N) were calculated from those currents evoked by stepping the cell potential to a 10 mV hyperpolarized value for 20 ms from a holding potential of -60 mV. Only recordings with an access resistance of < 30 MΩ were included in the analysis. Charge Q was estimated by time integration of evoked current during the step voltage. R_N was estimated from the steady-state evoked current during the step voltage. Light responses were defined as the maximum depolarization of the averaged trace during the first 30 s following light onset. Irradiance-response experiments were performed and analyzed as described previously (Schmidt et. al., 2008).

Retinas were allowed to dark adapt for 5 min. prior to the first stimulus, and stimuli were placed 5 min. apart to allow the cell to return completely to baseline. Curve fits for normalized, averaged irradiance-response data were determined by nonlinear regression using Origin 7.5 (MicroCal, Northampton, MA) according to the logistic dose-response function: $y = A_2 + [(A_1\text{-}A_20/1+(IR/IR_{50})\text{^}n_H]$, where A_1 is the maximum response plateau, A_2 is the minimum response plateau, IR is irradiance, IR_{50}

is the irradiance values that generate half-maximal response, and n_H is the Hill slope. Light stimuli for some experiments were full-field, broadband white light (7.6×10^{14} photons.cm^{-2}.s^{-1} measured at 480 nm by interposing a narrow bandpass filter) delivered from below the retina using the microscope's 100-W halogen lamp and transillumination optics. An electromechanical shutter (Vinicent Assoiates, Rochester, NY) was used to control the duration and timing of the light stimulus. In irradiance-response experiments, light stimulation was performed using a xenon lamp feeding the camera port. A filter wheel fitted with various neutral-density filters and narrow band-pass filters (Chroma Technologies, Rockingham, VT) and shutter (Lambda-3, Sutter Instruments) was used to control the wavelength, intensity, and duration of light stimuli. Irradiance measurements were made with a calibrated radiometer model S370 (UDT Instruments, San Diego, CA).

Statistical analyses were performed using Origin 7.5 (MicroCal). Statistical comparison of means was performed using a Student's *t*-test, and significance was concluded when $P < 0.05$. Data are presented as mean ± SE.

Immunocytochemistry

Immunocytochemistry, neurobiotin filling and image analysis of retinas were performed as published previously (Schmidt et al., 2008). Sholl analysis was performed using the Sholl analysis plugin for ImageJ software (http://rsb.info.nih.gov/ij/) on tracings from neurons using circles starting 10 μm from center and 15 μm steps. Relative fluorescence levels for EGFP were measured using ImageJ software by defining a fixed region of interest (ellipse) that encompassed most of the cell body for the EGFP-positive cells. Mean pixel intensity of the measured region was subtracted

from background levels for each cell and then EGFP signals were compared between cells in the same frame.

Pharmacology

Synaptic blocker cocktail included: 250 μM DL-2-amino-4-phosphonobutyrate (DL-AP4, a group III metabotropic glutamate receptor agonist); 10 μM 6,7-dinitroquinoxaline (DNQX, α-amino-3-hydroxy-5-methyl-4-isoxazolepropionic acid (AMPA)/kainate receptor antagonist); 0.3 μM strychnine (glycine receptor antagonist), 50 μM picrotoxin (GABA receptor antagonist). Extracellular solution sometimes also included 0.5 μM tetrodotoxin (TTX, sodium channel blocker). In some experiments, 200 μM hexamethonium bromide (nACh receptor antagonist) (MP Biomedicals, Solon, OH), 100 μM carbenoxelone (gap junction antagonist), and 2 mM cobalt chloride (to block all synaptic transmission) were included in the cocktail with all of the above blockers. DL-AP4, DNQX, and TTX were purchased from Tocris (Ellesville, MO). Picrotoxin, carbenoxelone, cobalt chloride, and strychnine were purchased from Sigma (St. Louis, MO).

RESULTS

M1 and M2 ipRGCs have distinct morphological characteristics

We first examined the overall morphological characteristics of M1 and M2 cells in the adult mouse retina using a transgenic mouse line in which ipRGCs are labeled *in vivo* with EGFP (Schmidt et al., 2008) to identify and fill 29 ipRGCs with the intracellular tracer neurobiotin. We then processed these retinas for immunocytochemistry and costained for ChAT, which is a marker for cholinergic amacrine cells whose cell bodies are found in both the GCL and the INL. This served as a visual marker for these two retinal layers. M1 cells were identified as those cells whose dendrites stratified solely in sublamina a (Figure 1A), while M2 cells were identified as those cells whose dendrites stratified solely in sublamina b (Figure 1B). When the dendritic arbors of these two populations were further examined, we observed M2 cells had significantly larger dendritic field diameters (422.9 ± 23.5 μm vs. 313.6 ± 17.3 μm; $P < 0.001$) as well as more overall dendritic length (4131.4 ± 273.7 μm vs. 2092.5 ± 145.9 μm; $P < 0.001$) (Figure 1C) and significantly larger soma diameter (21.8 ± 0.8 μm vs. 17.0 ± 0.4 μm, $P< 0.001$)(Figure 1D). We also observed that the dendritic arbors of M2 cells seemed more complex and highly branched than those of M1 cells. These differences in dendritic complexity of M1 versus M2 cells could be clearly seen after Sholl analysis (Figure 2A) as the M2 cells displayed a higher number of dendritic crossings than M1 cells (Figure 2*B*). Additionally, when we filled neighboring M1 and M2 cells with neurobiotin, we observed extensive overlap of the dendritic fields (Figure 1E,F), suggesting extensive overlap of the receptive fields of M1 and M2 cells.

Collectively, these results demonstrate morphological dissimilarities between M1 and M2 cells that go beyond differences solely in their stratification level within the IPL.

M1 and M2 ipRGCs have distinct light response characteristics

We used the EGFP reporter mouse, which labels both M1 and M2 cells (Schmidt et al., 2008) to test for physiological diversity in the intrinsic light responses of these two cell types. We performed simultaneous dual whole-cell recordings of the intrinsic light responses of neighboring ipRGCs to a 30 s fixed, bright white light stimulus in both current and voltage clamp mode in the presence of synaptic blockers and the sodium channel blocker TTX. Alexafluor-594 hydrazide (AF-594) was included in the intracellular solution, which allowed us to identify the morphological subtype of individual cells immediately following recordings. Current clamp recordings of ipRGC light responses to a 30 s white-light stimulus revealed noticeable differences in the light responses of identified M1 and M2 cells (Figure 3A). M1 cells responded to the 30 s white-light stimulus with a significantly larger depolarization than did M2 cells (30.5 ± 1.6 mV vs. 11.1 ± 1.0 mV, $P< 0.001$) (Figure 3C). We also performed the experiments in voltage clamp mode in order to compare the light-evoked current in each of these two cell types. Again, both cell types showed distinct light responses paralleling the differences observed in current clamp (Figure 3B). M1 cells responded to a 30 s white light stimulus with a significantly larger maximum light-evoked current than did M2 cells (-550.5 ± 65.7 pA versus -63.5 ± 6.5 pA, $P < 0.001$)(Figure 3D). The initial light-evoked current of M1 cells decayed rapidly until reaching a much smaller, steady-state current that lasted for the duration of the light

stimulus, while M2 cells responded to light with a small, but relatively sustained inward current.

Interestingly, we observed that M1 cells, in general, had a brighter EGFP signal than did M2 cells (Figure 3E). It is conceivable that the heterogeneity of EGFP expression among the ipRGCs in our reporter mouse line reflects a parallel heterogeneity of melanopsin expression among M1 and M2 cells. Previous research has indicated that M1 cells may express more melanopsin based on higher levels of anti-melanopsin antibody staining (Hattar et al., 2006; Baver et al., 2008). Consistent with this hypothesis, M1 cells showed a 10-fold higher sensitivity to 480 nm light than M2 cells as assessed in irradiance-response experiments (Figure 3F).

Though M2 cells do respond to light in the presence of synaptic blockers, it is still possible that light responses in this subpopulation are due to some residual chemical or electrical synaptic input. To determine conclusively whether M2 cells are intrinsically photosensitive, we performed whole-cell current clamp recordings in the same cocktail of drugs used for the initial light response experiments, but also containing cholinergic, synaptic, and gap junctional blockers. Light responses were recorded in all cells tested (Figure 4). Additionally, we performed nucleated patch experiments in which we isolated a portion of the membrane of M2 cells from the soma and tested the membrane for photosensitivity. We recorded responses to 5 or 30 s white light stimuli in all cells tested (6.7 ± 1.0 mV for 5 s stimuli, $P < 0.01$), demonstrating conclusively for the first time the intrinsic photosensitivity of M2 cells (Figure 3H-J).

M1 and M2 cells have distinct intrinsic membrane properties

It has been demonstrated that RGCs vary in their intrinsic membrane properties (O'Brien et al., 2002). We used whole cell recording methods to investigate whether the membrane properties and excitability of M1 and M2 cells differ. Indeed we found that M1 and M2 cells differ significantly in terms of their R_N (input resistance) and Vm (resting membrane potential), with M1 cells having a significantly higher R_N than M2 cells (709.0 ± 44.3 MΩ vs. 216.4 ± 13.0 MΩ; $P< 0.001$) and a significantly more depolarized Vm than M2 cells (-48.2 ± 1.1 mV vs. -66.0 ± 0.7 mV; $P < 0.001$) (Figure 5C). To further examine differences in the intrinsic membrane properties of these two ipRGC subtypes, we recorded responses from single M1 or M2 cells in current clamp mode to hyperpolarizing and depolarizing current pulses in the presence of synaptic blockers. For these experiments, current was injected to hold the Vm of both populations of cells at ~ -65 mV to facilitate direct comparison between current-voltage relationships of each subtype. Hyperpolarizing current steps of similar strength generated larger voltage responses in M1 cells than M2 cells (Figure 5A-B). Accordingly, I-V curves obtained from subthreshold responses to hyperpolarizing current pulses in M1 cells were much steeper than in M2 cells (Figure 5D).

Representative examples of the firing pattern of M1 and M2 cells are shown in Figure 6A-B. In both cell types, the temporal pattern of firing was characterized by an adaptation of spike frequency. In general, M2 cells showed firing over a wide range of depolarizing current pulses, while M1 cells were only able to sustain action potential firing through a narrower range of depolarization. While both cell types showed increases in instantaneous frequency of the first interspike interval with increasing strengths of current injection, M2 cells attained higher frequencies (242.3 ± 9.5 Hz)

than did M1 cells (76.6 ± 14.8 Hz) (Figure 6C,G). Additionally, if firing rate was averaged across the entire 1 s current injection, M1 cells attained lower average firing rates (10.8 ± 1.3 Hz) than did M2 cells (38.4 ± 4.0 Hz), and reached spike block much more quickly (Figure 6D,G). Both cell types also showed rapid frequency adaptation over the course of a given stimulus. Instantaneous frequency over time for the two example cells is shown in Figure 6E,F.

DISCUSSION

In this study, we utilized a transgenic mouse model in which ipRGCs are labeled *in vivo* with EGFP to identify several morphological and physiological properties of M1 and M2 cells. Previous morphological analyses of M1 cells have characterized their sparse dendritic arbors and stratification in sublamina a of the IPL (Berson et al., 2002; Hattar et al., 2002). Upon comparing the dendritic arbors of M1 cells with those of M2 cells, we found that M2 cells had not only more total dendritic length and larger dendritic field diameters, but also more complex dendritic arbors. The morphology of these cells is consistent with those morphologically classified as Mouse (M) 6 RGCs by Coombs et al., 2006, a population containing ON, OFF, and bistratified melanopsin positive RGCs. Other studies have randomly labeled ipRGCs via either viral or immunological methods, and determined the proportion of M1 and M2 cells to be 40-55% and 40-45% of the total ipRGC population respectively (Viney et al., 2007; Baver et al., 2008). Additionally, viral labeling has indicated that the dendritic field of these cells tile and cover the entire mouse retina (Viney et al., 2007). Our data indicate extensive overlap of dendritic fields between these two subtypes, which implies distinct functionality in signaling light information to the brain. These findings underscore differences in the morphology of M1 and M2 cells that go beyond dendritic stratification and suggest differences in their functional properties.

Some of these functional differences between M1 and M2 cells were revealed by examining their intrinsic light responses. M1 cells responded to light with a significantly larger depolarization and light-evoked current than did M2 cells. Additionally, M1 cells displayed generally brighter EGFP signals than M2 cells, which

because in this mouse model EGFP is driven by the melanopsin promoter, could imply proportionally higher levels of melanopsin in M1 cells. This would be in agreement with the observation that M1 cells show brighter anti-melanopsin antibody staining than M2 cells (Hattar et al., 2006; Baver et al., 2008). Our findings of an ~10 fold higher sensitivity of M1 cells to 480 nm light provides preliminary support for this idea. Our values for both threshold and IR_{50} are in agreement with previously published values for sensitivity of the intrinsic ipRGC response (Berson et al., 2002; Dacey et al., 2005; Tu et al., 2005). These differences in light sensitivity among ipRGCs parallel the physiological diversity seen by Tu et al., 2005, who demonstrated that what they called "Type III" cells showed an ~10 fold higher sensitivity to 480 nm light than what they called "Type II" cells. Because the action spectrum of M2 cells has not yet been experimentally determined it is also possible that the peak action spectra of these two subtypes are not the same and could underlie the differences in sensitivity to 480 nm light.

The functional heterogeneity between M1 and M2 cells extended to various intrinsic membrane properties. M2 cells had a lower R_N and more hyperpolarized Vm than M1 cells. Overall, M2 cells were capable of reaching higher peak and average firing rates than M1 cells, and were capable of spiking over a greater range of depolarizing current injections. Again these findings correlate with the results of Tu et al., 2005 in that their physiological "Type II" cells were capable of higher peak firing rates than their physiological "Type III" cells. This implies that perhaps the diversity reported in their MEA study could parallel the diversity reported here, with physiological "Type III" cells correlating with M1 cells and physiological "Type II"

cells correlating with M2 cells. These differences in R_N and ability to sustain spiking raise the question of what differences in ion channel expression might exist across these two subpopulations. Size alone cannot account for the differences in R_N because when average R_N is divided by average Cm to normalize for cell size, M1 cells show greater than fourfold higher (27.6) MΩ/pF compared to M2 cells (6.3). It is likely that M2 cells have a higher K^+ conductance at rest, which could also account for their more hyperpolarized Vm. In terms of spiking, it is possible that M1 and M2 cells express different subtypes or amounts of voltage-gated sodium channels, or that different types of other voltage-gated ion channels could influence spiking in each of these subtypes.

Previous research has demonstrated that likely all ipRGCs receive synaptic signals from the outer retina (Wong et al., 2007; Schmidt et al., 2008). These underlying differences in the intrinsic membrane properties likely affect how these synaptic signals are relayed to the different brain centers. M2 cells have a low input resistance, suggesting that a relatively large amount of current is needed to drive spiking, in contrast to their small and insensitive photocurrent. These findings suggest that perhaps most of the signals transmitted by M2 cells are driven by synaptic currents. This is in contrast to M1 cells which have a high input resistance and large, sensitive photocurrent, which implies that the intrinsic photosensivity of M1 cells is more influential than that of M2 cells in terms of how this subpopulation signals light information to the brain. It has been determined that M1 cells form a discrete plexus with dopaminergic amacrine cells and may even signal to these cells via dendro-dendritic synapses (Viney et al., 2007; Zhang et al., 2008). The divergent properties of the membranes, intrinsic light responses, and dendritic stratification of M1 and M2 cells

implies further divergence of not only the types but also the relative influences of synaptic inputs on these two ipRGC subtypes. The synaptic influences upon M1 and M2 ipRGCs will be an important question for future research.

M1 and M2 cells specifically and differentially innervate non-image forming and image-forming brain centers, and only for some of these areas has the proportion of M1 versus M2 projections been examined (Hattar et al., 2006; Baver et al., 2008). It is possible that these two subpopulations serve distinct roles in signaling light information to different brain areas.

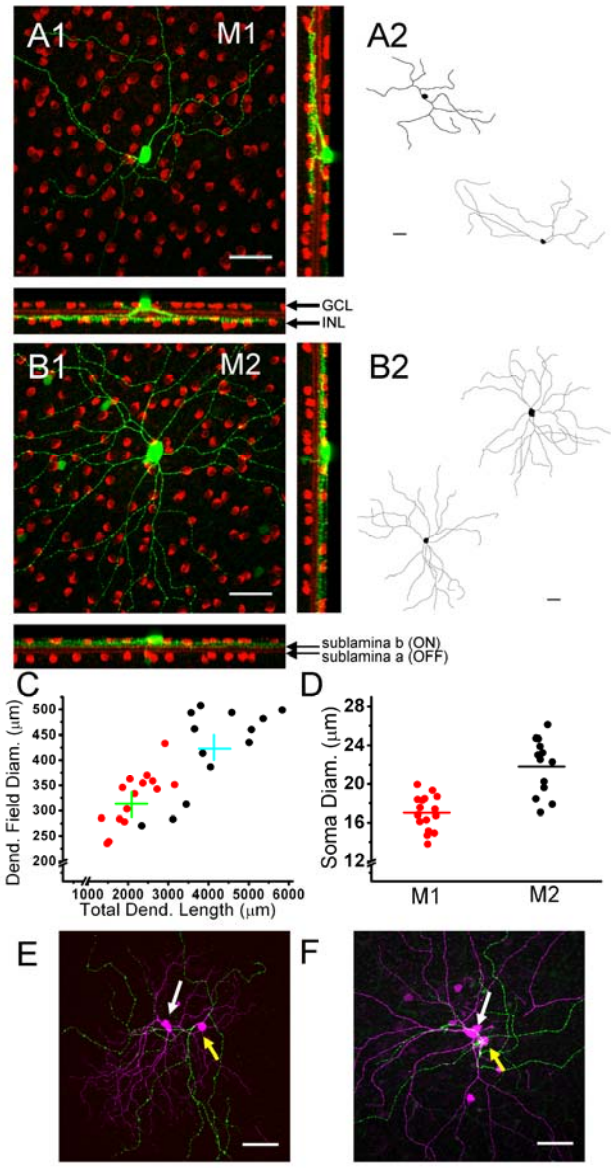

Figure 1. Morphological characteristics of M1 and M2 cells.
Whole mount retinas of M1 and M2 cells filled with neurobiotin (green) and immunostained for ChAT (red), a cholinergic amacrine cell marker (A1,B1). (A1), M1 cell with dendrites stratifying solely in sublamina a of the IPL. (A2) Tracings of M1 cells to show dendritic morphology. (B1) M2 cell with dendrites stratifying solely in the sublamina b of the IPL. (B2) Tracings of M2 cells to show dendritic morphology. (C) Dendritic field diameter and total dendritic length of M1 (red; n = 16) and M2 (black; n = 13) cells. Mean dendritic field diameter and total dendritic length of M1 (green) and M2 (blue) cells. (D) Soma diameter of M1 (red: n = 16) and M2 (black: n = 13) cells. Mean soma diameter of M1 (red bar) and M2 (black bar) cells. (E-F) M1 (green) and M2 (magenta) dendrites of neighboring M1 (yellow arrow) and M2 (white arrow) cells filled with neurobiotin. ChAT: choline acetyl transferase, IPL: inner plexiform layer. Scale bars: 50 µm.

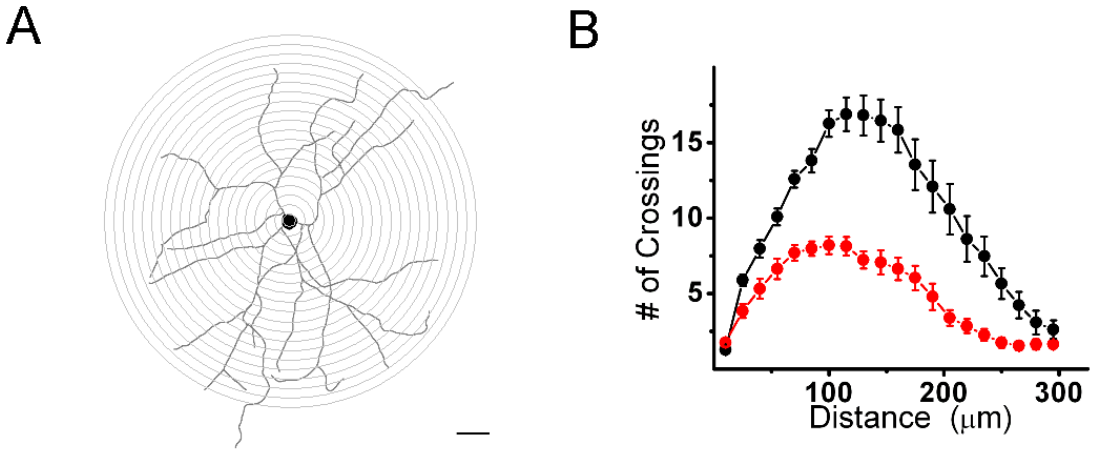

Figure 2. Sholl analysis of M1 and M2 dendritic arbors.
(A) Sholl analysis was performed starting 10 μm from the center of the soma with concentric circles at 15 μm radius steps. (B) Number of crossings measured from Sholl analysis shown from radii of 10 to 295 μm for M1 (red, n = 16) and M2 (black, n = 13) cells. Scale bar: 50 μm.

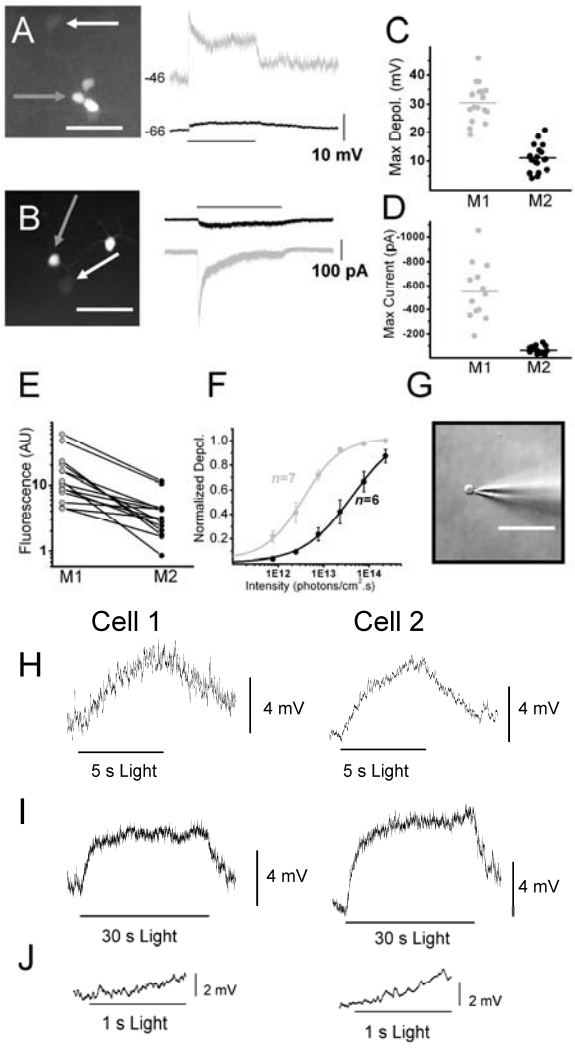

Figure 3. Intrinsic light responses of M1 and M2 cells in whole mount Opn4-EGFP mouse retinas.

All light responses recorded in the presence of synaptic blockers and TTX. (A, left panel), EGFP signal under epifluorescent illumination of M1 (gray arrow) and M2 (white arrow) cell targeted for dual whole cell current clamp recordings. (A, right panel), Responses in current clamp mode of M1 (gray trace) and M2 (black trace) cells shown in left panel to a 30 s white light stimulus. (B, left panel), EGFP signal under epifluorescent illumination of M1 (gray arrow) and M2 (white arrow) cell targeted for dual whole cell voltage clamp recordings. (B, right panel), Responses in voltage clamp mode of M1 (gray trace) and M2 (black trace) cells shown in left panel to a 30 s white light stimulus. (C) Maximum depolarization evoked by single 30 s white light stimulus measured in current clamp mode of M1 (gray; n = 17) and M2 (black; n = 19) cells. Mean depolarization of M1 (gray bar) and M2 (black bar) cells. (D) Maximum current evoked by single 30 s white light stimulus measured in voltage clamp mode of M1 (gray; n = 13) and M2 (black; n = 19) cells. Mean maximum current of M1 (gray bar) and M2 (black bar) cells. (E), Brightness (in AUs) of epifluorescence of EGFP signal for pairs containing one M1 and one M2 cell. (F) Irradiance response curves for M1 (gray; IR_{50} ~ 3.25 X 10^{12} photons/cm^2.s) and M2 (black; IR_{50} ~ 3.44 X 10^{13} photons/cm^2.s) generated by stimulating cells with increasing intensities of a 5 s 480 nm light stimulus. (G) Nucleated patch recordings were made in control solution from M2 cells (n = 5). (H-M) Average of 5-7 light responses recorded from nucleated patches of two cells (Cell 1 left panels,; Cell 2 right panels) in current clamp mode to a fixed, bright 5 s (*H*) or 30 s (I) white light stimulus. (L), Expanded view of first 1 s of 30 s light stimulation for Cell 1 (left panel) and Cell 2 (right panel). Scale bars: 50 μm. IR_{50}: irradiance yielding half-maximal response.

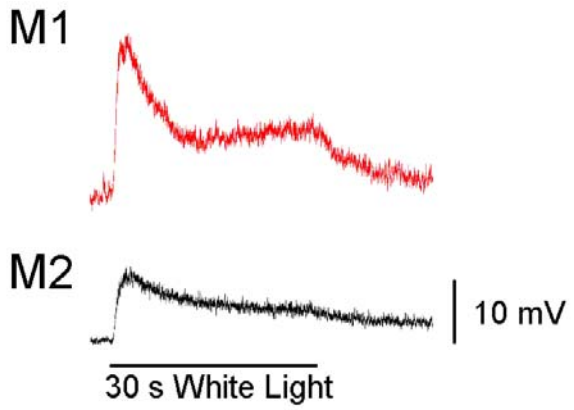

Figure 4. Intrinsic photosensivity of M1 and M2 cells.
Whole cell recordings of light evoked responses to a fixed, bright 30 s white light stimulus were performed from M1 (red trace, n = 4) and M2 (black trace, n = 6) cells in current clamp mode in a cocktail to block excitatory, inhibitory, and cholinergic receptors, synaptic transmission, electrical coupling, and spiking. Scale bar: 50 μm.

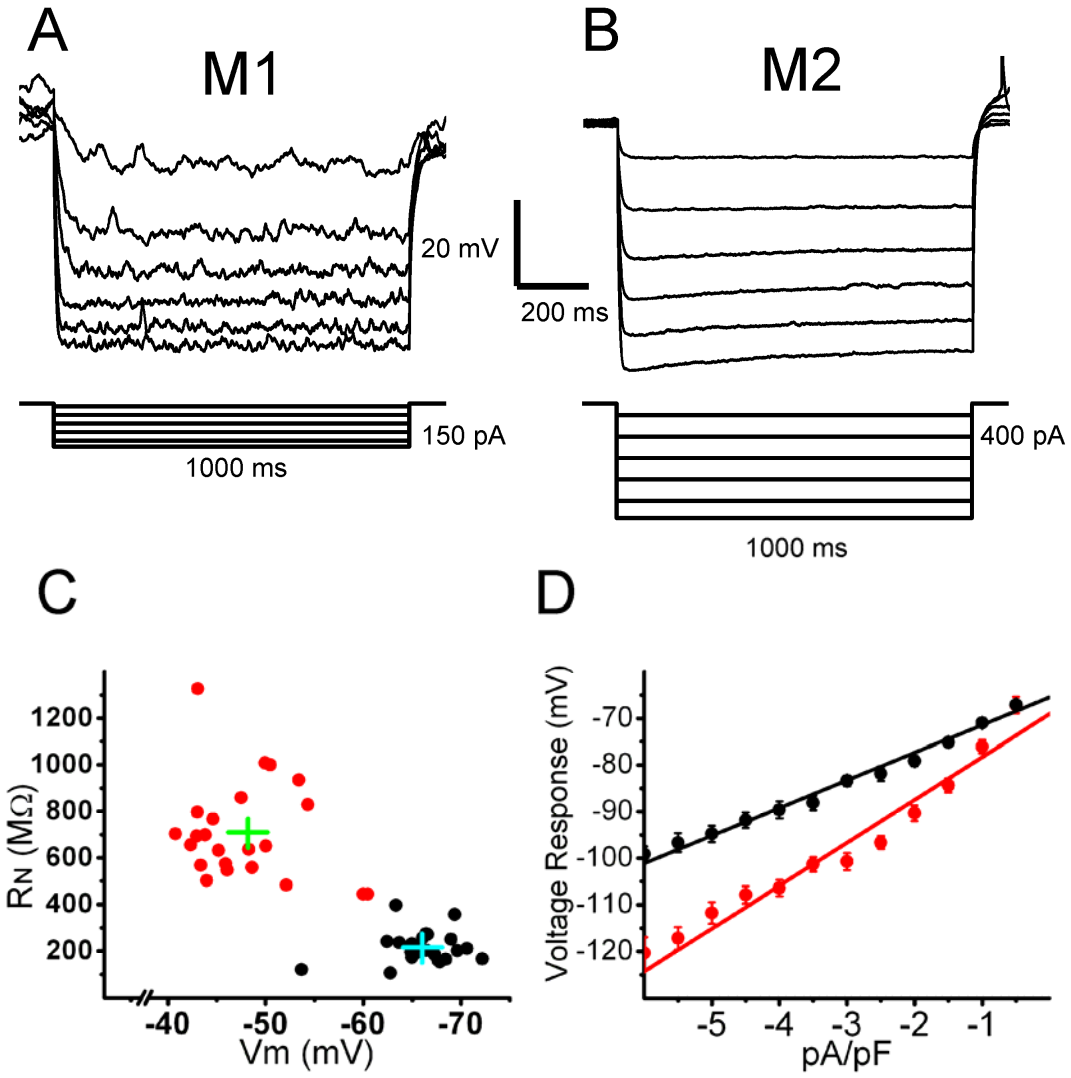

Figure 5. Responses of M1 and M2 cells to hyperpolarizing current pulses. Recordings were performed in the presence of synaptic blockers. (A-B) Responses of M1 (A) and M2 (B) cells to 1 s hyperpolarizing current injection. Values to the right of the steps indicate the maximum current injection shown. (C) R_N and Vm of M1 (red; $n = 23$) and M2 (black; $n = 25$) cells. Mean R_N and Vm shown for M1 (green bars) and M2 (blue bars) cells. (D) Mean ± SE voltage response of M1 (red, $n = 15$) and M2 (black, $n = 12$) cells to hyperpolarizing current steps. Current injections were divided by capacitance of the cells to facilitate averaging (Bin = 0.5 pA/pF). Points were fit with linear regression. R_N: input resistance. Vm: resting membrane potential.

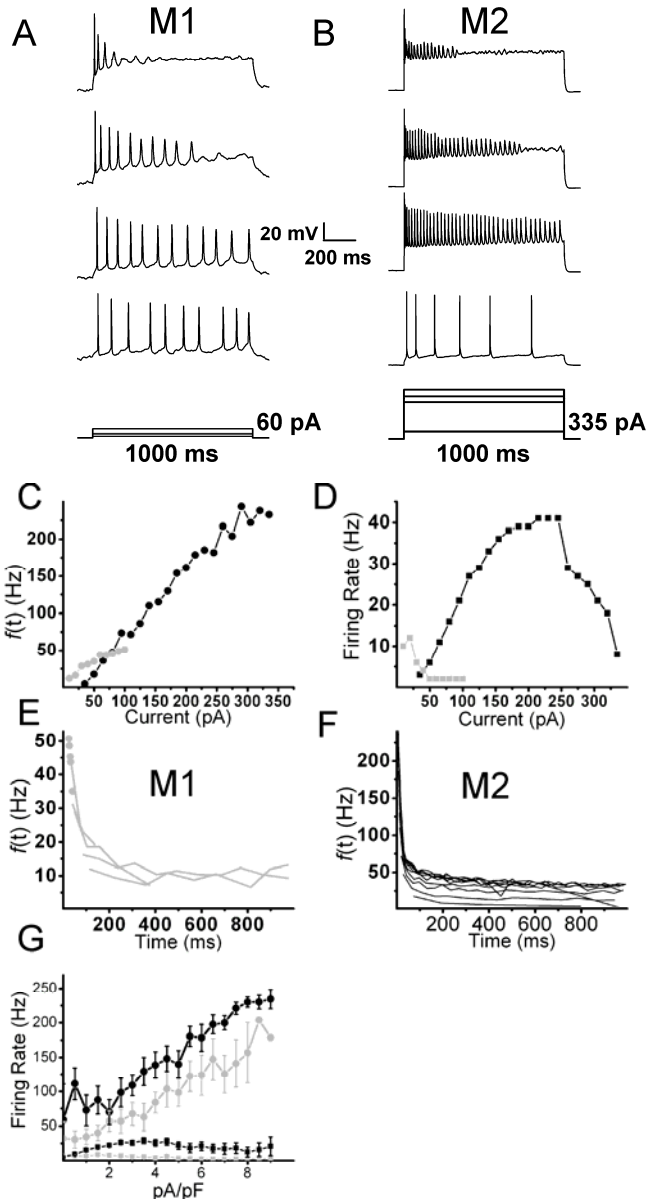

Figure 6. Responses of M1 and M2 cells to depolarizing current pulses.
Recordings were performed in the presence of synaptic blockers. (A-B) Representative response of M1 (A) and M2 (B) cells to 1 s depolarizing current injection. Values to the right of the current steps indicate maximum current injection shown. (C) Instantaneous frequency of the first interspike interval for M1 cell in (A) (gray) and M2 cell in (B) (black). (D) Average firing rate for duration of 1 s depolarizing steps for M1 cell in (A) (gray) and M2 cell in (B) (black). (E) Instantaneous frequency over time for M1 cell in (A). (F) Instantaneous frequency over time for M2 cell in (B). (G) Mean ± SE instantaneous frequency of the first interspike interval (circles) and mean ± SE firing rate (squares) during current injection for M1 (gray, n = 15) and M2 (black, n = 12) cells. Current injection for each cell was divided by its capacitance (Bin = 0.5 pA/pF) to facilitate averaging.

CHAPTER 4

Differential cone pathway influence on intrinsically photosensitive retinal ganglion cell subtypes

Schmidt TM and Kofuji P (2010) *J Neurosci* 30(48):16262-16271

ABSTRACT

A small subset of ganglion cells in the mammalian retina express the photopigment melanopsin and are intrinsically photosensitive (ipRGCs). These cells are the primary conduits through which photic information is relayed to non-image forming visual centers that mediate behaviors such as the pupillary light reflex and circadian entrainment. M1 and M2 cells comprise distinct morphological subpopulations of ipRGC, and possess physiological diversity in their intrinsic membrane properties and intrinsic light responses. Additionally, evidence now indicates that all ipRGCs receive photic information from rods/cones via synaptic signaling. It has recently been reported that OFF-stratifying M1 cells paradoxically receive input from the ON pathway within the OFF sublamina of the inner plexiform layer. The purpose of the current study was to examine the functional consequences of cone pathway signaling to M1 and M2 cells. Using pharmacological tools and single-cell recordings of synaptic responses in wild-type and melanopsin-null mice, we found that the ON pathway forms the primary excitatory synaptic input to both M1 and M2 cells. This input was much more influential in shaping the light-evoked responses and resting membrane properties of M2 cells than M1 cells. These findings indicate a surprising differential reliance upon cone-mediated phototransduction by ipRGC subpopulations. These findings also suggest that ipRGC subtypes signal diverse photic information to various non-image forming visual centers.

INTRODUCTION

In mammals, environmental irradiance information is conveyed to non-image forming centers in the brain primarily by a small population of retinal ganglion cells (RGCs) that express the photopigment melanopsin, rendering them intrinsically photosensitive (ipRGCs)(Berson et al., 2002; Hattar et al., 2002). A growing body of evidence indicates that ipRGCs also receive and integrate photic information from rods and cones via synaptic influences (Dacey et al., 2005; Wong et al., 2007; Goz et al., 2008; Guler et al., 2008; Hatori et al., 2008b; Schmidt et al., 2008; Pickard et al., 2009). ipRGCs project to brain areas involved in non-image-forming vision such as the olivary pretectal nucleus (OPN), which drives the pupillary light reflex, and the suprachiasmatic nucleus of the hypothalamus (SCN) which houses the main circadian pacemaker in the brain (Gooley et al., 2001; Hattar et al., 2002; Gooley et al., 2003; Hannibal and Fahrenkrug, 2004b; Hattar et al., 2006; Baver et al., 2008) .

Segregation of RGC dendrites in the retina is correlated with functional roles (Wassle, 2004). RGCs stratifying in the inner half of the inner plexiform layer (IPL) signal light increases via synaptic inputs from ON bipolar cells (BCs). RGCs stratifying in the outer half of the IPL signal light decrements via synaptic inputs from OFF BCs. ipRGCs can be divided into distinct subpopulations with distinct dendritic arborization within the IPL: M1 cells with dendrites stratifying in the OFF sublamina of the IPL, M2,4,5 cells with dendrites stratifying in the ON sublamina of the IPL, and bistratified (M3) ipRGCs with dendrites stratifying in both the ON and OFF sublaminas (Warren et al., 2003; Viney et al., 2007; Baver et al., 2008; Schmidt et al., 2008; Schmidt and Kofuji, 2009; Ecker et al., 2010). Surprisingly, M1 cells have recently been shown to

receive synaptic inputs from ON BCs within the OFF sublamina (Dumitrescu et al., 2009; Hoshi et al., 2009). However, the functional consequences of this atypical ON pathway input for the M1 cell light response have yet to be examined in detail. Furthermore, though On-stratifying M2 cells presumably receive ON pathway input, this has not been confirmed nor have the functional consequences of that input been addressed. M1 and M2 cells have been shown to have marked differences in their morphology, intrinsic membrane properties, and intrinsic light response (Schmidt and Kofuji, 2009), thus synaptic inputs could drastically and differentially affect the output of these physiologically and morphologically distinct ipRGC subtypes.

In the present study, we examined the functional influence of the cone-mediated ON pathway in shaping the light-evoked and resting discharge of M1 and M2 cells. We demonstrate that the ON pathway forms the primary excitatory synaptic input to both M1 and M2 cells. We find that this input is more influential in shaping the light-evoked and resting properties of M2 cells. M1 cells, however, rely primarily on the intrinsic photoreceptive system to respond to light stimulation. These results support the conclusion that ipRGC subpopulations signal distinct light information to various non-image forming centers in the brain.

MATERIALS AND METHODS

Animals

Recordings were performed on postnatal (P) 25-40 animals from the *Opn4-EGFP* mouse line described previously (Schmidt et al., 2008) as well as *Opn4-EGFP* mice crossed with animals on an $Opn4^{-/-}$ background provided by Dr. King-Wai Yau, Johns Hopkins University (Hattar et al., 2002). Animals were cared for in accordance with guidelines described in *Guide for the Care and Use of Laboratory Animals*, using protocols approved by the University of Minnesota Institutional Animal Care and Use Committee.

Electrophysiology

Dissections were performed as described previously (Schmidt et al., 2008). Briefly, animals were sacrificed by CO_2 asphyxiation and the eyes were enucleated in a dark room with minimal ambient light. Retinas were removed from eyecups under a standard dissection scope and placed in 95% O_2-5%CO_2 bicarbonate buffered Ames' solution (Sigma, St. Louis, MO) at room temperature. Prior to recording, retinas were treated with Ames' solution containing collagenase/hyaluronidase (240 and 1000 U/ml, respectively) at room temperature for 15 minutes to remove vitreous. Recordings were performed using an Axon 700B Amplifier (Molecular Devices, Union City, CA) with extracellular solution containing 95% O_2-5%CO_2 bicarbonate buffered Ames' solution at room temperature, which allowed for stable and robust synaptic responses. Recordings were made with fire-polished borosilicate pipettes (3-7 MΩ; Sutter Instruments, Novato, CA). For current clamp recordings, pipettes were filled with (in mM): 125 K-gluconate, 2 $CaCl_2$, 2 $MgCl_2$, 10 EGTA, 10 HEPES, 0.5 NaGTP, and 2

Na_2ATP, pH to 7.2 with KOH. For voltage clamp recordings, pipettes were filled with (in mM): 120 CsMethanesulfonate 2 $MgCl_2$, 5 Hepes, 5 EGTA, 0.5 $CaCl_2$, 1 Na_2ATP, 0.5 NaGTP, 2QX314, 5 TEA-Cl, 1 4-AP, pH to 7.2 with CsOH. Intracellular solutions also contained 10-20 µM Alexafluor-594 hydrazide (AF-594)(Invitrogen, Carlsbad, CA) and following recording dendritic stratification was classified by focusing in the proximal and distal layers of the IPL under epifluorescent illumination at 594 nm (Schmidt and Kofuji, 2009). Cells monostratifying in the OFF sublamina were classified as M1 while cells monostratifying in the ON sublamina were classified as M2. It is thus possible that the newly characterized M4 cells were included in our sample of M2 cells (Ecker et al., 2010). If a cell was bistratified or if its stratification could not be clearly identified, that cell was excluded from subsequent analyses. Current and voltage acquisitions were performed with a Digidata 1322 D/A and A/D converter connected to a personal computer running pClamp 10 software (Molecular Devices). Liquid junction potentials between the bath and electrode (14 mV for current clamp and 13 mV for voltage clamp solutions) were calculated using the Liquid Junction Potential Calculator (pClamp 10) and were corrected for in all recordings. Retinas were allowed to dark adapt for 5 min. prior to the first light stimulus, and any stimuli were placed 5 min. apart to allow the cell membrane potential to return completely to baseline.

Whole cell currents were analyzed off-line with Clampfit (Molecular Devices) or Igor Pro 6.0 (Portland, OR) over a 0.1 s sliding time window, and membrane potential values were measured from raw traces over a 1 s sliding time window to maximize the signal to noise ratio using Igor Pro 6.0 (Portland, OR). Resting membrane potential (Vm) values were calculated by taking the average membrane

voltage of the first 10 s of baseline prior to any light stimulation. For light response experiments if a cell's resting membrane potential (Vm) did not reach -40 mV negative current was injected to bring the resting membrane potential (Vm) to approximately -60mV.

Series resistance was noted in all recordings, but uncompensated and only recordings with series resistance of < 30 MΩ were included for analysis. Cell capacitance (Cm) and input resistance (R_N) were calculated from those currents evoked by stepping the cell potential to a 10 mV hyperpolarized value for 20 ms from a holding potential of -60 mV. Charge Q was estimated by time integration of evoked current during the step voltage. R_N was estimated from the steady-state evoked current during the step voltage. Light responses were defined as the maximum depolarization of the averaged trace during the first 30 s following light onset. Maximum current was defined as the maximum inward current measured from the .1 s smoothed trace during the 10 s light stimulus and total charge was calculated from the area measured during the 10 s light stimuli. For voltage clamp experiments, the 10 s prior to light stimulation was defined as baseline and set as the 0 current level. Irradiance-response experiments were performed and analyzed as described previously (Schmidt et al., 2008). For kinetics measurements, rise time (RT) was defined as the time for the cell membrane potential or whole-cell current to go from 10 to 90% of maximum, and decay time (DT) was defined as the time for recording to decline to 37% of the maximum value following light offset.

Curve fits for normalized, averaged irradiance-response data were determined by nonlinear regression using Origin 7.0 (MicroCal, Northampton, MA) according to

the logistic dose-response function: $y = A_2 + [(A_1-A_2)/(1+(IR/IR_{50})^{n_H})]$, where A_1 is the maximum response plateau, A_2 is the minimum response plateau, IR is irradiance, IR_{50} is the irradiance values that generate half-maximal response, and n_H is the Hill slope. Light stimuli for all experiments were full-field, broadband white light of 83 X 10^4 $\mu W.cm^{-2}$ (5.87 X 10^{16}, 5.03 X 10^{16}, 6.18 X 10^{14} photons.$cm^{-2}.s^{-1}$measured at 480, 500, and 360 nm respectively by interposing a narrow bandpass filter) delivered using a xenon lamp feeding the camera port. The field of the stimulus was sufficiently large to encompass the entire ipRGC arbors, and the focal plane of the stimulus was in the ganglion cell layer. A filter wheel fitted with various narrow bandpass (10 nm bandwidth) and neutral-density filters (Chroma Technologies, Rockingham, VT) and shutter (Lambda-3, Sutter Instruments) was used to control the intensity and duration of light stimuli. White light was used in most experiments so as to not preferentially activate either the melanopsin, M-cone, or rod photopigments, and so light intensities are reported in terms of the log relative intensity (LogI) for white-light experiments. For single intensity experiments, stimuli were delivered at -2LogI. Irradiance measurements were made with a calibrated radiometer model S370 (UDT Instruments, San Diego, CA). In spectral experiments, cells were stimuluated with full-field light at 360 nm or 500 light. Neutral density filters were interposed in the light path resulting in stimulation intensities of: -4.5, -3.0, -2,5, -2.0, -1.5, -1.0, -0.5, and -0 LogI for 360 nm and -7.5 to -0 LogI (increasing in intensity by 0.5 LogI/stimulation) for 500 nm stimuli. Threshold was defined as the intensity at which a light-evoked depolarization was first visible. The first stimulus of each wavelength was subthreshold and elicited no response in any cells tested. Though gradients of expression in M and S pigments have been

demonstrated across the retina (Applebury et al., 2000), we did not preferentially sample cells based on region.

For experiments where Vm was measured before and after L-AP4 application, cells were allowed 5-10 minutes of dark adaptation until a stable membrane potential was attained. After recording several minutes of baseline, recording continued as L-AP4 was applied and the cell was again allowed to attain a stable Vm. L-AP4 was then washed off and the cell Vm allowed to stabilize. Current was never injected in experiments were Vm was the variable being measured, and in this case cells where the Vm did not reach -40 mV were discarded.

Loose patch recordings were performed by obtaining a 100-700 MΩ seal and recording in voltage clamp mode with a holding potential of 0 mV. Cell-attached recordings were performed by obtaining a 1+GΩ seal and recording in voltage clamp mode with a holding current equal to that of the membrane potential (Perkins, 2006). Pipette solution consisted of (in mM) 150 NaCl, 10 HEPES.

Statistical analyses were performed using Origin 7.5 (MicroCal). Statistical comparison of means was performed using a Student's *t*-test or one-way *ANOVA* with Tukey's post-hoc test and significance was concluded when $P < 0.05$. Data are presented as mean ± SE.

Pharmacology

100 μM L-2-amino-4-phosphonobutyrate (L-AP4, a group III metabotropic glutamate receptor (mGluR) agonist) (Tocris, Ellesville, MO) that blocks photoreceptor to ON bipolar cell signaling (Slaughter and Miller, 1981), was sometimes included in the bath solution and used to silence ON pathway inputs.

In some experiments, we utilized Ionic Ames' media (Do et al., 2009) in which all calcium is replaced with cobalt to block synaptic transmission: (in mM) 120 NaCl, 23 $NaHCO_3$, 3.1 KCl, 0.5 KH_2PO_4, 2 $CoCl_2$, 1.2 $MgSO_4$, 6 Glucose. Ionic Ames' also differs from commercially available Ames' in that it is lacking the array of amino acids including L-Glutamine. 250 μM DL-2-amino-4-phosphonobutyrate (DL-AP4, a group III metabotropic glutamate receptor (mGluR) agonist) (Tocris, Ellesville, MO) was then bath applied to ensure no effect of this drug on resting membrane potential.

Immunocytochemistry

Immunocytochemistry, neurobiotin filling and image analysis of retinas were performed as published previously (Schmidt et al., 2008). Cells were filled with 0.3% neurobiotin (Vector Labs, Burlingame, CA) and visualized using Alexafluor-594-conjugated streptavidin (Invitrogen, Carlsbad, CA). Goat anti-choline acetyl transferase (ChAT) was used to stain cholinergic amacrine cells (Millipore, Bedford, MA) and visualized with Alexa-488 conjugated donkey anti-goat secondary antibody (Invitrogen). Colocalization of EGFP and Melanopsin immunostaining was performed using a custom-made antibody raised in rabbit to the N-terminus region of the mouse melanopsin protein and goat anti-GFP conjugated to FITC primary antibodies, as well as Alexa-594 conjugated anti-rabbit secondary antibody. Image acquisition was performed on an upright Olympus Fluoview 1000 laser scanning confocal microscope (Olympus, Center Valley, PA) Image J was used to adjust image brightness and contrast (http://rsb.info.nih.gov/ij/) and neurons were traced and analyzed using NeuroLucida (Microbrightfield, Williston, VT).

RESULTS

M1 and M2 cells retain similar morphology and intrinsic membrane properties in *Opn4*$^{-/-}$ mice

The purpose of this study was to examine the functional consequences of outer retinal signaling for ipRGCs. Because ipRGCs integrate synaptic input with their intrinsic, melanopsin-mediated photoresponse, it is difficult to measure synaptic inputs to ipRGCs in isolation. To circumvent this problem, we examined the light-evoked responses of ipRGCs in a mouse line which lacked expression of melanopsin (*Opn4*$^{-/-}$ mouse line where the melanopsin gene is replaced by a tau-lacZ coding sequence, generously provided by Dr. King-Wai Yau, Johns Hopkins University) (Hattar et al., 2002). In order to identify and target these cells for single cell electrophysiological recordings, we crossed the *Opn4* $^{-/-}$ mouse line with the previously characterized mouse line in which ipRGCs are labeled *in vivo* with enhanced green fluorescent protein (EGFP) (Schmidt et al., 2008). This strategy allowed us to identify and record from ipRGCs lacking the melanopsin protein and thus any intrinsic photosensitivity (Hattar et al., 2002). As expected, we observed excellent colocalization of EGFP and melanopsin in *EGFP-Opn4*$^{+/-}$ mice, with 242/250 (97%) of melanopsin positive cells costaining for EGFP, indicating the EGFP continues to reliably label ipRGCs in the *Opn4*$^{-/-}$mouse line (data not shown).

We first wanted to confirm that both M1 cells, with dendrites that stratify in the OFF sublamina, and M2 cells, with dendrites that stratify in the ON sublamina, are present in the *Opn4*$^{-/-}$ mouse because it has been reported that tau-lacZ is detectable only in the M1 cells (Hattar et al., 2002; Hattar et al., 2006; Baver et al., 2008) in *Opn4*$^{-}$

$^{-/-}$ mice. To test this, we recorded from EGFP positive cells in *Opn4*$^{-/-}$ mice with neurobiotin-filled pipettes. We then processed these retinas for expression of choline acetyl transferase (ChAT), a marker of cholinergic amacrine cells whose cell bodies are found in both the ganglion cell layer (GCL) and inner nuclear layer (INL), and visualized neurobiotin-filled cells with Alexafluor-594-conjugated streptavidin. The plexuses of cholinergic amacrine cells served as a visual marker for the OFF and ON sublaminas of the inner plexiform layer (IPL). Neurobiotin-filled EGFP positive cells revealed both Off- and On-stratifying cells in the *Opn4*$^{-/-}$ mouse, consistent with the presence of M1 and M2 subtypes in mice lacking expression of the melanopsin protein (Figure 1A,B).

Before examining the role of synaptic inputs in mediating the light-evoked responses of ipRGCs in the *Opn4*$^{-/-}$ mice, we needed first to examine whether ipRGCs develop normally in these mice. We carried out a quantitative examination of the morphological features of ipRGCs in *Opn4*$^{-/-}$ mice at adult stages and compared them with those obtained in WT mice to test for morphological abnormalities (Figure 1). Individual cells filled with neurobiotin were imaged and tracings were created to obtain an estimation of M1 and M2 cell soma size and dendritic field properties. M1 cells in the WT and *Opn4*$^{-/-}$ mice were similar in terms of their dendritic field diameter (WT: 391.2 ± 24.5 μm, $n = 12$; *Opn4*$^{-/-}$: 421.1 ± 35.8 μm, $n = 9$, $P > 0.05$, *t*-test), total dendritic length (WT: 2846.1 ± 379.0 μm, $n = 12$; *Opn4*$^{-/-}$: 2740.1 ± 278.2 μm, $n = 9$, $P > 0.05$, *t*-test), and soma diameter (WT: 16.9 ± 0.7 μm, $n = 12$; *Opn4*$^{-/-}$: 16.8 ± 0.6 μm, $n = 9$, $P > 0.05$, *t*-test). M2 cells were also similar in WT and *Opn4*$^{-/-}$ mice in their dendritic field diameter (WT: 445.4 ± 18.8 μm, $n = 7$; *Opn4*$^{-/-}$: 486.5 ± 22.1 μm, $n = 11$,

$P > 0.05$, *t*-test), total dendritic length (WT: 4919.8 ± 273.5 µm, $n = 7$; *Opn4*$^{-/-}$: 5244.8 ± 314.4 µm, $n = 11$, $P > 0.05$, *t*-test), and soma diameter (WT: 20.0 ± 0.6 µm, $n = 7$; *Opn4*$^{-/-}$: 20.8 ± 0.6 µm, $n = 11$, $P > 0.05$, *t*-test). Furthermore, when we analyzed the dendritic arbor complexity of ipRGCs utilizing Sholl analysis, we found that M1 and M2 cells were similar between WT and *Opn4*$^{-/-}$ (Figure 1C,D), demonstrating that ipRGCs develop normal morphology in the absence of the melanopsin protein.

To examine possible functional changes in *Opn4*$^{-/-}$ ipRGCs, we determined ipRGC intrinsic membrane properties and compared them with those in WT mice. We found that capacitance (Cm) and input resistance (R_N) of M1 cells in WT (Cm = 26.7 ± 2.2 pF, $n = 12$; R_N = 1027.6 ± 111.3 MΩ, $n = 12$) were not significantly different from M1 cells in the *Opn4*$^{-/-}$ mouse (Cm = 25.0 ± 2.2 pF, $n = 8$, $P > 0.05$, *t*-test; R_N = 1302.9 ± 173.0 MΩ, $n = 8$, $P > 0.05$, *t*-test). Similarly, in M2 cells, Cm and R_N were not significantly different between WT (Cm = 37.8 ± 2.5 pF, $n = 15$; R_N = 297.3 ± 18.3 MΩ, $n = 15$) and *Opn4*$^{-/-}$ (Cm = 31.1 ± 2.7 pF, $n = 7$, $p > 0.05$, *t*-test; R_N = 266.9 ± 25.7 MΩ, $n = 7$, $p > 0.05$, *t*-test). Consequently, lack of melanopsin expression in ipRGCs and therefore intrinsic photosensitivity did not affect the overall development of these cells, at least in regard to their structure and intrinsic membrane properties.

The ON pathway is the primary synaptic input to both M1 and M2 cells

Because M1 and M2 ipRGCs show apparently normal development in *Opn4*$^{-/-}$ animals, we proceeded to examine the light-evoked synaptic currents in *Opn4*$^{-/-}$ ipRGCs. We performed whole-cell voltage-clamp recordings in intact retinas from *Opn4*$^{-/-}$ mice. M1 and M2 cells were held at -73 mV and then light-evoked responses were recorded to a 10 s, bright, full-field, white light stimulus. Alexafluor-594 dye was included in the

pipette solution for these and all subsequent recordings so that following recordings, ipRGC subtypes could be identified using epifluorescence at 594 nm (Schmidt and Kofuji, 2009). Figure 2 shows examples of this experiment. Both M1 and M2 cells responded to light stimulation with an inward current at light onset (Figure 2A,B). Light-evoked currents in both M1 and M2 cells were sustained during the 10 s light stimulus although the currents decreased in amplitude during this time period. To test whether the light responses were mediated by the ON pathway, we subsequently added L-(+)-2–4-amino-4-phosphonobutyric acid (L-AP4) to the bath solution. L-AP4 is an agonist of the mGluR6 receptor and blocks the transmission of signals between rods/cones and ON BCs (Slaughter and Miller, 1981). Light-evoked currents in both M1 cells and M2 cells were completely abolished upon L-AP4 application (Figure 2A-C**;** M1: $n = 5$, M2: $n = 4$). The notable difference between the light-responses evoked in M1 and M2 cells was in their magnitude. Light-evoked currents amounted to only -58 ± 25.5 pA in M1 cells ($n = 10$) while in M2 cells they amounted to -200.3 ± 33.3 pA ($n = 8$) . These results indicate that the ON pathway does indeed signal light increases to ipRGCs by eliciting fast synaptic currents, albeit of distinct magnitude, in M1 and M2 cells.

To examine the efficiency of synaptically-mediated signaling to M1 and M2 cells, we performed whole cell current clamp recordings of light-evoked responses to 5 or 10 s light stimuli of ipRGCs in the *Opn4*$^{-/-}$ mouse. We found that all M1 cells responded to the light stimulus, but with a relatively weak depolarization that was somewhat sustained throughout the light stimulus and did not persist following stimulus offset (Figure 3A). M2 cells in the *Opn4*$^{-/-}$ mouse, in contrast, responded to bright

white-light with large, fast, and sustained depolarizations that terminated quickly following stimulus offset (Figure 3B). M2 cells had a significantly larger light-evoked maximum depolarization to a 5 s bright white-light stimulus than did M1 cells (M1: 13.1 ± 3.3 mV, $n = 8$; M2: 25.3 ± 2.4 mV, $n = 7$, $P < 0.05$). In general we observed more robust light-evoked action potential discharge in M2 than M1 cells, consistent with previous reports that M2 cells attain higher firing frequencies than M1 cells (Schmidt and Kofuji, 2009). As expected, light responses were completely and reversibly abolished for both M1 ($n = 3$) and M2 cells ($n = 3$) in the presence of L-AP4 (Figure 3A,B). These and the previous results indicate that the outer retinal input to ipRGCs is able to evoke light-mediated depolarization in both ipRGC subtypes, but that these responses are significantly larger in M2 than M1 cells. Differences in synaptic responses observed between M1 and M2 cells were not due to temperature because when preparations were acutely warmed to 34^{o}C, similar light response characteristics were observed for both M1 ($n = 3$) and M2 ($n = 3$) cells as seen at room temperature (data not shown).

To further examine the source of the synaptic input to M1 and M2 cells, irradiance response experiments using narrow-bandpass filtered 360 nm or 500 nm light were performed in *Opn4*$^{-/-}$ mice. At these wavelengths, light should effectively stimulate S-cone pigment (λ_{max} 360 nm) and M-cone pigment (λ_{max} 511 nm), with 360 nm light stimulating S-cone pigment ~ 10-fold more than M-cone pigment and 500 nm light stimulating M-cone pigment > 100,000 fold more than S-cone pigment (Jacobs et al., 1991; Nikonov et al., 2006). All M1 cells stimulated with either 500 nm ($n = 7$) or 360 nm ($n = 5$) light responded with a sustained depolarization (Figure 4A,C). The

average stimulus intensity at which a response was first observed in M1 cells was 12.3 ±0.7 log photons.cm^{-2}.s^{-1} for 500 nm light and 12.1 ±0.3 log photons.cm^{-2}.s^{-1} for 360 nm light, within the photopic range (Dacey et al., 2005) (Figure 4E). Furthermore, all M2 cells stimulated with either 500 nm (n = 7) or 360 nm (n = 5) light responded with a large, fast, and sustained depolarizations (Figure 4B,D). The average stimulus intensity at which a response was first observed for the M2 cell response was 11.6 ± 0.4 log photons.cm^{-2}.s^{-1} for 500 nm and 11.9 ± 0 log photons.cm^{-2}.s^{-1} for 360 nm, within the photopic range (Figure 4E)(Dacey et al., 2005). The fact that the threshold for M1 and M2 cell responses is within the photopic range indicates that the responses measured in this study are most likely originating from the cone ON pathway. This is unsurprising given that we are recording ipRGC responses in the isolated retinal preparation where the retina is physically isolated from the retinal pigmented epithelium so that cones, but not rods, are able to regenerate chromophore and avoid bleaching (Wang et al., 2009; Wang and Kefalov, 2009). Furthermore, the fact that ipRGCs receive light-evoked synaptic inputs at both 360 nm and 500 nm with similar thresholds indicates that both S (λ_{max} 360 nm) and M (λ_{max} 511 nm) cone pigments might participate in ipRGC synaptic signaling.

Integrated light-evoked current of M2, but not M1 cells, is dominated by ON pathway

Subsequent experiments were focused on comparing the magnitude of the contribution of intrinsic (i.e. melanopsin-mediated) and extrinsic (i.e. synaptically-mediated) light-evoked responses in M1 and M2 cells. We first recorded in voltage clamp mode from wild-type mice in which both the synaptic and melanopsin mediated

light responses are present. In these animals, M1 cell light responses to 10 s bright white light stimuli in WT mice were dominated by large, slow, and sustained inward currents similar to those reported previously (Berson et al., 2002; Schmidt and Kofuji, 2009) (Max Current: -206.3 ± 23.4 pA, $n = 8$; Total Charge: 796.9 ± 63.1 pC, $n = 8$) (Figure 5A,C-D). Light responses in WT M1 cells persisted for several seconds following the termination of light stimulus (DT: 3345.0 ± 651.3 ms, $n = 8$). M2 cells in WT mice showed a large, fast inward current that quickly terminated following light offset (Max Current: -125.0 ± 22.3 pA, $n = 6$; Total Charge: 829.4 ± 147.4 pC, $n = 6$; DT: 506.1 ± 72.0 ms, $n = 6$) (Figure 5A,C-D). In contrast, in *Opn4*$^{-/-}$ mice in which the intrinsic photosensitivity is lacking, M1 cells responded to light with a significantly smaller inward current and significantly less charge throughout the light stimulus compared to WT (Max Current: -58.0 ± 25.5 pA, $n = 10$, $P < 0.05$, *t*-test; Total Charge: 259.2 ± 111.5 pC, $n = 10$, $P < 0.05$, *t*-test) (Figure 5B,C-D). M1 cell light responses terminated significantly faster in the knockout mouse (DT = 324.1 ± 69.4 ms, $n = 10$, $P < 0.001$, *t*-test) compared to WT. M2 cells in the *Opn4*$^{-/-}$ mice, in contrast, had light responses that were indistinguishable from WT (Max Current: -200.3 ± 33.3 pA, $n = 8$, $P > 0.05$, *t*-test; Total Charge: 1333.7 ± 279.3 pC, $n = 8$, $P > 0.05$, *t*-test; DT: 366.9 ± 73.6 ms, $n = 8$, $P > 0.05$, *t*-test) (Figure 5B,C-D). Thus, light responses in M1 cells are driven primarily by their intrinsic photosensitivity and exhibit the long-latency and prolonged time course following light stimulation characteristic of melanopsin-mediated phototransduction. The dominant role of intrinsic photosensitivity for M1 cell photic responses is confirmed in the *Opn4*$^{-/-}$ mice where the light-evoked responses were significantly smaller than in WT. Light responses in M2 cells, on the other hand,

are driven primarily by the ON pathway via synaptic transmission at photopic light intensities. Light responses exhibit comparatively faster kinetics of activation and termination than M1 cells, and responses of M2 cells were largely preserved in the melanopsin null mice.

ON pathway input strongly modulates light response of M2 ipRGCs

Our results recorded in voltage clamp indicate that the integrated light-evoked current of M1 cells is dominated by the intrinsic photoreceptive system while the integrated light-evoked current of M2 cells is dominated by cone-mediated ON pathway input at bright light intensities. Given the diversity of the intrinsic membrane properties (Schmidt and Kofuji, 2009), and degree of intrinsic and extrinsic influences on M1 versus M2 cells, we hypothesized that the ON channel inputs might differentially modulate the light response of these two distinct ipRGC subtypes. To test this, we recorded light responses in whole-cell current-clamp mode from WT M1 and M2 ipRGCs to a 5 s bright, full-field, white light stimulus first in control Ames' media and then following inclusion of 100 μM L-AP4 in bath to selectively silence ON channel inputs. Both M1 and M2 cells responded to the light stimulation with large, rapid depolarizations (Figure 6A,B). Upon bath application of L-AP4, M2 cells responded to light with small, sluggish depolarizations (Figure 6B), consistent with the intrinsic, melanopsin-mediated response of M2 cells previously reported (Schmidt et al., 2008; Schmidt and Kofuji, 2009). M1 cells, however, continued to respond to bright light stimulation with large depolarizations, and only a small decrease in latency (Figure 6A). These effects were reversed upon washout (Figure 6A,B). When the maximum depolarization evoked by light was quantified, M2 cells did indeed show a significant

decrease in the maximum light-evoked depolarization in the presence of L-AP4 (control: 24.1 ± 2.4 mV vs. L-AP4: 8.7 ±1.6 mV, $n = 9$, $P < 0.05$, One-way *ANOVA*)(Figure 6C). L-AP4 application to M2 cells also resulted in a significant increase in10-90% rise time (RT) (2.1 ± 0.7 s, $n = 9$, $P < 0.05$, *t*-test) as well as a significant increase in decay time (DT) to 37% of maximum (20.8 ± 5.4 s, $n = 7$, $P < 0.01$, *t*-test). The light-evoked depolarization of M1 cells in control vs. L-AP4 conditions did not change (control: 21.1 ± 1.1 mV vs. L-AP4: 19.3 ± 1.6 mV, $n = 8$, $P > 0.05$, One-way *ANOVA*) (Figure6C). Furthermore, there were no significant changes in RT (0.18 ± 0.2 s, $n = 8$, $P > 0.05$, *t*-test) and DT (0.07 ± 0.8 s, $n = 8$, $P > 0.05$, *t*-test) following L-AP4 application to M1 cells. These results indicate that the On-pathway makes a relatively minor contribution to the total light-evoked depolarization observed in M1 cells and does not significantly affect the latency at light onset or offset for the M1 population as a whole. In contrast, the ON pathway evokes a sustained light-evoked depolarization in M2 cells that served to enhance both the magnitude and kinetics of the light response at photopic light intensities.

To ensure that the patterns observed were not attributable to washout of the intrinsic response due to dialysis of the intracellular contents as a result of the whole-cell recording mode, we also performed extracellular loose-patch or cell-attached recordings of M1 and M2 cells in the WT mouse (see Methods). We found that under control conditions, M2 cells ($n = 4$) responded to increasing intensities of white light with short-latency responses of increasing spike frequency similar to those observed in whole-cell recordings (Figure 7). M2 cells also showed cessation of firing at light offset followed by a rebound in the firing rate, consistent with patterns observed in whole-cell

current clamp mode (Figure 6B). Furthermore, application of L-AP4 to M2 cells (n = 5) resulted in a substantial reduction of both spike frequency and slower kinetics at light onset and offset (Figure 7), with cells continuing to fire following light offset in the presence of L-AP4. These patterns again support our observations made in whole-cell recordings (Figure 6B). Loose-patch or cell-attached recordings of M1 cells (n = 5) to increasing intensities of white light revealed responses that were relatively sluggish at lower light intensities and sustained at light offset, again similar to our whole cell recordings and consistent with the firing being driven primarily by melanopsin-mediated phototransduction (Figure 8). Furthermore, upon L-AP4 application, no substantial differences were observed in the kinetics of the light response of M1 cells at light onset or offset (n = 3), again similar to the sustained depolarization at light offset observed our whole-cell recordings (Figure 8, Figure 6A). Collectively, our extracellular recording results support the results obtained in our whole-cell recordings that the primary influence on the light response of M2 cells is driven by the ON pathway while M1 cells rely primarily on their intrinsic, melanopsin-mediated phototransduction.

We next investigated the effects of cone-driven ON pathway input on the intensity-response relations of M1 and M2 cells. Because M1 cells have been shown to be ~ 1 log unit more intrinsically sensitive to 480 nm light than M2 cells (Schmidt and Kofuji, 2009), we expected that the ON channel input would differentially influence the overall light sensitivity of these two subtypes. To test this, we recorded responses in whole-cell current clamp mode to increasing intensities of white light in the absence or presence of L-AP4. Both M1 and M2 cells responded to increasing intensities of light

with increasing depolarization under both conditions. We observed small, fast synaptic inputs to M1 cells at low light intensities (Figure 9A) that were not observed in the presence of L-AP4 (Figure 9*B*). These synaptic responses were often first observed at intensities at or just sub-threshold to the intrinsic response, which could clearly be discerned as a separate component at low light intensities in some M1 cells. When the normalized, maximum depolarization of M1 cells was averaged for each light intensity, we measured a significant increase in the maximum depolarization in control vs. L-AP4 only at higher light intensities (-4.5LogI and -4LogI, control: $n = 8$, L-AP4 $n = 5$, $P < 0.05$, *t*-test) but not near threshold. These results indicate that the ON channel did not significantly influence the sensitivity of M1 cells either near threshold or near the IR50 (Figure 9A-C), and may actually serve to saturate the light response at lower light intensities. We also observed robust synaptic inputs to M2 cells at low light intensities in control conditions. The threshold for synaptically-evoked responses occurred at intensities that were at least a log unit lower than the threshold for M2 cells observed in the presence of L-AP4 (Figure 9D,E). When the normalized maximum depolarization of M2 cells was averaged for at each light intensity, we measured a significant increase in the normalized maximum depolarization in control vs. L-AP4 at intensities near threshold (-6LogI, -5.5LogI, -5LogI, control: $n = 8$, L-AP4 $n = 6$, $P < 0.05$, *t*-test), but not at higher light intensities. In the case of M2 cells, the ON pathway greatly enhanced the response of M2 cells near threshold and served to increase the dynamic range of the response (Figure 9F). These experiments again demonstrate that the cone-driven On-pathway has fundamentally distinct roles in shaping the light-evoked responses and sensitivity of M1 and M2 cells.

ipRGCs are modulated by the ON pathway in the dark

In addition to mediating light-evoked signaling, previous research has demonstrated that the resting membrane potential (Vm) of ON and OFF RGCs is modulated by the ON pathway at rest (Zaghloul et al., 2003; Margolis and Detwiler, 2007). Because M1 and M2 ipRGCs have dendrites that stratify in the OFF and ON sublamina of the inner plexiform layer (IPL) respectively, we hypothesized that the ON pathway might also differentially modulate the resting discharge of M1 and M2 ipRGCs at rest. To test this hypothesis, we targeted single ipRGCs for whole-cell, current-clamp recordings. After whole-cell access, we allowed cells to dark adapt for 5-10 minutes and then continuously monitored Vm in the absence and then presence of 100 μM L-AP4 (Figure 10A,B). Compared to control conditions (Vm = -58.4 ± 1.8 mV), M2 cells were significantly more hyperpolarized in the presence of L-AP4 (Vm = -63.0 ± 1.5 mV, $n = 9$, *t*-test, $P < 0.01$; Figure 10B-D), consistent with patterns observed by previous studies of other ON RGC types (Margolis and Detwiler, 2007). M1 cells, in contrast, depolarized slightly upon L-AP4 application (-50.5 ± 0.7 mV) when compared to control conditions (-52.9 ± 1.1) though this trend was not significant ($n = 8$, $P = 0.053$, *t*-test; Figure 10A,C-D). DL-AP4 application in ionic Ames' solution containing 2mM cobalt (Do et al., 2009 and see Methods) to block all other synaptic transmission did not result in any changes in Vm of either M1 ($n = 3$) or M2 cells ($n = 4$) (data not shown), indicating that the effect of L-AP4 was not due to direct action on the ipRGCs themselves. Collectively these results indicate that the ON pathway exerts a tonic excitatory influence on M2 cells at rest, but not on M1 cells.

Note: "Atypical" M1 cells

Very infrequently (n = 4/36 M1 cells), we encountered M1 cells with physiological characteristics that mimicked those of M2 cells. "Atypical" M1 cells hyperpolarized in response to L-AP4 application in the dark (Figure 11A) and showed fast onset and offset kinetics when stimulated with light with little or none of the after-discharge following light offset typical of M1 cells (Figure 11B-D). These cells were qualitatively identifiable as outliers, and thus not included in the analyses though each cell had dendrites that clearly all stratified in the OFF sublamina of the IPL (Examples of each "Atypical" M1 cell can be seen in Figure 11). "Atypical" M1 cells have relatively dim EGFP signals and large dendritic arbors that extend through the ON sublamina before diving down into the OFF sublamina of the IPL (Schmidt TM and Kofuji P, unpublished observations). These cells are very rare, and may be a developmental anomaly or an actual physiological subset of the M1 population.

DISCUSSION

We have utilized pharmacological manipulations in a transgenic mouse line in which ipRGCs are labeled *in vivo* with EGFP in a wild-type or melanopsin null genetic background to examine the relative influence of the ON pathway on the light-evoked and resting discharge of M1 and M2 cells. The primary finding of this study is that the ON pathway constitutes the dominant excitatory synaptic input to both M1 and M2 cells at bright light intensities. While this pathway is critical in shaping the light-evoked and resting discharge of M2 cells, the M1 cells are only modestly affected. Instead, M1 cells rely primarily on melanopsin-mediated phototransduction to convey photic information to non-image forming visual centers.

M1 cells morphologically resemble the OFF RGCs in that the dendrites of M1 cells narrowly stratify in the outermost layer of the OFF sublamina of the IPL while the dendrites of M2 cells stratify narrowly in the innermost layer of the IPL, morphologically paralleling ON RGCs (Viney et al., 2007; Schmidt et al., 2008; Schmidt and Kofuji, 2009). It has been suggested that because M2 cells have such small, insensitive melanopsin-mediated photocurrent and low input resistance that synaptic inputs might be more influential in shaping the light response this ipRGC subtype (Schmidt and Kofuji, 2009; Bailes and Lucas, 2010). M1 cells, in contrast, with their large, sensitive melanopsin-mediated photocurrent and high input resistance, might be less influenced by synaptic inputs. Our results support these hypotheses, extending findings from our previous work to encompass diversity of not only intrinsic, but also synaptically-evoked influences on M1 and M2 cell light responses. Recordings from *Opn4*$^{-/-}$ mice indicate that M2 cells receive a large, excitatory cone-driven ON

pathway-synaptic input with light-evoked currents that displayed relatively fast kinetics upon light onset and offset and relatively sustained amplitude during the stimulus. Light-evoked synaptic currents in M1 cells were qualitatively similar, but their overall magnitude was consistently smaller than those recorded in M2 cells. These differences in the excitatory drive by the cone-mediated ON pathway were also seen in current clamp recordings, with larger depolarizations for M2 cells than M1 cells. Furthermore, when we measured the integrated light-evoked current and depolarizations in WT mice, we found that with melanopsin-mediated signaling intact, the ON pathway's contribution to the M1 cell light response was minimal. However, the light responses of M2 cells were largely unchanged in mouse lines where melanopsin mediated signaling was intact (WT) or nonfunctional (*Opn4*$^{-/-}$). Furthermore, application of L-AP4 reduced the amplitude and slowed the kinetics of the M2 cell light response, indicating that the ON pathway is the dominant influence during light stimulation for M2 cells.

We have demonstrated that M2 cells are depolarized by the ON pathway at rest, indicating that there is a tonic excitatory drive to M2 cells, even in the dark, that can be blocked by L-AP4 application. M1 cells, in contrast, are possibly hyperpolarized by the ON pathway in the dark, but the effect of L-AP4 application in depolarizing M1 cells was not significant. These data are in line with results reported previously indicating that other types of ON RGCs are modulated by the ON pathway at rest (Margolis and Detwiler, 2007). M2 cells have a very hyperpolarized Vm when synaptic inputs are blocked, as well as a low input resistance (Schmidt and Kofuji, 2009). It is thus possible that a tonic-depolarizing drive via the ON pathway serves to keep M2 cells close to or at threshold for action potential firing. The lack of a tonic excitatory drive to

M1 cells in the dark is suggestive that their input synapses have a relatively low rate of basal glutamate release in the dark or are perhaps occurring at such low densities that they are not able to influence Vm, especially with the large inhibitory drive these cells receive at rest (Wong et al., 2007; Dumitrescu et al., 2009).

Electron microscopy and immunohistochemical studies have identified synaptic contacts to ON and OFF-stratifying ipRGCs (Belenky et al., 2003; Jusuf et al., 2007; Ostergaard et al., 2007). Recent work in both rodent and rabbit has identified *en passant* or ectopic synapses of ON cone bipolar cells onto M1 ipRGCs as well as dopaminergic amacrine cells in the OFF sublamina of the IPL (Dumitrescu et al., 2009; Hoshi et al., 2009). The study by Dumitrescu et al. (2009) demonstrated functionality of the ON inputs to the displaced M1 cells, the somas of which are displaced in the INL and the dendrites of which never pass through the ON sublamina. Furthermore, in the macaque, both ON and OFF-stratifying ipRGCs (possible corollaries of M1 and M2 cells) were reported to receive similar excitatory drive at light onset, but differential influence of the ON pathway was not reported (Dacey et al., 2005). Our study provides the first evidence that excitatory synaptic sites are not equally effective in driving light-evoked responses in ipRGC subtypes. Our approach utilizing melanopsin-null mice to measure purely synaptic currents and depolarization of both non-displaced M1 and also M2 cells has allowed, for the first time, examination of the properties of the synaptic inputs throughout the duration of the light stimulus without contamination by melanopsin-mediated signaling. The synaptic currents and depolarizations evoked in both M1 and M2 cells are relatively sustained in comparison to other ganglion cell types (Wong et al., 2007). It has been suggested that perhaps ON bipolar cell inputs within

the OFF sublamina are more sustained than conventional ON bipolar cell synapses within the ON sublamina (Dumitrescu et al., 2009). However, the responses of M1 and M2 cells appear qualitatively similar, indicating that perhaps these subtypes of ipRGC could share input from a single cone bipolar cell subtype, which could be Type 6, 7 or 8 (Viney et al., 2007; Dumitrescu et al., 2009), with M1 cells receiving inputs within the "accessory ON sublamina" reported by Dumitrescu et al. (2009) and M2 cells receiving these inputs via more conventional synapses with cone ON bipolar cells in the ON sublamina. M1 synaptic responses measured in melanopsin-null mice in both current and voltage clamp were consistently smaller than those of M2 cells, which could be due to the relatively low density of synapses to M1 cells relative to M2 cells (Jusuf et al., 2007; Dumitrescu et al., 2009). Alternatively, the smaller responses of M1 cells could be due to smaller net excitation due to the presence of inhibitory inputs (Wong et al., 2007).

Stimulation of both M1 and M2 ipRGCs with narrow-bandpass filtered 500 nm or 360 nm light resulted in responses in both subtypes, indicating that both the S and M cone pigments might be involved in synaptic signaling to ipRGCs. Furthermore, because, in our preparation, the threshold for responses to both of these wavelengths occurred within the photopic range (Dacey et al., 2005), it can be concluded that we are principally measuring cone signaling to ipRGCs. This is also supported by the fact that most of the recordings were performed in response to bright white light after partial light adaptation of the isolated retinal preparation with epifluorescent illumination to localize EGFP positive cells.

M1 and M2 cells have been demonstrated to differentially and specifically project to different NIF nuclei in the brain, with M1 cells forming the primary projection to the SCN but both M1 and M2 cells substantially innervating the OPN (Baver et al., 2008; Ecker et al., 2010). Recent studies have highlighted an important role for rod, but apparently not cone, phototransduction in circadian photoentrainment (Altimus et al., 2010; Lall et al., 2010). Thus, our findings that M1 cells are not highly influenced by the cone pathway together with the fact that M1 cells form the primary projection to the SCN indicate that perhaps M1 cells serve mainly to relay rod and melanopsin-mediated information to NIF visual centers, while M2 cells are the primary conduit for cone-mediated information. This would implicate M2 cells in behaviors highly influenced by cone inputs through ipRGCs, such as the PLR (Lall et al., 2010). One might predict a larger influence of rod mediated input on M1 vs. M2 cell light responses, and this will be an important area for future study.

In summary, we demonstrate the distinctive synaptic influence from the ON pathway on M1 and M2 cells. Our results suggest that M1 cells carry primarily information related to melanopsin-mediated signaling while M2 cells are the primary conduit for cone-mediated signaling to non-image forming brain centers. These findings further support the idea that distinct ipRGC subtypes may signal distinct light information to the brain and have distinct influences on non-image forming behaviors.

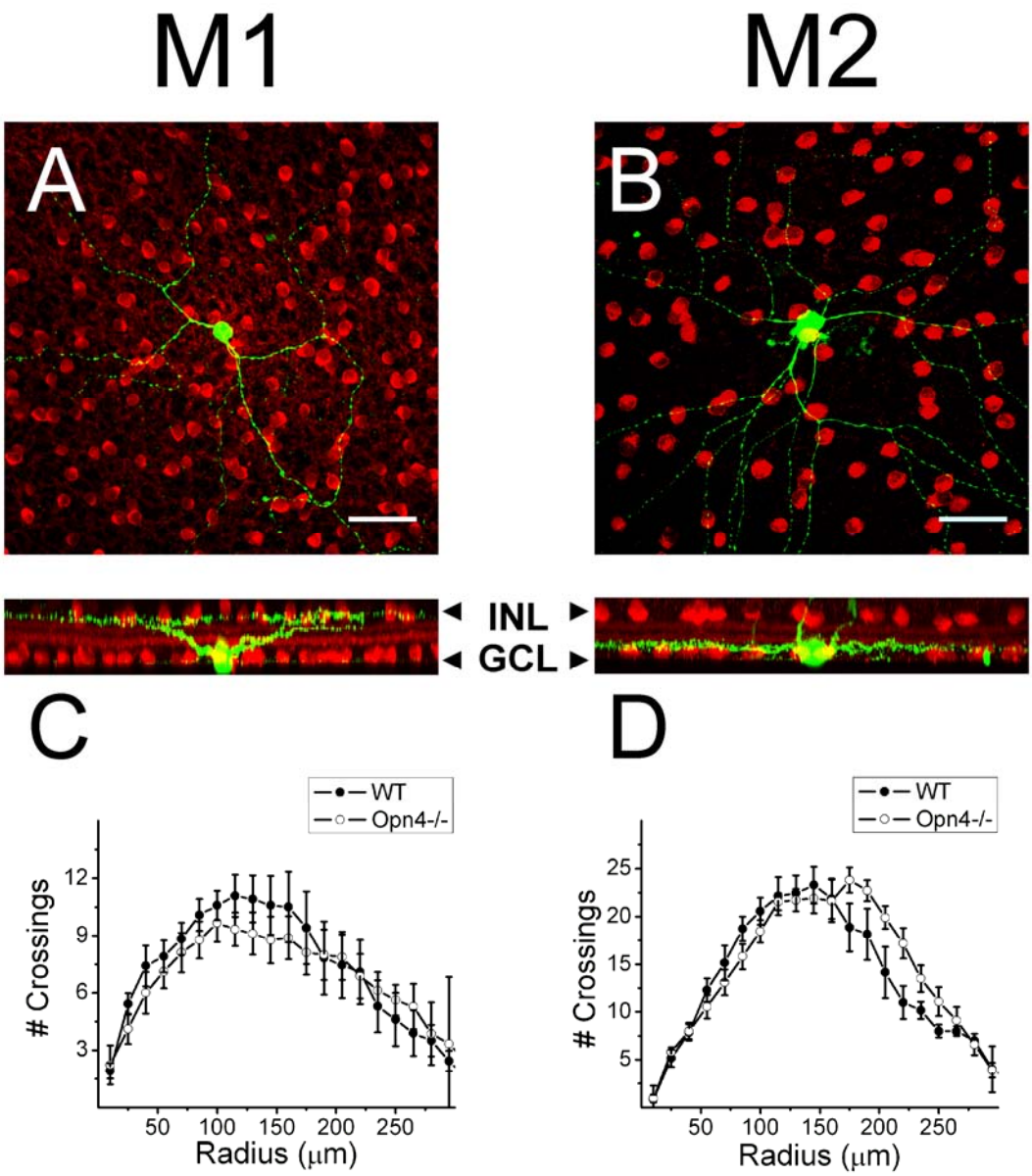

Figure 1. ipRGC morphology in *Opn4*$^{-/-}$ mice
(A,B) Confocal stacks of whole-mount retinas in which an M1 and M2 cell have been filled with neurobiotin (green) and co-stained for ChAT (red), a cholinergic amacrine cell marker. (A) M1 cell with dendrites stratifying near the border of the INL in the OFF sublamina of the IPL. (B) M2 cell with dendrites stratifying near the GCL in the ON sublamina of the IPL. Note: processes visible extending through IPL are those of Müller cells, which commonly take up dye during the patching procedure. (C-D) Sholl analysis (15 μm steps from starting diameter of 10 μm) of M1 (C) and M2 (D) dendritic arbors in WT (black circles) and *Opn4*$^{-/-}$ (open circles) mouse lines. ChAT, choline acetyl transferase, INL, inner nuclear layer, IPL, inner plexiform layer, GCL, ganglion cell layer. Scale bar: 50 μm (A,B).

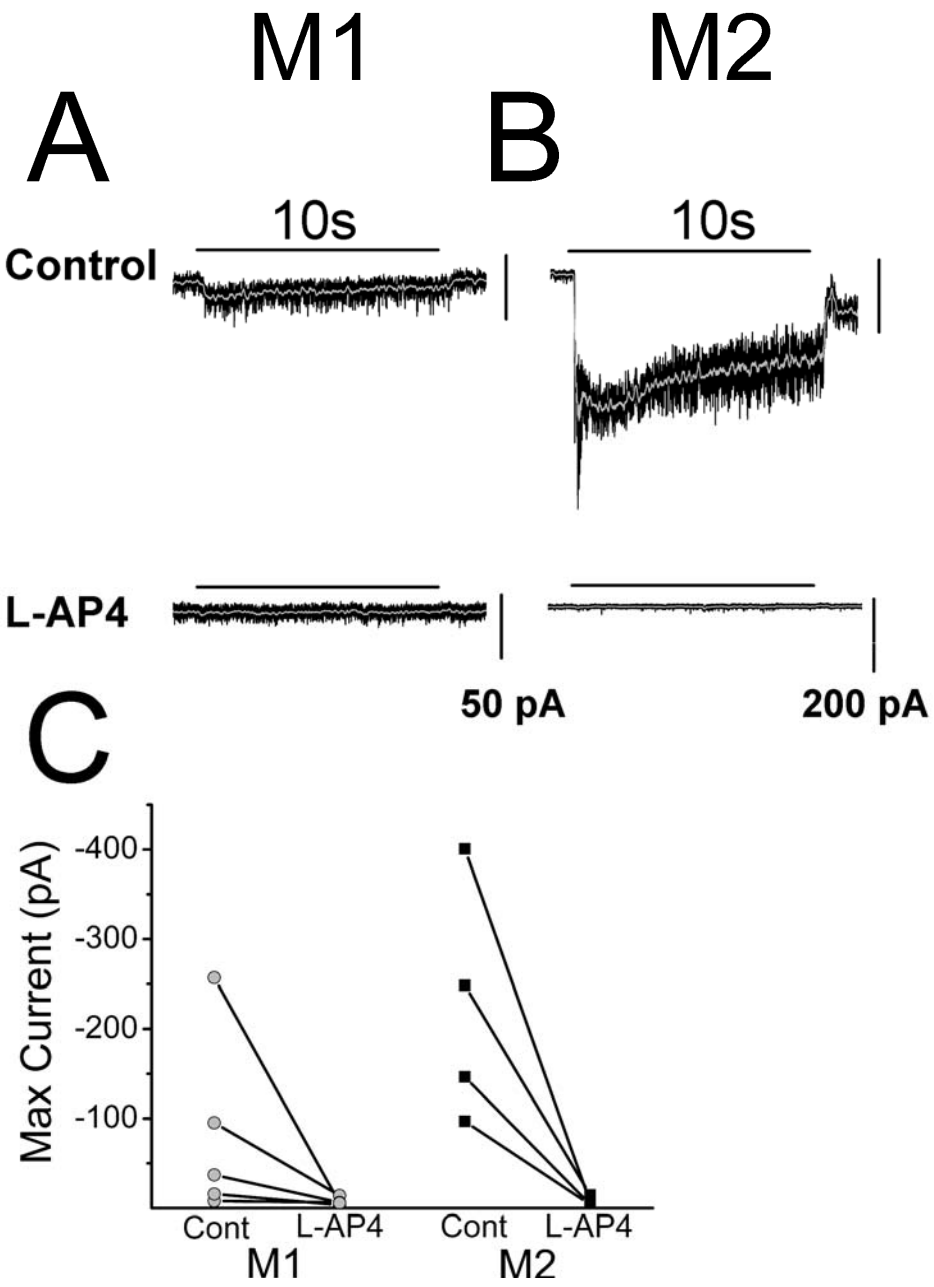

Figure 2. ON pathway-evoked currents in M1 and M2 cells of *Opn4*$^{-/-}$ mice
Voltage clamp recordings (V_{Hold} = -73 mV) of light-evoked current in M1 and M2 ipRGCs of the *Opn4*$^{-/-}$ mouse line to a 10 s, full-field, bright white-light stimulus at -2LogI before and after 100 μM L-AP4 application. (A-B) Light-evoked inward current of M1 (A) and M2 (B) cell in control (top panels) and after 5 min of 100 μM L-AP4 application (bottom panels) (*n* = 5 M1; *n* = 4 M2). (C) Maximum light evoked current in M1 (gray) and M2 (black) cells before and after L-AP4 application. Light-evoked currents were completely abolished following blockade of the ON pathway input. Gray line indicates 0.1 s smoothing of membrane current.

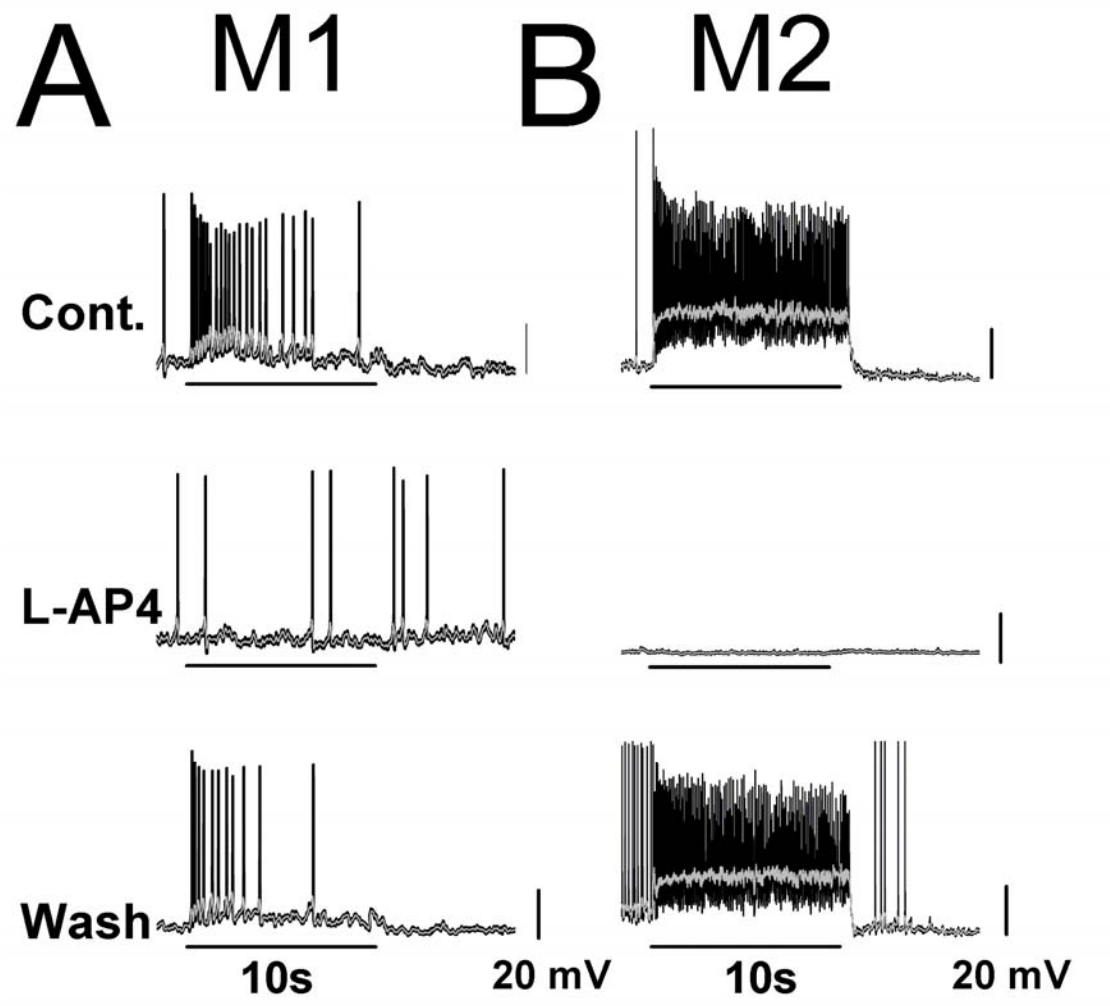

Figure 3. ON pathway-evoked depolarization in M1 and M2 cells of *Opn4*$^{-/-}$ mice
Current clamp recordings in Opn4$^{-/-}$ mouse line of M1 and M2 cell responses to a bright white light stimulus. (A) M1 cell response in current clamp mode to 10 s bright, full-field, white-light stimulus at intensity of -2LogI in control solution (top panel), in the presence of 100 μM L-AP4 in the bath (middle panel), and after washout (bottom panel). Light responses of M1 cells in *Opn4*$^{-/-}$ mouse were completely abolished in the presence of L-AP4. (B) M2 cell responses in current clamp mode to 10 s bright, full-field, white light stimulus at intensity of -2LogI in control solution (top panel), in the presence of 100 μM L-AP4 in the bath (middle panel), and after washout (bottom panel). Light response of M2 cells in *Opn4*$^{-/-}$ mouse were completely abolished in the presence of L-AP4. Gray lines indicate 0.1 s smoothing of membrane voltage.

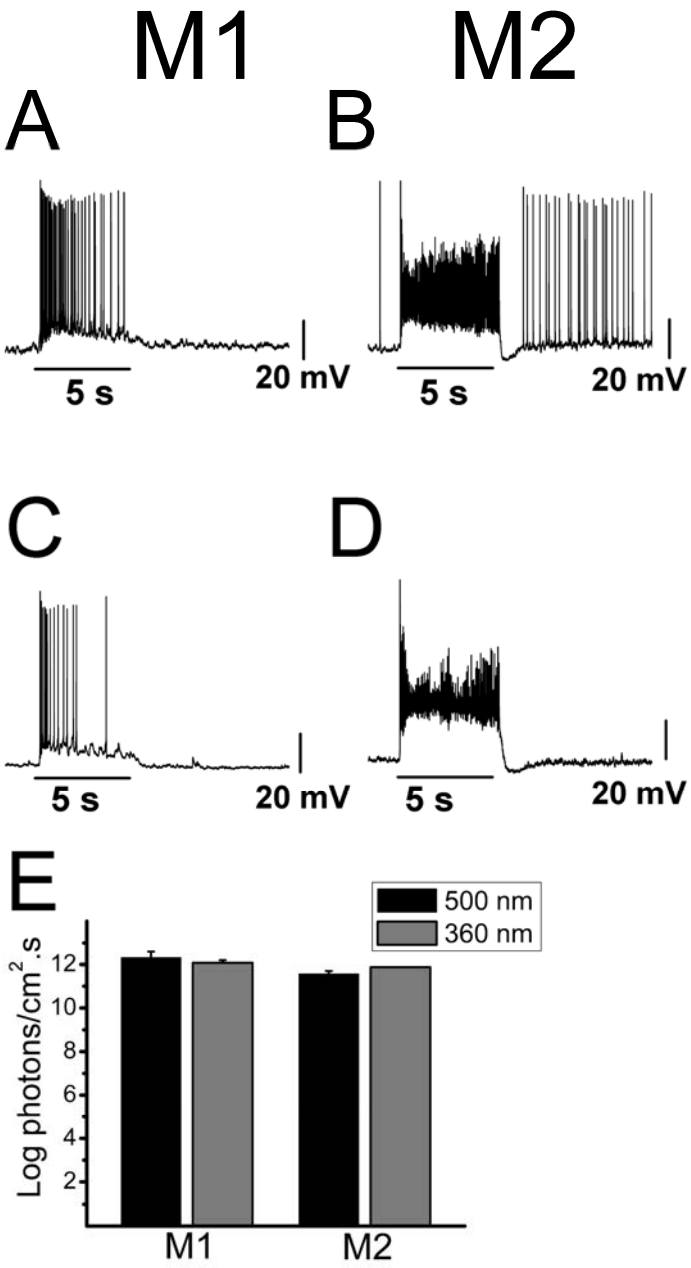

Figure 4. Synaptic responses of M1 and M2 cells in *Opn4*$^{-/-}$ mice to 500 nm and 360 nm light

Current clamp recordings of light-evoked depolarization of M1 and M2 cells to 5s 500 nm or 360 nm light stimulation of increasing intensities. (A-D) Representative examples of light-evoked depolarization of (A) M1 cell to 500 nm light stimulus at 15.2 log photons.cm^{-2}.s^{-1} (B) M2 cell to 500 nm light stimulus at 14.7 log photons.cm^{-2}.s^{-1} (C) M1 cell to 360 nm light stimulus at 13.4 log photons.cm^{-2}.s^{-1} (D) M2 cell to 360 nm light stimulus at 12.9 log photons.cm^{-2}.s^{-1}. (E) Average intensity (log photons.cm^{-2}.s^{-1}) at which a synaptic response was detectable for M1 and M2 cells to 500 nm (black bars) and 360 nm (gray bars) light stimuli.

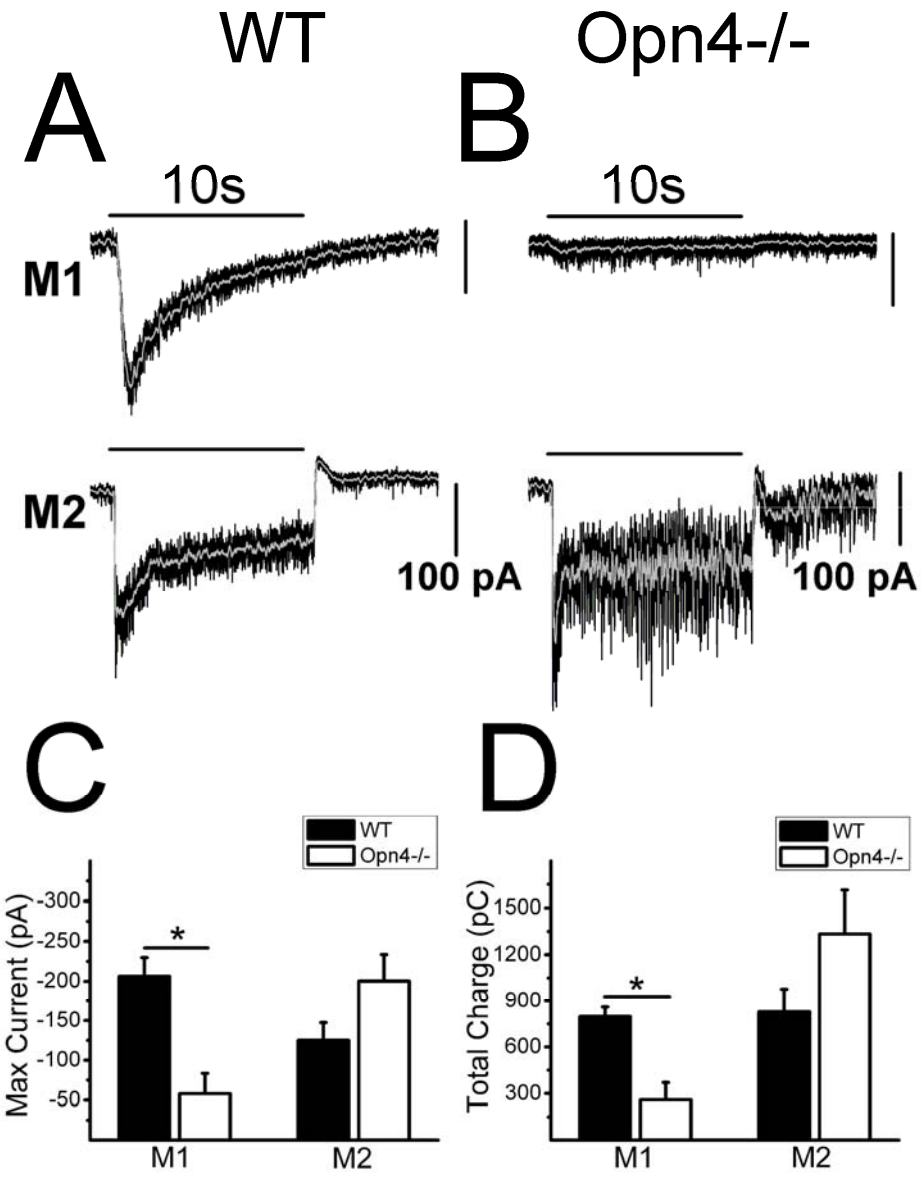

Figure 5. Light-evoked current in WT and *Opn4*$^{-/-}$- ipRGCs
Voltage clamp recordings (V_{Hold} = -73 mV) of light-evoked current to a 10 s, full-field, bright, white-light stimulus at -2LogI in M1 and M2 cells of WT and *Opn4*$^{-/-}$ mice. (A) Representative examples of light-evoked inward current of M1 (top panel) and M2 (bottom panel) cells in a WT mouse. (B) Representative examples of light-evoked inward current of M1 (top panel) and M2 (bottom panel) cells in an *Opn4*$^{-/-}$ mouse. (C) Mean ± SE maximum current measured during the 10 s light stimulus in M1 (n = 8 WT; n = 10 *Opn4*$^{-/-}$) and M2 (n = 6 WT; n = 8 *Opn4*$^{-/-}$) cells of WT (black bars) and *Opn4*$^{-/-}$ (white bars). Notice the reduced current in the *Opn4*$^{-/-}$ M1 but not M2 cells. (D) Mean ± SE total charge measured during 10 s light stimulus in M1 (n = 8 WT; n = 10 *Opn4*$^{-/-}$) and M2 (n = 6 WT; n = 8 *Opn4*$^{-/-}$) cells of WT (black bars) and *Opn4*$^{-/-}$ (white bars). Notice the reduced charge in the *Opn4*$^{-/-}$ M1 but not M2 cells. Gray lines indicate 0.1 s smoothing of membrane voltage. * $P < 0.05$, t-test.

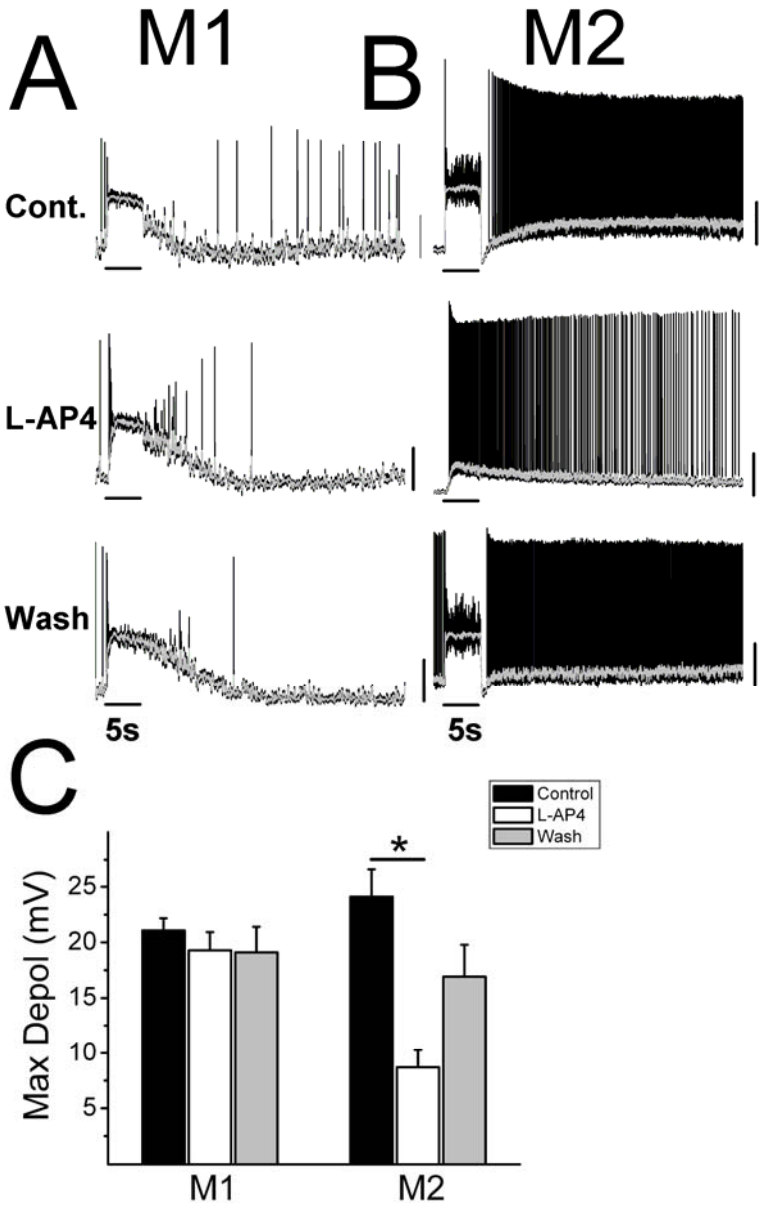

Figure 6. Contribution of ON channel input to light response of M1 and M2 ipRGCs in WT mouse

(A) M1 cell response in current clamp mode to 5 s bright, full-field, white-light stimulus at intensity of -2LogI in control solution (top panel), in the presence of 100 μM L-AP4 (middle panel) and after washout (bottom panel). (B) M2 cell response in current-clamp mode to 5 s bright, full-field, white-light stimulus at intensity of -2LogI in control solution (top panel), with 100 μM L-AP4 in the bath (middle panel) and after washout (bottom panel). (C) Mean ± SE maximum depolarization for M1 (n = 8 cells) and M2 (n = 9 cells) in control solution (black bars), 100 μM L-AP4 (white bars), and after washout (gray bars). Gray line in A,B indicates 0.1 s smoothing of membrane voltage. * $P < 0.05$, one-way *ANOVA*. Vertical scale bars (A,B) 20 mV.

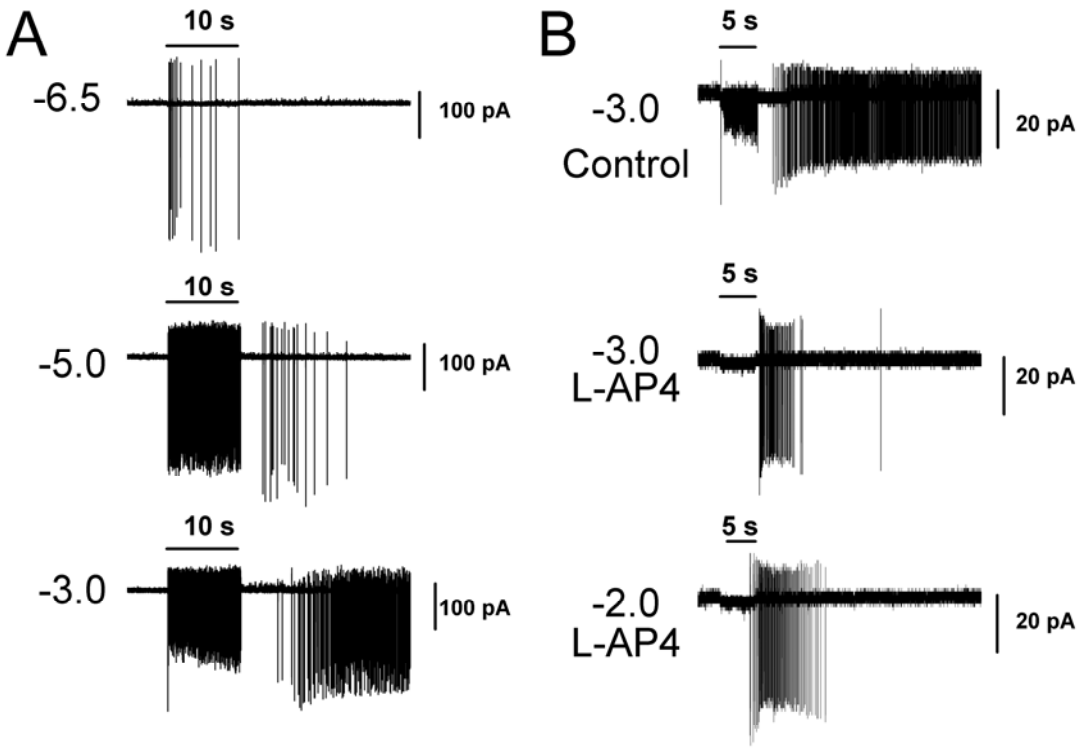

Figure 7. Extracellular recordings of M2 cell light responses in WT mouse
(A) Representative loose patch recording of M2 cell response to increasing intensities of full field white light stimulation ranging from -6.5 (top panel) to -3.0 (bottom panel) LogI. (B) Cell-attached recording of single M2 cell response to white light stimulus at -3.0 LogI in control conditions (top panel) and at -3.0 LogI (middle panel) and -2.0 LogI (bottom panel) following application of L-AP4.

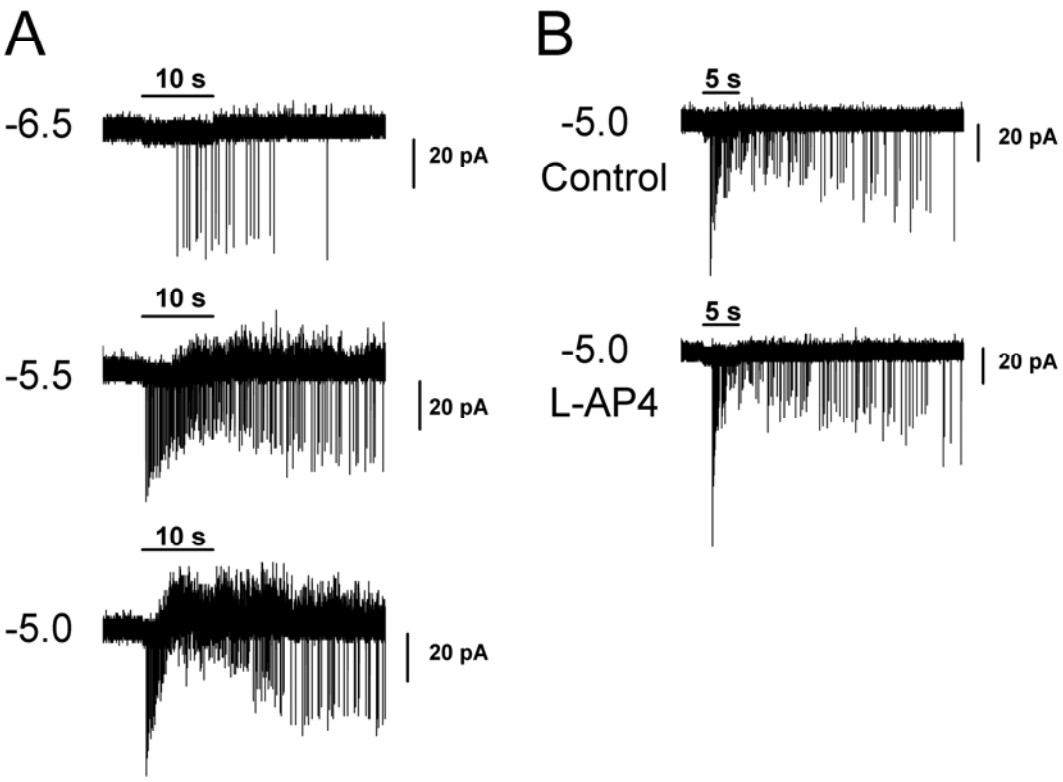

Figure 8. Extracellular recordings of M1 cell light responses in WT mouse
(A) Representative loose patch recording of M1 cell response to increasing intensities of full field white light stimulation ranging from -6.5 (top panel) to -5.0 (bottom panel) LogI. (B) Loose-patch recording of single M1 cell response to white light stimulus at -5.0 LogI in control conditions (top panel) and after application of L-AP4 (bottom panel).

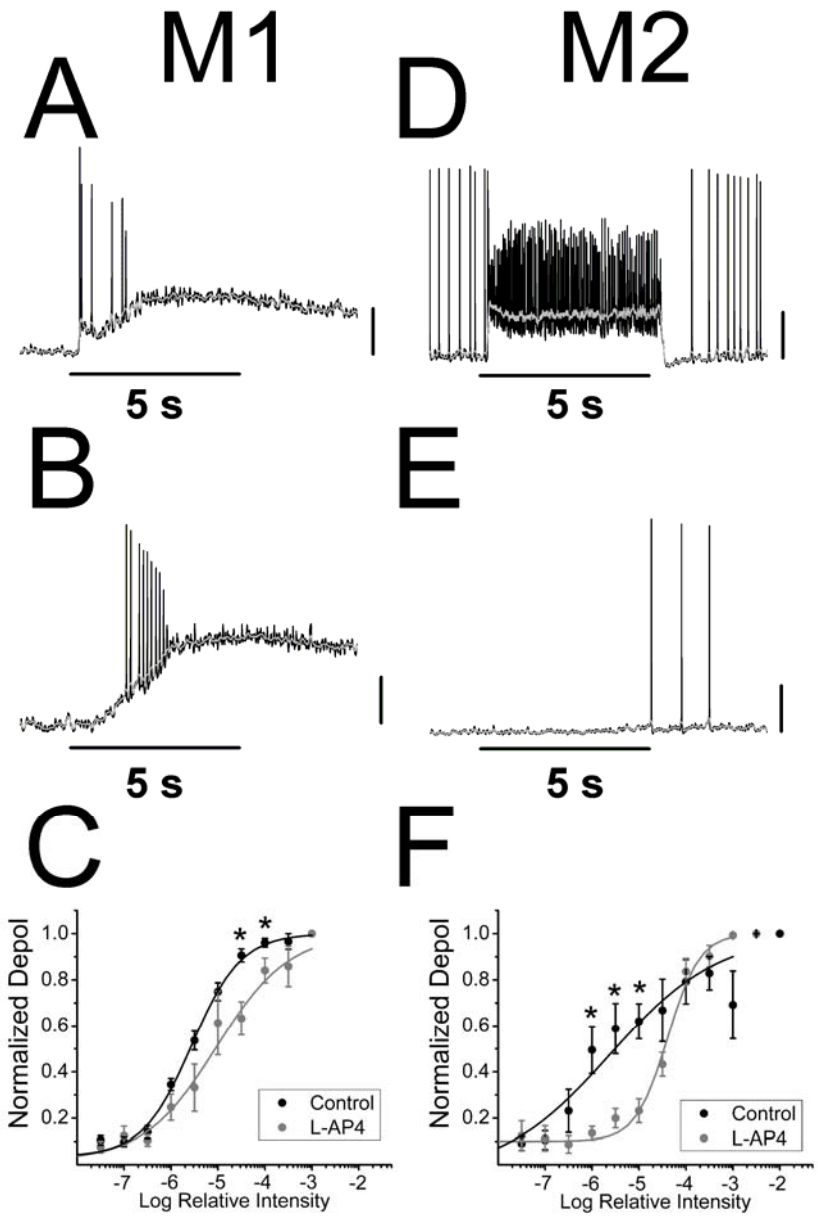

Figure 9. Effects of light-evoked ON pathway input on light sensitivity of M1 and M2 cells (A-B) Representative responses of two M1 cells to 5 s, full-field, white light stimulus at -5LogI in the absence (A) or presence (B) of 100 µM L-AP4. (C) Normalized, averaged responses of M1 cells in the absence (black, n = 8) and presence (gray, n =5) of 100 µM L-AP4 to increasing intensities of white light fit with logistic dose-response functions (see methods). (D-E) Representative responses of two M2 cells to 5 s, full-field, white light stimulus at -5LogI in the absence (D) or presence (E) of 100 µM L-AP4. (F) Normalized and averaged responses of M2 cells in the absence (black, n = 8) and presence (gray, n = 6) of 100 µM L-AP4 to increasing intensities of white light, fit with logistic dose-response functions (see methods). Gray lines indicate 0.1 s smoothing of membrane voltage. $P < 0.05$, t-test. Vertical scale bars (A-E) 20 mV.

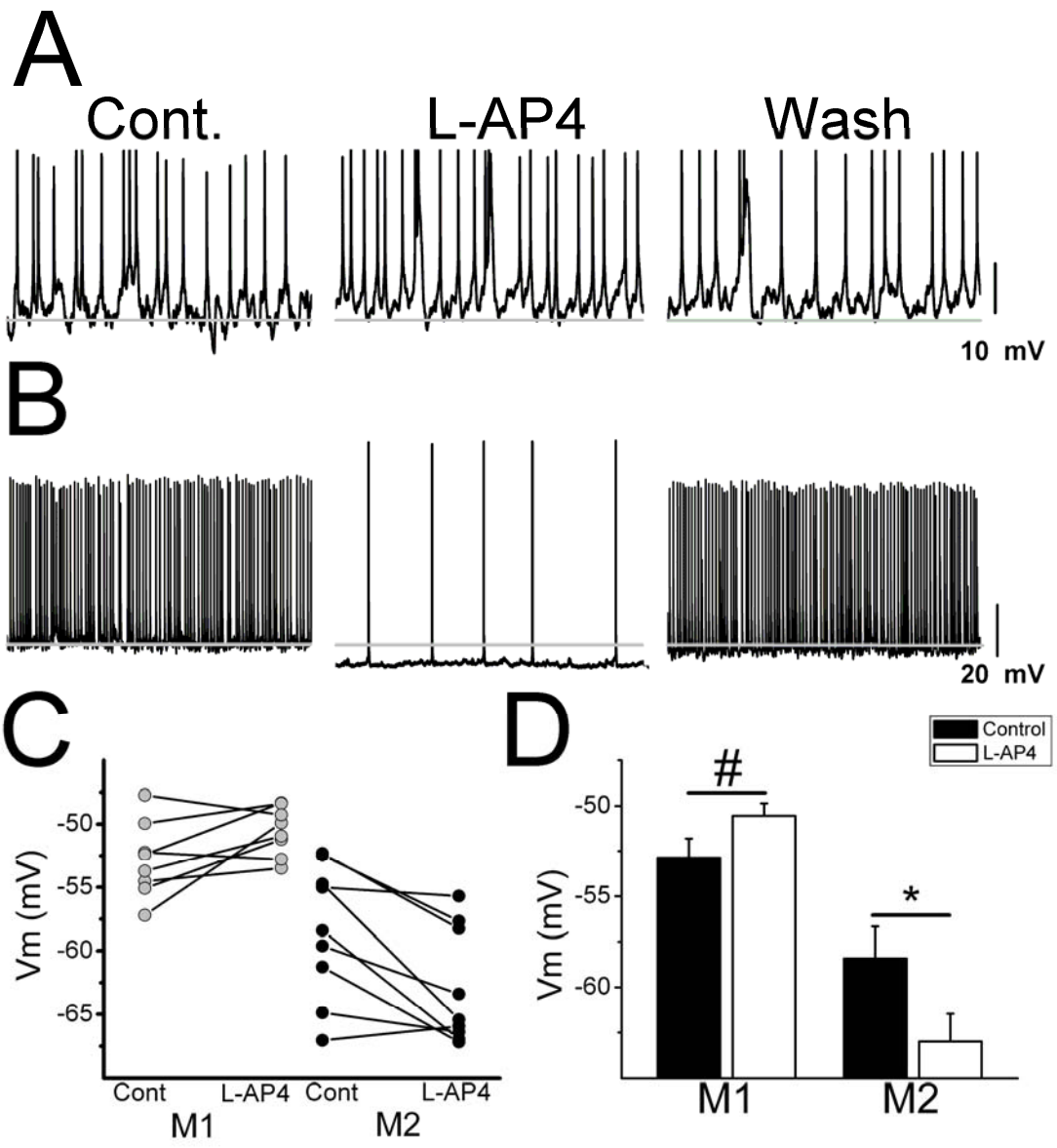

Figure 10. Modulation of ipRGC Vm by the ON pathway
(A,B) Whole-cell current clamp recording of M1 (A) and M2 (B) cells where Vm was recorded continuously (each panel indicates 10 s of recording) in the absence (left panels) and presence (middle panels) of 100 μM L-AP4. Right panels show washout. (C) Vm of individual M1 (gray, $n = 8$ cells) and M2 (black, $n = 9$ cells) cells in control solution and in the presence of 100 μM L-AP4. (D) Mean ± SE Vm of M1 ($n = 8$ cells) and M2 ($n = 9$ cells) in control solution (black bars) and in the presence of 100 μM L-AP4 (white bars). Gray line indicates -58 mV. Vm, resting membrane potential in mV. * $P < 0.05$, *t*-test, # $P < 0.06$, *t*-test.

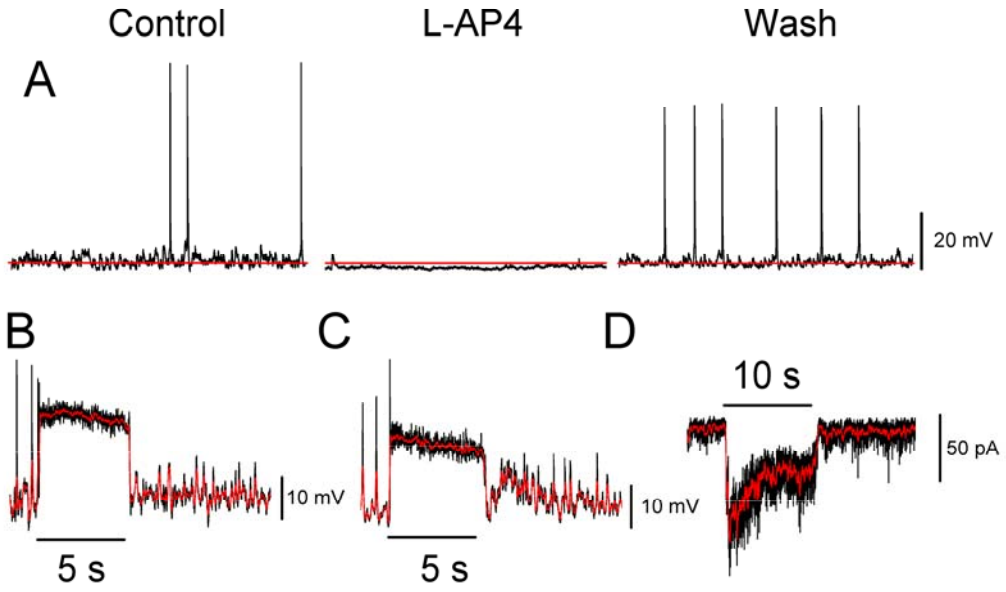

Figure 11. "Atypical" M1 cells are modulated by the ON pathway similarly to M2 cells

All recordings are from M1 cells in WT mice. (A) Whole-cell current clamp recording of M1 cell where Vm was recorded continuously in the absence (left panel) and presence (middle panel) of 100 μM L-AP4. Right panel shows washout. Note the hyperpolarized Vm of the cell and the further hyperpolarization in the presence of L-AP4. (B-C) Response of 2 M1 cells in current clamp mode to 5 s white-light stimulus at intensity of -3LogI (B) and -2LogI (C) in control solution. Note the lack of continued depolarization following stimulus offset that is typical of M1 cells (see Figure 6A). (D) Voltage clamp recording of M1 light-evoked current to a 10 s, full-field, bright, white-light stimulus at -2LogI. Note fast offset kinetics and lack of persistent inward current following stimulus offset that is typically observed in M1 cells (see Figure 5A) Red line (A) indicates -65 mV (B-C) 0.1 s smoothing of membrane voltage (D) 0.1 s smoothing of membrane current. Vm, resting membrane potential.

CHAPTER 5

Form and function of bistratified intrinsically photosensitive retinal ganglion cells in the mouse

Schmidt TM and Kofuji P (in press) *J Comp Neurol*

ABSTRACT

A subpopulation of retinal ganglion cells (RGCs) expresses the photopigment melanopsin, rendering these cells intrinsically photosensitive (ipRGCs). These cells are critical for competent circadian entrainment, pupillary light reflex, and other non-image-forming photic responses. Research has now demonstrated the presence of multiple subpopulations of ipRGC based on the dendritic stratification in the inner plexiform layer (IPL) , those monostratified in the OFF sublamina (M1), those monostratified in the ON sublamina (M2,4,5), and those bistratified in both the ON and OFF sublaminas (M3). Despite evidence that M1 and M2 cells are distinct subpopulations of ipRGC based on distinct morphological and physiological properties, the inclusion of M3 cells as a distinct subtype has remained controversial. Aside from the identification of M3 cells as a morphological subpopulation of ipRGC, to date there have been no functional descriptions of M3 cell physiology or synaptic inputs. We report that M3 cells form a morphologically heterogeneous population, but one that is physiologically homogeneous with properties similar to those of M2 cells. Our data provide the first in-depth description of M3 cell structural and functional properties and indicate that M3 cells may constitute a distinct ipRGC subtype.

INTRODUCTION

A small subpopulation of retinal ganglion cells (RGCs) express the photopigment melanopsin, rendering them intrinsically sensitive to light (Berson et al., 2002; Hattar et al., 2002)(ipRGCs). These cells project to a variety of brain areas, such as the suprachiasmatic nucleus of the hypothalamus (SCN), the mammalian circadian pacemaker, and the olivary pretectal nucleus (OPN), the structure responsible for driving the pupillary light reflex (PLR)(Hattar et al., 2002; Gooley et al., 2003; Hattar et al., 2006; Baver et al., 2008; Ecker et al., 2010). ipRGCs are critical for mediation of both circadian photoentrainment and the PLR (Goz et al., 2008; Guler et al., 2008; Hatori et al., 2008b)

Recent research has demonstrated that there are several morphological subpopulations of ipRGC classified by their dendritic ramification in the inner plexiform layer (IPL): M1 cells, which have dendrites monostratified in the OFF sublamina, M2, 4 and 5 cells, which have dendrites monostratified in the ON sublamina , and M3 cells, which have dendrites bistratified in both the ON and OFF sublaminas (Warren et al., 2003; Viney et al., 2007; Schmidt et al., 2008; Schmidt and Kofuji, 2009; Berson et al., 2010; Ecker et al., 2010). These morphological subpopulations are also physiologically dissimilar , with M1 cells having larger and more sensitive intrinsic light responses as well as a more depolarized resting membrane potential and higher input resistance than M2 cells (Schmidt and Kofuji, 2009). Both M1 and M2 cell dendrites have also now been shown to provide complete tiling of the retina, a criterion traditionally used to define a distinct RGC subtype (Wassle, 2004; Berson et al., 2010). Aside from their identification as a morphological population of

ipRGCs, no information regarding M3 cell functional properties has been reported. Furthermore, it has been proposed that because M3 cells are rare relative to M1 and M2 cells and do not provide complete tiling of the retina, that these cells are not a "true" ipRGC subtype but instead are some "anomalous hybrid" or are the result of an incomplete differentiation during ipRGC development (Berson et al., 2010).

We have utilized a transgenic mouse line in which ipRGCs are labeled *in vivo* with EGFP (Schmidt et al., 2008) to collect physiological and morphological data from the relatively rare and thus-far uncharacterized M3 ipRGC subtype. We provide the first in-depth descriptions of M3 morphology, intrinsic light responses, intrinsic membrane properties, and synaptic light responses. We find that M3 ipRGCs in adult mouse retinas, though morphologically heterogeneous, are physiologically a homogeneous population.

MATERIALS AND METHODS

Animals

Recordings were performed on postnatal (P) 22-40 animals from the *Opn4-EGFP* mouse line described previously (Schmidt et al., 2008) as well as *Opn4-EGFP* mice crossed with animals on an *Opn4*$^{-/-}$ background provided by Dr. King-Wai Yau, Johns Hopkins University (Hattar et al., 2002). Animals were cared for in accordance with guidelines described in *Guide for the Care and Use of Laboratory Animals*, using protocols approved by the University of Minnesota Institutional Animal Care and Use Committee.

Electrophysiology

Dissections were performed as described previously (Schmidt et al., 2008; Schmidt and Kofuji, 2011). Briefly, animals were sacrificed by CO_2 asphyxiation and the eyes were enucleated in a dark room with minimal ambient light. Retinas were removed from eyecup under a standard dissection scope and placed in 95% O_2-5%CO_2 bicarbonate buffered Ames' solution (Sigma, St. Louis, MO) at room temperature. Prior to recording, retinas were treated with Ames' solution containing collagenase/hyaluronidase (240 and 1000 U/ml, respectively; Worthington Biochemicals, Lakewood, NJ) at room temperature for 15 minutes to aide the removal of any remaining vitreous. Recordings were performed using an Axon 700B Amplifier (Molecular Devices, Union City, CA) with extracellular solution containing 95% O_2-5%CO_2 bicarbonate buffered Ames' solution at 32-34^{o}C for intrinsic light response and intrinsic membrane parameter measurements and room temperature for synaptic light response experiments, which allowed for stable and robust synaptic responses to be

recorded. Recordings were made with fire-polished borosilicate pipettes (3-7 MΩ; Sutter Instruments, Novato, CA). For current clamp recordings, pipettes were filled with (in mM): 125 K-gluconate, 2 $CaCl_2$, 2 $MgCl_2$, 10 EGTA, 10 HEPES, 0.5 NaGTP, and 2 Na_2ATP, pH to 7.2 with KOH. For voltage clamp recordings, pipettes were filled with (in mM): 120 CsMethanesulfonate 2 $MgCl_2$, 5 Hepes, 5 EGTA, 0.5 $CaCl_2$, 1 Na_2ATP, 0.5 NaGTP, 2 N-(2,6-dimethylphenyl carbamoylmethyl)triethylammonium bromide (QX314), 5 TEA-Cl, 1 4-aminopyridine (4-AP), pH to 7.2 with CsOH. Intracellular solutions also contained 10-20 μM Alexafluor-594 hydrazide (AF-594)(Invitrogen, Carlsbad, CA) and following recording, dendritic stratification was classified by focusing in the proximal and distal layers of the IPL under epifluorescent illumination with a rhodamine cube.(Schmidt and Kofuji, 2009; Schmidt and Kofuji, 2011). If a cell's stratification could not be clearly identified, that cell was excluded from subsequent analyses. Current and voltage acquisitions were performed with a Digidata 1322 D/A and A/D converter connected to a personal computer running pClamp 10 software (Molecular Devices). Liquid junction potentials between the bath and electrode (14 mV for current clamp and 13 mV for voltage clamp solutions) were calculated using the Liquid Junction Potential Calculator (pClamp 10, Molecular Devices) and were corrected for in all recordings. Retinas were allowed to dark adapt for 5 min prior to the first light stimulus, and any stimuli were placed 5 min apart to allow the cell membrane potential to return completely to baseline.

Whole cell currents were analyzed off-line with Clampfit (Molecular Devices) or Igor Pro 6.0 (Portland, OR) over a 0.1 s sliding time window, and membrane potential values were measured from raw traces over a 1 s sliding time window to

maximize the signal to noise ratio using Igor Pro 6.0 (Portland, OR). Resting membrane potential (Vm) values were calculated by taking the average membrane voltage in the presence of synaptic blockers and TTX (see "Pharmacology" section). For synaptic light response experiments, if a cell's resting membrane potential (Vm) did not reach -50 mV negative current was injected to bring the resting membrane potential (Vm) to approximately -60mV.

Series resistance was noted in all recordings, but uncompensated and only recordings with series resistance of < 30 MΩ were included for analysis. Cell capacitance (Cm) and input resistance (R_N) were calculated from those currents evoked by stepping the cell potential to a 10 mV hyperpolarized value for 20 ms from a holding potential of -60 mV. Charge Q was estimated by time integration of evoked current during the step voltage. R_N was estimated from the steady-state evoked current during the step voltage. Light responses were defined as the maximum depolarization of the averaged trace during the first 30 s following light onset.

Irradiance-response experiments were performed and analyzed as described previously (Schmidt et al., 2008; Schmidt and Kofuji, 2009). Curve fits for normalized, averaged irradiance-response data were determined by nonlinear regression using Origin 7.5 (OriginLab Corporation, Northampton, MA) according to the logistic dose-response function: $y = A_2 + [(A_1-A_2)/(1+(IR/IR_{50})\text{^}n_H)]$, where A_1 is the maximum response plateau, A_2 is the minimum response plateau, IR is irradiance, IR_{50} is the irradiance values that generate half-maximal response, and n_H is the Hill slope. Light stimuli for intrinsic light response experiments were full-field, broadband white light delivered from below the retina at 42 X 10^4 $\mu W.cm^{-2}$ (7.6 X 10^{14} $photons.cm^{-2}.s^{-1}$).

Light stimuli for synaptic and irradiance response experiments were 11 X 10^3 μW.cm^{-2} (7.63 x 10^{14} photons.cm^{-2}.s^{-1} measured at 480 nm by interposing a narrow bandpass filter) and delivered using a xenon lamp feeding the camera port. A filter wheel fitted with various neutral-density filters (Chroma Technologies, Rockingham, VT) and shutter (Lambda-3, Sutter Instruments) was used to control the intensity and duration of light stimuli. Irradiance measurements were made with a calibrated radiometer model S370 (UDT Instruments, San Diego, CA).

Statistical analyses were performed using Origin 7.5 (OriginLab Corporation). Statistical comparison of means was performed using a Student's *t*-test or one-way *ANOVA* with Tukey's post-hoc test and significance was concluded when $P < 0.05$. Data are presented as mean ± SE.

Pharmacology

For intrinsic light response and intrinsic membrane property measurements, synaptic blocker cocktail included: 250 μM DL-2-amino-4-phosphonobutyrate (DL-AP4, a group III metabotropic glutamate receptor agonist); 10 μM 6,7-dinitroquinoxaline (DNQX, α-amino-3-hydroxy-5-methyl-4-isoxazolepropionic acid (AMPA/kainate receptor antagonist); 0.3 μM strychnine (glycine receptor antagonist); 50 μM picrotoxin (GABA receptor antagonist). Extracellular solution sometimes also included 0.5 μM tetrodotoxin (TTX, sodium channel blocker). DL-AP4, DNQX, and TTX were purchased from Tocris (Ellesville, MO). Picrotoxin, and strychnine were purchased from Sigma (St. Louis, MO). For synaptic recordings 100 μM L-2-amino-4-phosphonobutyrate (L-AP4, a group III metabotropic glutamate receptor (mGluR) agonist) (Tocris, Ellesville, MO) that blocks photoreceptor to ON bipolar cell signaling

(Slaughter and Miller, 1981), was sometimes included in the bath solution and used to silence light-evoked ON pathway responses.

Immunocytochemistry

Immunocytochemistry and neurobiotin filling were performed as published previously (Schmidt et al., 2008). Cells were filled with either 0.3% neurobiotin (Vector Laboratories, Burlingame, CA) or 0.3% Lucifer Yellow (Sigma). For visualization of filled cells and immunostaining of retinas, retinas were then fixed overnight in 4% paraformaldehyde solution at 4^{o}C and washed extensively in PBS. Retinas were then placed in blocking solution containing 10% donkey serum and 0.5% Triton X100 (Sigma) in PBS overnight at 4^{o}C. Retinas were then placed in primary antibody solution containing 5% donkey serum, 0.5% Triton and a combination of goat polyclonal anti-choline acetyl transferase (ChAT) (1:250; Millipore, Bedford, MA; AB144P), rhodamine-conjugated streptavidin (1:500; Invitrogen, Carlsbad, CA), or rabbit polyclonal anti-lucifer yellow (1:500; Invitrogen; A5750) rotating for 3 days at 4^{o}C. ChAT is a marker of cholinergic amacrine cells, the dendrites of which form two plexuses and served as a marker for the ON and OFF sublaminas of the retina (Kang et al., 2004). The anti-Chat antibody (immunogen: human placental enzyme) has been well-characterized and previously demonstrated to recognize 68-70 kDa bands in Western blot analysis of brain extracts from rat and several species of fish that disappeared when the antibody was preincubated with human placental ChAT (Anadon et al., 2000). The same antibody has been used in the mouse retina to recognize cholinergic amacrine cells (Whitney et al., 2008). The anti-Lucifer Yellow antibody has been used previously and shown to specifically label cells filled with Lucifer Yellow

(Zhang et al., 2006; Xu et al., 2008). Following incubation in primary antibody solution, retinas were again washed extensively in PBS and the placed in secondary antibody solution containing 5% donkey serum, 0.5% TritonX100 and a combination of Alexa-488 conjugated donkey anti-goat or anti-rabbit (1:500; Invitrogen) or rhodamine-conjugated streptavidin (1:500) rotating for 2 days at 4^{o}C. Retinas were then washed extensively in PBS, mounted in Vectashield (Vector Laboratories), coverslipped, and sealed with nail polish. Image acquisition was performed on an upright Olympus Fluoview 1000 laser scanning confocal microscope (Olympus, Center Valley, PA). Image J was used to adjust image brightness and contrast (http://rsb.info.nih.gov/ij/). Multiple confocal stacks of filled neurons were merged and neurons were traced in 3 dimensions using NeuroLucida (Microbrightfield, Williston, VT). Dendritic field size was estimated in NeuroLucida by taking the area of a convex polygon linking the tips of the dendrites from a 2-dimensional tracing of a given cell and the diameter was then expressed as that of a circle having an equal area. Sholl Analysis (Sholl, 1953) was also performed in NeuroLucida with a starting radius of 10 μm from the center of the soma and the number of crossings were counted at circles increasing in radius by 15 μm.

RESULTS

M3 ipRGCs are morphologically heterogeneous

Though the existence of M3 cells has been described previously (Warren et al., 2003; Viney et al., 2007; Schmidt et al., 2008; Schmidt and Kofuji, 2009; Berson et al., 2010), the morphological properties of M3 cells have not been examined in detail. To provide further morphological characterization of M3 cells, we have filled ipRGCs in adult mouse retinas of a mouse line in which ipRGCs are labeled *in vivo* with EGFP (Schmidt et al., 2008) with 0.3% neurobiotin or Lucifer Yellow (LY). ipRGCs were classified as M1 if the cell had dendrites terminating in the OFF sublamina (Figure 1A), M2 if the cell had dendrites terminating in the ON sublamina (Figure 1B), and M3 if the cell had dendrites terminating in both the ON and OFF sublaminas of the IPL (Figure 1C). M3 ipRGCs had large dendritic arbors (diameter = 477.4 ± 20.1 μm, $n = 10$; dendritic length = 4441.2 ± 331.4 μm, $n = 10$). When compared to the arbors of M1 and M2 cells, M3 cells were found to have significantly larger dendritic field diameters and total dendritic length than M1 (diameter = 365.9 ± 16.3 μm, $n = 24$; dendritic length = 2350.1 ± 110.2 μm, $n = 24$) but not M2 cells (diameter = 425.4 ± 13.4 μm, $n = 15$, $P < 0.01$, *ANOVA*; dendritic length = 4603.6 ± 164.1 μm, $n = 15$, $P < 0.01$, *ANOVA*) (Figure 1D). Furthermore, when the dendritic arbor complexity was examined using Sholl analysis to quantify the degree of branching, we found that M3 cells had highly branched dendritic arbors, similar to M2 cells, while M1 cells had less branched, relatively simpler dendritic arbors (Figure 1E) (Schmidt and Kofuji, 2009; Berson et al., 2010). When the soma size of M3 cells was quantified (soma diameter = 17.8 ± 0.6 μm, $n = 10$) these cells were found to have significantly larger somas than M1 (soma

diameter = 15.7 ± 0.4 μm, n = 24) but not M2 cells (soma diameter = 18.9 ± 0.6 μm, n = 15, P< 0.0.1, *ANOVA*)(Figure 1F). Collectively these results indicate that M3 cells are similar to M2 cells in terms of the size and complexity of their dendritic arbors, but differ in terms of their dendritic stratification.

We next examined the proportion of dendrites of M3 cells residing in the ON or OFF sublaminas of the IPL. Notably, M3 cells had variable proportions of dendritic arbors stratifying in each sublamina. Examples of the dendritic arbors of 10 M3 cells are shown in Figure 2. 5 of 10 M3 cells had dendrites confined primarily to the OFF sublamina (Figure 2A), 4 of 10 M3 cells had dendrites stratifying approximately equally in both sublaminas (Figure 2C) and 1 of 10 M3 cells had dendrites confined almost entirely to the ON sublamina (Figure 2B). Altogether, these results indicate that M3 cells do not show a uniform pattern of dendritic stratification in either the ON or OFF sublamina.

Additionally, when we assessed the dendritic field overlap of ipRGCs in close proximity to each other by filling cells with either neurobiotin or LY, we found that M3 cells overlap extensively with M1 and M2 cells (Figure 3C-D). Furthermore, we found that M1 cell dendritic arbors overlap extensively with those of nearby M2 as well as M1 cells and that the dendrites of M2 cells likewise overlap extensively with nearby M2 cells (Figure 3A-B, E-F). These data are in agreement with previously reported findings (Schmidt and Kofuji, 2009; Berson et al., 2010) of extensive overlap of neighboring ipRGCs of hetero- and homotypic subtypes in mouse, but more extensive than seen in primate ipRGCs (Jusuf et al., 2007). This is contrast to some other ganglion cell subtypes in which dendrites show minimal overlap across the retina (Vaney, 1994).

When we analyzed the proportion of M3 ipRGCs across a sample of 213 cells from various experiments, we found that M3 cells formed 20% (43/213 cells) of the dataset while 42% (90/213) of cells were M2 and 38% (80/213) were M1 cells.

M3 cells have uniform intrinsic physiological characteristics

The functional properties of M3 cells have not yet been examined and compared to M1 and M2 cells in any study to date. We therefore examined the resting membrane potential and input resistance of M3 cells in the presence of a synaptic blocker cocktail and TTX (see methods). We found that M3 cells had a significantly more hyperpolarized resting membrane potential (Vm) (Vm = -73.3 ± 2.3 mV, $n = 9$) than M1 (Vm = -57.3 ± 1.7 mV, $n = 21$) but not M2 cells (Vm = -70.8 ± 1.3 mV, $n = 23$, $P < 0.05$, *ANOVA*) (Figure 4A). Furthermore, M3 cells had an input resistance (R_N= 280.3 ± 25.8 MΩ, $n = 11$) that was significantly lower than M1 cells (R_N=718.9 ± 72.5 MΩ, $n = 21$) but similar to M2 cells (R_N=233.7 ± 21.8 MΩ, $n = 23$, $P < 0.05$, *ANOVA*) (Figure 4A). Collectively, these results indicate that M3 cells have intrinsic membrane properties that are similar to M2 cells.

We also examined the spiking properties of M3 cells (again in the presence of synaptic blockers, but without TTX). To examine the spiking evoked by depolarizing current, we performed current clamp experiments where we first injected steady state current to bring the Vm to ~-70mV and then injected increasing amounts of depolarizing current (Figure 4B). We recorded from 3 M3 cells and found that, like M1 and M2 cells, M3 cells respond to increasing amounts of current injection with increasing spike frequency (Figure 4C). We found that M3 cells reached maximum average spike frequencies (27.6 ± 1.5 Hz, $n = 3$) comparable to those reported

previously for M2 cells (38.4 ± 4 Hz) and higher than reported previously for M1 cells (10.1 ± 1.3 Hz) (Figure 4C-D)(Schmidt and Kofuji, 2009) (Figure 4D). However, M3 cells reached depolarization block at lower amounts of current injection (2.6 ± 0.3 pA/pF), defined as the first current injection after which a submaximal spike frequency was attained, than M2 cells (4.4 ± 0.6 pA/pF) but higher than that for M1 cells (1.2 ± 0.3 pA/pF) (Figure 4C-D) (Schmidt and Kofuji, 2009). These results demonstrate that M3 cells respond to depolarizing current injections by attaining spike frequencies similar to those reported for M2 cells, but appear to reach depolarization block at lower frequencies than those reported previously for M2 cells, indicating that M3 cells have spiking properties unique to M1 and M2 cells.

We next sought to examine the properties of the intrinsic light response of M3 cells. We recorded light responses in current clamp mode to a 30 s bright, full-field white light stimulus from M1, M2, and M3 ipRGCs in the presence of a cocktail of synaptic blockers (see methods) and TTX. We found that M3 cells, like M1 and M2 cells, responded to light stimulation with a sustained depolarization that persisted following stimulus offset (Figure 5A). M3 cells responded to light with a significantly smaller depolarization (8.3 ± 1.3 mV, $n = 11$) than M1 cells (23.5 ± 1.9 mV, $n = 21$) and with a similar maximum depolarization to M2 cells (9.8 ± 1.1 mV, $n = 23$)(Figure 5B). M1 cells are ~1 log unit more sensitive to 480 nm light, the ~λ_{max} for melanopsin, than M2 cells, but this has not been examined for M3 cells (Lucas et al., 2001; Berson et al., 2002; Dacey et al., 2005; Qiu et al., 2005; Schmidt and Kofuji, 2009). We obtained full irradiance response curves for 3 M3 cells to 480 nm light. We found that the fitted LogIR50 for M3 cells of 12.8 Log photons/cm^2.s (range 12.5-13.2) was in between that

reported previously for M1 and M2 cells, shifted ~0.3 log units higher in intensity relative to that of M1 cells of 12.5 Log photons/cm^2.s (range 12-12.8) and ~0.7 log units lower in intensity relative to M2 cells of 13.5 Log photons/cm^2.s (range 13-14.1) collected under identical conditions (Schmidt and Kofuji, 2009) (Figure 5C). These results indicate that while M3 cells respond to light with a maximum intrinsically-evoked depolarization similar to that of M2 cells, these cells may display a unique sensitivity to 480 nm light compared to both M1 and M2 cells.

The ON pathway forms the primary synaptic input to M3 cells

We next examined the synaptic light response of M3 cells. M1 and M2 cells both receive synaptic input from the ON pathway in response to light stimulation, and this ON pathway input forms the primary light-evoked synaptic input to these two ipRGC subpopulations at bright light intensities(Schmidt and Kofuji, 2010a). In order to study the light-evoked synaptic inputs to M3 cells, we recorded light responses in current or voltage-clamp mode to a 5 or 10 s bright white light stimulus (see methods) in the absence of synaptic blockers. In current clamp mode, M3 cells responded to light with fast (< 1 sec onset) and sustained light-evoked depolarizations (Figure 6A). We next applied L-AP4, a Group III mGluR receptor agonist that selectively silences signaling at the photoreceptor-ON bipolar cell synapse (Slaughter and Miller, 1981). Following L-AP4 application, M3 cells responded with a smaller, sluggish depolarization that persisted following stimulus offset (Figure 6B). This effect was reversible upon washout (Figure 6C). When we quantified maximum depolarization in control (24.8 ± 2.2 mV, n = 4), L-AP4 (8.9 ± 4.5 mV, n = 4), and upon washout (19.5 ± 2.7 mV, n = 4) we found that in the presence of L-AP4, the maximum light-evoked

depolarization of M3 cells was significantly reduced relative to control ($P < 0.05$, *ANOVA*) (Figure 6D). Light responses in voltage clamp ($n = 2$) paralleled those seen in current clamp, with M3 cells showing a fast and sustained inward current that terminated quickly following light offset (Figure 6E). The effect of L-AP4 application on light-evoked depolarization of M3 cells was virtually identical to the effect of application of a cocktail of glutamatergic, GABAergic, and glycinergic blockers (Figure 7), indicating that, similar to M1 and M2 cells, the ON pathway forms the dominant synaptic input to M3 cells. Despite the fact that the bulk of dendrites for many M3 cells are almost entirely confined to the OFF sublamina (Figure 2), M3 cells show robust ON pathway-evoked depolarizations that are consistently similar to the synaptic light responses of M2 cells (Figure 6F)(Schmidt and Kofuji, 2010a).

In order to measure synaptic responses in isolation from the intrinsic photosensitivity of M3 cells, we crossed our EGFP reporter mouse line with a mouse line in which the *Opn4* gene coding region has been replaced with that of tau-lacZ (Hattar et al., 2002), to generate a melanopsin null mouse line ($Opn4^{-/-}$) in which ipRGCs are labeled with EGFP. When we recorded from M3 cells in the $Opn4^{-/-}$ mouse line we found that, in current clamp, the response of these cells to light was virtually identical to that seen in wild-type (WT) mice ($n = 2$, maximum depolarization 35.0 mV and 22.1 mV), with a fast onset and offset depolarization, but lacking the after-discharge often seen several seconds after light offset in the WT (Figure 8A). In voltage clamp mode, M3 cells responded to 10 s, bright, white light stimuli with fast and sustained inward currents that terminated quickly following light offset ($n = 4$). An example of a typical M3 cell light response in $Opn4^{-/-}$ mice recorded in voltage clamp

mode is shown in Figure 8B. Furthermore, all light-evoked currents were completely abolished in this cell upon application of L-AP4, providing further support for the idea that the ON pathway provides the dominant light-evoked synaptic input to M3 cells (Figure 8C). This is similar to both M1 and M2 cells in which the synaptic light response of ipRGCs in *Opn4*$^{-/-}$ mice is completely abolished following L-AP4 application (Schmidt and Kofuji, 2010a). Given the similarity of the light-evoked response in WT and *Opn4*$^{-/-}$ M3 cells, we conclude that the synaptic input via the ON pathway is primarily responsible for shaping the integrated light response of WT M3 cells under control conditions. The robust synaptic influence on the M3 cell light response is similar to that seen in WT M2 cells (Figure 6A,F) but not in M1 cells (Schmidt and Kofuji, 2010a).

DISCUSSION

ipRGCs are a distinct subpopulation of ganglion cell within the mammalian retina. It has become clear that ipRGCs are not a homogeneous population, but one that contains several morphological subtypes, each with distinct physiological characteristics (Warren et al., 2003; Tu et al., 2005; Viney et al., 2007; Schmidt et al., 2008; Schmidt and Kofuji, 2009; Ecker et al., 2010). In this study we demonstrate for the first time that the mouse retina contains a population of ipRGCs that are homogenous in regard to their physiological properties and yet are heterogeneous in regard to key morphological features. These ipRGCs, termed M3 cells, with a bistratified dendritic arborization in the inner plexiform layer (IPL), respond to light stimulation via intrinsic and synaptic mechanisms in a manner reminiscent of M2 cells. Intrinsic membrane properties and spiking properties are also more similar to M2 than M1 cells (Schmidt and Kofuji, 2009).

We first analyzed the detailed morphological properties of M3 cells. These cells have large and highly branched dendritic arbors and relatively large somas, similar to the arbors of M2 cells. The defining morphological characteristic of the M3 subpopulation is the bistratification of the dendrites within the innermost and outermost sublaminas of the IPL. What is perhaps most striking about the dendritic arbors of M3 cells is the lack of uniformity with regards to the proportion of dendrites stratifying in the ON and OFF sublaminas. It appears that M3 cell morphology forms a continuum with regard to the proportion of dendrites stratifying in either the ON or OFF sublaminas, with some cells having the vast majority of their dendrites confined to the OFF or ON sublamina and some stratifying in both sublaminas in roughly equal

proportions. Indeed this sparse branching into either the ON or the OFF sublamina could be at least partially responsible for some of the lower estimates of M3 cell density or lack of M3 cell projections reported in studies using immunostaining methods to identify various subtypes (Baver et al., 2008; Berson et al., 2010).

It has been proposed that M3 cells are some kind of developmental "anomalous hybrid" of the M1 and M2 subtypes (Berson et al., 2010). However, if this were the case, then one might expect to see a range of intrinsic properties and intrinsic light responses, some of which correlate with those of M1 cells and some that correlate with those of M2 cells. However, despite variation in the dendritic arborization of M3 cells, this was not observed in our experiments. The magnitude of the intrinsic light response, spike frequencies attained, resting membrane potential, and input resistance are all not only relatively consistent across the M3 cell population, but are also similar to the physiological properties of M2 cells. The apparent functional homogeneity of M3 cells, and the similarity of M3 functional properties to those of M2 cells is surprising, especially given that these cells displayed marked variability in the proportion of their dendritic arbors branching in the ON and OFF sublaminas of the IPL. Perhaps most surprising is that, regardless of the relative proportion of the M3 arbor stratifying in the OFF sublamina, M3 cells had remarkably uniform On-pathway mediated synaptically driven light responses. This seems to indicate that the synaptic inputs to M3 cells reside not only on the dendrites branching in the ON sublamina (which are often very sparse) but are perhaps distributed between the ON and OFF sublaminas. It has recently been demonstrated that M1 cell dendrites in the OFF sublamina form ectopic synapses with ON bipolar cells (Dumitrescu et al., 2009; Hoshi et al., 2009). M3 cell OFF arbors

costratify with the arbors of M1 cells and thus it is feasible that these cells receive a combination of both conventional and atypical ON pathway inputs.

M3 cell dendrites that terminate in the OFF sublamina stratify in the same sublamina as the dendrites of both M1 cells as well as the dopaminergic amacrine cells (DACs) (Vugler et al., 2008; Zhang et al., 2008; Dumitrescu et al., 2009; Hoshi et al., 2009). Bidirectional signaling between M1 cells and DACs has been proposed (Zhang et al., 2008). The close proximity of the dendritic arbor of M3 cells to DACs could expose M3 cells to levels of dopaminergic signaling that M2 cells would not experience. Furthermore, whether M3 cells might also contribute to the centrifugal flow of information from ipRGCs to the DACs (Zhang et al., 2008) is an intriguing possibility that has yet to be explored.

It is unclear whether this M2-like photic information conveyed by M3 cells is particularly relevant to a specific non-image forming (NIF) behavior. It has recently been demonstrated that the SCN and OPN receive distinct proportions of innervation of M1 and M2 cells (Baver et al., 2008). M3 cell projections were not reported in this study, perhaps because these cells do not project to these areas in high enough proportions or because it might be difficult to identify these cells using immunostaining methods as there are often only sparse dendritic branching in the ON or OFF sublaminas. If M3 cells do not project to the SCN or OPN, however, it will be important to determine whether any other NIF nuclei receive preferential projections from M3 cells. Whether M3 cells project in specific proportions to different NIF nuclei or play a specialized role in certain NIF behaviors will be an important question in future research.

Are M3 cells a "true" ipRGC subtype? RGCs are divisible into over a dozen morphological subtypes in the mammalian retina and a key feature of RGCs is that their dendrites create a mosaic that covers the surface the retina and exhibit consistent dendritic morphology (Sun et al., 2002; Wassle, 2004; Coombs et al., 2006). By using this criterion, we would expect M3 cell dendrites to cover the retina completely. However, a recent study by Berson et al. (2010) shows that M3 cell dendrites do not completely tile the retina, and that M3 cells are relatively rare. We find that the morphological features of M3 cells are consistently similar to M2 cells in terms of their dendritic length, dendritic field size, soma size, and dendritic arbor complexity. However, M3 cells show marked variation with regards to the proportion of dendrites stratifying in either the ON or the OFF sublamina. Stratification in the ON or OFF sublamina is an important indicator of synaptic connectivity for RGCs (Wassle, 2004), but we find that the ON channel provides the primary synaptic input to M3 cells regardless of the proportion of dendrites stratifying in the ON or OFF sublamina for a given cell.

While tiling and morphological homogeneity are valid arguments for a "regular" RGC to be consider a distinct subtype, these stringent criteria need not necessarily apply to ipRGCs because of their unique functional features. First, because ipRGCs function primarily as irradiance detectors (Berson et al., 2002; Dacey et al., 2005), spatial discrimination as provided by the orderly and complete tiling of ganglion cell dendrites may not be required to mediate various NIF functions (but see (Ecker et al., 2010). The extensive overlap of ipRGC dendritic fields with nearby ipRGCs of the same or different subtype indicates that spatial segregation of the receptive field is not important

for the mediation of ipRGC function. Furthermore, we find that 20% (43 cells) of a sample of 213 ipRGCs are bistratified by our criteria, in agreement with ~21% reported by (Viney et al., 2007) where the ipRGC population was randomly virally labeled with GFP, and less than the 26% we have reported previously based on single-cell neurobiotin filling (Schmidt et al., 2008). A recent study reported extremely low density of M3 cells of <10% though this study used immunostaining and the authors acknowledge that the bistratified arbors were not easily identifiable using their methods (Berson et al., 2010). Even if areas of the retina are not sampled by the dendritic arbors of a particular ipRGC subtype, collectively they still may function as efficient irradiance detectors. A relatively small number of ipRGCs is still expected to exert a large physiological impact as cell ablation studies have indicated that 17% percent of ipRGCs are able to sustain a significant proportion of NIF behaviors such as pupillary light reflex and circadian photoentrainment (Guler et al., 2008).

In this study, we have provided the first comprehensive assessment of the morphological and physiological properties of M3 ipRGCs. We find that though M3 cells show heterogeneity in the proportion of their dendritic arbors stratifying in either the ON or OFF sublaminas, these cells show remarkable homogeneity in their physiological properties. Many of M3 cell morphological features as well as many, though not all, of their functional features are similar to those of the previously described M2 cells (Schmidt and Kofuji, 2009). Whether these properties of M3 cells warrant their classification as a "true" ipRGC subtype depends on the criterion for classification used. Further analysis of whether M3 cells receive distinct patterns of synaptic inputs, receive differing amounts of inhibitory or excitatory synaptic inputs, or

play distinct roles in mediating various NIF behaviors will be important questions for future research. Thus, though our data indicate that M3 ipRGCs may constitute a unique ipRGC subtype based on both their bistratification as well as their uniform physiological properties, further research will be necessary to conclusively answer this question.

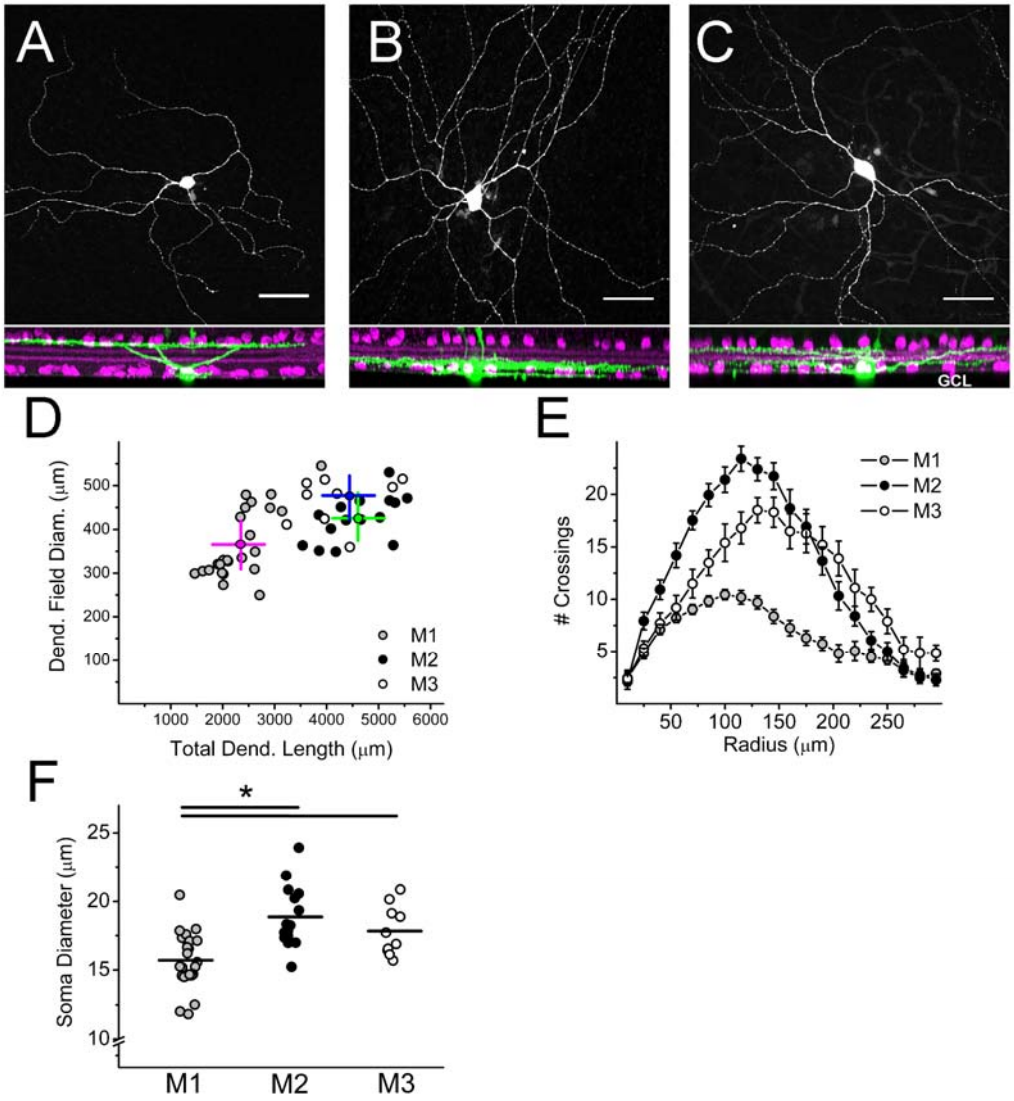

Figure 1. Morphological properties of M3 cells.
(A-C) Confocal stack in which ipRGCs have been filled with neurobiotin (green) and costained for ChAT (magenta), a cholinergic amacrine cell marker. (A) M1 cell with dendrites terminating in the outer (OFF) sublamina of the inner plexiform layer (IPL). (B) M2 cell with dendrites terminating in the inner (ON) sublamina of the IPL. (C) M3 cell with dendrites terminating in the inner (ON) and outer (OFF) sublaminas of the IPL. Note: processes visible extending through IPL in A-C are those of Müller cells, which often take up dye during the patching procedure. (D) Plot showing total dendritic length (μm, x-axis) and dendritic field diameter (μm, y-axis) of M1 (gray circles), M2 (black circles), and M3 (open circles). Magenta (M1), green (M2), and blue (M3) lines represent the mean value for each cell type. (E) Sholl analysis (15 μm steps from starting diameter of 10 μm) of M1 (gray circles), M2 (black circles), and M3 (open circles) dendritic arbors. (F) Soma diameter (μm) of M1 (gray circles), M2 (black circles), and M3 (open circles) cells. Lines represent mean values. Scale bar (A-C): 50 μm. *$P < 0.05$ *ANOVA*. INL, Inner Nucelar Layer, GCL, Ganglion Cell Layer.

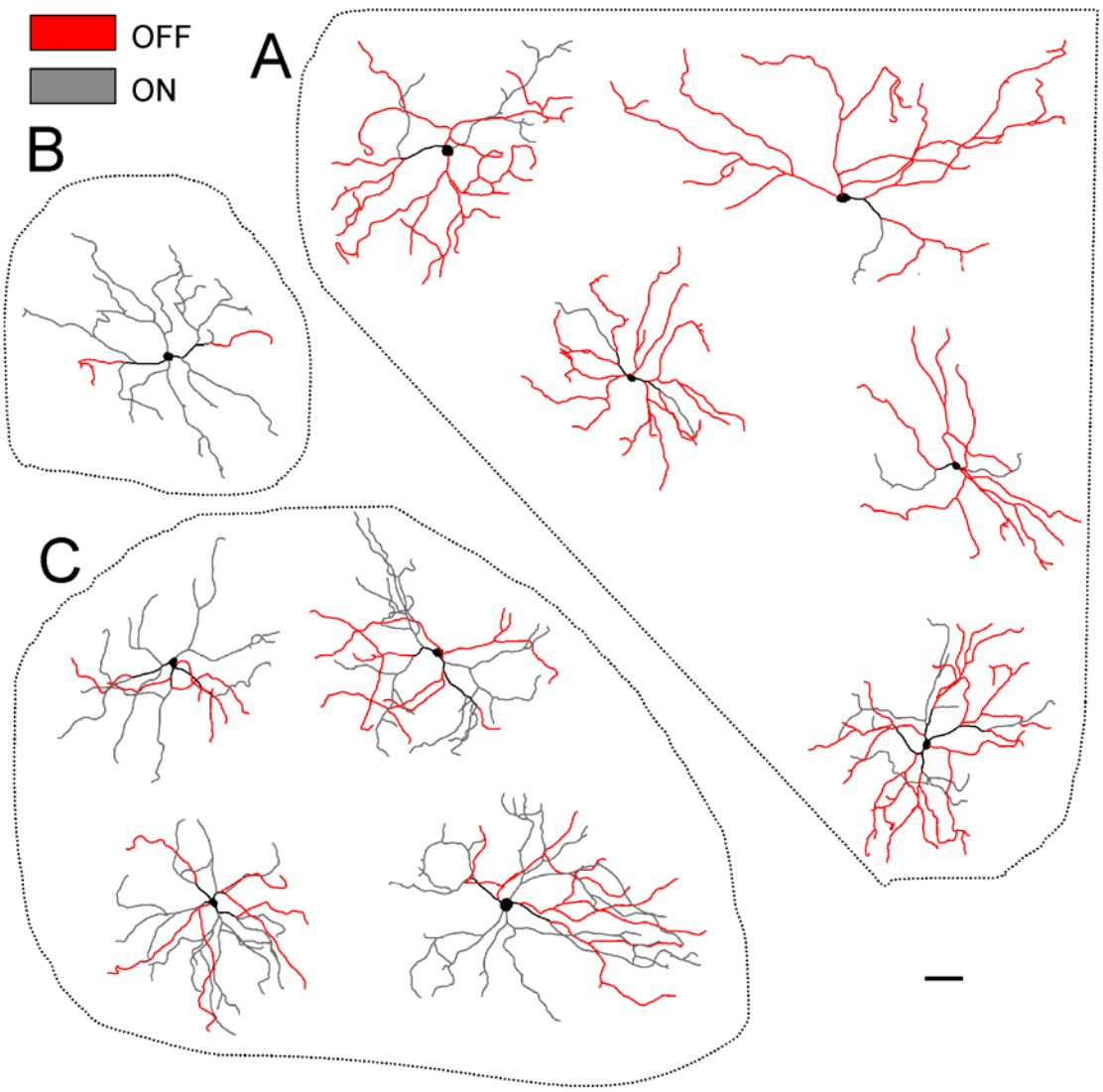

Figure 2. Dendritic arbors of M3 cells.
Traced dendritic arbors of neurobiotin or LY-filled M3 cells. Red-colored arbors represent those dendrites terminating in the OFF sublamina of inner plexiform layer. Gray colored processes represent dendrites terminating in the ON sublamina. (A) M3 cells with dendrites confined mainly to the OFF sublamina. (B) M3 cell with dendrites confined mainly to the ON sublamina (C) M3 cells with substantial dendritic stratification in both the ON and OFF sublaminas. LY: Lucifer yellow. Scale bar: 100 μm.

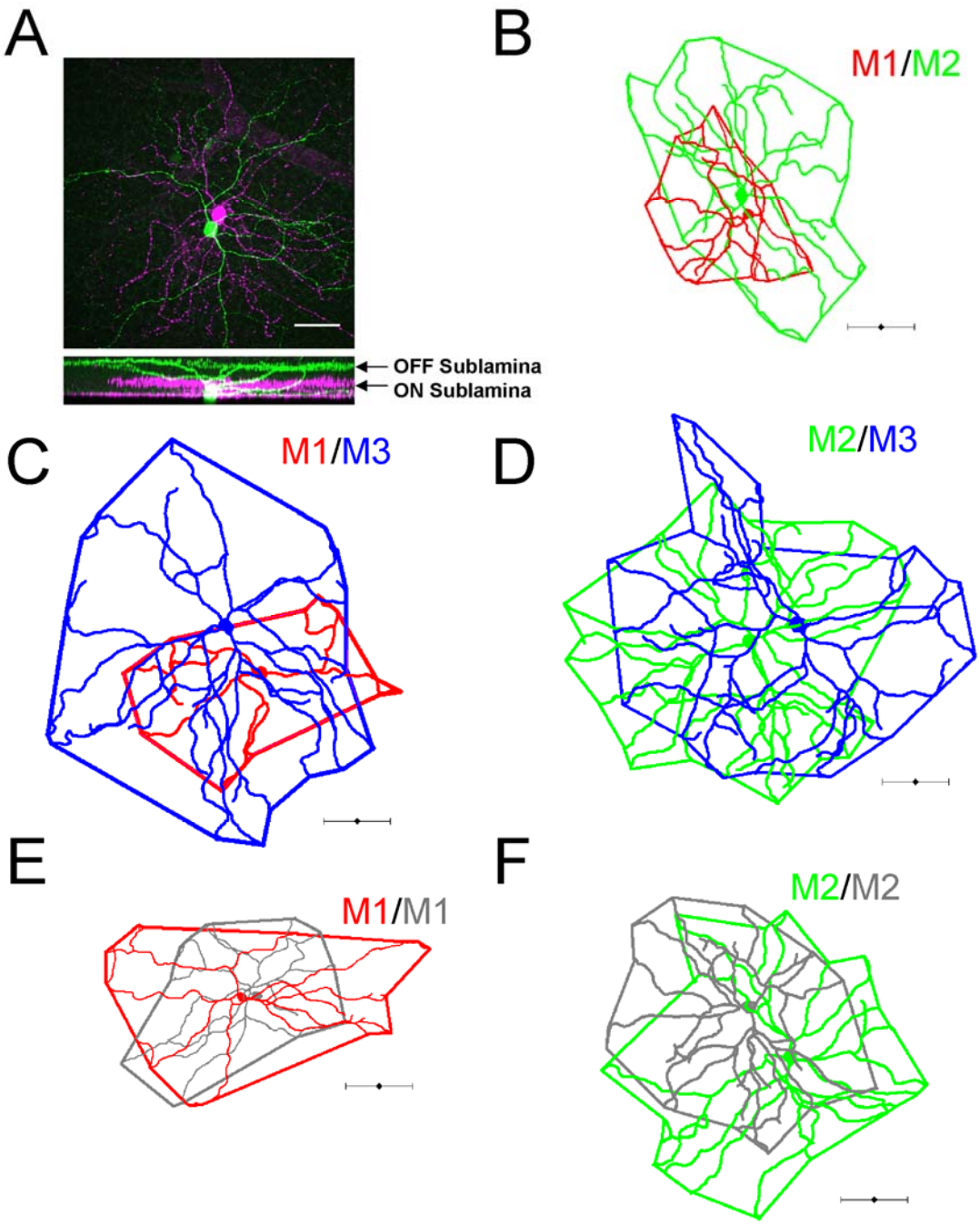

Figure 3. Dendritic field overlap of neighboring ipRGCs.
Neighboring ipRGCs were filled with 0.3% neurobiotin or LY and their arbors traced and dendritic field overlap mapped. Extensive dendritic field overlap was observed between heterotypic (A-D) and homotypic (E-F) filled pairs. (A) Confocal image where an M1 cell (green) was filled with LY and an M2 cell (magenta) with neurobiotin. Scale bar 50µm. (B) Neighboring M1 (red) and M2 (green) cell. (C) Neighboring M1 (red) and M3 (blue) cell. (D) Neighboring M2 (green) and M3 (blue) cell. (E) Neighboring M1 cells. (F) Neighboring M2 cells. Scale bar (A) 50 µm (B-F) 100 µm.

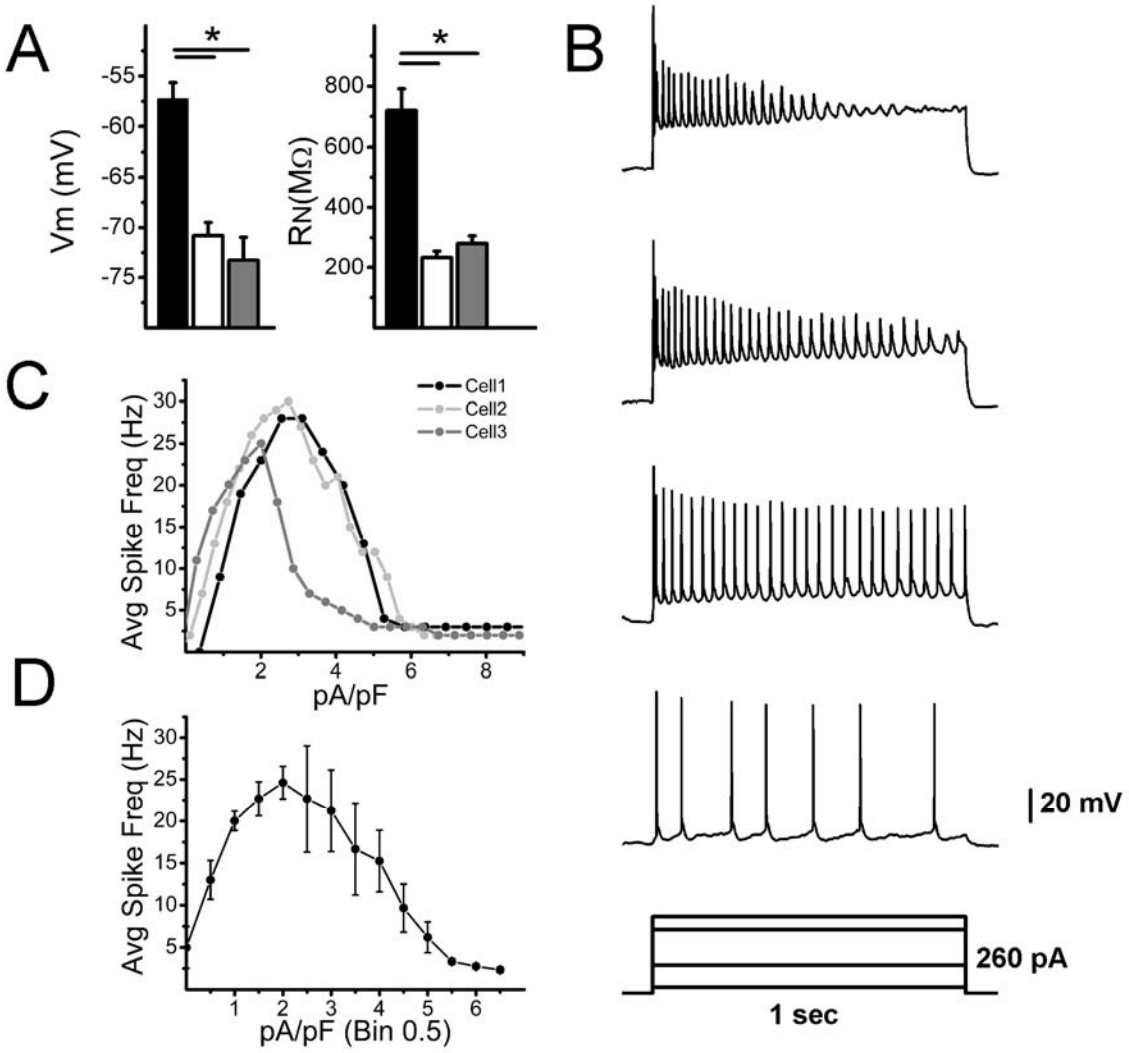

Figure 4. Intrinsic membrane properties of M3 cells.
(A) Recordings were performed in the presence of synaptic blockers and TTX. (left panel) Mean ± SE Vm (mV) of M1 (black bar), M2 (white bar), and M3 cells (gray bar). (right panel) R_N (MΩ) of M1 (black bar), M2 (white bar), and M3 (gray bar) cells. (B-D) Recordings were performed in the presence of synaptic blockers. (B) Representative response of M3 cell to 1 s depolarizing current injection over a range of 260 pA. (C) Average firing frequencies of 3 M3 cells to increasing amounts of depolarizing current injection. (D) Mean ± SE average firing frequency of M3 cells to increasing amounts of 1 s depolarizing current injections. Current injection for each cell was divided by its capacitance (in D, Bin = 0.5 pA/pF) to facilitate averaging. Vm: resting membrane potential, R_N: input resistance. *$P < 0.05$ *ANOVA*

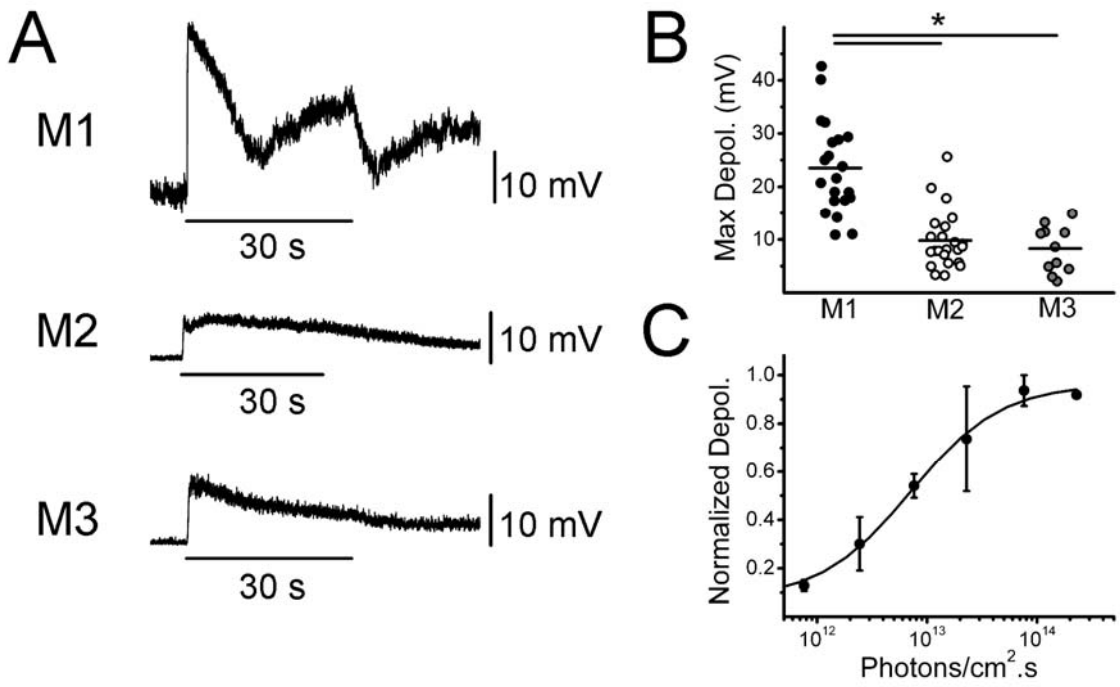

Figure 5. Intrinsic light responses of M3 cells.
All light responses recorded in the presence of synaptic blockers and TTX. (A) Response in current clamp mode of M1 (top panel), M2 (middle panel), and M3 (bottom panel) cells to 30 s full-field, bright, white light stimulus. (B) Maximum depolarization evoked by single 30 s white light stimulus measured in current clamp mode of M1 (black circles), M2 (white circles), and M3 (gray circles) cells. Black bars represent mean maximum depolarization. (C) Irradiance response curve fitted with logistic dose-response function for M3 cells generated by stimulating cells with increasing intensities of a 5 s 480 nm light stimulus. *$P < 0.05$ *ANOVA*.

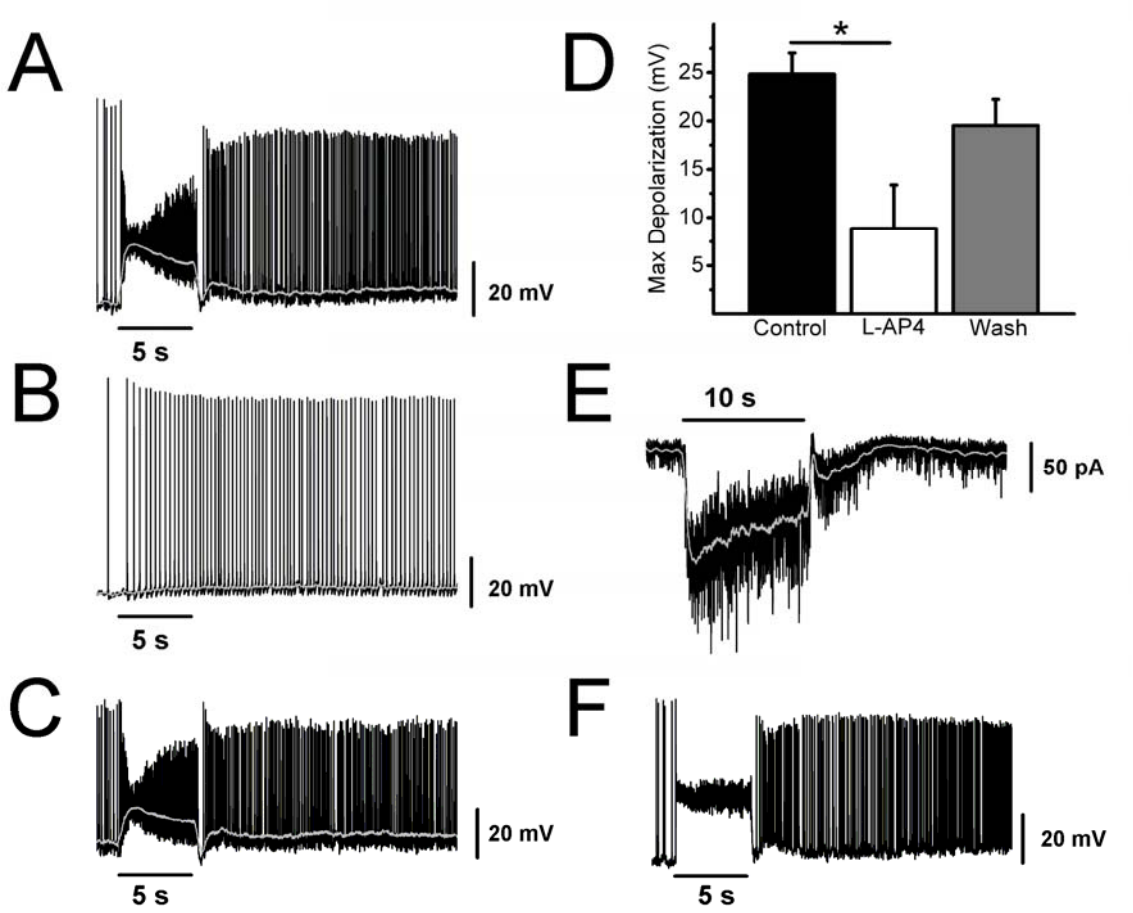

Figure 6. Synaptically-evoked light response of M3 cells in WT mice.
(A-C) Example of typical synaptic light response of an M3 cell recorded in current clamp mode to a 5 s, full-field, bright white light stimulus first in control conditions (A), in the presence of 100 µM L-AP4 (B), and following washout (C). (D) Mean ± SE maximum depolarization evoked by 5 s full-field bright white light stimulus in control (black bar), 100 µM L-AP4 (white bar), and after washout (gray bar). (E) Voltage clamp recording of M3 cell response to 10 s full field, bright, white light stimulus. (F) Example of typical synaptic light response of an M2 cell recorded in current clamp mode to a 5 s, full-field, bright white light stimulus in the absence of synaptic blockers. Gray lines (A-C) represent 0.1 s smoothing of membrane voltage. * $P < 0.05$ *ANOVA*.

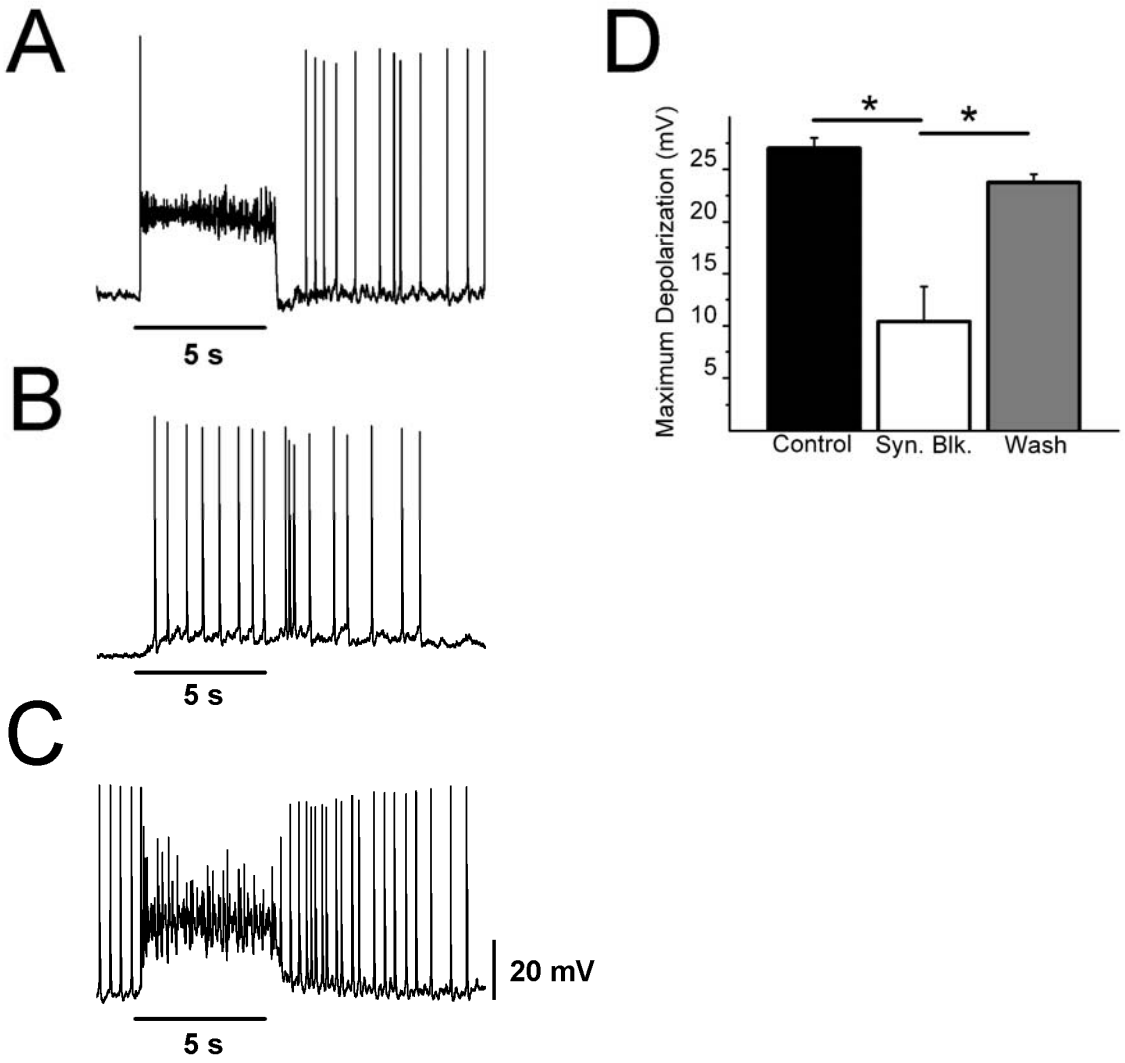

Figure 7. Light response of M3 cells before and after application of a cocktail of synaptic blockers.
(A-C) Example of typical light response of an M3 cell recorded in current clamp mode to a 5 s, full-field, bright white light stimulus first in control conditions (A), in the presence of a cocktail of synaptic blockers (B), and following washout (C). (D) Mean ± SE maximum depolarization evoked by 5 s full-field bright white light stimulus in control (black bar), in the presence of a synaptic blocker cocktail (white bar), and after washout (gray bar). **P* < 0.05, *ANOVA*. Synaptic blocker cocktail included: 100 µM L-AP4, 10 µM DNQX (Tocris, Ellesville, MD), 50 µM picrotoxinin (Sigma), and 5 µM strychnine.

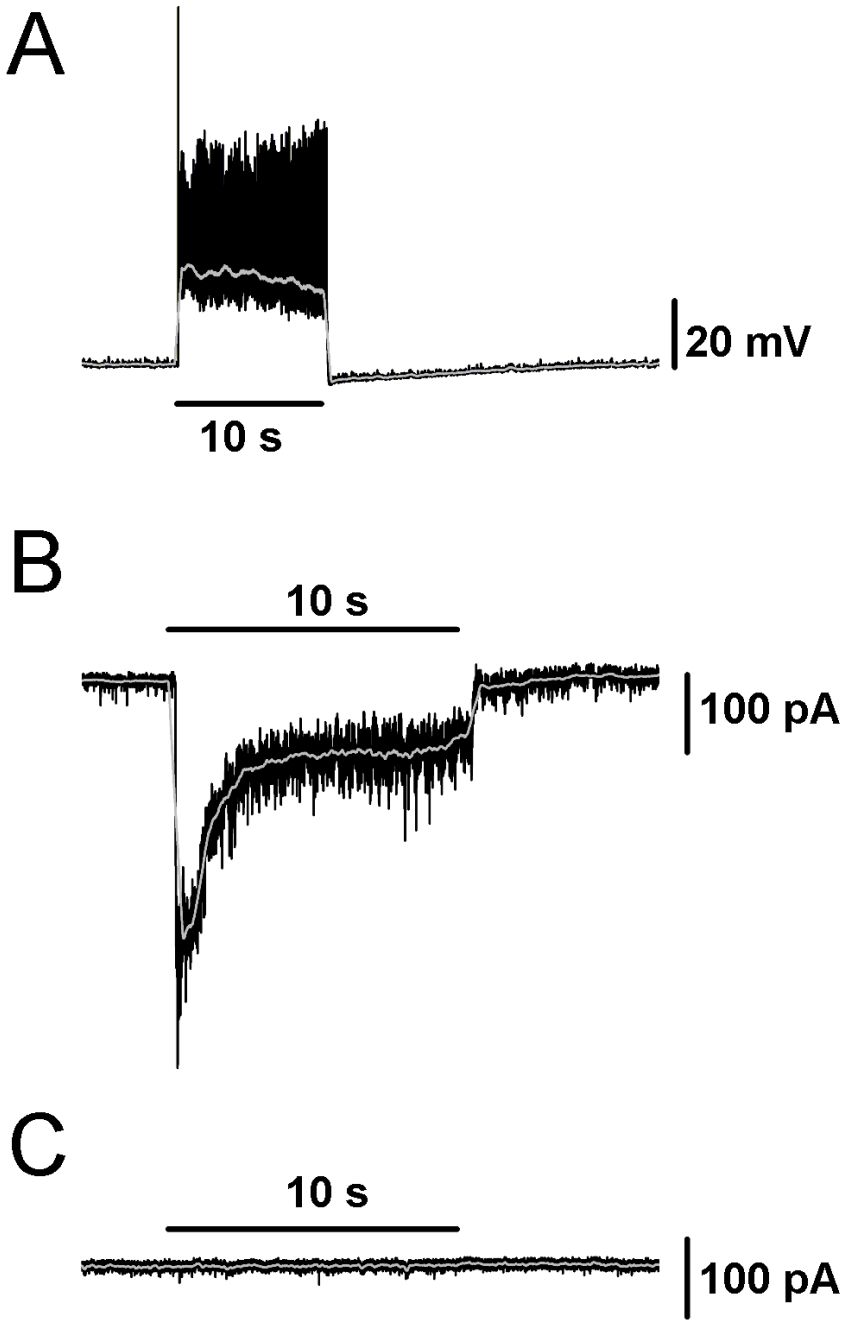

Figure 8. Synaptic input to M3 cells recorded in *Opn4*$^{-/-}$ mice.
(A) Current clamp recording of M3 cell light response to 10 s full-field, bright, white light stimulus in *Opn4*$^{-/-}$ mouse. (B-C) Voltage clamp recording of M3 cell light response to 10 s full field, bright, white light stimulus in *Opn4*$^{-/-}$ mouse first in control conditions (B) and then in the presence of 100 μM L-AP4 (C). In the presence of L-AP4 the light response of this cell is completely abolished. Gray lines (A-C, E) represent 0.1 s smoothing of membrane voltage.

CHAPTER 6

Intrinsic phototransduction persists in melanopsin-expressing ganglion cells lacking diacylglycerol-sensitive TRPC subunits

Perez-Leighton CE,* **Schmidt TM**,* Abromovitz J, Birnbaumer L, Kofuji P (in press)

Eur J Neurosci

*Denotes equal co-author

ABSTRACT

In mammals, intrinsically photosensitive retinal ganglion cells (ipRGCs) mediate various non-image-forming photic responses such as circadian photoentrainment, pupillary light reflex, and pineal melatonin suppression. ipRGCs directly respond to environmental light by activation of the photopigment melanopsin followed by the opening of an unidentified cation-selective channel. Studies in heterologous expression systems and in the native retina have strongly implicated diacylglycerol-sensitive transient receptor potential channels containing TRPC3, TRPC6, and TRPC7 subunits in melanopsin-evoked depolarization. Here we show that melanopsin-evoked electrical responses largely persist in ipRGCs recorded from early postnatal (P6-P8) and adult (P22-P50) mice lacking expression of functional TRPC3, TRPC6, or TRPC7 subunits. Multielectrode array recordings performed at P6-P8 stages under conditions that prevent influences from rod/cone photoreceptors show comparable light sensitivity for the melanopsin-evoked responses in these mutant mouse lines in comparison to wild-type mice. Patch-clamp recordings from adult mouse ipRGCs lacking TRPC3 or TRPC7 subunits show intrinsic light-evoked responses equivalent to those recorded in wild-type mice. Persistence of intrinsic light-evoked responses was also noted in ipRGCs lacking TRPC6 subunits, however of significantly smaller magnitudes. These results demonstrate that the melanopsin-evoked depolarization in ipRGCs is not mediated by either TRPC3, TRPC6, or TRPC7 channel subunits alone. They also suggest that the melanopsin signaling pathway includes TRPC6-containing heteromeric channels in mature retinas.

INTRODUCTION

Intrinsically photosensitive retinal ganglion cells (ipRGC) express the photopigment melanopsin (*Opn4*) and respond directly to light with a sustained depolarization and increase in intracellular calcium (Berson et al., 2002; Hattar et al., 2002; Sekaran et al., 2003; Hartwick et al., 2007). ipRGCs densely innervate brain areas related to non-image-forming (NIF) photic responses (Hattar et al., 2006; Baver et al., 2008). These cells integrate light information from rod and cone photoreceptors with their intrinsic light response (Dacey et al., 2005; Schmidt et al., 2008; Schmidt and Kofuji, 2009, 2010a), and their axonal projections are the main source of photic input to elicit various NIF visual behaviors (Goz et al., 2008; Guler et al., 2008; Hatori et al., 2008b).

It has been suggested that mammalian ipRGCs and *Drosophila* rhabdomeric photoreceptors share similar phototransduction mechanisms (Berson, 2007; Peirson et al., 2007). Sequence analysis of *Opn4* has indicated its closer evolutionary relationship to invertebrate rhodopsins than vertebrate opsins (Nickle and Robinson, 2007). Like ipRGCs, *Drosophila* photoreceptors depolarize in response to light (Hardie and Raghu, 2001). Additionally, as in *Drosophila* photoreceptors (Hardie and Raghu, 2001), ipRGC phototransduction engages a membrane-anchored mechanism and requires activation of a $G_{q/11}$ protein and phospholipase-C activity (Graham et al., 2008). However, identification of the channel(s) that mediate the melanopsin-evoked depolarization in ipRGCs remains elusive (Do and Yau, 2010).

In *Drosophila* photoreceptors, the transient receptor potential (TRP) channel mediates the initial depolarization upon light stimulation (Hardie and Minke, 1992;

Phillips et al., 1992). There are seven mammalian TRP homologues, denominated TRP canonical (TRPC) subunits 1-7 (Clapham et al., 2001) that combine to form tetrameric channels (Hofmann et al., 2002). Pharmacological evidence implicates the diacylglycerol-sensitive TRPC channels (formed by different combinations of subunits TRPC3, TRPC6 and TRPC7), in ipRGC intrinsic phototransduction. However, evidence has been contradictory with regard to which of these TRPC subunits are involved (Warren et al., 2006; Hartwick et al., 2007; Sekaran et al., 2007). Furthermore, immunocytochemical evidence has been scarce, but supports cellular colocalization of melanopsin with TRPC6 and possibly TRPC7 (Warren et al., 2006; Sekaran et al., 2007). Messenger RNA analysis of ipRGC-enriched primary cultures has also indicated the presence of all three subunits and enrichment of TRPC7 (Hartwick et al., 2007). Finally, the melanopsin photopigment can trigger activation of TRPC3 channels in various heterologous expression systems (Panda et al., 2005; Qiu et al., 2005).

Perhaps the greatest hurdle in identifying whether and which TRPC channel subunits are involved in melanopsin phototransduction *in situ* is the lack of pharmacological tools specifically affecting individual TRPC channels (Birnbaumer, 2009). Because of this lack of specificity of various TRPC inhibitors, we utilized mouse lines lacking either TRPC3, TRPC6 or TRPC7 subunits to examine the role of these TRPC subunits in ipRGC phototransduction. By means of multielectrode array (MEA) and single cell patch-clamp recordings, we demonstrate that melanopsin-evoked responses of ipRGCs are not mediated by TRPC3, TRPC6, or TRPC7 subunits as homomeric channels. Our data also suggest that TRPC6 subunits contribute to the nonselective cation conductance mediating the ipRGC intrinsic photoresponse.

MATERIALS AND METHODS

Animals

TRPC3$^{-/-}$ (Hartmann et al., 2008), *TRPC6*$^{-/-}$ (Dietrich et al., 2005), and *TRPC7*$^{-/-}$ lines in 129Sv:C57BL/6J background (see next section) were backcrossed to the *Opn4-EGFP* mouse line (Schmidt et al., 2008) for electrophysiological recordings. The *Opn4-EGFP* mice in a C57BL/6J background have been described previously (Schmidt et al., 2008) and were used as wild-type controls as well. The *Opn4*$^{-/-}$ mouse line (Hattar et al., 2002) was generously provided to us by Dr. King-Wai Yau. Animals were cared for in accordance with guidelines described in *Guide for the Care and Use of Laboratory Animals*, using protocols approved by the University of Minnesota Institutional Care and Use Committee.

Generation of *TRPC7*$^{-/-}$ mice

TRPC7$^{-/-}$ mice were generated by disrupting the *Trpc7* gene in a four step process. First, the targeting vector containing loxP sites flanking exon 5 and the PGK-neo cassette was generated (Figure 3). Second, in embryonic stem cells (ES) cells, loxP recombination sites were introduced by homologous recombination into the introns bordering exon 5 of the murine *Trpc7* gene. Electroporation and isolation of neomycin resistant cell clones were performed as described (Rudolph *et al.*, 1994). Third, the F0 generation of chimeric mice generated from blastocysts that had received the targeted ES cells were interbred and used to generate mice homozygous for the *Trpc7* gene with floxed exon 5 (*Trpc7* flx/flx). Fourth, male *Trpc7* flx/flx mice were crossed to female mice carrying a transgene directing the expression of Cre recombinase under the control of the Sox2 promoter (Tg[Sox2-Cre] mice, Jackson Laboratories, Bar Harbor, ME,

USA). The resulting heterozygous null mice were bred and mice which were *TRPC7*$^{-/-}$ and negative for the Sox2-Cre transgene were identified by PCR analysis of tail biopsies (Figure 3).

RNA extraction and reverse transcription

Retinas from postnatal P6-P8 animals were dissected in 95% O_2-5% CO_2 bicarbonate buffered Ames' medium (Sigma, St. Louis, MO, USA) at room temperature and stored in RNALater (Qiagen, Valencia, CA, USA) at -80°C. RNA was extracted using RNeasy kit (Qiagen) and immediately quantified using Nanodrop 1000 spectrophotometer (Thermo Scientific, Wilmington, DE, USA). Equal amounts of RNA for all samples were subjected to reverse transcription using Quantitect Reverse Transcription Kit (Qiagen) and cDNA stored at -20°C until use.

Real time Polymerase Chain reaction (PCR)

Real Time PCR was conducted on the cDNA from WT, *TRPC3*$^{-/-}$, *TRPC6*$^{-/-}$, and *TRPC7*$^{-/-}$ retinal samples employing the TaqMan system (Roche Applied Science, Indianapolis, IN, USA) in a LightCycler 2.0 Thermocycler (Roche Applied Science). All primers used were designed using the Universal Probe Library Assay Design Center and were: β-actin (fwd: 5'-AAGGCCAACCGTGAAAAGAT-3, rev: 5'-GTGGTACGACCAGAGGCATAC-3), TRPC3 (fwd: 5'-TGGATTGCACCTTGTAGCAG-3', rev: 5'-ACCCAGAAAGATGATGAAGGAG-3'), TRPC6 (fwd: 5'-TACTGGTGTGCTCCTTGCAG-3', rev: 5'-CAAACTTCATGAACGGTCCTC-3'), TRPC7 (fwd: 5'-GTGGCCTACTTCACCTACGC-3', rev: 5'-CGAGATGATCTGGGGGTCT-3') and Opn4 (fwd:5'-CTCTCTGTTAGCCCCACGAC-3',rev:5'-

GACATCGACTGTGGGGAAG-3'). Opn4, TRPC3, TRPC6 and TRPC7 mRNA levels were normalized against β-actin mRNA levels correcting by PCR efficiencies determined by the dilution curve method (Pfaffl, 2001).

End Point PCR

Primers for murine TRPC3 exon 7 (fwd: 5'- AGTGACTTCTGTTGTCCTCA-3', rev: 5'-CTCGATCTCTTGGTATGAGCTA-3'), murine TRPC6 exon 7 (fwd: 5'-TGGGACCCTACTGATCCTCAGA-3', rev: 5'-ATGCTTCATTCTGTTTTGCGCC-3'), murine TRPC7 exon 5 (fwd: 5'-GGACAAACCCTGAGGAGCCC-3', rev: 5'-TTAACGCCCTCAAACCGGTCG-3') were designed using Perl scripts. PCR reactions were performed using HotStart Taq Plus DNA polymerase kit (Qiagen). PCR protocol consisted of 5 min at 95°C followed by 30 cycles of 1 min at 94°C, 30 sec at 58°C, and 1 min at 72°C. Extension was concluded at 72°C for 10 min.

Immunohistochemistry

Immunocytochemistry was performed essentially as previously described (Connors and Kofuji, 2002; Schmidt et al., 2008). The primary antibodies used in this study as well as their dilutions are listed in Table 1. We used goat anti-mouse AlexaFluor (AF) 488 (A11029), goat anti-rabbit AF488 (A11034) and donkey anti-mouse AF594 (A11058) as secondary antibodies (all from Invitrogen, Carlsbad, CA, USA). Controls with omission of either primary or secondary antibodies revealed no detectable signal. In addition, the localization and morphology of the stained cells with each primary antibody matched previous descriptions in retina (Haverkamp and Wassle, 2000) and see Table 1, confirming the specificity of the antibodies used in this study. For the anti-melanopsin antibody, its specificity was tested upon immunostaining of

WT and *Opn4*$^{-/-}$ retinas. Staining of a subset of wide-field ganglion cells in the ganglion cell layer in WT retinas, and lack of staining in the *Opn4*$^{-/-}$ retinas shows that the antibody labels ipRGCs specifically (Figure 1).

Image Observation and ipRGC cell count

All fluorescent specimens were imaged with an Olympus Fluoview 1000 confocal microscope. For the retinal markers and melanopsin cell count, we used 40X and 20X oil-immersion lens respectively. Optical sections were collected at 0.2- to 1.0-μm intervals and reconstructions of several optical images onto a single plane were performed using National Institutes of Health ImageJ 1.42q (http://rsb.info.nih.gov/ij/). Contrast and brightness of the images for retinal markers were adjusted using Adobe Photoshop CS2 (Adobe System, San Jose, CA, USA). For melanopsin cell density analysis, all images were processed with Adobe Photoshop CS2 (Adobe System). Images were converted to their negative to observe dark stained nuclei. The image levels and contrast were adjusted to match a standard image. This step assigned the same contrast level to all the images to make easier the identification of stained nuclei. Dark melanopsin immunoreactive nuclei were counted semi automatically using ImageJ Cell Counter plugin (http://rsbweb.nih.gov/ij/plugins/cell-counter.html). Averages from 4-5 images from each retina were used to calculate cell density for each retina. Melanopsin positive cell density data was analyzed using the R Statistical Project v2.11 software (http://www.R-project.org) with a one-factor *ANOVA* with genotype as experimental factor. Significance criterion was set at 0.05.

MEA Recordings: Data recording

Retinas of P6-P8 animals were dissected as described (Schmidt et al., 2008; Schmidt and Kofuji, 2011) and mounted ganglion cell layer down over the MEA electrode array. The electrodes were arranged in a 8X8 grid with no corner electrodes, 200 μm inter-electrode spacing, and 30 μm electrode diameter. The MEA system was purchased from Multi Channel Systems (Reutlingen, Germany) and included the 60-electrode array (200/30-Ti), headstage (MEA1060-2-BC), filter amplifier (FA60SBC) and PCI-bus data acquisition system (MCCard 64). Retinas were dark adapted for 15-20 minutes before start of the light stimulation protocol. During all recordings retinas were superfused with 95% O_2-5%CO_2 bicarbonate buffered Ames' medium (Sigma) with synaptic blockers at 36°C. Data recorded was amplified and digitized with a sampling frequency of 25 kHz.

MEA Recordings: Light Stimulation

Stimulation protocol consisted of 1 min baseline in the dark, 1 min light stimulation (480 nm, narrow band pass filter), and 4 min post-stimulation in the dark. Light stimulation was generated using a Xenon lamp feeding a fiber optic to the preparation interposed with a filter wheel fitted with neutral-density and narrow band-pass filters (Chroma Technologies, Rockingham, VT, USA). We used light intensities (in photons / $cm^2 \cdot sec$) of 7.32×10^{10}, 2.31×10^{11}, 7.32×10^{11}, 1.16×10^{12}, 2.31×10^{12}, 3.67×10^{12}, 7.32×10^{12}, 3.67×10^{13}, 7.32×10^{13} as measured with a calibrated radiometer model S370 (UDT Instruments, San Diego, CA, USA).

MEA Recordings: Data analysis

MEA data was processed using high (200 Hz) and low (3000 Hz) band pass filters. Extracellular spikes were extracted using a threshold filter of -4.5 standard

deviations calculated independently for each electrode using MCRack v 4.0.0 software (Multi Channel Systems). Extracted spikes from all light intensities corresponding to a single electrode were concatenated into a single file using MCData Tool v2.6.0 software (Multi Channel Systems). Only electrodes that showed at least twice the number of spikes during the light stimulation period than during baseline were used for further analysis. Spikes were aligned to reduce jitter and clustered using principal component analysis with Offline Sorter v 2.8.6 software (Plexon Inc, Dallas, TX, USA). ipRGC light responses were identified based on the time lock between light stimulation and the appearance of spikes. ipRGC response features were further analyzed using Igor Pro 5.04 software (WaveMetrics, Portland, OR, USA) and the extracted features were: 1) IR_{50} of the light response, defined after fitting a Hill function to the number of light induced spikes normalized to maximum versus the log of light intensity (log (IR)), 2) Light induced spikes, defined as the total number of spikes during light stimulation, 3) Maximal spiking frequency, defined as the maximal spiking frequency after light onset using 5 second bins, 4) Latency, defined as time between light onset and maximal spiking frequency.

MEA Recordings: Statistical Analysis

Initial analysis ipRGC intrinsic light responses showed the data had non-normality, lack of homocedasticity and unequal sample size. Therefore, we decided to use randomization tests for the analysis of the data (Edgington & Onghena, 2007). We analyzed the IR_{50} with a randomization-based t-test to compare directly between each $TRPC^{-/-}$ and WT responses followed by a false discovery rate (FDR) correction for multiple testing. We analyzed the dose response curves between each $TRPC^{-/-}$ and WT

by means of a randomization 2-way *ANOVA* using genotype (*TRPC*$^{-/-}$ vs WT) and light intensity as experimental factors. Pairwise comparisons between genotypes at each light intensity were done by t-test using the residual error of the *ANOVA* as variance followed by an FDR correction. We analyzed the number of light induced spikes and other features of the ipRGC intrinsic light response using a randomization t-test followed by a FDR correction for each of the comparison between WT and TRPC responses at each of the light intensities. All statistical analyses were implemented using the R Statistical Project v2.11 software (http://www.R-project.org). We generated all graphs using the R Statistical Project Software. For all tests the significance criterion was set at 0.05. Data are shown as mean ± SEM.

MEA Recordings: Pharmacology

Synaptic blocker cocktail added to the extracellular Ames' medium included: 250 μM DL-2-amino-4-phosphonobutyrate (DL-AP4, a group III metabotropic glutamate receptor agonist); 10 μM 6,7-dinitroquinoxaline (DNQX, α-amino-3-hydroxy-5-methyl-4-isoxazolepropionic acid (AMPA)/kainate receptor antagonist); 0.3 μM strychnine, 50 μM picrotoxin, and 10 nM (±)-epibatidine dihydrochloride. All reagents were purchased from Tocris (Ellesville, MO, USA).

Whole-cell Patch Clamp Recordings

Recordings were performed on P 22-50 animals from the *Opn4-EGFP* mouse line described previously (Schmidt and Kofuji, 2009, 2010a) on a WT, *TRPC3*$^{-/-}$, *TRPC6*$^{-/-}$, *or TRPC7*$^{-/-}$ background. Dissections were performed as described previously (Schmidt et al., 2008; Schmidt and Kofuji, 2011). Retinas were removed from the eyecups and bubbled with 95% O_2-5% CO_2 bicarbonate buffered Ames' solution

(Sigma) at room temperature in a dark room with minimal ambient light. Prior to recording, retinas were treated with Ames' solution containing collagenase/hyaluronidase (240 and 1000 U/ml, respectively) at room temperature for 15 minutes to remove vitreous. Recordings were performed using an Axon 700B Amplifier (Molecular Devices, Union City, CA) with extracellular solution containing 95% O_2-5% CO_2 bicarbonate buffered Ames' solution (Sigma) at 32-34^oC. For current clamp recordings, pipettes were filled with (in mM): 125 K-gluconate, 2 $CaCl_2$, 2 $MgCl_2$, 10 EGTA, 10 HEPES, 0.5 NaGTP, and 2 Na_2ATP, pH to 7.2 with KOH. For voltage clamp recordings, pipettes were filled with (in mM): 125 CsMethanesulfonate, 10 $CsCl_2$, 5 EGTA, 1 $MgCl_2$, 2 Na_2ATP, 10 NaHepes, 10 Phosphocreatine, 2 QX314, 0.5 NaGTP, pH to 7.6 with KOH. Intracellular solutions also contained 10 μM Alexafluor-594 hydrazide (AF-594) (Invitrogen) and dendritic stratification was classified by focusing in the proximal and distal layers of the IPL. Series resistance was noted in all recordings, but uncompensated and only recordings with series resistance of < 30 MΩ were included for analysis. For whole cell recordings, the synaptic blocker cocktail was identical to that employed in the MEA recordings (see above) but without the cholinergic blocker epibatidine dihydrochloride. We also included 0.5 μM tetrodotoxin (TTX, sodium channel blocker) (Ascent, Princeton, NJ, USA) to prevent action potential firing.

Whole cell patch clamp recordings: Light stimulation

A filter wheel fitted with various narrow bandpass (10 nm bandwidth) and neutral-density filters (Chroma Technologies, Rockingham, VT) and shutter (Lambda-3, Sutter Instruments, Novato, CA, USA) was used to control the intensity and duration of

light stimuli. Light stimuli for all experiments were full-field, 480 nm light (5.87 X 10^{16} photons.cm^{-2}.s^{-1} unattenuated) generated by interposing a narrow bandpass filter. Stimuli were delivered using a xenon lamp feeding the camera port at -2.1LogI for current clamp and -1.5LogI for voltage clamp experiments. Cells were given 5 min to dark adapt prior to light stimulation.

Whole cell patch clamp: Analysis

Whole cell currents were analyzed off-line with Clampfit (Molecular Devices), and membrane potential values were measured from raw traces over a 1 s sliding time window to maximize the signal to noise ratio using Igor Pro 6.0 (Portland, OR, USA). Resting membrane potential (Vm) values were calculated by taking the average membrane voltage of the first 10 s of baseline prior to any light stimulation.

Whole cell patch clamp: Statistics

Statistical analysis of whole-cell data was performed using Origin 7.5 (OriginLab, Northampton, MA, USA). Statistical comparison of means was performed using a two-tailed Student's t-test or one way *Analysis of Variance* (*ANOVA*) and significance criterion was set at 0.05. Data are presented as mean ± SE.

RESULTS

MEA analysis suggests two subtypes of ipRGC light responses in WT mice.

We first examined the light-evoked responses of ipRGC in isolated retinas of WT mice using MEA recordings. We chose to record from early postnatal mice (P6-P8) as it has been shown that ipRGCs constitute the only light-responsive ganglion cells at this developmental stage (Sekaran et al., 2005; Tu et al., 2005) allowing for isolated recording of ipRGC intrinsic light responses. Though outer retinal signaling to ganglion cells is not present at this developmental stage (Sernagor et al., 2001), we included a cocktail of synaptic blockers in the Ames' medium to inhibit any glutamatergic, GABAergic, and glycinergic signaling to ipRGCs (see Methods). This ensured that all light responses recorded originated from ipRGC intrinsic photoresponses. We also added cholinergic blockers to minimize interference from retinal waves present at this developmental stage (Sun et al., 2008). The MEA technique allowed for simultaneous recording of light responses from multiple ipRGCs per retina. Following a period of dark adaptation for 15-20 min, the retinas were submitted to diffuse, uniform light stimulation of increasing irradiance (from 7.3 X 10^{10} to 7.3 X10^{13} photons / cm^2·sec) for 60 sec at 480 nm, the peak wavelength for melanopsin activation (Berson, 2007; Do and Yau, 2010). The retinas were then allowed to readapt to dark for 4 min following each stimulation episode. Figure 2A shows the light induced spike activity from ipRGCs of two apparently distinct subtypes (see below). Similar to previous studies, we observed that all ipRGCs responded to increasing light intensities with increasing firing rates that reached their maximum several seconds following light onset. Upon termination of the light stimulus, most

ipRGCs continued to display substantial spike activity that persisted for several seconds. The relatively sluggish initiation and termination of spike responses are consistent with previous reports of melanopsin-evoked light responses (Berson et al., 2002; Dacey et al., 2005; Tu et al., 2005; Schmidt et al., 2008). Spike discharge rates returned to baseline 5-30 seconds following light offset (Figure 2A).

Previous studies have demonstrated considerable heterogeneity in the sensitivity, response latency, and maximal spike frequency of melanopsin-evoked light responses (Sekaran et al., 2003; Sekaran et al., 2005; Tu et al., 2005; Schmidt and Kofuji, 2009). Likewise we found that ipRGCs could be qualitatively separated into subpopulations with high and low light sensitivities (LS), consistent with previous reports at this developmental stage (Tu et al., 2005). Figure 2A shows representative voltage traces from a high (Figure 2A, left) and a low (Figure 2A, right) LS ipRGC. The $\log IR_{50}$ histogram of the normalized ipRGC intrinsic light responses (n = 93 cells, from 5 retinas) showed an apparent bimodal distribution (Figure 2B) that could be arbitrarily separated into high (n = 66 cells) and low (n = 27 cells) LS cell populations using a cutoff of log(IR) = 12.70 photons / $cm^2 \cdot sec$ (Figure 2B-C). We also found that high LS ipRGCs had significantly higher average spike frequency and maximal spike frequency as well as a significantly shorter latency to response onset than low LS ipRGCs (Table 2).

Generation of *TRPC7*$^{-/-}$ mouse line.

To examine the contribution of the diacylglycerol-sensitive TRPC channel subunits to the melanopsin-mediated light responses we utilized *TRPC3*$^{-/-}$, *TRPC6*$^{-/-}$ and *TRPC7*$^{-/-}$ mouse lines. The generation of the *TRPC3*$^{-/-}$ and *TRPC6*$^{-/-}$ mouse lines has

been described elsewhere (Dietrich et al., 2005; Hartmann et al., 2008). To generate *TRPC7*$^{-/-}$ mice, the TRPC7 gene was ablated in mice through homologous recombination using a targeting construct to delete the exon 5 within the putative 4th transmembrane domain (Figure 3A). The deletion of exon 5 was catalyzed by Cre-recombinase and verified by PCR analyses of genomic DNA (Figure 3A,B). In addition, RT-PCR analyses of transcripts from brain WT and *TRPC7*$^{-/-}$ mice confirm the deletion of exon 5 at mRNA level (Figure 3C,D). The *TRPC7*$^{-/-}$ mouse line was viable and showed no obvious differences from WT in weight and size.

***TRPC3*$^{-/-}$, *TRPC6*$^{-/-}$ and *TRPC7*$^{-/-}$ mouse retinas develop normally.**

To examine whether diacylglycerol-sensitive TRPC channels are expressed at early postnatal stages in the mouse retina, we performed real-time RT-PCR on P6-P8 mouse retinas. We found evidence for the expression of TRPC3, TRPC6, and TRPC7 at this developmental stage, with higher levels for the TRPC3 subunit (Figure 4). End-point RT-PCR analysis also detects expression of these subunits in WT retinas at adult stages, in agreement with previous reports (Warren et al., 2006; Hartwick et al., 2007; Sekaran et al., 2007). As expected, the transcripts of exons deleted by genetic targeting were not detectable by end-point RT-PCR in *TRPC3*$^{-/-}$, *TRPC6*$^{-/-}$, and *TRPC7*$^{-/-}$ mouse retinas (Figure 5A). We next asked whether the lack of expression for these TRPC channel subunits affected the overall development of the retinas as TRPC channels have been implicated in guidance of nerve growth cones (Li *et al.*, 2005) and in neuronal development (Tai *et al.*, 2009). DAPI nuclear staining showed no apparent abnormalities in the nuclear layers in the retinas of any of the mutant mouse lines (Figure 5B). Furthermore, immunohistochemical analysis of Müller cells, rod bipolar

cells, dopaminergic amacrine cells and cholinergic amacrine cells yielded no observable differences between WT and mutant mice (Figure 6). Analysis of melanopsin-immunoreactive cells revealed no differences in ipRGC cell density between genotypes (Figure 5C, *ANOVA*, $P = 0.736$). These results suggest that lack of expression of TRPC 3/6/7 channel subunits does not affect the morphological development of the retinal cell types and ipRGCs.

Early postnatal WT, *TRPC3*$^{-/-}$, *TRPC6*$^{-/-}$, and *TRPC7*$^{-/-}$ ipRGCs have similar intrinsic light responses.

To examine whether TRPC3, TRPC6, and TRPC7 subunits participate in melanopsin-evoked phototransduction, we next performed MEA recordings of ipRGC light responses from *TRPC3*$^{-/-}$, *TRPC6*$^{-/-}$ and *TRPC7*$^{-/-}$ mice using the same stimulation protocols as those employed in the WT mice. For these experiments we used P6-P8 retinas from *TRPC3*$^{-/-}$ ($n = 83$ cells from 5 retinas), *TRPC6*$^{-/-}$ ($n = 50$ cells from 3 retinas) and *TRPC7*$^{-/-}$ ($n = 38$ cells from 3 retinas) mice. ipRGCs from *TRPC3*$^{-/-}$, *TRPC6*$^{-/-}$, and *TRPC 7*$^{-/-}$ mice responded to light stimulation with similar overall characteristics as WT ipRGCs (Figure 7). At lower light intensities, the initiation of responses was relatively sluggish and spike activity persisted for several seconds following light-offset. Figure 7 shows voltage traces for a typical cell from *TRPC3*$^{-/-}$ (Figure 7A), *TRPC6*$^{-/-}$ (Figure 7B), and *TRPC7*$^{-/-}$ (Figure 7C) retinas. The persistence of light responses in these mutant mice indicates that the individual expression of TRPC3, TRPC6, or TRPC7 subunits is not required for melanopsin-driven photoresponses. Though we were able to separate WT ipRGCs into two subpopulations of high- and low-sensitivity groups based on a bimodal distribution of IR_{50} (see above),

the distribution of IR_{50}'s in the TRPC$^{-/-}$ mice, especially *TRPC7*$^{-/-}$ mice, did not show an apparent bimodal distribution. Thus we considered all ipRGCs as a homogeneous population for further comparison between the mouse lines. Figure 8A,C,E shows the histograms for the log(IR_{50}) distributions for the TRPC $^{-/-}$ retinas. Analysis of the log(IR_{50}) values (in photons / cm^2·sec) using a randomization t-test followed by a FDR multiple testing correction (See Methods) showed no differences between WT (12.5 ± 0.05) and *TRPC3*$^{-/-}$ (12.7 ± 0.05, $P = 0.096$), *TRPC6*$^{-/-}$ (12.4 ± 0.06, $P = 0.133$) and *TRPC7*$^{-/-}$ (12.4 ± 0.05, $P = 0.094$). Next, we compared the dose-response curve between WT and each TRPC$^{-/-}$ by means of a randomization based two-way *ANOVA* with genotype and light intensity as experimental factors. The statistical analysis showed no significant differences between WT and *TRPC3*$^{-/-}$ (Figure 8B) or *TRPC6*$^{-/-}$ (Figure 8D). Pair-wise comparisons at each light intensity between WT and *TRPC7*$^{-/-}$ showed only significant differences at 2 light intensities in the middle of the dose-response curve (Figure 8F). Together, this evidence shows that ipRGCs from all three TRPC $^{-/-}$ mice maintain their intrinsic light responses with similar light sensitivity compared to the WT mice.

The previous results indicate that the light sensitivity of the melanopsin phototransduction pathway is not appreciably altered upon genetic inactivation of TRPC3, TRPC6 or TRPC7 channels. Next we tested whether the light-evoked spike output of the ipRGCs is modified in these mouse lines. We compared the average light-evoked spike frequency of ipRGCs in WT, *TRPC3*$^{-/-}$, *TRPC6*$^{-/-}$, and *TRPC7*$^{-/-}$ mice at various light intensities (Figure 9). We did not observe a statistically significant

difference in firing frequency for either *TRPC6*$^{-/-}$ or *TRPC7*$^{-/-}$ ipRGCs with the exception of an enhanced spike activity in the *TRPC6*$^{-/-}$ mouse at one light intensity (See Methods for details on statistical analyses). However, we observed a small but significant decrease in the firing frequency of *TRPC3*$^{-/-}$ ipRGCs at most light intensities tested, indicating that ipRGCs in *TRPC3*$^{-/-}$ mice, though they display similar sensitivity to ipRGCs in the WT mouse, do not attain similar spike frequencies in response to light stimulation (See Figure 9 legend for details).

Persistence of intrinsic light-evoked responses in M1 and M2 ipRGCs recorded from *TRPC3*$^{-/-}$ *TRPC6*$^{-/-}$, and *TRPC7*$^{-/-}$ adult mice.

One potential limitation of MEA recordings is that they sample only light responding ipRGCs. If genetic inactivation of a TRPC channel subunit renders subpopulations of ipRGCs unresponsive to light then they would escape detection using this method. In addition, MEA recordings are unable to identify the ipRGC subtype using morphological criteria. There are at least three and perhaps as many as five major subtypes of ipRGCs based on their morphological and physiological characteristics (Viney et al., 2007; Schmidt et al., 2008; Ecker et al., 2010). To allow for identification of and recording from single ipRGCs in the various TRPC knockout lines, we crossed our *Opn4-EGFP* reporter mouse line with the *TRPC3*$^{-/-}$, *TRPC6*$^{-/-}$, and *TRPC7*$^{-/-}$ mouse lines. At adult stages, ipRGCs subtypes can be recognized based on their pattern of dendritic stratification in the inner plexiform layer (IPL). M1 cells have dendrites branching in the outermost layers of the IPL while the M2 cells have dendrites branching in the innermost layers of the IPL (Viney et al., 2007; Schmidt et al., 2008; Schmidt and Kofuji, 2009). When we recorded intrinsic light responses of M1 and M2

cells to full-field, bright, 480 nm light in WT and *TRPC6*$^{-/-}$ mice in current clamp mode, we found that all ipRGCs in the *TRPC6*$^{-/-}$ mice responded to light stimulation, but with a significantly reduced amplitude (maximum depolarization) (M1 = 7.24 ± 1.30 mV, *n* = 12; M2 = 2.77 ± 0.16 mV, *n* = 9) relative to WT (M1 = 24.57 ± 1.67 mV, *n* = 9, *P* = 0, *t*-test; M2 = 5.77 ± 0.45 mV, *n* = 10, *P* = 0.00001, *t*-test)(Figure 10A,B,E). Similar results were obtained when light responses of WT and *TRPC6*$^{-/-}$ M1 and M2 cells were recorded in voltage clamp mode with ipRGCs in *TRPC6*$^{-/-}$ mice all responding to light, but with significantly smaller inward current (maximum current) (M1 = -149.28 ± 31.51 pA, *n* = 14; M2 = -37.9 ± 10.50 pA, *n* = 12) than that of WT ipRGCs (M1 = -524.50 ± 54.10 pA, n = 11, *P* = 0, *t*-test; M2 = -82.79 ± 0.85 pA, *n* = 11, *P* = 0.0073, *t*-test)(Figure 10C,D,F). ipRGCs in *TRPC3*$^{-/-}$ (M1 = -347.65 ± 99.25 pA, n = 6; M2 = -53.62 ± 2.30 pA, *n* = 4) and *TRPC7*$^{-/-}$ (M1 = -337.47 ± 48.75 pA, *n* = 3; M2 = -64.57 ± 26.6 pA, *n* = 4) also all responded to light with a sustained inward current similar to that seen in WT (M1 = -415.91 ± 42.53 pA, *n* = 7, *P* = 0.72, one-way *ANOVA*; M2 = -44.51 ± 8.61 pA, *n* = 5, *P* = 0.65, *ANOVA*) (Figure 11A-C) . Collectively, these results support our results using MEA and indicate that ipRGCs continue to respond to light in the absence of TRPC3, TRPC6, or TRPC7 subunits. Furthermore, data from *TRPC6*$^{-/-}$ mice indicate that this subunit may play a significant role in melanopsin phototransduction for both M1 and M2 cells.

DISCUSSION

Using a combination of MEA and whole-cell electrophysiological recordings from retinas of various TRPC knockout mouse lines, we demonstrate that genetic inactivation of either TRPC3, TRPC6, and TRPC7 channel subunits does not ablate intrinsic light-evoked responses in melanopsin-expressing ganglion cells at early postnatal (P6-P8) or adult (P22-P50) stages. A key finding of this study is the persistence of intrinsic light-evoked responses in ipRGCs in all tested TRPC knockout lines. At early postnatal stages, we found no differences in the irradiance-response curves between *TRPC3*$^{-/-}$ and *TRPC6*$^{-/-}$ and only a small change in the slope of *TRPC7*$^{-/-}$ compared to WT ipRGC responses. In adult mouse retinas, the melanopsin-evoked light responses were largely unaltered in the *TRPC3*$^{-/-}$ and *TRPC7*$^{-/-}$ in both M1 and M2 cells. However, consistent diminished melanopsin-mediated photoresponses were noted in *TRPC6*$^{-/-}$ retinas for both ipRGC subtypes. No major developmental abnormalities were observed in the TRPC knockout mouse retinas, which contained similar numbers of melanopsin-expressing ganglion cells and cytoarchitecture similar to WT retinas.

Previous MEA studies of ipRGCs in mice and chicks have revealed different types of light responses supporting the existence of ipRGC subtypes in early postnatal and adult retinas (Tu et al., 2005; Neumann et al., 2008). However another study failed to reveal the heterogeneity of light responses in adult rat (Weng et al., 2009). In our study, two types of ipRGC responses were present at P6-P8 based on the apparent bimodal distribution of ipRGC light sensitivities. Contrary to previous studies, (Tu et al., 2005; Neumann et al., 2008) our analysis did not reveal a third functional subtype of ipRGCs at this age. While it is possible that technical factors in the preparation of the

sample or the recording conditions may account for this discrepancy, we do not have a consistent explanation for this difference between the current study and previous work (Tu et al., 2005; Neumann et al., 2008). Interestingly, the apparent bimodal distribution of light sensitivities of ipRGCs was less well defined in the mutant mouse lines. It is tempting to speculate that lack of expression of TRPC channels altered the functional properties or development of one specific ipRGC subtype but we do not have data to support that conclusion at this time.

Several lines of evidence are suggestive that the photopigment melanopsin is at least capable of activating diacylglycerol-sensitive TRPC channels formed by subunits TRPC3, TRPC6 or TRPC7 in heterologous expression systems. For example, coexpression of the photopigment melanopsin with homomeric TRPC3 channels in various heterologous expressions systems results in light-evoked conductance increases with the expected spectral properties (Panda et al., 2005; Qiu et al., 2005). Pharmacological studies are also supportive that melanopsin activates diacylglycerol-sensitive TRPC channels in the mammalian retina. It has been shown that the membrane permeant analog of diacylglycerol,1-oleoyl-2-acetyl-sn-glycerol (OAG) moderately potentiates the intrinsic light responses of ipRGCs (Warren et al., 2006)(but see below). Furthermore, studies have shown that several agents known to block TRPC channels can block ipRGC light responses (Warren et al., 2006; Hartwick et al., 2007; Sekaran et al., 2007). Finally, TRPC6 or TRPC7 subunits immunoreactivities have been described in melanopsin-expressing ganglion cells (Warren et al., 2006; Sekaran et al., 2007).

While this hypothesis that melanopsin requires a diacylglycerol-sensitive TRPC channel for phototransduction is generally accepted, some results are difficult to

reconcile. For instance, one study finds TRPC6 expression principally in dendrites and soma of ipRGCs (Warren et al., 2006) while another study reports its preferential nuclear localization (Sekaran et al., 2007) casting doubts on the specificity of currently available antibodies. Moreover, TRPC7 was suggested as a candidate for the melanopsin transducing channel because of its relative enrichment in ipRGCs to other ganglion cells (Hartwick et al., 2007). However, a recent study has shown that ectopic expression of melanopsin in "regular" RGCs is able to confer upon these RGCs an intrinsic photosensitivity similar to that reported in ipRGCs (Lin et al., 2008). This suggests that melanopsin is able to gate channels, possibly of the TRPC family, that are ubiquitously expressed within the retina and therefore need not be enriched in the ipRGC population to serve as a candidate for melanopsin-mediated phototransduction. Finally, there are contradictory results in regard to the pharmacological evidence for the diacylglycerol sensitivity of melanopsin-transducing channels. A recent study has failed to demonstrate either OAG-induced currents in ipRGCs or occlusion of light-evoked currents in ipRGCs exposed to diacylglycerol analogs (Graham et al., 2008). Thus, a fuller exploration into the role of other TRPC channels in the native ipRGCs may be warranted at this point.

Our results do indicate that TRPC3, TRPC6, TRPC7 subunits are expressed in the retina at P6-P8 and that retinal development seems to proceed as usual in the absence of each of these three TRPC subunits. It was our expectation that at earlier postnatal stages the issues of compensation would be minimized and therefore we would detect large deficits in the light-evoked responses in the mouse null lines. However, MEA recordings from neonatal ipRGCs in *TRPC3*$^{-/-}$, *TRPC6*$^{-/-}$, and *TRPC7*$^{-/-}$

mouse lines continued to show robust light-evoked increases with half-maximal responses (IR_{50}) similar to those recorded in WT mice. We did observe a significant decrease in spike frequency attained at several light intensities in *TRPC3*$^{-/-}$ mice. Single cell recordings from adult ipRGCs allowed us to address the question whether lack of expression of specific TRPC channels affects differentially M1 or M2 ipRGC subtypes with regard to their intrinsic light responses. We found that lack of TRPC3 or TRPC7 subunit expression did not induce significant changes in the intrinsic light responses of either M1 or M2 cells. Interestingly in the *TRPC6*$^{-/-}$ adult mice, the melanopsin-evoked currents and membrane depolarizations were substantially smaller than those recorded in age-matched WT mice. Together, these findings indicate subtle changes in the ipRGC light responses across the analyzed *TRPC3*$^{-/-}$, *TRPC6*$^{-/-}$, and *TRPC7*$^{-/-}$ mouse lines and again were not supportive of the notion that melanopsin promotes depolarization of ipRGCs by activation of homomeric TRPC3/6/7 ion channels. The results gathered in the *TRPC6*$^{-/-}$ mice are however suggestive that the phototransduction channel does include TRPC6 subunits, at least in mature retinas.

Although issues of developmental compensation may complicate the interpretation of our data, the most parsimonious explanation for the previous accounts and our results is to consider that TRPC7 and TRPC3 homomeric channels do not constitute the long sought transduction channels in ipRGCs. Alternatively, these subunits may do so by forming heteromultimeric assemblies among themselves or with other unidentified TRPC channels. For instance, TRPC3 subunits have recently been shown to heteromultimerize with TRPC1 subunits in smooth muscle cells (Chen *et al.*, 2009) and a similar scenario may apply to ipRCGs. Further work, and in particular a

better biophysical characterization and usage of compound TRPC knockout mouse lines, should help to decipher the molecular nature of the transducing channel in ipRGCs.

Table 1. Primary antibodies used in this study.

Antibody against	Host	Dilution	Immunogen	Specificity	Reference	Source	Catalog number	Retina reference
Glutamine synthetase	Mouse	1:400	Sheep enzyme 1-373	Western bolot 45 kDa	Manufacturer	BD Biosciences	610518	(Zhang *et al.*, 2005)
Protein kinase C-α	Mouse	1:400	Purified bovine brain PKC, amino acids 296-317	Western blot 80KDa	(Young *et al.*, 1988)	Abcam	Ab31	(Kim *et al.*, 2008)
choline acetyl transferase	Goat	1:200	human placental enzyme	Western blot 70KDa	Manufacturer	Millipore	Ab144p	(Gaillard *et al.*, 2008)
Tyrosine hydroxylase	Rabbit	1:400	tyrosine hydroxylase from rat pheochromocytoma	Western blot 62kDa	Manufacturer	Millipore	Ab152	(Acosta *et al.*, 2008)
Melanopsin	Rabbit	1:500	1-19 aa mouse melanopsin	*		Home made		

*****Specificity of anti-melanopsin antibody was tested upon immunostaining in WT, and *Opn4*$^{-/-}$ mouse retinas (see methods).

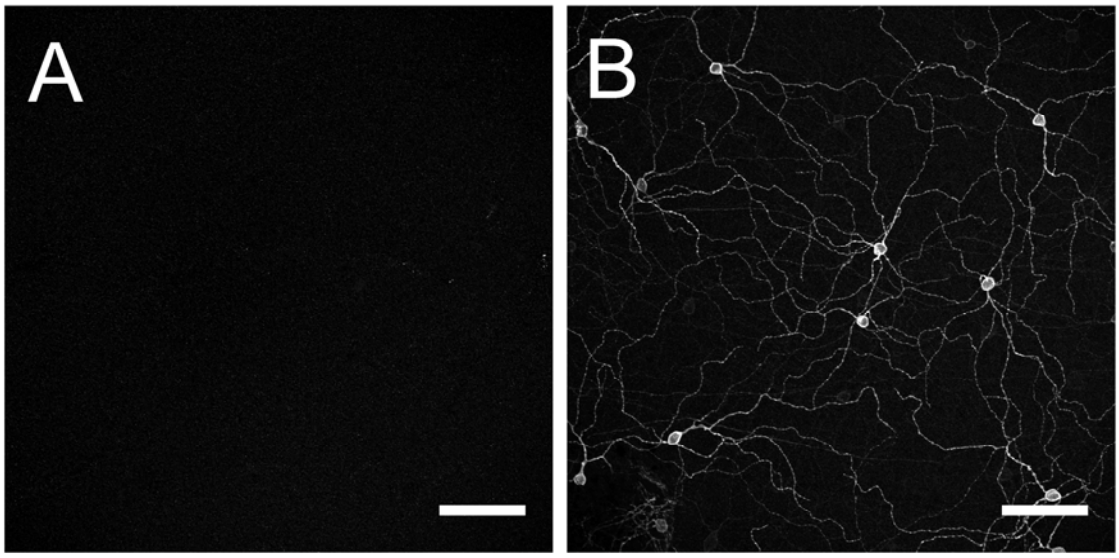

Figure 1. Specificity of anti-melanopsin antibody.
Confocal images of *Opn4*$^{-/-}$ (A) and WT (B) adult retinas imaged at the GCL. Retinas were immunostained and imaged for melanopsin using the anti-melanopsin antibody under identical conditions. Notice the staining of ganglion cells in the WT retina (B) and lack of staining in the *Opn4*$^{-/-}$ retina (A). Scale bar = 100 μm.

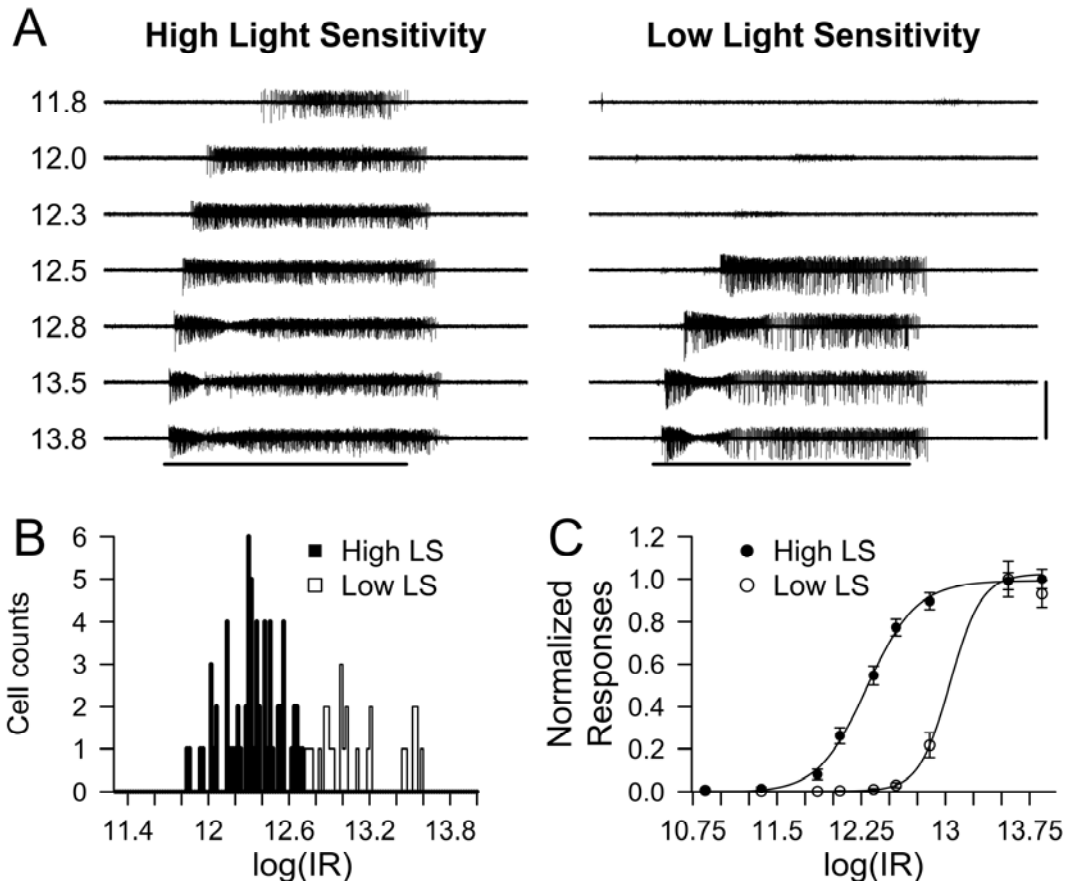

Figure 2. Intrinsic light responses of P6-P8 WT ipRGCs.
(A) Representative voltage traces for high light sensitivity (LS) and low LS ipRGCs obtained using MEA recording. Numbers on the left of the traces indicate the logarithmic of light stimulation intensity in photons / cm^2·sec. Horizontal bar indicates 480 nm light stimulus with duration of 60 sec. Vertical bar represents 300 μV. (B) Histogram of $log(IR_{50})$ values (in photons / cm^2·sec) for ipRGC intrinsic light responses calculated from the Hill Function fit over normalized light induced spikes. High and low LS responses were separated at $log(IR_{50}) = 12.70$. (C) Dose-response graph of the normalized light responses (mean ± SEM) and the fitted Hill function for high ($log(IR_{50}) = 12.30$ in photons / cm^2·sec) and low ($log(IR_{50}) = 13.04$ photons / cm^2·sec) LS ipRGCs.

Table 2. Analysis of ipRGC intrinsic light responses in WT P6-P8 retinas.

	Average Spike frequency (Hz)		Maximal Spike Frequency (Hz)		Latency to Maximal Spike Frequency (s)	
log (IR)	High LS**	Low LS	High LS	Low LS	High LS	Low LS
12.56	7.27 ± 0.37	0.19 ± 0.07 *	10.96 ± 0.51	0.43 ± 0.15 *	14.39 ± 0.65	40 ± 6.07 (n=7)*
12.86	8.42 ± 0.37	1.36 ± 0.36 *	12.66 ± 0.68	2.72 ± 0.62 *	9.62 ± 0.59	34.17 ± 8.88 (n=18)*
13.56	9.31 ± 0.38	6.26 ± 0.53 *	14.85 ± 0.72	8.61 ± 0.63 *	7.12 ± 0.82	18.33 ± 2.28
13.86	9.39 ± 0.42	5.83 ± 0.40 *	14.78 ± 0.74	7.54 ± 0.57 *	5.83 ± 0.64	15.93 ± 1.36

**High LS, High and Low light sensitive (LS) groups as defined by a cutoff of log(IR) = 12.70 photons / cm^2·sec (see results section)

*Represents significant values ($P < 0.05$) when comparisons are made between the High and Low LS groups.

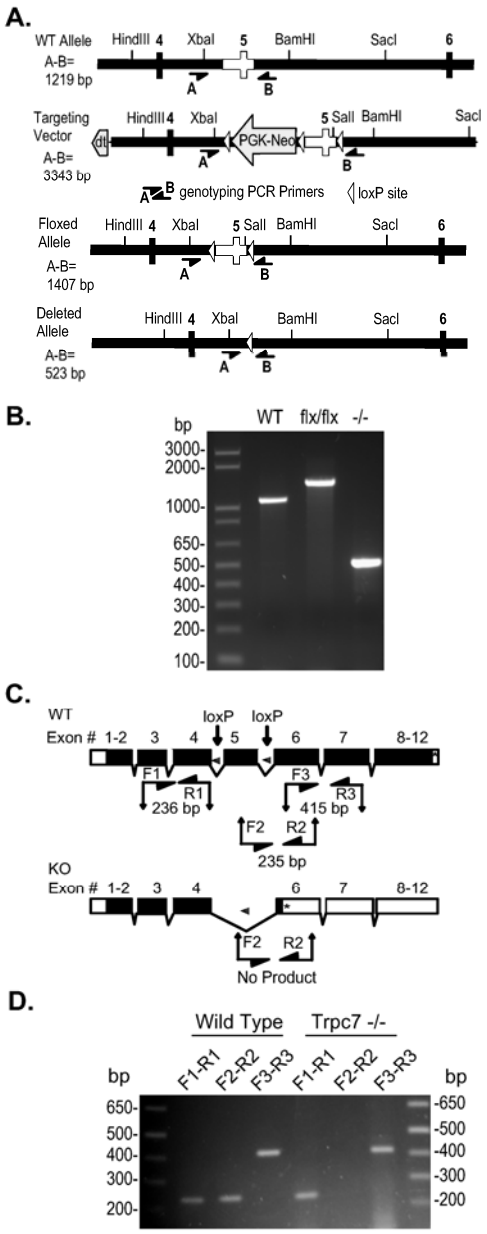

Figure 3: Disruption of the murine *TRPC7* locus.
(A) Targeting strategy. WT Allele: depicts the region of the wild type *TRPC7* gene containing the targeted exon 5 (clear) used to construct the targeting vector. Targeting Vector: depicts the portion of the targeting vector used to target the *TRPC7* locus by homologous recombination. Floxed Allele: depicts the structure of the targeted allele after Cre-mediated excision of the PGK-Neo cassette with exon 5 flanked by loxP sites. Deleted Allele: depicts the structure of the disrupted allele from which exon 5 has been removed by the action of Cre recombinase. The position of key restriction endonuclease sites and the location of genotyping primers A (5'- CCTTC CTCTC TAGGT TCCTT CTAG) and B (5'- GTAGT ATCAG GAAGC TCGCG GCTCT) are indicated. Rectangles, exons included in targeting vector; heavy black line, intronic sequence

Figure 3. Disruption of the murine *TRPC7* locus (Continued)
included in the targeting vector; open triangle, loxP site; PGK-Neo, neomycin selection cassette; dt, diptheria toxin selection cassette. (B) PCR analysis of mouse genomic DNA using primers A and B. F1 recombinant mice (flx/WT) were interbred, and then bred to Sox2-Cre mice (Jackson Laboratories) to promote excision of exon 5, and then interbred to generate exon 5 null mice that had also lost the cre transgene. All *TRPC7* genotypes produce PCR products of the expected sizes given in A. WT, DNA from wild-type mouse; flx/flx, DNA from mouse homozygous for the floxed allele; $^{-/-}$, DNA from mouse homozygous for the deleted allele which exon 5 has been excised by a Cre transgene driven by the uniquitous *Sox2* promoter. (C) (Top) Diagram of the wild-type intron/exon organization of the *TRPC7* gene. Locations of loxP sites in the floxed allele and RT-PCR primers are indicated. (Bottom) Diagram of the deleted allele. Deletion of exon 5 by Cre recombinase is predicted to result in a frameshift and premature stop codon in exon 6. The lengths of the depicted amplicons include the primers. Primer F1 (5'-ATGTG AACTT GCAAG TCTGG TCCG), R1 (5'- AGCAA TCCAA TAGGC TATGG CGAG), F2 (5'-GACGG AGATG CTCAT CATGA AGTG), R2 (5'- TGAGA CGTTG TGCAG CGTTA CATC), F3 (5'-TGCTA CACTT GTGGA ACCTT CTGG), R3 (5'- CGGTA GTAGG AGTAC AGGTT GAAC). Black boxes, coding sequence; open boxes, untranslated exon sequence; *, stop codon. (D) RT-PCR analysis of brain RNA from a wild-type and a *TRPC7*$^{-/-}$ mouse. Primer pairs are indicated, their position in the gene and predicted product sizes are given in C. Sequencing of the RT-PCR products confirmed splicing from exon 4 to exon 6 and the presence of a premature stop codon in mRNA transcribed from the deleted allele.

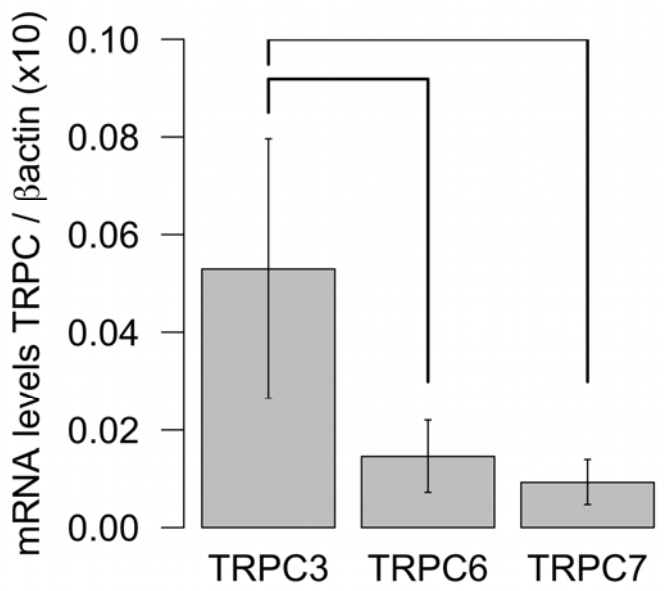

Figure 4. Real Time PCR Analysis in P6-P8 retinas.
mRNA expression levels of TRPC3, TRPC6 and TRPC7 subunits were analyzed in P6-P8 WT retinas. mRNA expression levels in for TRPC transcripts are normalized to β-actin. One-way ANOVA indicated a significant differences between TRPC subunits expression (P = 0.0001). A Tukey HSD showed significant differences between TRPC3 and TRPC6 (P < 0.0001) and TRPC7 (P = 0.0001) and no differences between TRPC6 and TRPC7 (P = 0.065). Data is presented as mean ± S.E.M. n = 4 retinas per group.

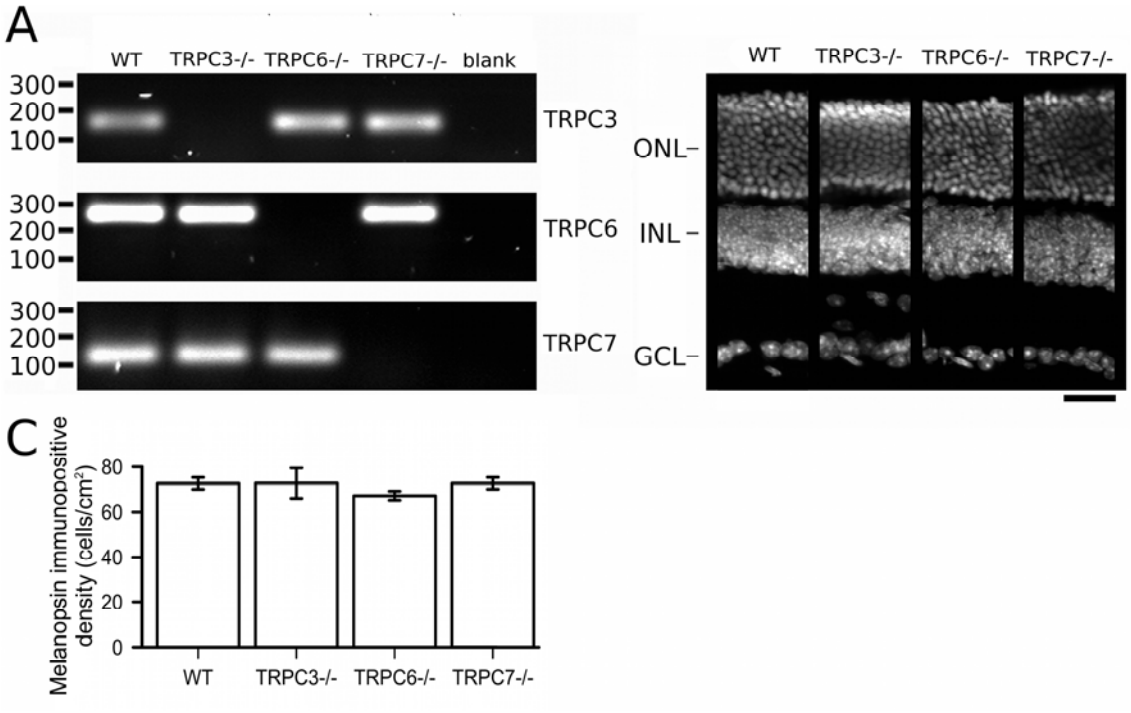

Figure 5. Characterization of *TRPC3*$^{-/-}$, *TRPC6*$^{-/-}$ and *TRPC7*$^{-/-}$ retinas.
(A) End-point RT-PCR analysis from adult retinal samples shows the absence of respective ablated exons in *TRPC3*$^{-/-}$, *TRPC6*$^{-/-}$ and *TRPC7*$^{-/-}$ retinal transcripts. RT-PCR for TRPC3 exon 7 (145 bp), TRPC6 exon 7 (247 bp), TRPC7 exon 5 (110 bp) shows the presence in WT retinas but not in the respective mutant mouse line samples. Blank controls are RT-PCR reactions with H_2O instead of cDNAs. (B) Cross sections of DAPI stained adult retinas show apparent normal morphology in *TRPC3*$^{-/-}$, *TRPC6*$^{-/-}$ and *TRPC7*$^{-/-}$ mice compared to WT mice (scale bar 20 μm). (C) Densities of melanopsin immunoreactive cell bodies in WT, *TRPC3*$^{-/-}$, *TRPC6*$^{-/-}$, and *TRPC7*$^{-/-}$ mouse retinas (mean ± SEM). ONL, outer nuclear layer; INL, inner nuclear layer; GCL, ganglion cell layer.

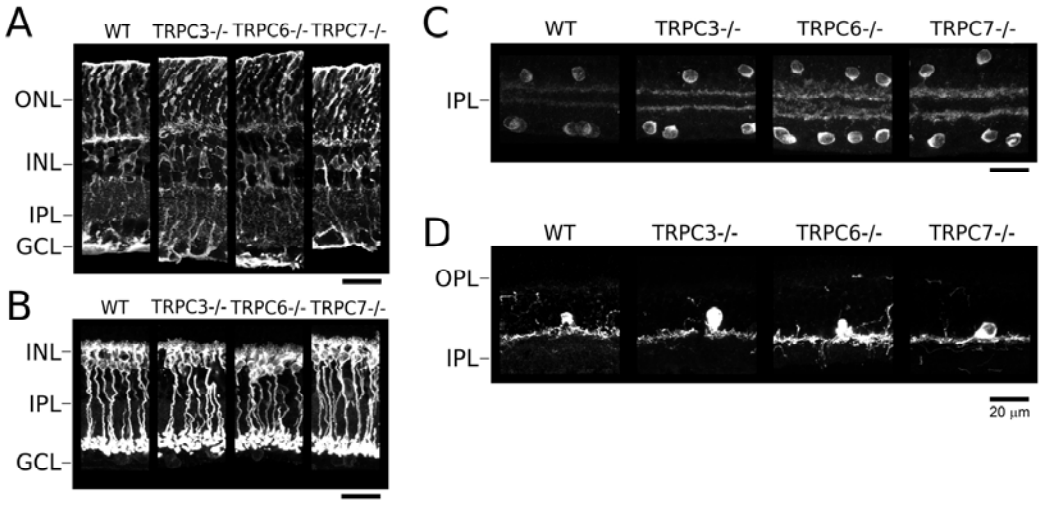

Figure 6. Immunohistochemical analysis of *TRPC*$^{-/-}$ adult retinas.
Analysis of different cell types in adult retinas revealed no qualitative differences between genotypes. The cells types analyzed were: (A) Muller cells, anti-glutamine synthetase antibody, (B) Rod bipolar cells, anti-PKCα, (C) Cholinergic amacrine cells, anti-ChAT antibody, (D) Dopaminergic amacrine cells, anti-tyrosine hydroxylase antibody. (see Methods for additional antibody information). The scale bar is 20 um.

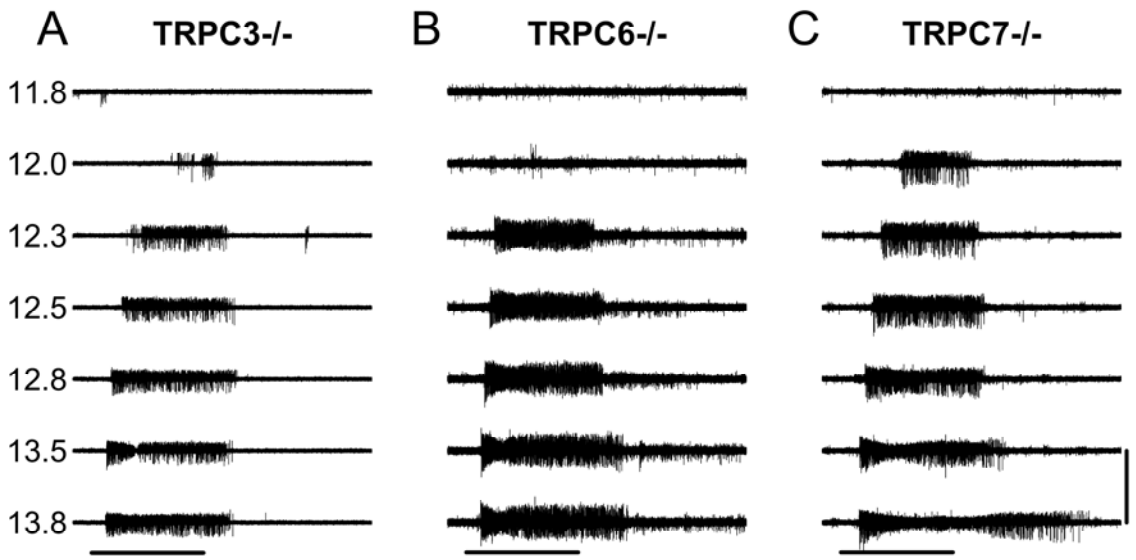

Figure 7. Intrinsic light responses of *TRPC3*$^{-/-}$, *TRPC6*$^{-/-}$ and *TRPC7*$^{-/-}$ ipRGCs.
Representative voltage traces for ipRGC intrinsic light responses in *TRPC3*$^{-/-}$ (A), *TRPC6*$^{-/-}$ (B) and *TRPC7*$^{-/-}$ (C) retinas. Numbers on the left of the traces indicate the logarithmic of light stimulation intensity in photons / cm^2·sec. Horizontal bar represents light stimulation (60 sec). Vertical scale bar is 300 μV. Each one of the traces represents the light response at a given 480 nm light intensity.

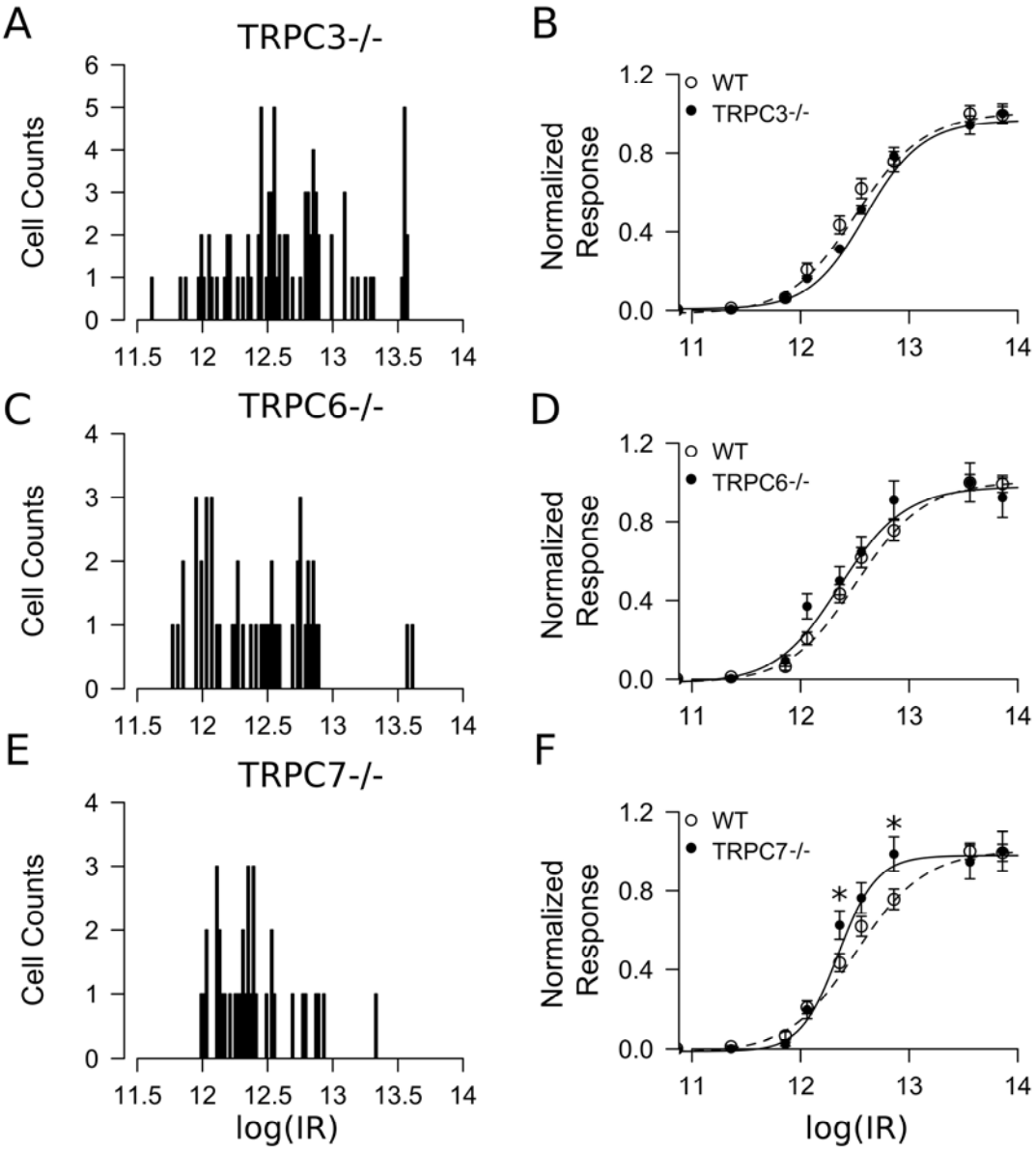

Figure 8. Summary of intrinsic light responses in *TRPC3*$^{-/-}$, *TRPC6*$^{-/-}$ and *TRPC7*$^{-/-}$ ipRGCs.

(A,C,E) .Histograms of the log(IR_{50}) in photons / cm^2·sec for (A) *TRPC3*$^{-/-}$ (n =84 cells), (C) *TRPC6*$^{-/-}$ (n = 49 cells) and (E) *TRPC7*$^{-/-}$ (n = 37 cells) ipRGC light responses. (**B,D,F**) Normalized light responses (mean ± SEM) and the fitted Hill function for (B) *TRPC3*$^{-/-}$ (log(IR_{50}) = 12.52), (D) *TRPC6*$^{-/-}$ (log(IR_{50}) = 12.30) and (F) *TRPC7*$^{-/-}$ (log(IR_{50}) = 12.28). The WT normalized light response shown here was calculated using all WT ipRGC responses (n = 93, log(IR_{50}) = 12.44).

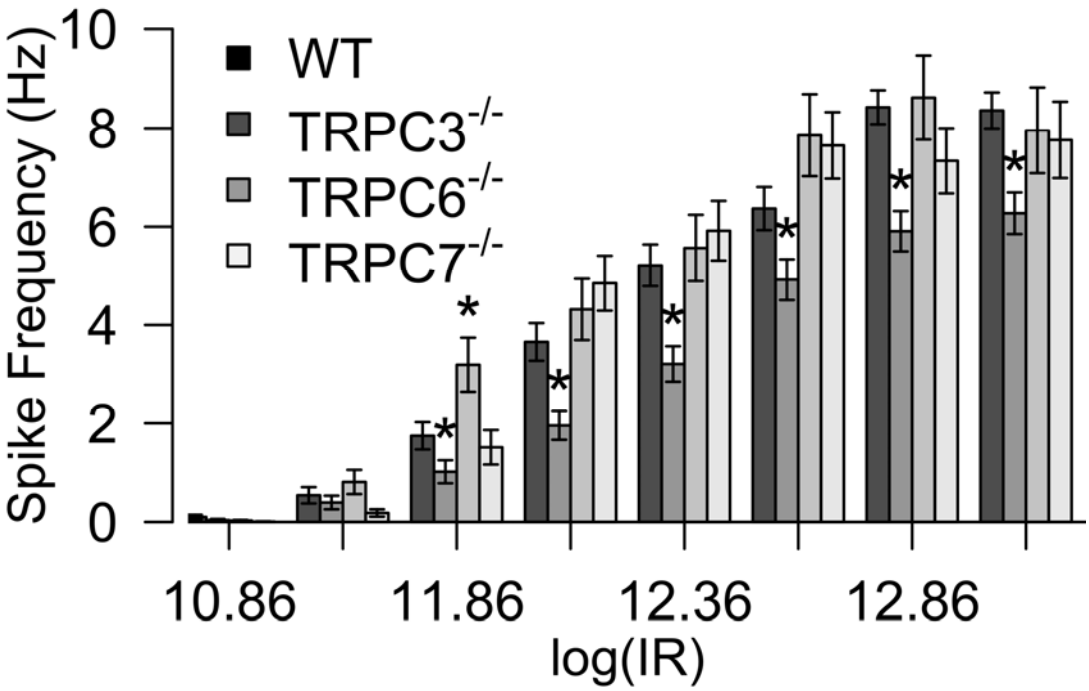

Figure 9. Irradiance-response relationships for WT, *TRPC3*$^{-/-}$, *TRPC6*$^{-/-}$ and *TRPC7*$^{-/-}$ ipRGCs.

Average spike frequency in WT and mutant mice ipRGCs recorded at various light intensities (Log photons/cm^2.s). Significant differences were recorded across various light intensities for *TRPC3*$^{-/-}$ retinas and one light intensity for *TRPC6*$^{-/-}$ retinas. * indicates *P* value < 0.05 in a randomization based t-test comparing WT and the corresponding TRPC$^{-/-}$ response at each light intensity after a FDR correction for multiple comparisons.

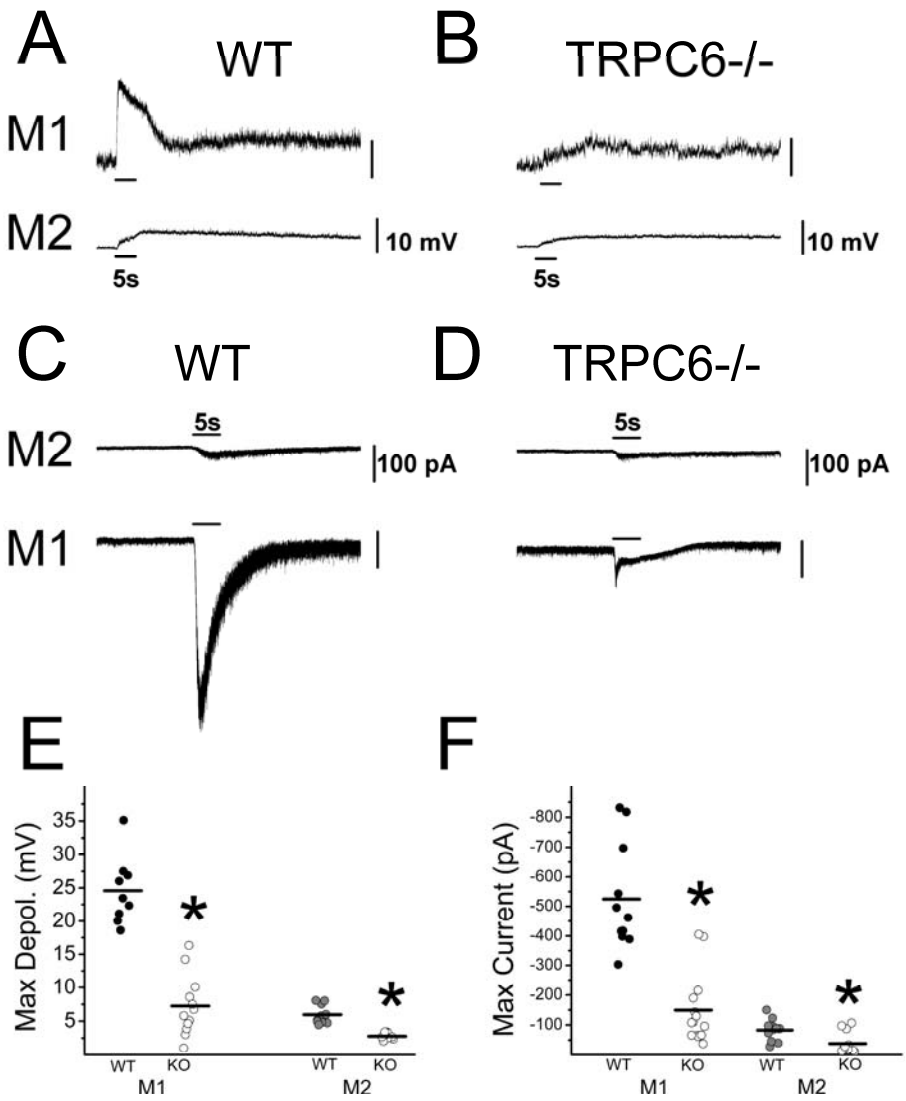

Figure 10. Current and voltage clamp recordings of light responses of M1 and M2 ipRGCs in WT and *TRPC6*$^{-/-}$ mice.

(A) Representative intrinsic light responses of M1 (top trace) and M2 (bottom trace) cells in adult WT mice to a 5 s full-field 480 nm light stimulus at -2.1LogI recorded in current clamp mode. (B) Representative intrinsic light responses of M1 (top trace) and M2 (bottom trace) cells in adult *TRPC6*$^{-/-}$ mice to a 5 s full-field 480 nm light stimulus at -2.1LogI recorded in current clamp mode. (C) Representative intrinsic light response of M2 (top trace) and M1 (bottom trace) cells in adult WT mice to a 5 s full-field 480 nm light stimulus at -1.5LogI recorded in voltage clamp mode (V_{hold} -80mV). (D) Representative intrinsic light response of M2 (top trace) and M1 (bottom trace) cells in adult *TRPC6*$^{-/-}$ mice to a 5 s full-field 480 nm light stimulus at -1.5LogI recorded in voltage clamp mode (V_{hold} -80mV). (E) Maximum depolarization evoked by a 5s full-field 480 nm light stimulation in WT and *TRPC6*$^{-/-}$ M1 and M2 cells. Black bars indicate mean. (F) Maximum inward current evoked by a 5 s full-field 480 nm light stimulus in WT and *TRPC6*$^{-/-}$ M1 and M2 cells. Black bars indicate mean. * $P < 0.05$, *t*-test.

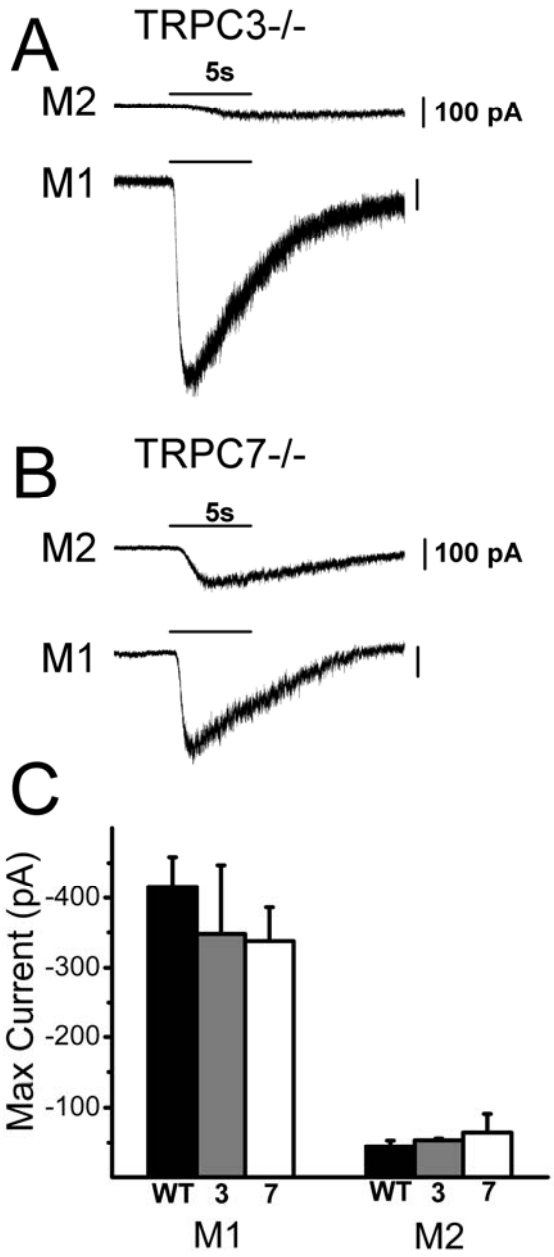

Figure 11. Voltage clamp recordings of light responses of M1 and M2 ipRGCs in *TRPC3*$^{-/-}$ and *TRPC7*$^{-/-}$ mice.

(A) Representative intrinsic light response of M2 (top trace) and M1 (bottom trace) cells in adult *TRPC3*$^{-/-}$ mice to a 5 s full-field 480 nm light stimulus at -1.5LogI recorded in voltage clamp mode (V_{hold} -60mV). (B) Representative intrinsic light response of M2 (top trace) and M1 (bottom trace) cells in adult *TRPC7*$^{-/-}$ mice to a 5 s full-field 480 nm light stimulus at -1.5LogI recorded in voltage clamp mode (V_{hold} -60mV). (C) Mean ± SE maximum inward current to a 5 s full-field 480 nm light stimulus in WT, *TRPC3*$^{-/-}$, and *TRPC7*$^{-/-}$ M1 and M2 cells (V_{hold} -60mV).

CHAPTER 7

General Conclusions

Summary

We have developed a mouse line in which ipRGCs are labeled *in vivo* with EGFP, allowing us to reliably target ipRGCs for analysis at the single-cell level (Chapter 2). Using this mouse line, we have demonstrated the ipRGCs are photosensitive from postnatal day (P)0. During development, the light response of ipRGCs evolves from one that is purely intrinsic and maximally sensitive to 480 nm light, to one that is influenced by synaptic inputs starting around P11, just before eye opening. These synaptic inputs render the light response of ipRGCs more sensitive to both 480 nm and 610 nm light, and shift the λ_{max} closer to 500 nm. Morphologically, ipRGCs develop as a population of cells with relatively small dendritic arbors that evolves into one consisting of at least three morphologically distinct subpopulations of cells with large dendritic arbors: those with dendrites monostratified in the OFF sublamina (M1, or Type I), those with dendrites monostratified in the ON sublamina (M2, or Type II), and those with dendrites bistratified in both the ON and OFF sublaminas (M3, or Type II)(Chapter 2,3).

When we further examined the morphology of M1 and M2 cells, we found that M2 cells have larger, more complex dendritic arbors as well as larger somas than M1 cells. What was perhaps most striking, however, were the distinct physiological characteristics of these two morphological subpopulations. We found that M1 cells had significantly larger input resistance, more depolarized resting membrane potential, spike at lower frequencies, and have larger, more sensitive intrinsic light responses. In contrast, M2 cells had smaller input resistance, more hyperpolarized resting membrane potential, attain higher spike frequencies, and have smaller and less sensitive intrinsic

light responses (Chapter 3). These distinct intrinsic physiological characteristics of M1 and M2 cells highlights an additional layer of diversity within the ipRGC population that goes beyond simple differences in level of dendritic stratification within the IPL. This changes the initially held view of ipRGCs that the population consists of a single, physiologically uniform population with dendrites ramifying in the OFF sublamina of the IPL (Berson et al., 2002; Berson, 2003; Wong et al., 2007). The findings that ipRGCs can be divided into populations that are morphologically and physiologically distinct raises the possibility that ipRGC subtypes could signal distinct light information to the brain.

Though ipRGCs are intrinsically photosensitive, it has been known for some time that these cells also receive light-evoked synaptic signals from the rod/cone pathways. When we examined the consequences of cone-mediated signaling to ipRGCs we found that not only is the cone-mediated ON pathway the primary synaptic input to ON-stratifying M2 cells, but also to OFF-stratifying M1 cells. Furthermore, this ON pathway input is more influential in shaping the light-evoked and resting properties of M2 cells than M1 cells, which rely primarily upon melanopsin-mediated phototransduction to signal light information to the brain at bright light intensities (Chapter 4). These results, combined with our findings regarding the intrinsic diversity of M1 and M2 cells, provide further support for the idea that M1 and M2 ipRGCs signal distinct light information to the brain.

Additionally, though the existence of bistratified, or M3 ipRGCs had been reported anecdotally in the literature, the physiological and morphological properties of M3 cells had not yet been examined in detail. One major question regarding this

population of ipRGC is whether it constitutes a “true” ipRGC subpopulation or whether these cells are some kind of developmental “accident” forming an anomalous hybrid of the M1 and M2 subtypes. When we analyzed the morphological properties of M3 cells, we encountered a surprising degree of heterogeneity in the dendritic architecture of M3 cells, with some cells having dendrites almost entirely confined to the OFF sublamina and others with dendrites stratifying in the ON and OFF sublaminas in relatively equal proportions. However, with regard to intrinsic physiological properties as well as synaptic inputs we found that not only were M3 cells remarkably homogeneous, but that these characteristics were largely similar to M2 cells (Chapter 5). Though M3 cells do not tile the retina (Berson et al., 2010), we argue that this might not be a necessary feature for an ipRGC to be considered a true subtype as only 15% of ipRGCs are present they can still mediate competent circadian photoentrainment and pupillary light reflex (PLR) (Guler et al., 2008). Furthermore, the physiological homogeneity of M3 cells indicates that these cells may indeed constitute a distinct ipRGC population. However, more research into whether M3 cells receive distinct synaptic inputs or have unique influences on non-image forming (NIF) behaviors is needed to conclusively answer this question.

Finally, we examined the phototransduction pathway of ipRGCs in order to determine the identity of the non-specific cation channel involved in melanopsin-evoked depolarization of ipRGCs. Because of the similarity of the melanopsin phototransduction cascade with that of the invertebrate rhodopsin cascade, it has been widely hypothesized that melanopsin activation results in the opening of a cation channel of the canonical transient receptor potential (TRPC) family of the TRP channels,

specifically those composed of the TRPC3,6, or 7 subunits (Warren et al., 2006; Hartwick et al., 2007; Sekaran et al., 2007; Graham et al., 2008). We utilized a mouse knockout approach to determine the consequences of knockout of TRPC3, TRPC6, or TRPC7 subunits on melanopsin-mediated phototransduction as assessed by multi-electrode array or whole-cell patch clamp recordings. We found that intrinsic phototransduction persisted in mouse lines where each of these TRPC subunits was absent at neonatal and adult stages, but that both M1 and M2 cells in adult mice showed a reduction in the intrinsic light response in *TRPC6*$^{-/-}$ mice (Chapter 6). This indicates that a single TRPC3,6, or 7 subunit alone is not responsible for melanopsin-mediated depolarization, but that TRPC6 subunits likely form part of the as-yet unidentified phototransduction channel.

Differential and specific ipRGC projections

In addition to their unique morphological and physiological properties, evidence is emerging that ipRGC subpopulations differentially and specifically project to different NIF visual centers. For example, it has been reported that M1 cells are the primary ipRGC subtype innervating the SCN, with about 80% of the projection being formed by the M1 cells and 20% by M2 cells (Baver et al., 2008; Ecker et al., 2010). However 50% of the projection to the olivary pretectal nucleus (OPN) and the superior colliculous (SC) is formed by M1 and 50% by M2 cells (Baver et al., 2008). A more recent study has demonstrated an even more substantial innervation of the OPN core by M2 cells, with M1 cells forming the primary projection to the OPN shell (Ecker et al., 2010). This same study also highlighted a previously unappreciated projection of M2 cells to areas involved in image forming vision, such as the dorsal lateral geniculate

nucleus (dLGN), and even demonstrated the ability of melanopsin-only mice lacking rods/cones to mediate a rudimentary form of pattern vision (Ecker et al., 2010). This study also further divided the ON-stratifying ipRGCs into M2,4, and 5 subpopulations, though the physiological properties of these subdivisions were not examined in great detail (Ecker et al., 2010). This differential and specific innervation of M1 and non-M1 ipRGCs of different NIF nuclei implies that these subtypes may play distinct roles in mediating different NIF behaviors.

Differential and specific rod/cone/melanopsin influences on behavior

Though it is now well-accepted that ipRGCs form the primary conduit for rod, cone, and melanopsin signals to mediate various NIF behaviors, it was not well understood which systems were primarily responsible for mediation of specific NIF behaviors such as the PLR and circadian photoentrainment and phase shifting. Two recent papers have tackled this problem using mouse genetics. The first study by Lall et al. utilized a mouse line in which the human L-opsin (λ_{max} 556 nm) is knocked into the mouse M-opsin (λ_{max} 511 nm) locus (Lall et al., 2010). This results in normal development and wiring of the mouse visual system, but allows for a better spectral separation between rods and cones. This study found that the PLR was almost entirely mediated by cones, whereas rods and melanopsin played very little role in mediation of this reflex. Circadian photoentrainment, in contrast, was found to be mediated by rods at low light intensities and melanopsin at high light intensities, with very little influence of the cone pathway (Lall et al., 2010).

A separate study also utilized mouse genetics to tackle the question of the role of rods, cones, and melanopsin in circadian photoentrainment, but with a knockout/loss of

function approach to generate melanopsin only, cone only, and rod only mouse lines. This study, like that of Lall et al. (2010) also found that rods play a large role in influencing circadian photoentrainment (Altimus et al., 2010). Furthermore, this study found that rods are able to drive this behavior at much brighter light intensities than those for which rods can influence image forming vision and that this influence at brighter light intensities is dependent upon the presence of cone photoreceptors in a dark-adapted state. When cones are either chronically hyperpolarized or absent altogether, then the influence of rods is confined to the scotopic range (Altimus et al., 2010).

Collectively, these new studies highlight a previously unappreciated role for rods in circadian photoentrainment, and imply that the RGCs influencing circadian photoentrainment must receive rod input (Altimus et al., 2009; Lall et al., 2010). Furthermore, the strong influence of cones on the PLR implies that the cells influencing this behavior might receive strong cone inputs (Lall et al., 2010).

Conclusions/Model

This differential influence of rods and cones on circadian photoentrainment and the PLR has been interpreted by above-mentioned studies to be the result, not of differential signaling by ipRGC subpopulations, but of differences in propensity for light adaptation by rods vs. cones integrated differently by the SCN and OPN (Figure 1).

We have now demonstrated that M2 cells rely primarily on cone-mediated signals to shape the light-evoked response while M1 cells rely primarily on melanopsin-mediated signals at bright light intensities to shape the light-evoked response, paralleling differences in behavioral outputs at bright light intensities seen by Lall et al.

(2010) and Altimus et al. (2010). Because the SCN receives substantially more innervation from the M1 vs. the non-M1 population (Hattar et al., 2002; Hattar et al., 2006; Baver et al., 2008; Ecker et al., 2010) and because rods play a large role in circadian photoentrainment (Altimus et al., 2010; Lall et al., 2010), one explanation could be that M1 cells receive substantially larger innervation from the rod pathway. Alternatively, M1 and non-M1 cells could receive equivalent rod pathway inputs that for non-M1 cells are filtered by circadian effects in the downstream nuclei.

It has been proposed that because non-M1 cells do not appear to innervate the shell of the OPN that they cannot play a role in the PLR (Ecker et al., 2010). Previous work using c-fos induction in the OPN of rats has demonstrated an ability to induce c-fos expression in the shell but not the core of the OPN in response to light, leading some to conclude that core-innervating cells do not play a role in the PLR (Prichard et al., 2002; Ecker et al., 2010; Lall et al., 2010). The M1 cells, identified using tau-lacZ staining, which also labels M3 cells (Pires et al., 2009), form the primary projection to the shell of the OPN (Hattar et al., 2002; Hattar et al., 2006; Ecker et al., 2010), while the non-M1 shells show substantial innervation of the core (Ecker et al., 2010). However, the substantial innervation of the OPN, as well as the dominance of cone-mediated signals in influencing non-M1 (including M3 cells), but not M1 cell light responses indicates that M2 or other non-M1 cells could play a role in mediating the PLR.

Taking together our single cell data with behavioral and anatomical studies, I propose an alternative model to that of Lall et al. (2010) whereby light information from rods and cones is routed differentially at the level of the retina via M1 and non-M1 cells

respectively. I propose that M1 cells function to relay primarily rod and melanopsin mediated information for circadian entrainment (Figure 2A). Furthermore, cone input is primarily responsible for driving the PLR, though research has shown that melanopsin-mediated phototransduction is required to maintain the PLR over long durations (Zhu et al., 2007; Mure et al., 2009; Lall et al., 2010). As M2 (and other non-M1) cells form a large proportion of the projection to the OPN, I propose that M2 cells play a large role in mediating the PLR, primarily by relaying cone-mediated signals, and perhaps some melanopsin-mediated signals, to the OPN (Figure 2B). The specific roles of various ipRGC subtypes in influencing NIF behaviors will be an important focus for future research in the field.

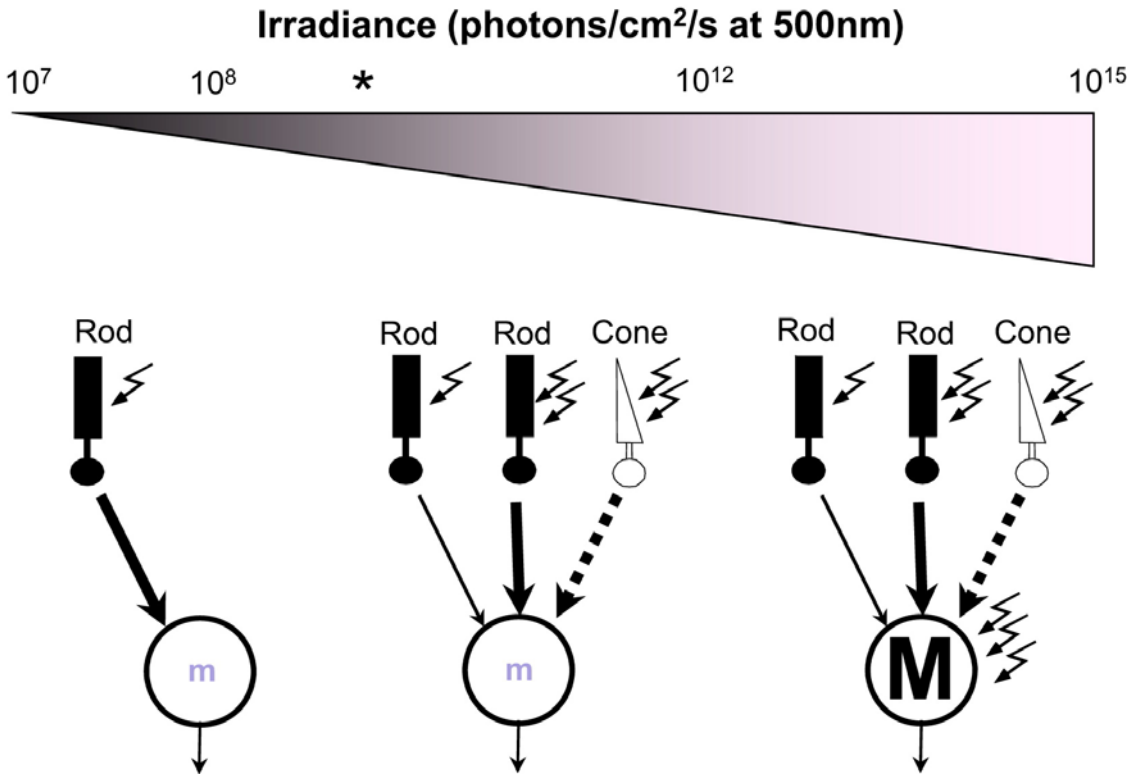

Figure 1. Model proposed by Lall et al. (2010) for rod/cone/melanopsin signals conveyed to NIF nuclei.
Lall et al. (2010) propose a model whereby a single subtype of ipRGC (M1) conveys rod, cone, and melanopsin-mediated signals to drive both circadian photoentrainment and PLR from scotopic to photopic intensities. The cone signal is interpreted not to influence photoentrainment due to the fast adaptation of cones in the presence of constant light, and is only capable of doing so in response to repeated "intermittent" light stimuli.

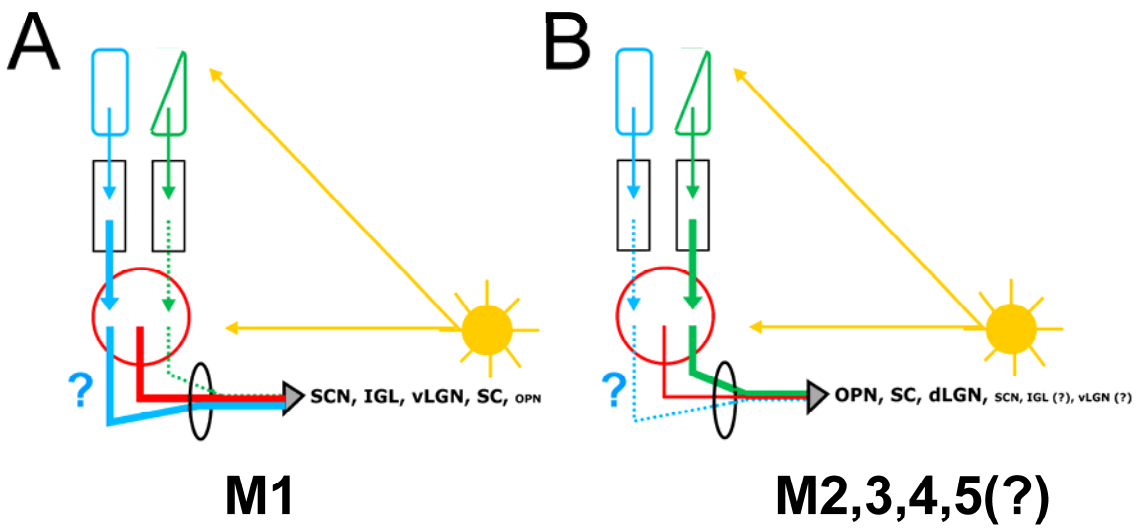

Figure 2. Proposed model for differential signals relayed by diverse ipRGC subtypes to NIF nuclei

(A) M1 cells have large sensitive intrinsic light responses (red line) but small inputs from the cone ON pathway (green line) that exert relatively little influence in shaping the integrated light response. Given behavioral and projection data, I hypothesize that M1 cells may receive a strong input from the rod pathway (blue line) at low light intensities. (B) M2 (and other non-M1 cells) have small, insensitive intrinsic light responses (red line) but receive strong inputs from the cone ON pathway (green line) that exert a substantial influence in shaping the integrated light response. Given behavioral and projection data, I hypothesize that M2 and other non-M1 cells will not receive substantial drive from the rod pathway (blue line) at low light intensities. "?" reflects lack of data regarding M5 cell intrinsic properties or synaptic inputs, and these cells have been provisionally placed with the other non-M1 cells. Lettering size for brain structures indicative of relative strength of influence on respective behaviors driven by these nuclei.

CHAPTER 8

References

Aggelopoulos NC, Meissl H (2000) Responses of neurones of the rat suprachiasmatic nucleus to retinal illumination under photopic and scotopic conditions. J Physiol 523 Pt 1:211-222.
Altimus CM, LeGates T, Hattar S (2009) Circadian and Light Modulation of Behavior. In: Neuromethods (Gould TD, ed), pp 47-65: Humana Press.
Altimus CM, Guler AD, Villa KL, McNeill DS, Legates TA, Hattar S (2008) Rods-cones and melanopsin detect light and dark to modulate sleep independent of image formation. Proc Natl Acad Sci U S A 105:19998-20003.
Altimus CM, Guler AD, Alam NM, Arman AC, Prusky GT, Sampath AP, Hattar S (2010) Rod photoreceptors drive circadian photoentrainment across a wide range of light intensities. Nat Neurosci.
Anadon R, Molist P, Rodriguez-Moldes I, Lopez JM, Quintela I, Cervino MC, Barja P, Gonzalez A (2000) Distribution of choline acetyltransferase immunoreactivity in the brain of an elasmobranch, the lesser spotted dogfish (Scyliorhinus canicula). J Comp Neurol 420:139-170.
Applebury ML, Antoch MP, Baxter LC, Chun LL, Falk JD, Farhangfar F, Kage K, Krzystolik MG, Lyass LA, Robbins JT (2000) The murine cone photoreceptor: a single cone type expresses both S and M opsins with retinal spatial patterning. Neuron 27:513-523.
Badea TC, Cahill H, Ecker J, Hattar S, Nathans J (2009) Distinct roles of transcription factors brn3a and brn3b in controlling the development, morphology, and function of retinal ganglion cells. Neuron 61:852-864.
Bailes HJ, Lucas RJ (2010) Melanopsin and inner retinal photoreception. Cell Mol Life Sci 67:99-111.
Barlow HB, Levick WR (1969) Changes in the maintained discharge with adaptation level in the cat retina. J Physiol 202:699-718.
Barnard AR, Appleford JM, Sekaran S, Chinthapalli K, Jenkins A, Seeliger M, Biel M, Humphries P, Douglas RH, Wenzel A, Foster RG, Hankins MW, Lucas RJ (2004) Residual photosensitivity in mice lacking both rod opsin and cone photoreceptor cyclic nucleotide gated channel 3 alpha subunit. Vis Neurosci 21:675-683.
Baver SB, Pickard GE, Sollars PJ, Pickard GE (2008) Two types of melanopsin retinal ganglion cell differentially innervate the hypothalamic suprachiasmatic nucleus and the olivary pretectal nucleus. Eur J Neurosci 27:1763-1770.
Belenky MA, Smeraski CA, Provencio I, Sollars PJ, Pickard GE (2003) Melanopsin retinal ganglion cells receive bipolar and amacrine cell synapses. J Comp Neurol 460:380-393.
Bellingham J, Foster RG (2002) Opsins and mammalian photoentrainment. Cell Tissue Res 309:57-71.
Berson DM (2003) Strange vision: ganglion cells as circadian photoreceptors. Trends Neurosci 26:314-320.
Berson DM (2007) Phototransduction in ganglion-cell photoreceptors. Pflugers Arch.
Berson DM, Dunn FA, Takao M (2002) Phototransduction by retinal ganglion cells that set the circadian clock. Science 295:1070-1073.

Berson DM, Castrucci AM, Provencio I (2010) Morphology and mosaics of melanopsin-expressing retinal ganglion cell types in mice. J Comp Neurol 518:2405-2422.
Birnbaumer L (2009) The TRPC Class of Ion Channels: A Critical Review of Their Roles in Slow, Sustained Increases in Intracellular Ca(2+) Concentrations (*). Annu Rev Pharmacol Toxicol 49:395-426.
Clapham DE, Runnels LW, Strubing C (2001) The TRP ion channel family. Nat Rev Neurosci 2:387-396.
Clarke RJ, Ikeda H (1985) Luminance and darkness detectors in the olivary and posterior pretectal nuclei and their relationship to the pupillary light reflex in the rat. I. Studies with steady luminance levels. Exp Brain Res 57:224-232.
Connors NC, Kofuji P (2002) Dystrophin Dp71 is critical for the clustered localization of potassium channels in retinal glial cells. J Neurosci 22:4321-4327.
Coombs J, van der List D, Wang GY, Chalupa LM (2006) Morphological properties of mouse retinal ganglion cells. Neuroscience 140:123-136.
Czeisler CA, Shanahan TL, Klerman EB, Martens H, Brotman DJ, Emens JS, Klein T, Rizzo JF, 3rd (1995) Suppression of melatonin secretion in some blind patients by exposure to bright light. N Engl J Med 332:6-11.
Dacey DM, Liao HW, Peterson BB, Robinson FR, Smith VC, Pokorny J, Yau KW, Gamlin PD (2005) Melanopsin-expressing ganglion cells in primate retina signal colour and irradiance and project to the LGN. Nature 433:749-754.
Dietrich A, Mederos YSM, Gollasch M, Gross V, Storch U, Dubrovska G, Obst M, Yildirim E, Salanova B, Kalwa H, Essin K, Pinkenburg O, Luft FC, Gudermann T, Birnbaumer L (2005) Increased vascular smooth muscle contractility in TRPC6-/- mice. Mol Cell Biol 25:6980-6989.
Dkhissi-Benyahya O, Gronfier C, De Vanssay W, Flamant F, Cooper HM (2007) Modeling the role of mid-wavelength cones in circadian responses to light. Neuron 53:677-687.
Do MT, Yau KW (2010) Intrinsically photosensitive retinal ganglion cells. Physiol Rev 90:1547-1581.
Do MT, Kang SH, Xue T, Zhong H, Liao HW, Bergles DE, Yau KW (2009) Photon capture and signalling by melanopsin retinal ganglion cells. Nature 457:281-287.
Dowling JE (1970) Organization of vertebrate retinas. Invest Ophthalmol 9:655-680.
Dowling JE, Werblin FS (1969) Organization of retina of the mudpuppy, Necturus maculosus. I. Synaptic structure. J Neurophysiol 32:315-338.
Doyle SE, Castrucci AM, McCall M, Provencio I, Menaker M (2006) Nonvisual light responses in the Rpe65 knockout mouse: rod loss restores sensitivity to the melanopsin system. Proc Natl Acad Sci U S A 103:10432-10437.
Dumitrescu ON, Pucci FG, Wong KY, Berson DM (2009) Ectopic retinal ON bipolar cell synapses in the OFF inner plexiform layer: contacts with dopaminergic amacrine cells and melanopsin ganglion cells. J Comp Neurol 517:226-244.
Ecker JL, Dumitrescu ON, Wong KY, Alam NM, Chen SK, LeGates T, Renna JM, Prusky GT, Berson DM, Hattar S (2010) Melanopsin-expressing retinal ganglion-cell photoreceptors: cellular diversity and role in pattern vision. Neuron 67:49-60.

Famiglietti EV, Jr., Kolb H (1976) Structural basis for ON-and OFF-center responses in retinal ganglion cells. Science 194:193-195.
Foster RG, Provencio I, Hudson D, Fiske S, De Grip W, Menaker M (1991) Circadian photoreception in the retinally degenerate mouse (rd/rd). J Comp Physiol A 169:39-50.
Freedman MS, Lucas RJ, Soni B, von Schantz M, Munoz M, David-Gray Z, Foster R (1999) Regulation of mammalian circadian behavior by non-rod, non-cone, ocular photoreceptors. Science 284:502-504.
Fu Y, Liao HW, Do MT, Yau KW (2005a) Non-image-forming ocular photoreception in vertebrates. Curr Opin Neurobiol 15:415-422.
Fu Y, Zhong H, Wang MH, Luo DG, Liao HW, Maeda H, Hattar S, Frishman LJ, Yau KW (2005b) Intrinsically photosensitive retinal ganglion cells detect light with a vitamin A-based photopigment, melanopsin. Proc Natl Acad Sci U S A 102:10339-10344.
Gamlin PD, McDougal DH, Pokorny J, Smith VC, Yau KW, Dacey DM (2007) Human and macaque pupil responses driven by melanopsin-containing retinal ganglion cells. Vision Res 47:946-954.
Gooley JJ, Lu J, Fischer D, Saper CB (2003) A broad role for melanopsin in nonvisual photoreception. J Neurosci 23:7093-7106.
Gooley JJ, Lu J, Chou TC, Scammell TE, Saper CB (2001) Melanopsin in cells of origin of the retinohypothalamic tract. Nat Neurosci 4:1165.
Goz D, Studholme K, Lappi DA, Rollag MD, Provencio I, Morin LP (2008) Targeted destruction of photosensitive retinal ganglion cells with a saporin conjugate alters the effects of light on mouse circadian rhythms. PLoS ONE 3:e3153.
Graham DM, Wong KY, Shapiro P, Frederick C, Pattabiraman K, Berson DM (2008) Melanopsin ganglion cells use a membrane-associated rhabdomeric phototransduction cascade. J Neurophysiol 99:2522-2532.
Guler AD, Ecker JL, Lall GS, Haq S, Altimus CM, Liao HW, Barnard AR, Cahill H, Badea TC, Zhao H, Hankins MW, Berson DM, Lucas RJ, Yau KW, Hattar S (2008) Melanopsin cells are the principal conduits for rod-cone input to non-image-forming vision. Nature 453:102-105.
Hanifin JP, Brainard GC (2007) Photoreception for circadian, neuroendocrine, and neurobehavioral regulation. J Physiol Anthropol 26:87-94.
Hankins MW, Peirson SN, Foster RG (2008) Melanopsin: an exciting photopigment. Trends Neurosci 31:27-36.
Hannibal J, Fahrenkrug J (2004a) Melanopsin containing retinal ganglion cells are light responsive from birth. Neuroreport 15:2317-2320.
Hannibal J, Fahrenkrug J (2004b) Target areas innervated by PACAP-immunoreactive retinal ganglion cells. Cell Tissue Res 316:99-113.
Hardie RC, Minke B (1992) The trp gene is essential for a light-activated Ca2+ channel in Drosophila photoreceptors. Neuron 8:643-651.
Hardie RC, Raghu P (2001) Visual transduction in Drosophila. Nature 413:186-193.
Hartmann J, Dragicevic E, Adelsberger H, Henning HA, Sumser M, Abramowitz J, Blum R, Dietrich A, Freichel M, Flockerzi V, Birnbaumer L, Konnerth A (2008)

TRPC3 channels are required for synaptic transmission and motor coordination. Neuron 59:392-398.
Hartwick AT, Bramley JR, Yu J, Stevens KT, Allen CN, Baldridge WH, Sollars PJ, Pickard GE (2007) Light-evoked calcium responses of isolated melanopsin-expressing retinal ganglion cells. J Neurosci 27:13468-13480.
Hastings MH, Reddy AB, Maywood ES (2003) A clockwork web: circadian timing in brain and periphery, in health and disease. Nat Rev Neurosci 4:649-661.
Hastings MH, Herzog, E. D. (2004) Clock genes, oscillators, and cellular networks in the suprachiasmatic nuclei. J Biol Rhythms 19:400-413.
Hatori M, Le H, Vollmers C, Keding SR, Tanaka N, Schmedt C, Jegla T, Panda S (2008a) Inducible ablation of melanopsin-expressing retinal ganglion cells reveals their central role in non-image forming visual responses. PLoS ONE 3:e2451.
Hatori M, Le H, Vollmers C, Keding SR, Tanaka N, Buch T, Waisman A, Schmedt C, Jegla T, Panda S (2008b) Inducible ablation of melanopsin-expressing retinal ganglion cells reveals their central role in non-image forming visual responses. PLoS One 3:e2451.
Hattar S, Liao HW, Takao M, Berson DM, Yau KW (2002) Melanopsin-containing retinal ganglion cells: architecture, projections, and intrinsic photosensitivity. Science 295:1065-1070.
Hattar S, Kumar M, Park A, Tong P, Tung J, Yau KW, Berson DM (2006) Central projections of melanopsin-expressing retinal ganglion cells in the mouse. J Comp Neurol 497:326-349.
Hattar S, Lucas RJ, Mrosovsky N, Thompson S, Douglas RH, Hankins MW, Lem J, Biel M, Hofmann F, Foster RG, Yau KW (2003) Melanopsin and rod-cone photoreceptive systems account for all major accessory visual functions in mice. Nature 424:76-81.
Haverkamp S, Wassle H (2000) Immunocytochemical analysis of the mouse retina. J Comp Neurol 424:1-23.
Herzog ED (2007) Neurons and networks in daily rhythms. Nat Rev Neurosci 8:790-802.
Hofmann T, Schaefer M, Schultz G, Gudermann T (2002) Subunit composition of mammalian transient receptor potential channels in living cells. Proc Natl Acad Sci U S A 99:7461-7466.
Hoshi H, Liu WL, Massey SC, Mills SL (2009) ON inputs to the OFF layer: bipolar cells that break the stratification rules of the retina. J Neurosci 29:8875-8883.
Jacobs GH, Neitz J, Deegan JF, 2nd (1991) Retinal receptors in rodents maximally sensitive to ultraviolet light. Nature 353:655-656.
Johnson RF, Moore RY, Morin LP (1988) Loss of entrainment and anatomical plasticity after lesions of the hamster retinohypothalamic tract. Brain Res 460:297-313.
Jusuf PR, Lee SC, Hannibal J, Grunert U (2007) Characterization and synaptic connectivity of melanopsin-containing ganglion cells in the primate retina. Eur J Neurosci 26:2906-2921.

Kang TH, Ryu YH, Kim IB, Oh GT, Chun MH (2004) Comparative study of cholinergic cells in retinas of various mouse strains. Cell Tissue Res 317:109-115.
Kumbalasiri T, Provencio I (2005) Melanopsin and other novel mammalian opsins. Exp Eye Res 81:368-375.
Lall GS, Revell VL, Momiji H, Al Enezi J, Altimus CM, Guler AD, Aguilar C, Cameron MA, Allender S, Hankins MW, Lucas RJ (2010) Distinct contributions of rod, cone, and melanopsin photoreceptors to encoding irradiance. Neuron 66:417-428.
Lamb TD (1995) Photoreceptor spectral sensitivities: common shape in the long-wavelength region. Vision Res 35:3083-3091.
Lamb TD, Collin SP, Pugh EN, Jr. (2007) Evolution of the vertebrate eye: opsins, photoreceptors, retina and eye cup. Nat Rev Neurosci 8:960-976.
Lee YT, Wang Q (1999) Inhibition of hKv2.1, a major human neuronal voltage-gated K+ channel, by meclofenamic acid. Eur J Pharmacol 378:349-356.
Lin B, Koizumi A, Tanaka N, Panda S, Masland RH (2008) Restoration of visual function in retinal degeneration mice by ectopic expression of melanopsin. Proc Natl Acad Sci U S A 105:16009-16014.
Lockley SW, Skene DJ, Arendt J, Tabandeh H, Bird AC, Defrance R (1997) Relationship between melatonin rhythms and visual loss in the blind. J Clin Endocrinol Metab 82:3763-3770.
Lucas RJ, Douglas RH, Foster RG (2001) Characterization of an ocular photopigment capable of driving pupillary constriction in mice. Nat Neurosci 4:621-626.
Lucas RJ, Hattar S, Takao M, Berson DM, Foster RG, Yau KW (2003) Diminished pupillary light reflex at high irradiances in melanopsin-knockout mice. Science 299:245-247.
Lupi D, Sekaran S, Jones SL, Hankins MW, Foster RG (2006) Light-evoked FOS induction within the suprachiasmatic nuclei (SCN) of melanopsin knockout (Opn4-/-) mice: a developmental study. Chronobiol Int 23:167-179.
Margolis DJ, Detwiler PB (2007) Different mechanisms generate maintained activity in ON and OFF retinal ganglion cells. J Neurosci 27:5994-6005.
Mawad K, Van Gelder RN (2008) Absence of long-wavelength photic potentiation of murine intrinsically photosensitive retinal ganglion cell firing in vitro. J Biol Rhythms 23:387-391.
Maywood ES, O'Neill J, Wong GK, Reddy AB, Hastings MH (2006) Circadian timing in health and disease. Prog Brain Res 153:253-269.
Melyan Z, Tarttelin EE, Bellingham J, Lucas RJ, Hankins MW (2005) Addition of human melanopsin renders mammalian cells photoresponsive. Nature 433:741-745.
Metea MR, Newman EA (2006) Glial cells dilate and constrict blood vessels: a mechanism of neurovascular coupling. J Neurosci 26:2862-2870.
Moore RY, Lenn NJ (1972) A retinohypothalamic projection in the rat. J Comp Neurol 146:1-14.

Morin LP, Blanchard JH, Provencio I (2003) Retinal ganglion cell projections to the hamster suprachiasmatic nucleus, intergeniculate leaflet, and visual midbrain: bifurcation and melanopsin immunoreactivity. J Comp Neurol 465:401-416.
Mure LS, Rieux C, Hattar S, Cooper HM (2007) Melanopsin-dependent nonvisual responses: evidence for photopigment bistability in vivo. J Biol Rhythms 22:411-424.
Mure LS, Cornut PL, Rieux C, Drouyer E, Denis P, Gronfier C, Cooper HM (2009) Melanopsin bistability: a fly's eye technology in the human retina. PLoS One 4:e5991.
Muyrers JP, Zhang Y, Testa G, Stewart AF (1999) Rapid modification of bacterial artificial chromosomes by ET-recombination. Nucleic Acids Res 27:1555-1557.
Nelson R, Famiglietti EV, Jr., Kolb H (1978) Intracellular staining reveals different levels of stratification for on- and off-center ganglion cells in cat retina. J Neurophysiol 41:472-483.
Neumann T, Ziegler C, Blau A (2008) Multielectrode array recordings reveal physiological diversity of intrinsically photosensitive retinal ganglion cells in the chick embryo. Brain Res 1207:120-127.
Newman EA, Bartosch R (1999) An eyecup preparation for the rat and mouse. J Neurosci Methods 93:169-175.
Nickle B, Robinson PR (2007) The opsins of the vertebrate retina: insights from structural, biochemical, and evolutionary studies. Cell Mol Life Sci.
Nikonov SS, Kholodenko R, Lem J, Pugh EN, Jr. (2006) Physiological features of the S- and M-cone photoreceptors of wild-type mice from single-cell recordings. J Gen Physiol 127:359-374.
O'Brien BJ, Isayama T, Richardson R, Berson DM (2002) Intrinsic physiological properties of cat retinal ganglion cells. J Physiol 538:787-802.
Ostergaard J, Hannibal J, Fahrenkrug J (2007) Synaptic contact between melanopsin-containing retinal ganglion cells and rod bipolar cells. Invest Ophthalmol Vis Sci 48:3812-3820.
Pan F, Mills SL, Massey SC (2007) Screening of gap junction antagonists on dye coupling in the rabbit retina. Vis Neurosci 24:609-618.
Panda S (2007) Multiple photopigments entrain the Mammalian circadian oscillator. Neuron 53:619-621.
Panda S, Nayak SK, Campo B, Walker JR, Hogenesch JB, Jegla T (2005) Illumination of the melanopsin signaling pathway. Science 307:600-604.
Panda S, Sato TK, Castrucci AM, Rollag MD, DeGrip WJ, Hogenesch JB, Provencio I, Kay SA (2002) Melanopsin (Opn4) requirement for normal light-induced circadian phase shifting. Science 298:2213-2216.
Panda S, Provencio I, Tu DC, Pires SS, Rollag MD, Castrucci AM, Pletcher MT, Sato TK, Wiltshire T, Andahazy M, Kay SA, Van Gelder RN, Hogenesch JB (2003) Melanopsin is required for non-image-forming photic responses in blind mice. Science 301:525-527.
Peirson S, Foster RG (2006) Melanopsin: another way of signaling light. Neuron 49:331-339.

Peirson SN, Oster H, Jones SL, Leitges M, Hankins MW, Foster RG (2007) Microarray analysis and functional genomics identify novel components of melanopsin signaling. Curr Biol 17:1363-1372.
Peretz A, Degani N, Nachman R, Uziyel Y, Gibor G, Shabat D, Attali B (2005) Meclofenamic acid and diclofenac, novel templates of KCNQ2/Q3 potassium channel openers, depress cortical neuron activity and exhibit anticonvulsant properties. Mol Pharmacol 67:1053-1066.
Perez-Leon JA, Warren EJ, Allen CN, Robinson DW, Lane Brown R (2006) Synaptic inputs to retinal ganglion cells that set the circadian clock. Eur J Neurosci 24:1117-1123.
Perkins KL (2006) Cell-attached voltage-clamp and current-clamp recording and stimulation techniques in brain slices. J Neurosci Methods 154:1-18.
Pfaffl MW (2001) A new mathematical model for relative quantification in real-time RT-PCR. Nucleic Acids Res 29:e45.
Phillips AM, Bull A, Kelly LE (1992) Identification of a Drosophila gene encoding a calmodulin-binding protein with homology to the trp phototransduction gene. Neuron 8:631-642.
Pickard GE (1980) Morphological characteristics of retinal ganglion cells projecting to the suprachiasmatic nucleus: a horseradish peroxidase study. Brain Res 183:458-465.
Pickard GE, Baver SB, Ogilvie MD, Sollars PJ (2009) Light-induced fos expression in intrinsically photosensitive retinal ganglion cells in melanopsin knockout (opn4) mice. PLoS One 4:e4984.
Pires SS, Hughes S, Turton M, Melyan Z, Peirson SN, Zheng L, Kosmaoglou M, Bellingham J, Cheetham ME, Lucas RJ, Foster RG, Hankins MW, Halford S (2009) Differential expression of two distinct functional isoforms of melanopsin (Opn4) in the mammalian retina. J Neurosci 29:12332-12342.
Prichard JR, Stoffel RT, Quimby DL, Obermeyer WH, Benca RM, Behan M (2002) Fos immunoreactivity in rat subcortical visual shell in response to illuminance changes. Neuroscience 114:781-793.
Provencio I, Rollag MD, Castrucci AM (2002) Photoreceptive net in the mammalian retina. This mesh of cells may explain how some blind mice can still tell day from night. Nature 415:493.
Provencio I, Jiang G, De Grip WJ, Hayes WP, Rollag MD (1998) Melanopsin: An opsin in melanophores, brain, and eye. Proc Natl Acad Sci U S A 95:340-345.
Provencio I, Rodriguez IR, Jiang G, Hayes WP, Moreira EF, Rollag MD (2000) A novel human opsin in the inner retina. J Neurosci 20:600-605.
Qiu X, Kumbalasiri T, Carlson SM, Wong KY, Krishna V, Provencio I, Berson DM (2005) Induction of photosensitivity by heterologous expression of melanopsin. Nature 433:745-749.
Rea MA (1998) Photic entrainment of circadian rhythms in rodents. Chronobiol Int 15:395-423.
Ruby NF, Brennan TJ, Xie X, Cao V, Franken P, Heller HC, O'Hara BF (2002) Role of melanopsin in circadian responses to light. Science 298:2211-2213.

Sather W, Dieudonne S, MacDonald JF, Ascher P (1992) Activation and desensitization of N-methyl-D-aspartate receptors in nucleated outside-out patches from mouse neurones. J Physiol 450:643-672.
Schmidt TM, Kofuji P (2009) Functional and morphological differences among intrinsically photosensitive retinal ganglion cells. J Neurosci 29:476-482.
Schmidt TM, Kofuji P (2010a) Differential cone pathway influence on intrinsically photosensitive retinal ganglion cell subtypes. J Neurosci 30(48): 16262-16271.
Schmidt TM, Kofuji P (2011) An isolated retinal preparation to record light responses from genetically labeled retinal ganglion cells. J Vis Exp: in press.
Schmidt TM, Taniguchi K, Kofuji P (2008) Intrinsic and extrinsic light responses in melanopsin-expressing ganglion cells during mouse development. J Neurophysiol 100:371-384.
Sekaran S, Foster RG, Lucas RJ, Hankins MW (2003) Calcium imaging reveals a network of intrinsically light-sensitive inner-retinal neurons. Curr Biol 13:1290-1298.
Sekaran S, Lall GS, Ralphs KL, Wolstenholme AJ, Lucas RJ, Foster RG, Hankins MW (2007) 2-Aminoethoxydiphenylborane is an acute inhibitor of directly photosensitive retinal ganglion cell activity in vitro and in vivo. J Neurosci 27:3981-3986.
Sekaran S, Lupi D, Jones SL, Sheely CJ, Hattar S, Yau KW, Lucas RJ, Foster RG, Hankins MW (2005) Melanopsin-dependent photoreception provides earliest light detection in the mammalian retina. Curr Biol 15:1099-1107.
Semo M, Peirson S, Lupi D, Lucas RJ, Jeffery G, Foster RG (2003) Melanopsin retinal ganglion cells and the maintenance of circadian and pupillary responses to light in aged rodless/coneless (rd/rd cl) mice. Eur J Neurosci 17:1793-1801.
Sernagor E (2005) Retinal development: second sight comes first. Curr Biol 15:R556-559.
Sernagor E, Eglen SJ, Wong RO (2001) Development of retinal ganglion cell structure and function. Prog Retin Eye Res 20:139-174.
Sholl DA (1953) Dendritic organization in the neurons of the visual and motor cortices of the cat. J Anat 87:387-406.
Slaughter MM, Miller RF (1981) 2-amino-4-phosphonobutyric acid: a new pharmacological tool for retina research. Science 211:182-185.
Sollars PJ, Smeraski CA, Kaufman JD, Ogilvie MD, Provencio I, Pickard GE (2003) Melanopsin and non-melanopsin expressing retinal ganglion cells innervate the hypothalamic suprachiasmatic nucleus. Vis Neurosci 20:601-610.
Sun C, Speer CM, Wang GY, Chapman B, Chalupa LM (2008) Epibatidine application in vitro blocks retinal waves without silencing all retinal ganglion cell action potentials in developing retina of the mouse and ferret. J Neurophysiol 100:3253-3263.
Sun W, Li N, He S (2002) Large-scale morphological survey of mouse retinal ganglion cells. J Comp Neurol 451:115-126.
Takahashi JS, DeCoursey PJ, Bauman L, Menaker M (1984) Spectral sensitivity of a novel photoreceptive system mediating entrainment of mammalian circadian rhythms. Nature 308:186-188.

Terakita A, Tsukamoto H, Koyanagi M, Sugahara M, Yamashita T, Shichida Y (2008) Expression and comparative characterization of Gq-coupled invertebrate visual pigments and melanopsin. J Neurochem 105:883-890.
Trejo LJ, Cicerone CM (1984) Cells in the pretectal olivary nucleus are in the pathway for the direct light reflex of the pupil in the rat. Brain Res 300:49-62.
Tu DC, Zhang D, Demas J, Slutsky EB, Provencio I, Holy TE, Van Gelder RN (2005) Physiologic diversity and development of intrinsically photosensitive retinal ganglion cells. Neuron 48:987-999.
Tu DC, Owens LA, Anderson L, Golczak M, Doyle SE, McCall M, Menaker M, Palczewski K, Van Gelder RN (2006) Inner retinal photoreception independent of the visual retinoid cycle. Proc Natl Acad Sci U S A 103:10426-10431.
Vaney DI (1994) Territorial organization of direction-selective ganglion cells in rabbit retina. J Neurosci 14:6301-6316.
Viney TJ, Balint K, Hillier D, Siegert S, Boldogkoi Z, Enquist LW, Meister M, Cepko CL, Roska B (2007) Local retinal circuits of melanopsin-containing ganglion cells identified by transsynaptic viral tracing. Curr Biol 17:981-988.
Vugler AA, Semo M, Joseph A, Jeffery G (2008) Survival and remodeling of melanopsin cells during retinal dystrophy. Vis Neurosci 25:125-138.
Vugler AA, Redgrave P, Semo M, Lawrence J, Greenwood J, Coffey PJ (2007) Dopamine neurones form a discrete plexus with melanopsin cells in normal and degenerating retina. Exp Neurol.
Wang JS, Kefalov VJ (2009) An alternative pathway mediates the mouse and human cone visual cycle. Curr Biol 19:1665-1669.
Wang JS, Estevez ME, Cornwall MC, Kefalov VJ (2009) Intra-retinal visual cycle required for rapid and complete cone dark adaptation. Nat Neurosci 12:295-302.
Warren EJ, Allen CN, Brown RL, Robinson DW (2003) Intrinsic light responses of retinal ganglion cells projecting to the circadian system. Eur J Neurosci 17:1727-1735.
Warren EJ, Allen CN, Brown RL, Robinson DW (2006) The light-activated signaling pathway in SCN-projecting rat retinal ganglion cells. Eur J Neurosci 23:2477-2487.
Wassle H (2004) Parallel processing in the mammalian retina. Nat Rev Neurosci 5:747-757.
Weaver DR, Reppert SM (1995) Definition of the developmental transition from dopaminergic to photic regulation of c-fos gene expression in the rat suprachiasmatic nucleus. Brain Res Mol Brain Res 33:136-148.
Weng S, Wong KY, Berson DM (2009) Circadian modulation of melanopsin-driven light response in rat ganglion-cell photoreceptors. J Biol Rhythms 24:391-402.
Werblin FS, Dowling JE (1969) Organization of the retina of the mudpuppy, Necturus maculosus. II. Intracellular recording. J Neurophysiol 32:339-355.
Whitney IE, Keeley PW, Raven MA, Reese BE (2008) Spatial patterning of cholinergic amacrine cells in the mouse retina. J Comp Neurol 508:1-12.
Wong KY, Dunn FA, Berson DM (2005) Photoreceptor adaptation in intrinsically photosensitive retinal ganglion cells. Neuron 48:1001-1010.

Wong KY, Dunn FA, Graham DM, Berson DM (2007) Synaptic influences on rat ganglion-cell photoreceptors. J Physiol 582:279-296.
Wong RO (1999) Retinal waves and visual system development. Annu Rev Neurosci 22:29-47.
Xu Y, Vasudeva V, Vardi N, Sterling P, Freed MA (2008) Different types of ganglion cell share a synaptic pattern. J Comp Neurol 507:1871-1878.
Yang XW, Model P, Heintz N (1997) Homologous recombination based modification in Escherichia coli and germline transmission in transgenic mice of a bacterial artificial chromosome. Nat Biotechnol 15:859-865.
Yoo SH, Yamazaki S, Lowrey PL, Shimomura K, Ko CH, Buhr ED, Siepka SM, Hong HK, Oh WJ, Yoo OJ, Menaker M, Takahashi JS (2004) PERIOD2::LUCIFERASE real-time reporting of circadian dynamics reveals persistent circadian oscillations in mouse peripheral tissues. Proc Natl Acad Sci U S A 101:5339-5346.
Yoshimura T, Ebihara S (1996) Spectral sensitivity of photoreceptors mediating phase-shifts of circadian rhythms in retinally degenerate CBA/J (rd/rd) and normal CBA/N (+/+)mice. J Comp Physiol A 178:797-802.
Zaghloul KA, Boahen K, Demb JB (2003) Different circuits for ON and OFF retinal ganglion cells cause different contrast sensitivities. J Neurosci 23:2645-2654.
Zhang DQ, Wong KY, Sollars PJ, Berson DM, Pickard GE, McMahon DG (2008) Intraretinal signaling by ganglion cell photoreceptors to dopaminergic amacrine neurons. Proc Natl Acad Sci U S A 105:14181-14186.
Zhang J, Zhang AJ, Wu SM (2006) Immunocytochemical analysis of GABA-positive and calretinin-positive horizontal cells in the tiger salamander retina. J Comp Neurol 499:432-441.
Zhu Y, Tu DC, Denner D, Shane T, Fitzgerald CM, Van Gelder RN (2007) Melanopsin-dependent persistence and photopotentiation of murine pupillary light responses. Invest Ophthalmol Vis Sci 48:1268-1275.